ABSTRACT

ENERGY DEPENDENCE OF PROTON
INELASTIC SCATTERING FROM Ca^{40}

By

Thomas Yao-Ting Kuo

Inelastic proton scattering from the nucleus ^{40}Ca has been performed at 25, 30, 35 and 40 MeV beam energies. The target used was 99.97% enriched in the ^{40}Ca isotope. Spectra were taken simultaneously by two surface barrier Ge(Li) detectors. The overall resolution (FWHM) was 30-35 KeV. Angular distributions from 13° to 97° for elastic scattering and about 40 inelastic states were obtained.

The L-transfer quantum numbers for most of the observed states have been obtained and compared with the results of other experiments. Some ambiguities existing in previous experiments were clarified. States with L-transfer larger than 5 were observed. The deformation δ_L were extracted from DWBA collective model analysis of the angular distributions. It was found that the deformations were more or less energy independent, but exceptions are expected. The reduced transition probabilities B(EL) scaled for the (p,p') experiment were obtained using Fermi equivalent uniform-density-distribution.

Thomas Yao-Ting Kuo

Antisymmetrized distorted wave calculations were performed for some negative parity states using the Kallio-Kolltveit force and T. T. S. Kuo's R.P.A. wave functions. The particle-hole configurations of these states were investigated. It was found that the central force used in the ADW calculations is adequate in predicting the distributions of the normal parity states, but a tensor force may be essential to reproduce those of the unnatural parity states.

ENERGY DEPENDENCE OF PROTON INELASTIC SCATTERING FROM CA^{40}

By

Thomas Yao-Ting Kuo

Department of Physics

ACKNOWLEDGEMENT

I am greatly indebted to Professor C. R. Gruhn for suggesting this experiment and for his guidance, encouragement, and assistance throughout my graduate work. I am very grateful to him and to Dr. Wildenthal for his careful and critical reading of the manuscript.

I would like to thank Dr. B. Preedom for his great assistance in introducing me to the distorted wave theory and to the use of the JULIE code. Special thanks go to Professor H. McManus and Dr. F. Petrovich for teaching me to understand their microscopic theory of scattering as well as to use the form factor program.

I am indebted to Professor A. Galonsky for his constant concern for my work, to Professor H. Blosser for training me to operate the Cyclotron, and to Professor W. Kelly, Professor S. Austin, Dr. H. Wildenthal, Dr. G. Crawley, Dr. R. St. Onge, Dr. R. Jolly and Dr. R. Hinrichs for many helpful discussions.

I would like to thank Mr. Mercer and the staff of the machine shop; Mr. R. deForest and the staff of the electronics shop; Mr. R. Au and computer people; Mr. Hilbert and his fellow staff; Mr. A. Kaye and his secretary for their kind assistances in many occasions.

To my fellow graduate or ex-graduate students like Carl Maggiore who shared the hard work in making Ge(Li) detectors, Ken Thompson who designed and built the goniometer, Larry Samuelson, Richard Todd, Fred Trentelman, Larry Learn, Doug Bayer, Lolo Panggabean, Duane Larson, Bill Chaffee, I extend my thanks for their aid and cooperation.

I acknowledge the financial support of the research program at MSU provided by the National Science Foundation.

Finally, I would like to thank my wife, Monica, for her patience and understanding during these few years of my graduate study.

TABLE OF CONTENTS

Chapter

LIST OF TABLES

LIST OF FIGURES

Figure

CHAPTER I

INTRODUCTION

^{40}Ca is a nucleus of considerable theoretical interest because of its double closed shell structure. The degree of deviation from this simple structure is of great interest. Recent advances in the theories of nuclear shell models (RPA and deformed), effective nucleon-nucleus force, and the distorted wave treatment of direct reaction enable one to formulate a microscopic description of the inelastic scattering of protons by nuclei. A microscopic DWBA theory including anti-symmetrization for the (p,p') reaction at medium energy has been developed at Michigan State University and elsewhere. ^{40}Ca is one of the nuclei of interest. However, previous inelastic proton scattering data for ^{40}Ca in the range of 20-50 MeV were insufficient to provide a test for this theory. Rectification of this situation is one of the main motivations of performing the present experiment. The ^{40}Ca nucleus was chosen because in order to test the (p,p') reaction as a probe of nuclear structure, one needs:

1) a target which allows to examine all the components of the proton-nucleus force.

2) a target in which the eigenvectors describing the excited states are well established both experimentally and theoretically.

3) a target for which good optical model parameters exist.

The structure of ^{40}Ca has also been investigated in other experiments such as (α,α'), (e,e'), $(^3He,d)$ and (d,n). The (α,α') reaction is a predominantly surface dominated reaction and it leads to diffraction scattering. It provides information for L-transfer for the excited normal parity states, as well as the information on the isoscalar component of the projectile-nucleus force. The (e,e') reaction gives reduced electromagnetic transition probabilities and multipolarities. The $(^3He,d)$ and (d,n) proton stripping reactions allow one to study a component of the vectors of the excited states.

Previous $^{40}Ca(p,p')$ experiments giving some angular distributions were reported by Gray et al. (Colorado) and Yagi et al. (Japan). The experiment at Colorado was performed at 14 and 17 MeV with resolution about 80-100 KeV. The one at Japan was done at 55 MeV with 500 KeV resolution. The present experiment was conducted at 24.93, 30.04, 34.78 and 39.83 MeV beam energies. The target used is 99.97% enriched and is 2 mg/cm^2 thick. Spectra were taken simultaneously by two surface barrier Ge(Li) detectors which

were fabricated by the author of the present work and his collaborator. The overall resolution (FWHM) was 30-35 KeV. A goniometer was specially designed to facilitate the use of Ge(Li) counters and to provide a mechanism for transferring Ca targets into the scattering chamber under vacuum environment.

Angular distributions from 13° to 97° for elastic scattering and about 40 inelastic states were obtained. The weak excited states were of interest and the development of the high resolution Ge(Li) detectors with the best peak to valley ratio obtainable was directed toward this goal. The usefulness of thick and enriched target is also apparent.

In this thesis, the experimental apparatus and methods of obtaining and analyzing the data are described in Chapter II and III. The collective model analysis and the extraction of nuclear deformation are presented in Chapter IV. Chapter V is devoted to the summary of results of experimental sources. The microscopic DW calculations are described in Chapter VI, where the effective force and RPA wave functions used in the calculations are discussed.

CHAPTER II

EXPERIMENTAL APPARATUS AND PROCEDURES

2.1 Cyclotron and Beam Transport System

2.1.1 The Cyclotron

The proton beams of variable energy were produced by the sector-focus cyclotron (Bl 61) at Michigan State University. The principle and the details of the design of the machine as well as its operation have been reported elsewhere (Bl 66, Go 68). The most important objective in the operation of the cyclotron is a well tuned beam with high extraction efficiency. This can be accomplished by setting the main magnetic field precisely, centering the beam carefully to reduce the effect of RF ripple and selecting a narrow phase group to get an optimum single turn (resonant) extraction.

The H^+ beam is extracted at a radius of about 29 inches (212 turns), using a small first harmonic bump field to induce a coherent radial oscillation, together with a guiding electrostatic deflector and a focusing air-core magnetic channel. The beam is then balanced on the exit slits S1 as shown in Fig. 2.1. Typical internal beam currents were

1 to 5 microamperes and extraction efficiencies were about 80% during this experiment.

2.1.2 Beam Transport System

The external beam transport system is shown in Fig. 2.1. Detailed discussions of the optical properties of the beam and of the energy analysis system have been published (Ma 67, Sn 67, Be 68). M1 and M2 are horizontal bending magnets used to align the beam through the object slit S3 and the divergence slit S4. S2 is a vertical slit which was not used in this experiment. Two quadrupole doublets Q_1, Q_2 and Q_3, Q_4 are used to focus the beam on S3. The distance between S3 and S4 is approximately 48 inches. Thus the openings of S3 and S4 determine the divergence of the beam. M3 and M4 are two 45° analyzing magnets the fields of which are adjusted so as to direct the beam to the image slit, S5. Nuclear magnetic resonance fluxmeters (Scanditronix, NMR-656C) in M3 and M4 are used to measure the magnetic fields which determine the energy of the proton beam. Q5 and Q6 are quadrupole magnets used for refocusing.

The beam has to be balanced on S3, S4 and S5 simultaneously. The balancing can be exercised by adjusting the current on each side of the individual slit. The geometry of beam can be viewed from the scintillators in front of S3 and S5. After these conditions are satisfied, beam is then deflected into the target chamber by the distributing

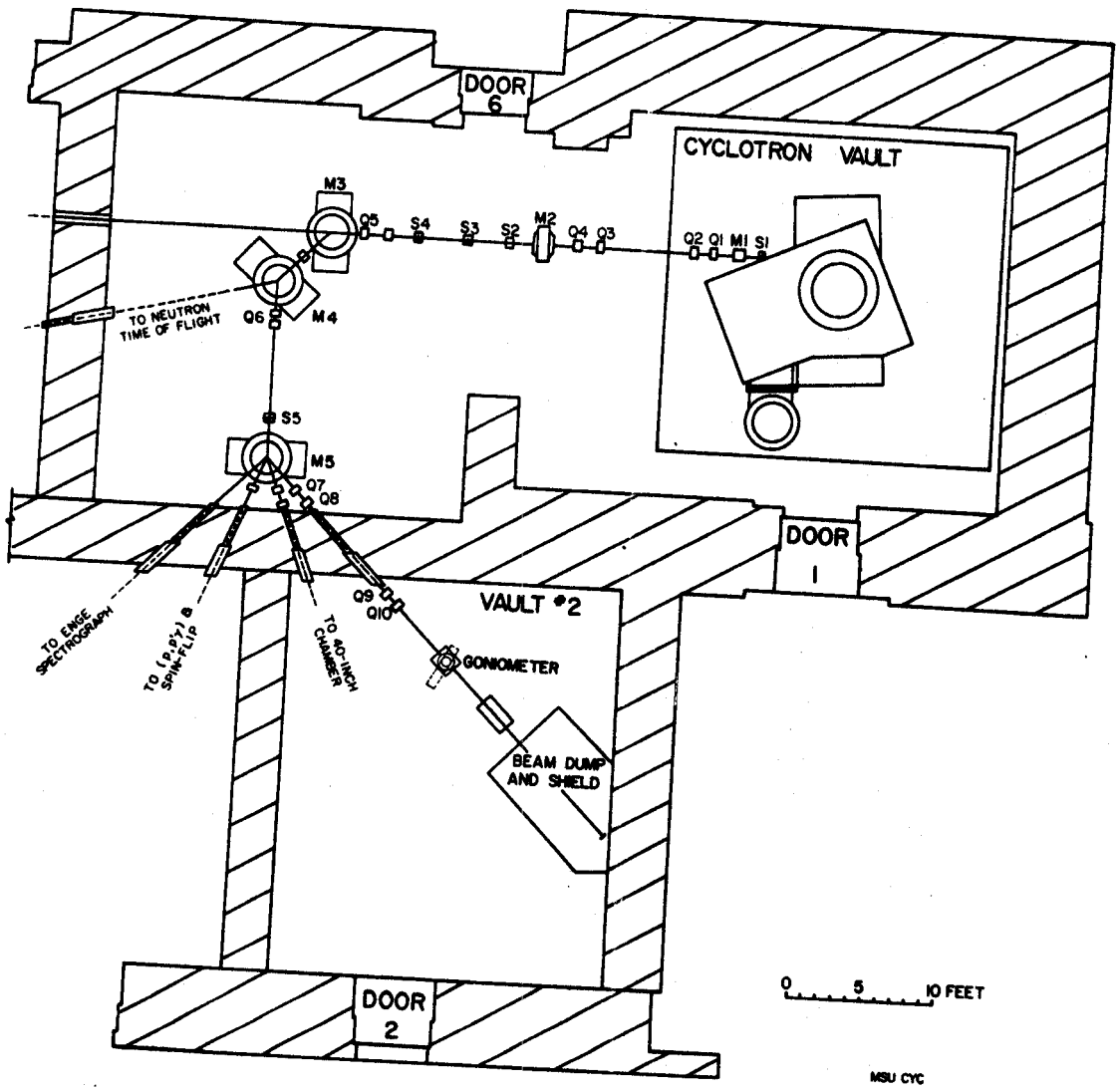

Figure 2.1.--Cyclotron and beam transport layout used in this experiment at the Michigan State University Cyclotron Laboratory.

magnet M5. Two more quadrupole doublets Q7, Q8 and Q9, Q10 are used to focus the beam on the target.

For the final beam preparation the following procedures were exercised. A plastic scintillator with a 1/16 inch hole in the middle was used for centering the beam on the target. The sharp and greatly enlarged image of the hole and the boundaries of the scintillator viewed by TV camera were first marked on the TV screen. When the beam hit the scintillator, the location of the spot could be seen clearly and the best focusing and centering could be achieved. In addition there were two more devices used for maintaining the correct alignment of the beam in the course of the experiment. One was the neutron background in the vicinity of the target chamber, the other was the current monitored by a tantalum ring which is shown in Fig. 2.2. The neutron background and the ring current must be kept in a minimum with respect to the beam current detected at the Faraday cup. The ring current was probably due to the particles which were scattered in the slit, S5.

2.1.3 Beam Energies

In this experiment, typical slit apertures were about 25 mils for S3 and S5, 100 mils for S4. These settings yield a beam divergence of ±0.8 milliradians which is equivalent to an 8-10 KeV energy spread on target at E_p=40 MeV.

The absolute energies of the proton beams were calculated from the NMR reading in M3 and M4. The uncertainty in absolute scale was 0.1% (Ma 67). The calibrated absolute energies for this experiment were 24.926 MeV ± 25 KeV, 30.044 MeV ± 30 KeV, 34.775 MeV ± 35 KeV and 39.828 MeV ± 40 KeV.

2.2 Target Chamber

The goniometer used in this experiment was designed by K. Thompson (Th 69). The target chamber, designed by C. Maggiore (Ma 70), is 16 inches in diameter and shown in Fig. 2.2. Two beam pipe adapters were plugged into the chamber with a double O-ring seal. On the right hand side (following the beam direction), an opening of 100° wide and 1½ inches high was covered by a 5 mil stainless steel sliding seal. A block of brass with two 3/4 inch brass tubes was soldered to the steel sheet. The center of the chamber could be viewed through the brass tubes. This block was attached to the main arm so that the sliding seal could be moved in either direction by the action of the arm.

There were baffles made of 50 mil tantalum sheet which encircled the target holder, two standing on the bottom, and another two hanging from the top of the chamber. The vertical opening of the strips was 1/2 inch. The end of the brass tubes was covered by tantalum rings with 3/8 inch holes. This arrangement was designed to minimize the multi-scattering into the detector.

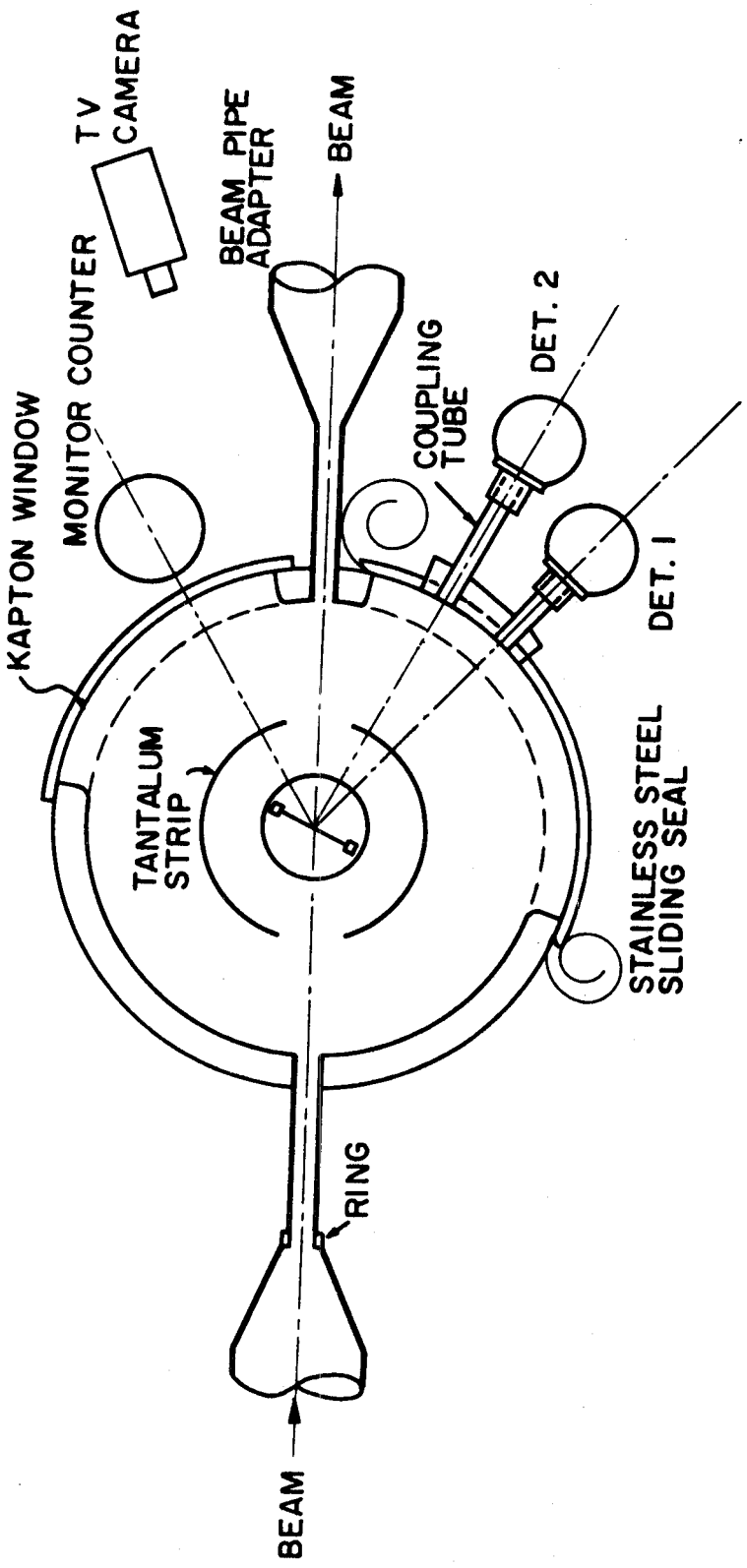

Figure 2.2.--Target chamber and detector arrangement.

The detectors were coupled to the tubes by sliding O-ring seals. Detector 2 was always placed at the smaller angle tube so that the solid angle was constant from one energy run to another. The angular separation between these two detectors was also mechanically fixed and was measured to be 14.7° (see Section 3.1). The mylar window on the detector cap was the only material through which the scattered protons had to pass before being detected.

On the other side of the chamber, an opening covered by 1/2 mil kapton foil served as viewing window for the TV camera in the monitoring of the beam spot. It also allowed scattered particles to be detected by various kinds of monitor counters. A secondary arm provided a convenient platform for mounting these counters.

The target holder could be rotated and moved vertically by remote control. On the top of the chamber was the target transfer system (Th 69) and the coupling pipe to the diffusion pump. The vacuum inside the chamber was maintained at about 5×10^{-3} microns and monitored in data room by television.

2.3 Faraday Cup and Integrated Charge

The monitor counter becomes standard equipment for normalization in this thesis. The Faraday Cup used was a half-inch aluminum beam stop isolated from the target chamber and shielded by concrete blocks 6 foot wide and 7 foot high. As seen in Fig. 2.1, additional shielding was

provided by a cylinder of paraffin surrounding the beam pipe about 3 feet from the target chamber. The neutron background was reduced about 10 times below the case of no shielding. Data so taken were much cleaner and the lifetime of detectors were extended.

The relative integrated charged was measured by an Ortec 439 current digitizer along with an Ortec 430 scaler. The current digitizer triggered the scaler every time after it has collected preset charge level (in the order of 10^{-12} to 10^{-8} coulomb). From the calculation of absolute cross section, the charge lost were found to be ~30%. There were cases in which the charge was fully collected. Those cases were found about 30% higher than those after loss. The causes of charge loss were probably due partly to multiple scattering after the beam travelled through the target, to leakage to the ground and to the malfunction of the current meters.

2.4 Detectors

Two Ge(Li) surface barrier detectors were used to take data simultaneously. These detectors were fabricated in this laboratory, one by the author of this thesis and the other by C. Maggiore who investigated the $^{48}Ca(p,p')$ reaction using the identical experimental setup. Details about the fabrication of Ge(Li) detectors are discussed in Appendix I of Maggiore's thesis.

As shown in Fig. 2.2, these two detectors were fastened to the coupling mechanism on the sliding seal. Detector 1 and 2 were always attached to the same coupling tube and the distances from the detectors to the center of the target chamber were also fixed. The angular separation was measured to be 14.7° (see Section 3.1).

The monitor counter employed throughout this experiment was a Ge(Li) detector of side entry geometry mounted in a Harshaw satelite cryostat. It was mounted outside of the target chamber on a secondary arm whose angle could be manually adjusted. Scattered protons were detected after passing through the 1/2 mil kapton windows of the target chamber, about 1/2 inch of air and then the 1/4 mil diminized mylar window of the detector cap. The overall resolution of this counter obtained with the above arrangement was about 100 KeV. The peak to valley ratio was 1000:1. The electronics used will be described in Section 2.6.

2.5 Target

The target used in this work was a 99.973% isotopically enriched Ca^{40} foil. Its thickness was 2 mg/cm^2. This target was purchased from Oak Ridge National Laboratory (ORNL) and shipped in a vacuum tube. Mounting the foil on a target frame was done in Argon atmosphere. The mounted target was immediately placed in a target storage chamber (Ma 70)

which was evacuated to a vacuum of the order of 5×10^{-6} mm by an absorption pumping system.

After having been transferred from the vacuum shipment tube into the storage chamber, the target was never exposed to air or argon. This was accomplished by the coupling scheme of target storage and transfer system designed by K. Thompson (Th 69) and C. Maggiore (Ma 70).

The target thickness of 2 mg/cm^2 was so chosen that the "signal to noise" ratio would be good enough to observed the first excited 0^+ state and that higher efficiency of data taking could be achieved, without unduly high beam currents on target. The energy straggling of protons passing through this target at normal incidence was about 12 KeV more or less. It increased to 18 KeV when the target plane was set at about 50° with respect to the beam.

The amount of contamination in the target due to oxidation and condensation of pump oil molecules were obtained from the elastic scattering data. It was found that the thickness of oxygen was about 0.019 ± 0.002 mg/cm^2, carbon 0.0026 ± 0.0003 mg/cm^2 and hydrogen 0.0017 ± 0.0002 mg/cm^2. There was also a small amount of F^{19} whose elastic peak showed up clearly in some spectra. However, there is no

proton elastic scattering data in the energy range of 20-40 MeV, and therefore the amount of F^{19} was not estimated.

The isotopic and spectrographic analysis supplied by ORNL is listed in Table II-1.

TABLE II-1.--Isotopic and Spectrographic Analysis* of Ca^{48} Target Used.

Isotopic Analysis		Spectrographic Analysis			
Ca^{40}	99.973%	Ag	<0.02%	Mo	<0.05%
Ca^{42}	0.008	Al	<0.05	Na	0.01
Ca^{43}	0.001	B	<0.01	Ni	<0.05
Ca^{44}	0.018	Ba	<0.02	Pb	<0.05
Ca^{46}	<0.001	Co	<0.05	Pt	<0.05
Ca^{48}	0.001	Cr	<0.05	Rb	<0.02
		Cu	<0.05	Si	<0.05
		Fe	<0.02	Sn	<0.05
		K	<0.01	Sr	0.02
		Li	<0.01	Ti	<0.02
		Mg	<0.05	V	<0.02
		Mn	<0.02	Zr	<0.1

*supplied by Oak Ridge National Laboratory

2.6 Electronics

Fig. 2.3 shows the block diagram of the electronics used in this experiment. The electronics used for detector 1 and 2 are identical and only slightly different for the monitor counter. The 1500 volt bias supply (Model 250) for the data taking detectors was purchased from Mech-tronic Nuclear Corporation. The voltage applied to detector 1 and 2 were 1500 and 1200 volts respectively.

Modified Ortec 109A preamplifiers were used for the first stage amplification. The modified model was designed for up to 90 MeV proton detection using Ge(Li) counter (Wi 67). A shaping amplifier board was added between the charge sensitive loop and the cable driver of model 109A. The pole-zero network and voltage amplifier were bypassed. The shaping time constant τ was 2μ sec for both differentiator and integrator.

The preamplified pulses were fed into the second stages of Tennelec TC 200 amplifiers. This section of the amplifierswas found to have the least noise at the time when this experiment was being performed. Since the shaping preamps were used, only one step of differentiation and integration in the TC 200 amplifier was needed. Therefore, this arrangement of preamplifier and main amplifier was capable of providing optimum electronic resolution.

The outputsignals from the TC 200 amplifiers were always monitored by a RM41A Oscilloscope (Tektronix,

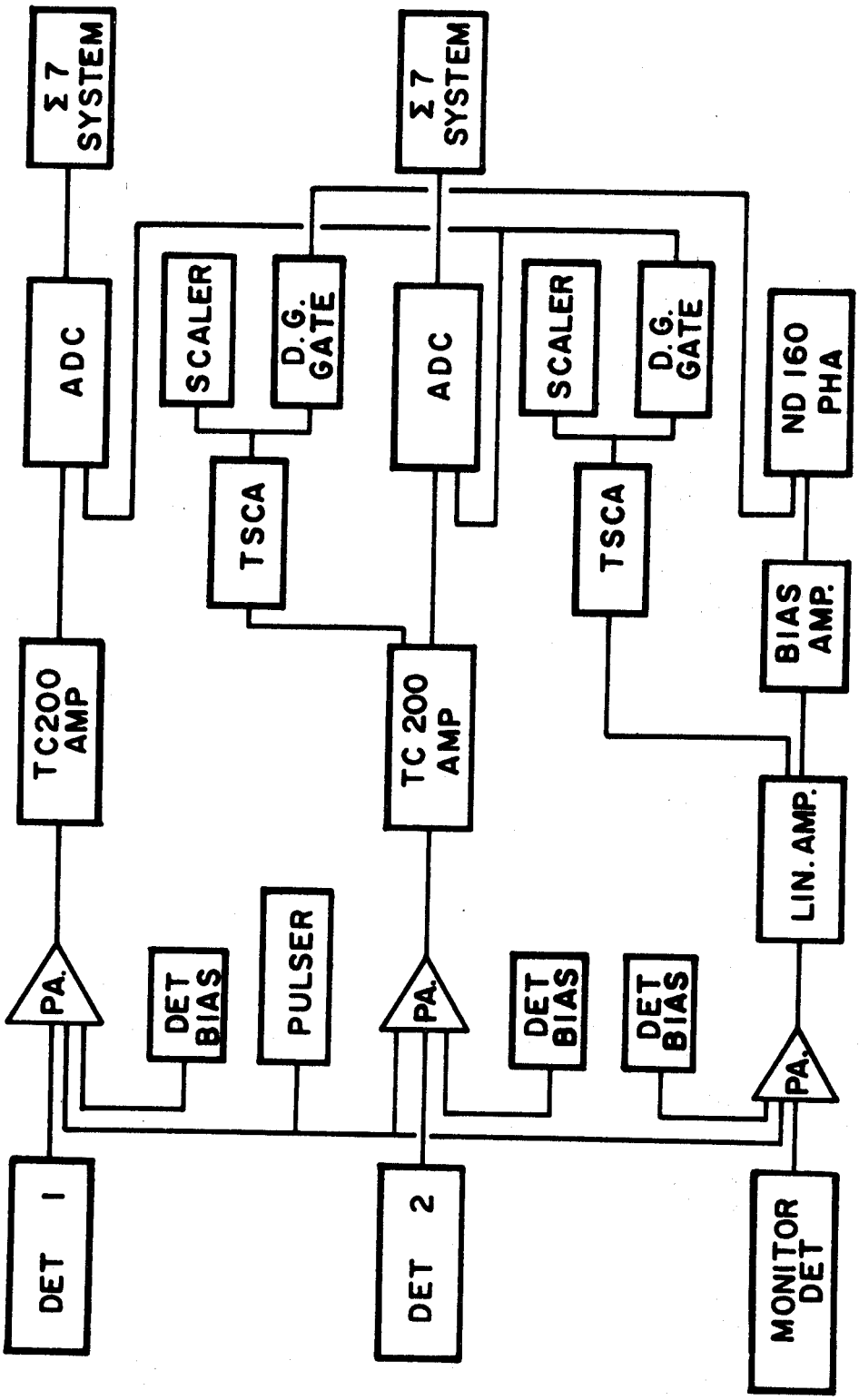

Figure 2.3.--Block diagram of the electronics used with the Ge(Li) detectors.

Inc.). In the course of data taking, pulses from the detector with the higher counting rate were displayed so that pile up problems could be prevented. On the other hand, the beam current could be adjusted to give maximum efficiency of data taking.

Output signals were tested by feeding them into a Nuclear Data 160 1024-channel analyzer. Signals from a Canberra stabilized pulser (Model 1501) were used to check the total noise level of the setup. The overall noise was less than 6 KeV when the pulses were equivalent to those coming from protons at 40 MeV. This method provided a way to single out faulty components, i.e., a poor cable connection or a damaged preamplifier. The pulser was also used in setting the gain of the amplifier.

The electronics setup thus far was further examined by a γ-ray test using Cs^{137} as a source. Resolutions of 3 KeV were obtained with the modified preamplifier at 661 KeV. The pulser and γ-ray tests were essential prior to the data accumulation. A number of malfunctions of equipments were found and corrected by this procedure.

The output pulses of the amplifier were finally fed into a NS-629 Analog-Digital Converter. The conversion gain of the ADC was set at 8192 channels and the upper 4096 channels were interfaced to the laboratory's Sigma 7 computer. Program POLYPHEMUS written by Richard Au was used in command of data storage and data dumpout.

The electronics used for the monitor counter was very similar to those used for data taking except that optimum resolution was not vigorously sought. 1000 volts bias was applied to the counter by an Ortec 210 power supply. Ortec 109A preamplifier and 410 multimode linear amplifier were used for amplification. The pulses from the linear amplifier were fed into an Ortec 408 biased amplifier to discriminate the lower 30 MeV signals. The upper 10 MeV pulses were finally imput into a ND 160 analyzer. Data could be dump out in punched cards by Sigma-7 computer. Tests using pulser and γ-ray were also performed for the monitor counter.

Dead time corrections were made for all the ADCs used (two NS-629s and one ND 160). Pulses were taken from the amplifiers and fed into an Ortec 420 timing single channel analyzer (TSCA). The E setting depended on beam energy and the window ΔE was set wide open. Since only random signals were needed, there was no particular adjustment for the window. Positive signals were put into an Ortec 430 scaler and an Ortec 416 gate and delay generator which the final pulses from the monitor counter were fed into the zero channels of two NS-629 ADCs. Similarly pulses from detector 2 entered the live time clock of the ADC of ND 160. Dead time corrections in percentage were computed by the equation

$$\text{D.T. Correction } (\%) = \frac{\text{counts (scaler)}}{\text{counts (zero channel of ADC)}} - 1.$$

2.7 Accumulation of Data

With the preparation of beam and detector-electronics in readiness, preliminary spectra were taken for final inspection and correction. Using the program POLYPHEMUS a spectrum could be displayed and analyzed on a scope while data were still being accumulated. The resolution of the spectrum normally provided the sole indication of the degree of perfection of the whole setup. Data accumulation started after every aspect has been judged functioning properly.

The angular range of detection was from 12° to 97° in 5° step. Data were taken twice at 27° and 72° by each detector for the relative normalization. The time to be spent at each angle was from an hour and half to two hours. At the beginning of the angular distribution, the beam current was limited by the pile up effect of the detector sitting at smaller angle. In this case the beam current was less than 10na and it took about three hours to obtain the necessary statistics for the spectrum taken by the detector at larger angle. Usually, the statistics required for the first excited 0^+ state at 3.35 MeV was set at about 10 ~ 15%. The efficiency of gathering data as a function of cyclotron time was also taken into account.

At the end of each run, data were dumped out by the Sigma-7 computer in cards and listings. Spectra could be obtained immediately using the Calcomp plotter. After

the angular distribution for Ca^{40} was completed, mylar runs were made at the same angles to collect information for contaminant corrections. The total run time for beam energies at 35 and 40 MeV was 72 hours each due to some difficulties in cyclotron and computer operation. For 25 and 30 MeV, it took only 72 hours to collect all the data of two angular distributions.

2.8 Representative Spectra

Representative spectra with counts in logarithmic scale are shown in Fig. 2.4 to Fig. 2.8. A spectrum in linear scale is shown for E_p=35 MeV (Fig. 2.4). In the group of elastic peaks two small ones can be seen. One of which is from high Z contaminants and the other was identified as ^{19}F. The first excited 0^+ (3.35 MeV) state was clearly seen due to the cleanness of the valley. Peaks below 7 MeV were well isolated.

States up to 10.3 MeV excitation energy were observed and the angular distributions of many of them were obtained for E_p=35 MeV. The broad peak of bell shape was due to the Ta degrader of the antislit scattering system in front of the surface barrier Ge(Li) detector. The ground state of the $^{40}Ca(p,d)$ reaction with Q-value of -13.863 MeV was also observed.

The overall resolution was about 30 to 35 KeV (FWHM). The sources and their contributions to the energy resolution is tabulated in Table II-2.

TABLE II-2.--Contributions to the Energy Resolution (40 MeV Proton on Ca^{40}).

Sources	ΔE(KeV)	$(\Delta E)^2$
Straggling		
Target	10.0	
Package Windows	5.3	
Detector Windows	8.0	
Total	25.3	642
Electronic	7.2	52
Ion Pair Statistics	7.3	53
Beam Spread	10.0	100
Kinematic (at 45°)	7.5	56
Electronic Drift	5.0	25
Overall	30.2	928

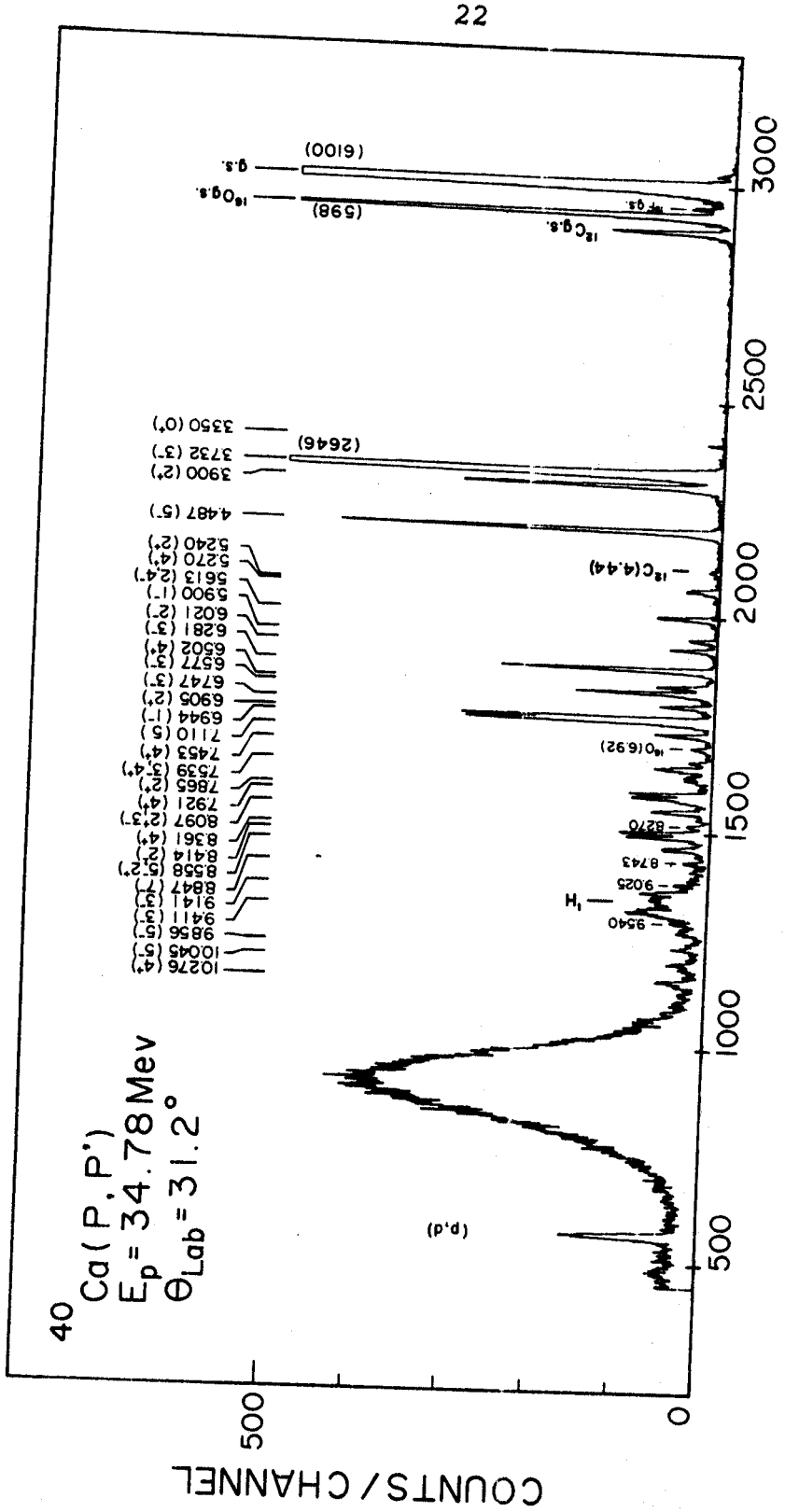

Figure 2.4.--$^{40}Ca(p,p')^{40}Ca^*$ spectrum taken at θ_{Lab}=31.2° for E_p=34.78 MeV. Linear scale in count number is used for illustration of the relative strengths of various peaks at this angle.

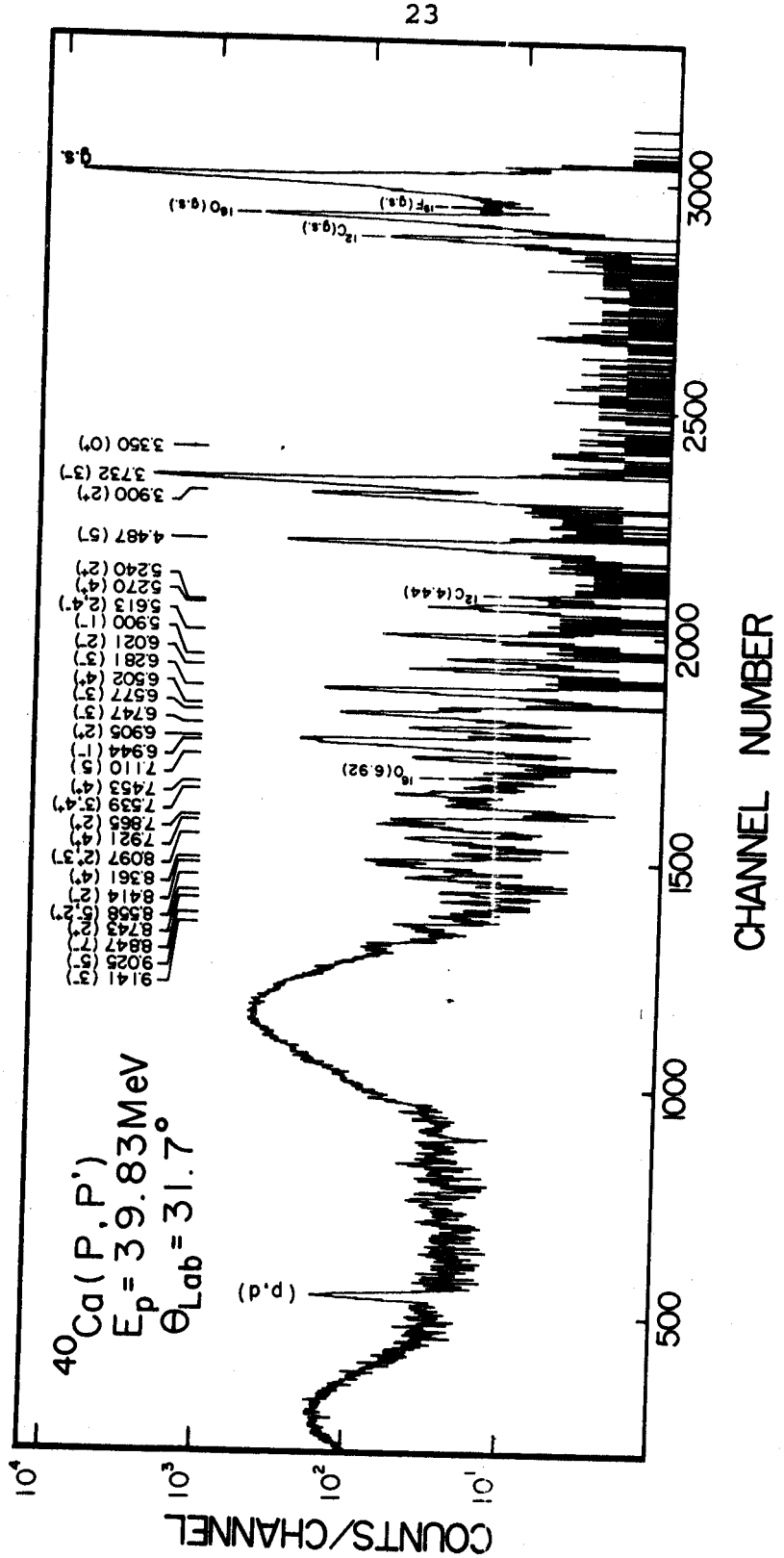

Figure 2.5.--^{40}Ca(p,p')^{40}Ca* spectrum taken at θ_{Lab}=31.7° for E_p=39.83 MeV.

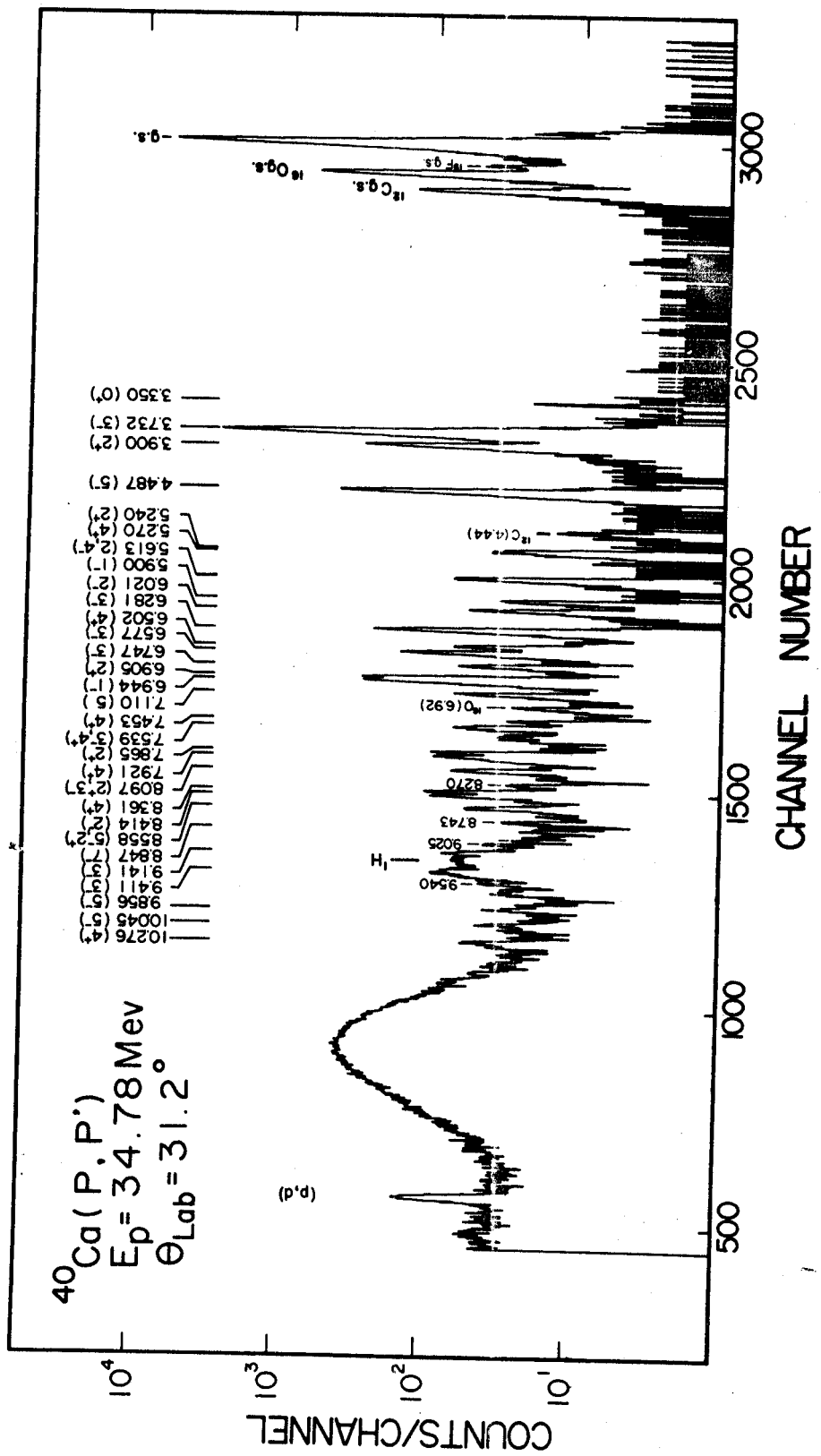

Figure 2.6.--$^{40}Ca(p,p')^{40}Ca^*$ spectrum taken at $\theta_{Lab}=31.2°$ for $E_p=34.78$ MeV.

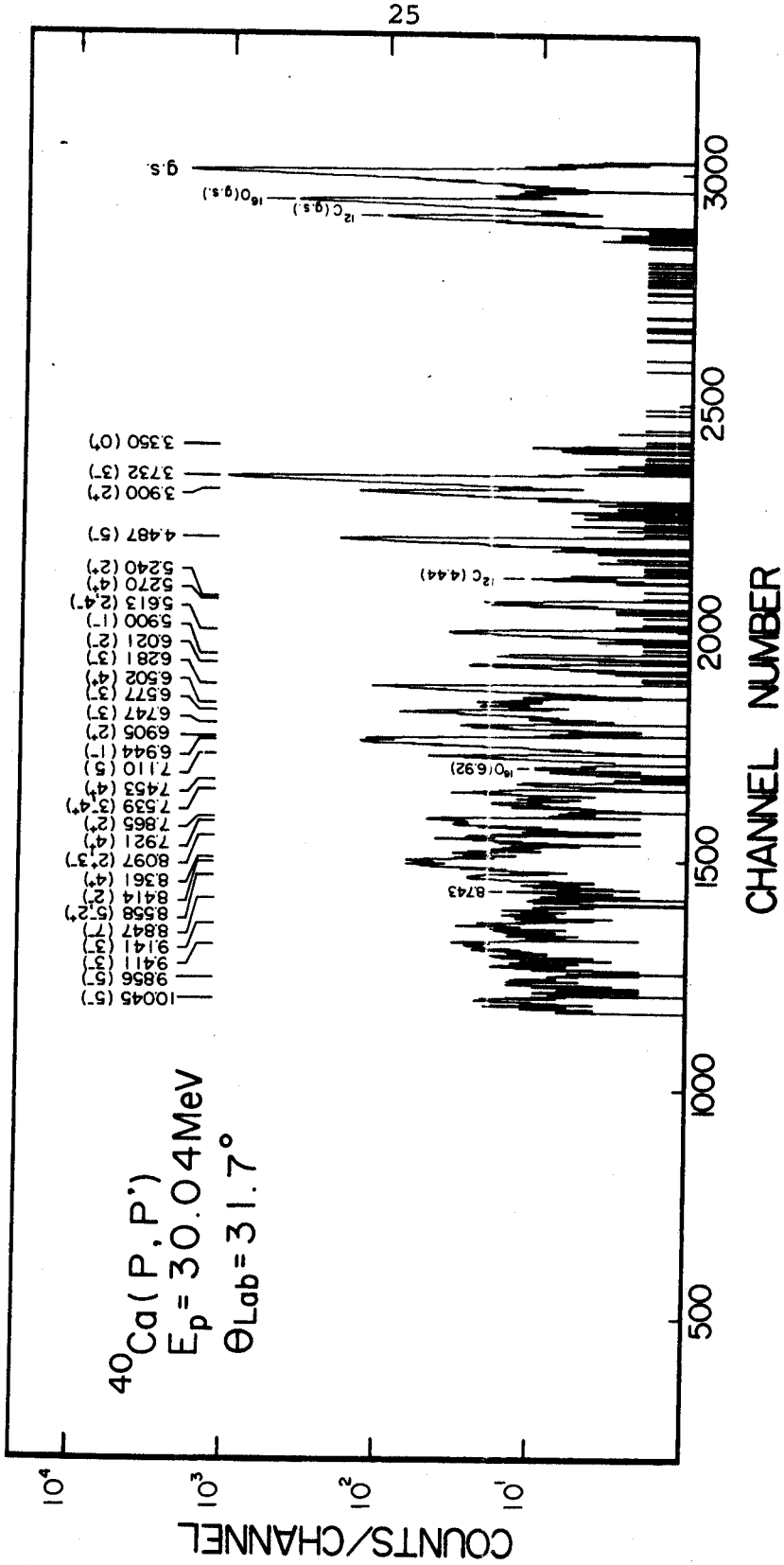

Figure 2.7.--$^{40}Ca(p,p')^{40}Ca^*$ spectrum taken at $\theta_{Lab}=31.7°$ for $E_p=30.04$ MeV.

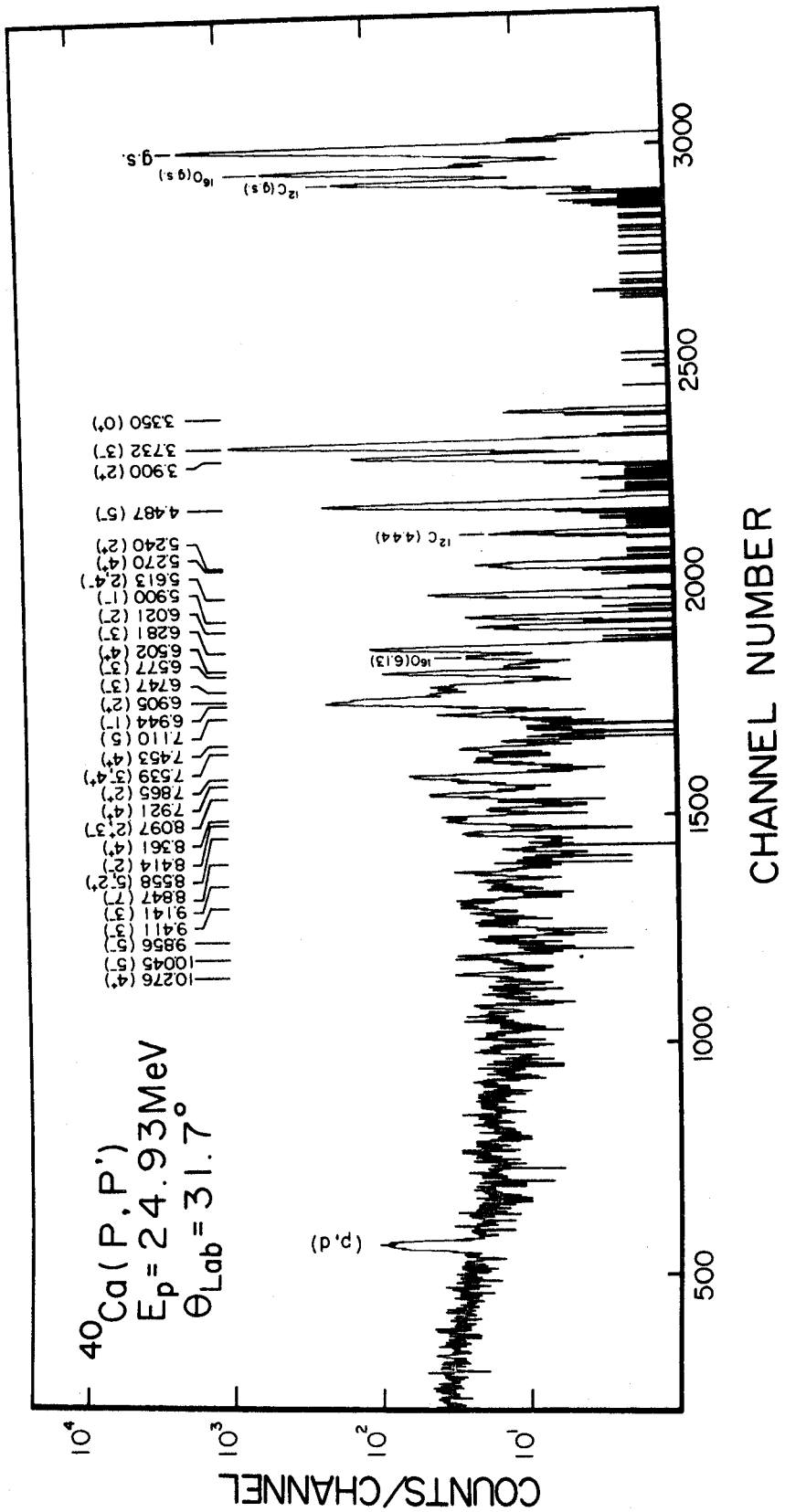

Figure 2.8.--^{40}Ca(p,p')^{40}Ca* spectrum taken at θ_{Lab}=31.7° for E_p=24.93 MeV.

CHAPTER III

EXPERIMENTAL DATA ANALYSIS

3.1 Laboratory Angle Calibration

The laboratory angle for each spectrum was determined by the energy separations between the elastic peaks of Ca^{40}, O^{16} and C^{12} and the 3^- excited state of ^{40}Ca at 3.731 MeV. Using the program FASTKINE written by W. Plauger, the relativistic kinematics of the scattered protons were calculated for each nucleus in 0.1° steps in the vicinity of the estimated laboratory angles. The laboratory energies for each nucleus were plotted with respect to laboratory angle together on one linear graph. Thus the calculated energy spacings could be read continuously as the function of laboratory angle.

The experimental energies of the forementioned peaks were calculated from the positions of their centroids. With the known energy difference between the ^{40}Ca [0.000 MeV] and the $^{40}Ca^*$ [3.731 MeV] states at a particular angle, the energy spacing between these four peaks were computed. However, without knowing the exact angle, the energy calculation is only approximate. It was, therefore, necessary to reiterate this angle and energy calibration

procedure. Since the energy difference between the $^{40}Ca^*$ [3.731 MeV] and ^{40}Ca [0.000 MeV] states changes slowly with respect to angle (about 0.8 KeV/deg. at 25° and 1.7 Kev/deg. at 100°), most computations required only two iterations. By fitting the experimental energy differences to those calculated, the laboratory angle was determined.

For laboratory angles less than 28°, the H(p,p)H reaction was also used. The fact that the kinematics of this reaction is stongly dependent on angle provided an acute test of the accuracy of the method described above. The agreement between these two calibration methods agreed within 0.04 degree.

The effect upon the accuracy of determinations of the laboratory angle of the uncertainties in the beam energy and in the centroids of peaks was studied. Two kinematic calculations were done using E_p=35.000 MeV and 34.775 MeV. The laboratory angles calibrated by these two calculations were within 0.1 degree. When the centroids were allowed to fluxuate ±0.2%, the calibrated angles varied by ±0.04 degree.

In addition to the above, other checks of the angle calibration were made. For example, the angular separation between two detectors used was mechanically fixed. This separation was obtained by computing the difference between the calibrated angles of these two detectors when they were taking data simultaneously. The angular difference between the counters was found 14.7° throughout. On the other hand,

these two detectors overlapped at about 27° where the differential cross-section of the elastic peak changes drastically. Should the angle be measured incorrect by more than 0.1 degree the matching of the elastic angular distribution would be very difficult. In this experiment, each distribution was matched to with 1%.

3.2 Normalization of Data

3.2.1 Dead Time Correction

Dead time corrections were made for all spectra including those taken by the monitor counter. The percentage corrections were obtained by taking the ratio of counts registered by the scaler to those registered by the zero channel of the analyzer (see Section 2.6 for electronic setup). The dead times for most spectra were under 2%. For only a very few cases (5 out of 100) in which the detector was set at small angle, were corrections found to exceed 5%, the largest being 12%.

3.2.2 The Monitor Counts

The entire monitor spectrum was taken by the ND 160 analyzer for each run. In the early stage of data analysis, the effect of the window width of the differential discriminator was investigated, for it was feared that elastic counts might get lost in the long tail of background. As mentioned in Section 2.4, the peak to valley ratio of the monitor counter

used was about 1000:1. Consequently when a window was consistently chosen, the relationships between monitor counts, integrated charges and target angles were found to remain almost the same. The monitor counts used for normalization were obtained by setting a window which covered all the elastic peaks of Ca^{40}, O^{16} and C^{12} so as to minimize tail losses even though they were small.

3.2.3 Charge and Target Angle

Ratios of monitor counts (after dead time correction) to integrated charge were computed to examine the charge collection system for relative errors. An average value was obtained for each target angle and deviations from the average were also computed. Most of these deviations were less than 1%. The average value of ratios also provided a way to check the target angle. The ratio of two mean values should be equal to the ratios the cosines of the corresponding angles. When the backlash of the target frame driving system was treated properly, the readout for target angle was found accurate to ±1 degrees.

The consistency between monitor counts and integrated charge enabled either of them to be used for normalization. In this experiment monitor counts were preferred because they were obtained by a somewhat more reliable and controllable electronic setup and hence believed to be more accurate.

Throughout about 100 data taking runs, there were only two successive runs in which the integrated charges showed a 30% discrepancy. On the other hand, from the calculation of absolute normalization, the integrated charge was found consistently 30% lower than expected. Probably this was due to a loss of charge between the Faraday cup and current digitizer system.

3.2.4 The Solid Angles of Detectors

The solid angles of the two detectors used in this thesis and their measurements in area and distance from the center of target chamber are listed as follows:

	Detector 1	Detector 2
Width	2.2 ±0.05 mm	1.9 ±0.05 mm
Area	14.5 ±0.4 mm^2	10.5 ±0.35 mm^2
Distance	32.45±0.25 CM	36.65 ±0.25 CM
Solid Angle	1.38±0.04 $x10^{-4}$Sr	0.786±0.024$x10^{-4}$Sr

The relative ratio of solid angle of detector 1 and 2 so obtained was $\Delta\Omega_1/\Delta\Omega_2$ = 1.755±0.105. The ratio of effective detection efficiencies was determined by matching the relative differential cross section for the elastic peak at the overlap angle of 72°. This was done for each beam energy. The result of the four measurements yield an average value of 1.78±0.01, for the efficiency ratio.

3.3 Method of Normalization

The differential cross section is defined as the probability of finding scattered particles through a unit solid angle per unit incoming flux per unit scattering center. It can be written as

$$\frac{d\sigma}{d\Omega}(\theta_{Lab}) = \frac{N_{event}}{N_{Scatt} \cdot I \cdot \Delta\Omega \cdot \varepsilon_{ff}}$$

where N_{event} is the number of events detected within solid angle $\Delta\Omega$

N_{scatt} is the number of scatterers per unit area

I is the number of incoming particles

ε_{ff} is the efficiency of the detection. (equal to 1 for ideal detector).

For the present experiment, these physical quantities were more specifically defined. N_{event} is the number of counts extracted from a spectrum after correction for analyzer dead time loss. N_{scatt} can be obtained by calculating the number of atomic weight per unit area, that is t/A where t is the thickness of target in mg/cm^2 and A is the atomic weight in mg, and then converting it to the number of target nuclei ($t/A \times 6.023 \times 10^{23}$). Normalization to target angle should also be taken into account. The number of incoming particles I is computed from the recorded integrator charge. I is also proportional to the monitor counts in a given run. This ratio may differ from runs with unequal target angles.

For the convenience in the data analysis two simplified expressions for differential cross section were used

$$\frac{d\sigma}{d\Omega}(\theta_{Lab}) = \text{Counts x Abs. Norm. factor}$$

$$= \text{Counts x } k \frac{A}{t}$$

where k is the relative normalization factor belong to a given spectrum. The former one implies that once the peak counts are given, the cross section can be obtained by just one step multiplication. The latter is used for computing the amount of contaminants in a target.

To test the overall accuracy of the calibration works described in Section 3.1 and 3.2, and to examine the correctness of the formula used in computing absolute differential cross sections, several calculations were tried. For example, the hydrogen peak counts were first extracted from a mylar spectrum at θ_{Lab}=26.7 degree and at E_p=40 MeV. By assuming the efficiency of the detector be 98.75% (Ja 66), the absolute cross section in the center of mass system was found to be 14.6 mb/sr (θ_{CM}=53.96°). This was about 30% higher than 11.12±0.5 mb/Sr obtained by Johnston (Jo 58). Calculations for C^{12}, O^{16} and Ca^{40} and comparisons with other experiments are listed below where θ_{CM} is the angular location of a maximum or a flat region in the distribution.

Target	E_p	θ_{CM}	$\frac{d\sigma}{d\Omega}\pm\Delta$ (Trial Cal.)	$\frac{d\sigma}{d\Omega}\pm\Delta$ (Ref., Abs.ERR.)	Ratio (Cal./Ref.)
C^{12}	40	60°	13.9±2.4%	10.3±2.0% (Bl 66a,±5.0%)	1.35±6.1%
O^{16}	40	50°	26.2±2.0%	20.2±1.0% (Ca 67,±1.7%)	1.29±2.8%
Ca^{40}	40	41°	126.0±0.2%	96.7±2.0% (Bl 66a,±5.0%)	1.31±5.4%
Ca^{40}	30	46°	143.6±0.2%	110.1±1.7% (Ri 64,±3.0%)	1.31±3.4%

It can be seen that all results of the trial calculations were consistently 30% higher than other measurements indicating that the combined systematic error of the integrated charge and the detector solid angle was about 30%. We have attributed this discrepency to a malfunction in the integrator.

Viewing this matter from another angle, one finds that once the charge loss of this experiment was corrected, good agreement between this experiment and various others was obtained. Most important of all, the results of elastic scattering from Ca^{40} obtained by ORNL and Oxford groups were confirmed. Consequently the elastic and inelastic scattering data of this work were believed to be normalized within ±3%.

3.4 Treatment of Contaminant Data

The main contaminants observed were H, C^{12} and O^{16}. The hydrogen and carbon came from the deposition of pumping oil on the target while the oxygen came from the oxidation of the Ca during the mounting of the target foil.

A complete analysis was made for C^{12} and O^{16}. First, it was necessary to know the number of counts for the individual inelastic peaks of these two contaminants in a spectrum of interest. To do this, a mylar target was used to measure the ratio of counts of the inelastic to the elastic peaks at the identical angles at which Ca^{40} data were taken. This method provided a reference to monitor the intensity of the contaminant peaks in Ca^{40} spectrum, because the mylar spectra did not need to be analyzed in detail. Once the ratio of counts in the mylar run was computed, the number of counts for the same inelastic contaminant peak in Ca^{40} spectrum was easily determined as long as the elastic counts were known.

The corrections for contaminants at small angles, where the C^{12} and O^{16} elastic peaks could not be separated from that of Ca^{40}, required the knowledge of the thickness of each contaminant. To determine the amount of O^{16}, a complete analysis was done as follows. Take the case of 40 MeV for example. The angular distribution of relative cross sections in laboratory system for the O^{16} elastic peak

was first obtained. This result was compared with the measurement reported by Cameron (Ca 67). Good agreement in the shape of the distribution was noted. This suggested that the buildup of O^{16} on the target remained essentially constant in the course of the whole experiment. Secondly, the amount of O^{16} in the target was calculated by using Cameron's data and the equations described in Section 3.3. Several values were computed over a few angles around $\theta_{Lab}=50°$ where the distribution is flat. The average value of the amount of O^{16} in the Ca^{40} target used was found 0.0192 ± 0.002 mg/cm^2. Thirdly, the amount of correction for contamination in the number of counts in the composite elastic peak at 12° and 17° were obtained by inverting the procedure of the second step.

data from ORNL was used (Bl 66a). The thickness of C^{12} was measured to be 0.00258 ± 0.0003 mg/cm^2. Similar corrections were made for 35, 30 and 25 MeV data.

3.5 Elastic Angular Distribution

The elastic peak counts were obtained by first drawing consistent peak tails extended to each side of the peak and then calculating the area under the boundaries. Since the average peak to valley ratio was 5000:1, the uncertainty due to the extraction process was very small. Peak counts were then corrected for dead time loss and normalized by monitor counts to obtain relative cross

sections prior to the relative normalization between two counters. Relative cross sections for each counter were plotted and carefully matched at the overlap angle at about 72 degree and the accuracies of matching were checked at 27° (see Section 3.1 and 3.2.4). An average value of 1.78 for relative counter normalization was obtained.

Although various measurements in this work would hypothetically enable us to obtain independent absolute cross sections, we have not done so because of the apparent large amount of integrated charge loss previously mentioned. Rather, our cross section normalization were obtained by normalizing our relative cross sections to the existing data reported in literature. For 40 MeV, data from Oak Ridge National Laboratory was used (Bl 66a). For 30 MeV, those from Harwell, England (Ri 64) was compared. It was found that the normalization factor computed from the comparisons at 40 MeV and 30 MeV agreed to better than 0.3%. There were no existing data to compare with for 25 MeV and 35 MeV. However, judging from the good agreement at 40 and 30 MeV, It was decided that the same normalization factor be used.

The angular distributions of the differential cross sections for elastic scattering in the center of mass system are shown in Fig. 3.1. Data are tabulated in Appendix II.

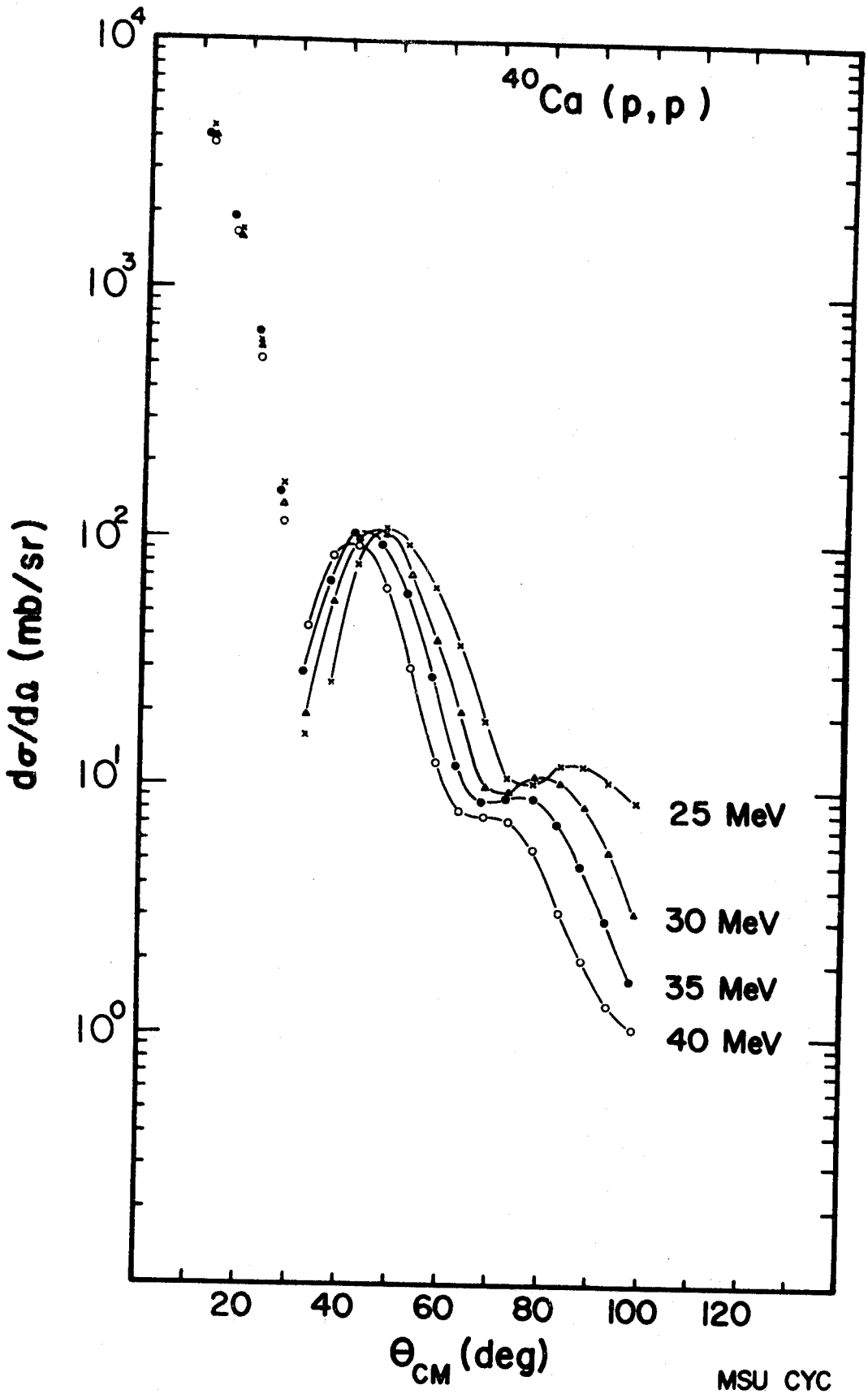

Figure 3.1.--Cross sections of elastic scattering of proton from Ca^{40} at 25,30,35 and 40 MeV. Curves between data points are drawn to guide the eyes and have no physical significance.

3.6 Inelastic Angular Distributions

Priot to the analysis of inelastic angular distributions, the spectra were subjected to careful inspection and study. Peaks which lie below 7 MeV excitation in the spectra were well separated and well resolved except for 5.24 and 6.92 triplets. These separated peaks were easily identified and were analyzed first. The region between 7 and 9 MeV was densely populated. A spectrum taken by Grace and Poletti with a magnetic spectrograph was used to help identify these closely spaced states.

The absolute laboratory energies were calculated for the inelastic states of ^{12}C and ^{16}O at the calibrated angles using program FASTKINE. The states involved were

C^{12} 0.000, 4.440 and 7.660 MeV (Le 68)

O^{16} 0.000, 6.052, 6.131, 6.916, 7.115 and 8.890 MeV (Le 68)

The kinematically determined energies of these states were tabulated and then transformed into channel numbers. Consequently the positions of these contaminant peaks were marked in each spectrum. The overall quality of all spectra were summarized in a chart which showed the conditions of each peak such as resolvability, intensity, freedom from contaminant, etc.

After this preliminary inspection the spectra were ready for cross section analysis. The areas, centroids

and statistical uncertainties of the peaks of interest were computed by the program PEAKSTRIP written by R. Paddock. The output of this program was in turn used as a part of input of another program, RELTOMON also by R. Paddock which calculated the absolute cross sections for both the laboratory and the center of mass system. The output of RELTOMON included printed listings, graphs of angular distributions in usual 4-cycle semi-log plot and punched card decks.

The results of the complete analysis will be discussed in detail in the following sections and chapters.

3.7 Errors

Aside from the statistical and normalization errors, the sources of other errors can originate from the uncertainties in background substraction, setting of peak boundaries and contaminant counts in the analysis.

Most of the spectra displayed a clean background below 7 MeV due to the excellent peak to valley ratio of the Ge(Li) detectors used. Above 7 MeV, the background is higher because of the greater density of states and the slow-dropping tail of the scattering from the degrader slit. The effect of uncertainty in background level assignment was studied by setting upper and lower limits for background levels to see the differences in peak counts. It was less than 1% for 3.731, 3.900, 4.487 MeV states and about 3 to 10% for others.

The effect due to errors in setting peak boundaries would be sizable for closely spaced peaks. Usually consistent boundaries were assigned before peak areas were extracted.

A large amount of error may result when a weak Ca^{40} peak was overlapped by a strong contaminant peak, for example, the 6.131 MeV state of O^{16}. If the net counts of the Ca^{40} peak were of the order of the statistical error of the contaminant peak, this datum point would be discarded.

Extraction of the peak areas for weak states at small angles, typically 12° and 17°, was most difficult. This situation was characterized by small peak counts, a large normalization factor, high background and the worst of all, peaks were not distinguishable from the flutuations in the background. In these cases, cross sections for weak states at those angles were not obtained.

To minimize these possible errors, data were treated as follows: For a given state, the preliminary angular distributions at all four energies were displayed on one 4-cycle semi-log graph. The shapes of distribution were carefully examined and compared. If some data points appeared to be off course, they were rechecked for accuracy. Very frequently every datum point in a spectrum was checked for its credit of confidence, i.e., taking all sources of error into account to determine the permissible range of correction. Only points with poor confidence levels were corrected if indications showed this to be desirable and the corrections

were required to lie within the limit of total possible error. Usually smooth distributions were normally obtained. But one must not push too far to make the final distribution satisfy his own taste. For in the case of weakly excited states whose data points were associated with large error bars, any alteration of the shape of distributions would be possible. An example is the angular distributions of the first excited state. The distribution of 25 MeV looks different from other three at 30, 35 and 40 MeV. These cross section points were then reanalyzed for many cycles and the distinction between the result of 25 MeV from others was confirmed.

Extreme care was taken in the analysis of small angle data because they play an important role in the determination of the spin transfer. Effort was also made to obtain the distributions for composite peaks as accurately as possible so that meaningful decomposition of these multiplets could be carried out (see Section 3.8 and Fig. 3.2).

3.8 The Decomposition of Multiplets

From the knowledge of the exact position of excited states which we have on the basis of Grace and Poletti's spectrum (Gr 66), we know that several pairs of doublets with about 20 KeV separation were seen as single peaks in our spectra. Individual distributions could not be extracted directly from spectra for these states. It was decided that the angular distribution for the composition peak be analyzed first. Then, decomposition was done whenever it was possible.

Fig. 3.2 illustrates the decomposition of the doublet at 8.558 MeV. The spins of the component states were tentatively determined by examining the overall shape of the combined distribution and by intelligent guessing. In this case they are 5^- and 2^+. The experimental angular distributions of 4.48 (5^-) and 3.90 (2^+) states were used for mixing, with a proportional ratio. The resultant distribution was compared with that of the experimental doublet. The best ratio could be obtained by finding the best fit to all distributions at four energies. As shown in Fig. 3.2, these fits were very good except at E_p=25 MeV.

Aside from the criteron of being a good fit for all four beam energies, the difference in differential cross section at various angles must also be in consistent with the change of peak shape and centroid from one spectrum to another. It was found that, by careful inspection, the change of peak shape for this multiplet agreed with the above analysis. This also provided a way to determine the association of the spin and the excitation energy of the component states. The differential cross sections so obtained were estimated to be accurate to 30%.

Similar analyses applied to the doublets at 7.539 and 8.097 MeV. The results were shown in Fig. 3.3 and 3.4. For the composite peak at 7.539 MeV, a fit was obtained by using the distributions of the 3^- (3.73 MeV) and 4^+ (6.50 MeV). One may argue that the differentiation in angular distributions between ℓ=3 and ℓ=4 states is not significant enough

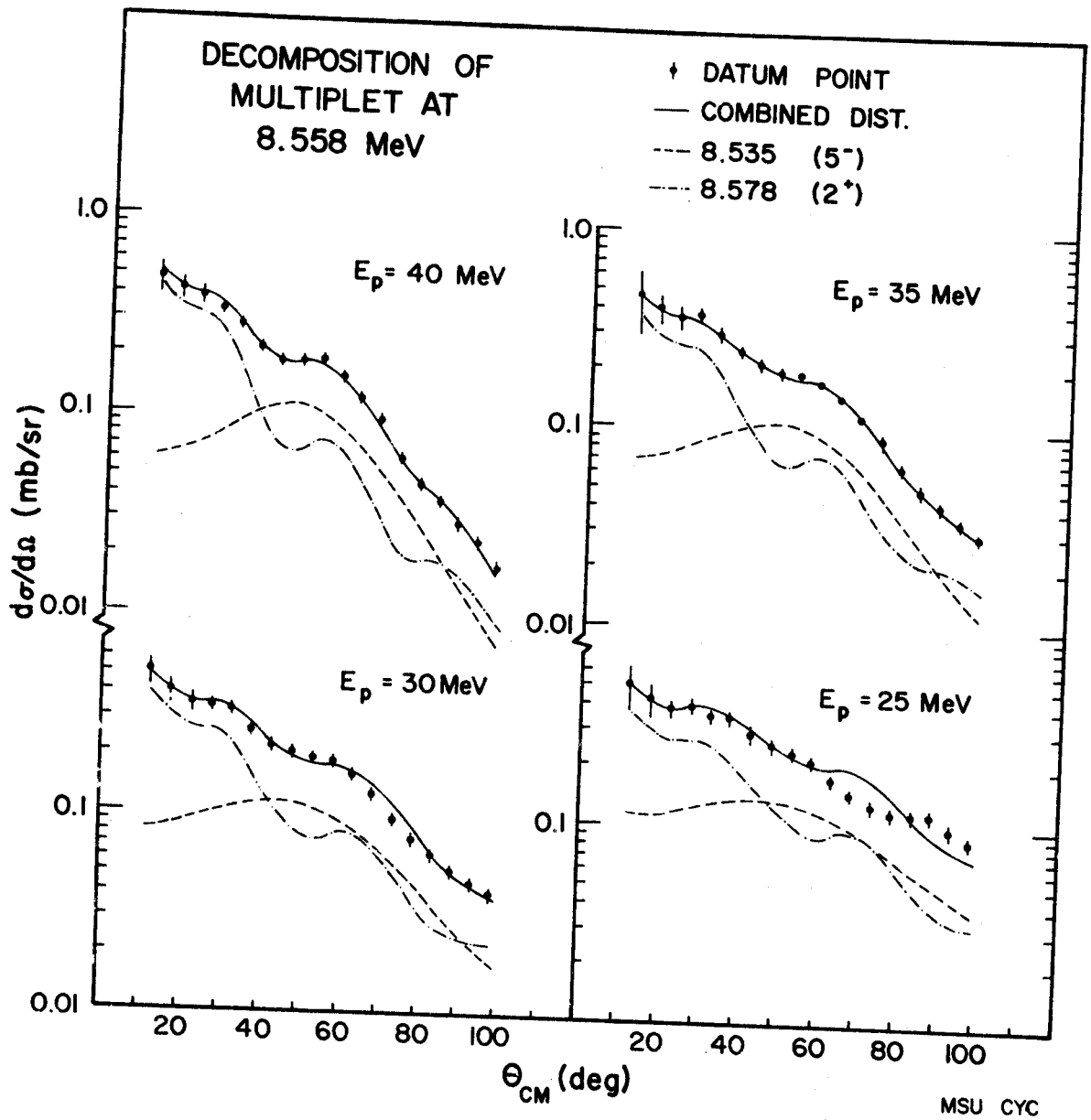

Figure 3.2.--The decomposition of doublet at E_x=8.558 MeV.

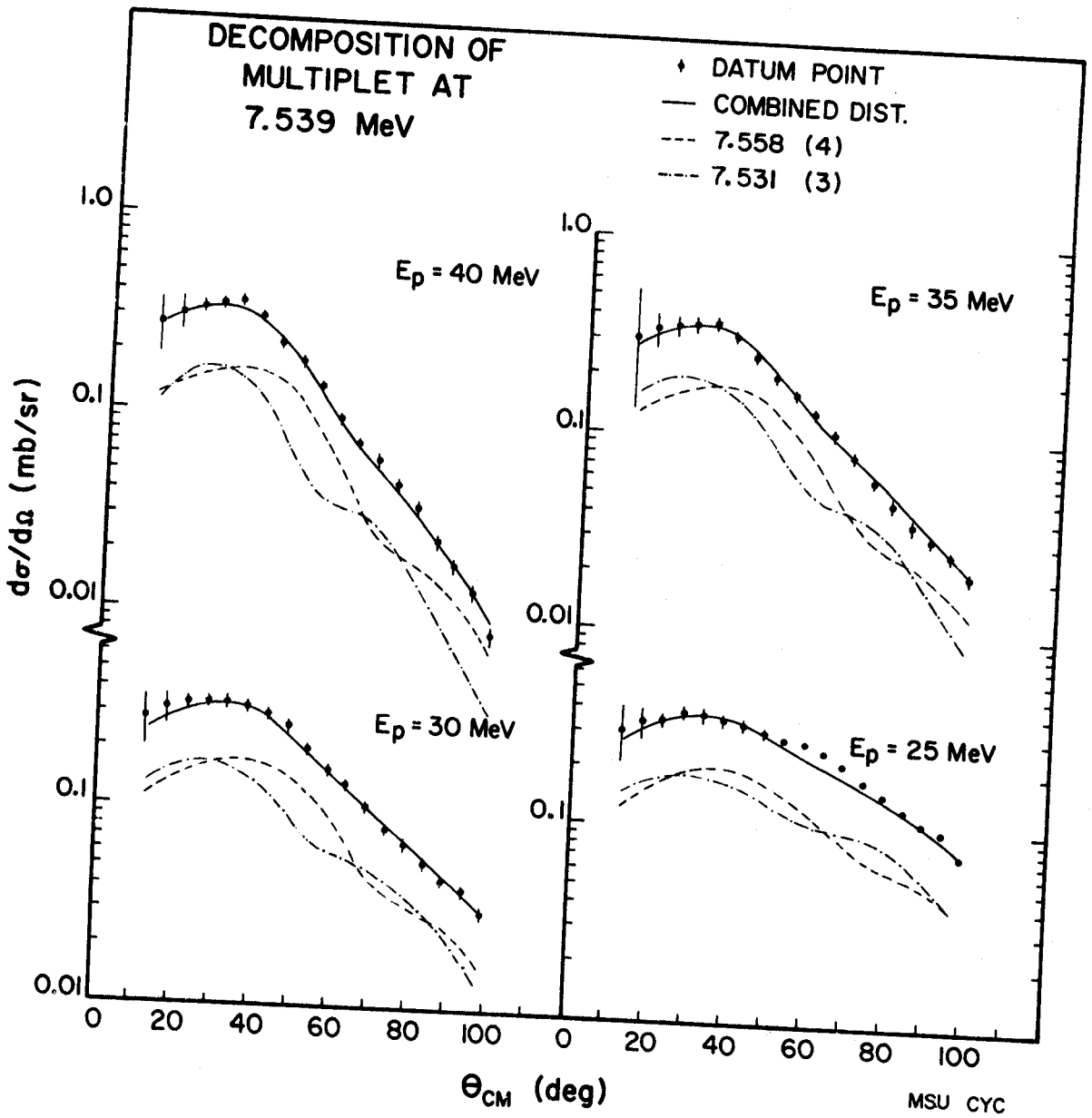

Figure 3.3.--The decomposition of doublet at E_x=7.539 MeV.

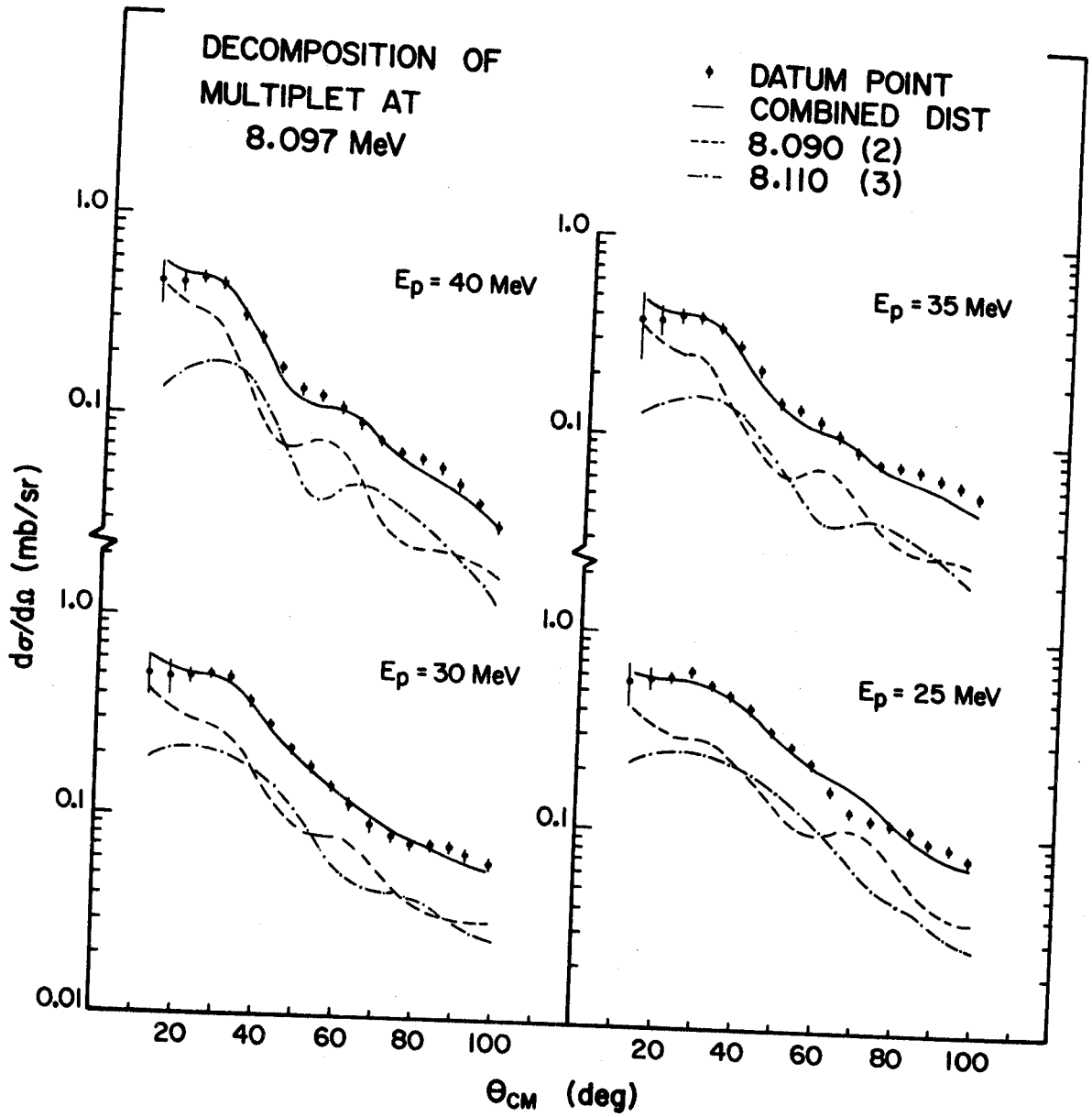

Figure 3.4.--The decomposition of doublet at E_x=8.097 MeV.

to allow a definite conclusion to be drawn. It was true that the uncertainties in the differential cross sections of the component states were quite high. However, judging from the smallness of the relative errors in cross sections, the angular position of the maximum, the lack of structure of the distribution, as well as the consistency between the proposed decomposition and peak features, it was thought that the result of this analysis would not be far from the truth.

The components of 8.097 MeV were assigned 2^+ and 3^-. It should be noted that the experimental distribution of 6.28 MeV state, instead of that of 3.73 MeV state, was used for 3^- to obtain the best overall fit.

3.9 The Analysis of 6.905 and 6.944 States

Grace and Poletti observed a triplet with excitation energies at 6.909, 6.930 and 6.948 MeV. The 6.930 level was seen to be the strongest among this triplet in their spectrum taken at 87.5° at E_p=13.065 MeV. In the present experiment the level energies were assigned (see Section 3.10) 6.905, 6.926 and 6.944 MeV. As shown in Fig. 3.5, the first and third of this triplet were quite well resolved at smaller angles while the middle one was not seen. At larger forward angles, they were partially resolved and the 6.926 level could be recognized. It can be inferred from this and Grace and Poletti's observations that the differential cross section of the 6.926 state is probably small and its spin may be at least higher than 2.

A program was written to analyze this multiplet. Only the first and third levels were analyzed. The program was to find the best fit to this part of the spectrum by superimposing two standard peaks 40 KeV apart. Various standard peak shapes observed in this experiment were stored in the program as options to be selected. The input includes the spectrum deck and a control card which indicates the approximate centroids of the component peaks, background levels and an option number. The program will search for the heights of the individual ideal peaks, add total counts per channel, compare with the experimental spectrum and calculate a χ^2. It will also move the ideal peaks one-fifth channel per step on both sides across the pre-set channel for their centroids, to search for the minimum χ^2. The output consists of the area and the centroid of each peak, comparison of total net area and most important of all, a printed graph of fitting. Searches can be repeated by putting in more control cards.

The result of this analysis is illustrated in Fig. 3.5. It was found that the fitting was very sensitive to the resolution of the standard peak used. In this result, best fits were obtained by choosing a standard peak with resolution of 33 Kev (FWHM).

At laboratory angles equal to 12° and 27°, the quality of fit and the cleanness in the valley suggested that the

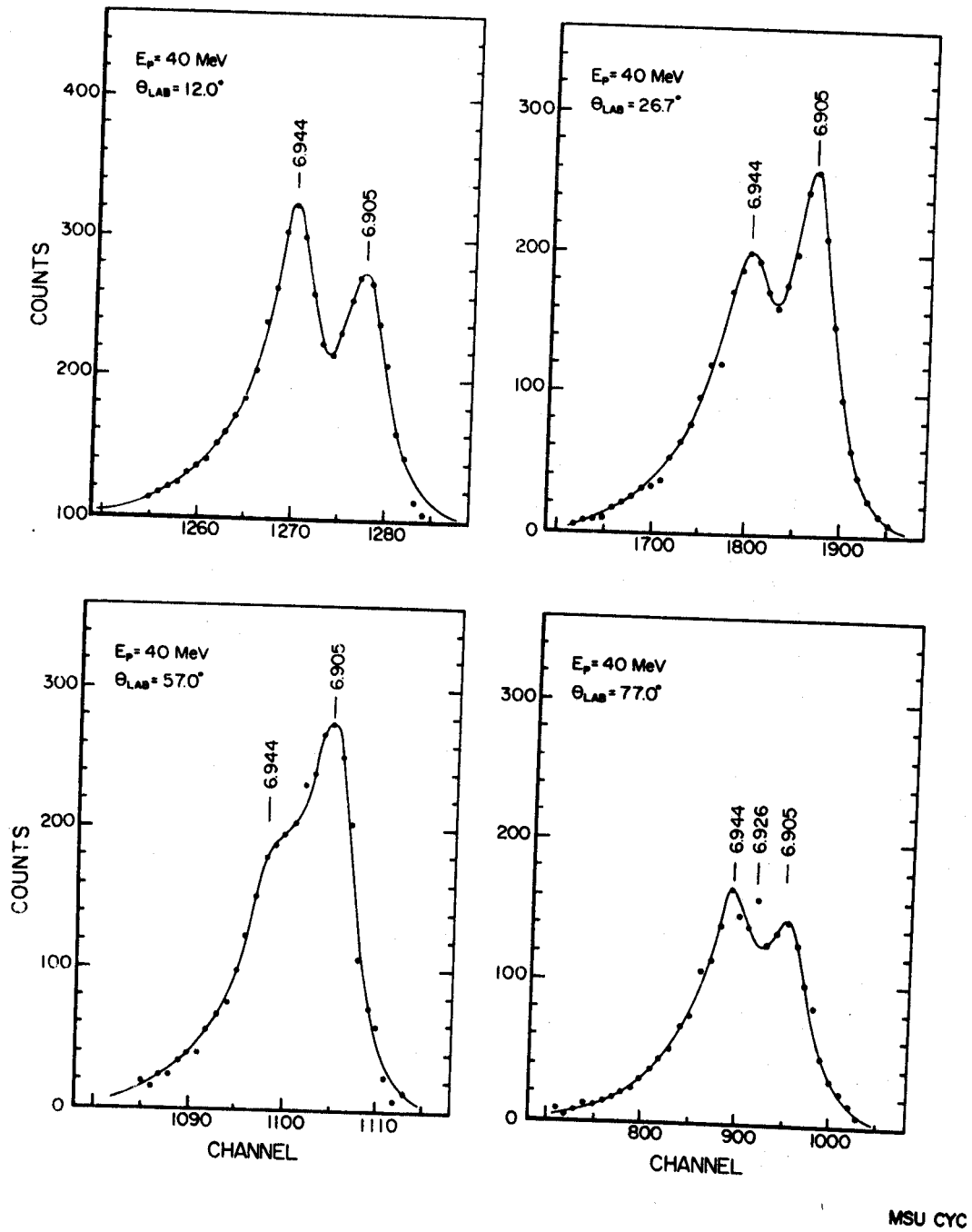

Figure 3.5.--Spectrum fits using two superimposed standard peaks for the analysis of 6.905, 6.926, 6.944 triplet.

differential cross section of the middle level at 40 MeV beam energy is less than 0.02 mb/sr in this angular range. Hence the differential cross sections for the 6.905 and 6.944 states are believed to be fairly accurate, and the spin assignments for these two states can be made more or less unambiguiously. At larger angles good fits were still achieved, although the middle level started to show up. The angular distributions and the spin assignments of the 6.905 and 6.944 states are discussed in Chapters IV and V.

3.10 Excitation Energies

The excitation energies of the observed levels of Ca^{40} have been measured in previous works (see Section 5.1). Below 9 MeV, every state seen in this experiment was also reported by Grace and Poletti. However, it was decided to carry out the energy calibration to check the linearity of the data taking system used in this work and to determine the excitation energies for those states lie above 9 MeV.

Program FOILTARCAL written by R. Paddock was employed. The input to the program consisted of beam energy, target thickness and orientation, detector angle, type of reaction, centroids of peaks in channel number and the calibration energies of

reference peaks. The program calculated the laboratory energies for the reference peaks using relativistic kinematics and then made corrections for the energy loss due to straggling through the target. These calculations so far were independent of any knowledge of centroids fed into the computer. Now using the calculated energies and the experimental centroids of the reference peaks as two independent variables, points of reference peaks were located. A least-squares fit of linear or quadratic order could be drawn through these points. Fixing the theoretical absolute energy, a calculated centroid corresponding to the calibration energy for a given reference peak was obtained. The experimental centroid of the same peak is converted to the observed energy after the calibration. The determination of energies for non-reference peaks is then straightforward.

The calibration energies for reference peaks were 3.731 MeV (3^-), 4.482 MeV (5^-) and 6.285 MeV (3^-) taken from ref. (Gr 66). The results of the calculation are listed in Table III-1. The energy shown for a given peak was obtained by averaging over the results from all but few spectra of each beam energy and again over all four energies. As can be seen in the table, the consistency of the experimentally determined Q-value for every state was within ±1 KeV. A comparison with the Aldermaston measurement showed that agreement at both ends of the spectrum (3.732 vs 3.731 and 8.847 vs

8.848) is very good indeed. Comparisons with other experiments are shown in Fig. 5.1 and discussed in Section 5.1.

No attempt was made to calibrate the energies for closely spaced multiplets. Absolute energies were assigned in consistant with all other levels and the separations were taken from the results given by Grace et al.

It was found that the calibrated energy for a given state was independent of beam energy, i.e., independent of the absolute energies of the inelastic scattered protons. This fact reflected that both Ge(Li) detectors used possessed good relative charge collection characteristics. It is concluded that the linearity of the electronic setup in this experiment was within 0.1% over about 9 MeV difference in proton energies.

TABLE III-1.--Energy Calibration and Determination for Ca^{40} (in MeV).

Peak No.	E_p=40 MeV		E_p=35 MeV		E_p=30 MeV		E_p=25 MeV		Over all Energies	
	E_x	Δ	E_x	Δ	E_x	Δ	E_x	Δ	E_x	Δ
1	3.73228	±0.00052	3.73224	±0.00038	3.73228	±0.00071	3.73236	±0.00141	3.73229	±0.00087
2	3.89979	±0.00109	3.89989	±0.00066	3.89892	±0.00108	3.89944	±0.00074	3.89949	±0.00097
3	4.48634	±0.00045	4.48687	±0.00065	4.48699	±0.00096	4.48727	±0.00176	4.48699	±0.00109
4*	5.26076	±0.00400	5.26187	±0.00423	5.26060	±0.00645	5.26080	±0.00501	5.26097	±0.00501
5	5.61436	±0.00340	5.61226	±0.00243	5.61347	±0.00212	5.61246	±0.00216	5.61312	±0.00273
6	5.89936	±0.00301	5.89936	±0.00197	5.89877	±0.00342	5.89911	±0.00334	5.89912	±0.00301
7	6.02163	±0.00358	6.02130	±0.00178	6.02075	±0.00307	6.02123	±0.00278	6.02134	±0.00293
8	6.26033	±0.00094	6.28087	±0.00037	6.28111	±0.00066	6.28155	±0.00161	6.28109	±0.00106
9	6.30306	±0.00327	6.30448	±0.00326	6.30115	±0.00330	6.30032	±0.00565	6.30220	±0.00435
10	6.57736	±0.00151	6.57748	±0.00190	6.57739	±0.00226	6.57672	±0.00207	6.57718	±0.00198
11	6.74806	±0.00429	6.74683	±0.00296	6.74756	±0.00345	6.74719	±0.00327	6.74738	±0.00357
12*	6.92152	±0.00372	6.92160	±0.00466	6.92222	±0.00453	6.92350	±0.00428	6.92215	±0.00438
13	7.11008	±0.00193	7.10885	±0.00167	7.10990	±0.00338	7.11044	±0.00224	7.10980	±0.00247
14*	7.45436	±0.00491	7.45495	±0.00375	7.45347	±0.00383	7.45260	±0.00373	7.45376	±0.00423
15*	7.53463	±0.00473	7.53496	±0.00259	7.53685	±0.00350	7.53337	±0.00391	7.53568	±0.00556
16*	7.66988	±0.00422	7.67053	±0.00287	7.67036	±0.00623	7.66924	±0.00568	7.66990	±0.00531
17	7.86677	±0.00254	7.86646	±0.00159	7.86330	±0.00514	7.86412	±0.00320	7.86512	±0.00371
18	7.92292	±0.00386	7.92326	±0.00775	7.92031	±0.00405	7.92036	±0.00704	7.92163	±0.00605
19*	8.09971	±0.00334	8.09792	±0.00362	8.09632	±0.00337	8.09502	±0.00383	8.09714	±0.00396
20	8.36396	±0.00374	8.36410	±0.00271	8.35999	±0.00442	8.35744	±0.00548	8.36121	±0.00509
21	8.41312	±0.00360	8.41513	±0.00383	8.41369	±0.00434	8.41315	±0.00601	8.41370	±0.00463
22*	8.55975	±0.00559	8.55866	±0.00474	8.55770	±0.00467	8.55820	±0.00412	8.55827	±0.00468
23	8.74453	±0.00508	8.74301	±0.00429	8.74401	±0.00458	8.74035	±0.00637	8.74302	±0.00536
24	8.84569	±0.00291	8.84501	±0.00278	8.84697	±0.00364	8.84979	±0.00446	8.84668	±0.00339
25			8.97438	±0.00486					8.97439	±0.00486
26			9.02538	±0.00489					9.02538	±0.00489
27*			9.14133	±0.00445					9.14133	±0.00445
28			9.23745	±0.00609					9.23745	±0.00609
30			9.35755	±0.00531					9.35755	±0.00531
31*			9.41061	±0.01141					9.41061	±0.01141
32			9.59009	±0.00790					9.59009	±0.00790
33*			9.63711	±0.00490					9.63711	±0.00490
34			9.85590	±0.00396					9.85590	±0.00396
35			10.04548	±0.00596					10.04548	±0.00596
36			10.27642	±0.00649					10.27642	±0.00649

* indicate doublet

CHAPTER IV

COLLECTIVE MODEL ANALYSIS

4.1 DWBA Theory

The distorted waves theory of direct nuclear reactions and the treatment of the inelastic scattering have been summarized by Satchler (Sa 64, Sa 67). The formulation is based on the transition amplitude

$$T_{DW}=\langle\chi_f^{(-)}|V|\chi_i^{(+)}\rangle \qquad (4\text{-}1)$$

where the $|\chi\rangle$'s are the "distorted" wave functions of the interacting system. This matrix element can be obtained from the formal scattering T-matrix theory using a perturbation method (Ma 64). Lectures on deriving the above equation have been presented in this laboratory by F. Petrovich and B. Preedom who also gave the detailed prescriptions for the calculation of this matrix element in terms of various types of reactions and specific nuclear models.

The transition amplitude for the reaction A(a,b)B can be written as

$$T_{DW}=J\sum_{m_f m_i}\int\int\chi^{(-)*}_{m_f m_f}(\vec{k}_b,\vec{r}_b)\langle b,B|V|aA\rangle\,\chi^{(+)}_{m_i m_i}(\vec{k}_a,\vec{r}_a)\,d\vec{r}_a\,d\vec{r}_b \qquad (4\text{-}2)$$

where $\vec{r}_a$ and $\vec{r}_b$ are the coordinates of the projectile relative to the target in the initial and final state, and J is the Jacobian of the transformation to these relative coordinates. The function $\chi(\vec{k},\vec{r})$ is the spatial part of the distorted wavefunction of the projectile. The matrix element $\langle bB|V|aA\rangle$ is referred to as a nuclear form factor and contains all the information on nuclear structure, spin and isospin selection rules, the type of reaction involved and so on. It should be noted that the operator V and state vector $|aA\rangle$ are written in an abstract basis. Their expansions over the space of a chosen representation are implied.

The distorted waves $\chi^{(\pm)}_{m'm}(\vec{k},\vec{r})$ are the elastic scattering wavefunctions which describe the relative motion of the pair. They are generated from a Schrödinger equation which contains the one-body optical potential. The subscript m'm denotes the spin projection m' of the distorted wave due to the action of the spin-orbit component of the optical potential on the original impinging wave with spin projection m.

If an unpolarized beam and target are used, the differential cross section is obtained by introducing kinematical factors and appropriately summing and averaging over the spin projections of projectile and target nuclei.

$$\frac{d\sigma}{d\Omega} = \left(\frac{\mu_a \mu_b}{2\pi\hbar^2}\right)^2 \frac{k_b}{k_a} \frac{1}{(2s_a+1)(2J_A+1)} \sum_{\substack{M_A M_B \\ m_a m_b}} |T_{DW}|^2 \qquad (4\text{-}3)$$

where μ is the reduced mass of the projectile.

The matrix element $\langle bB|V|aA\rangle$ is rewritten in angular momentum representations

$$\langle bB|V|aA\rangle \rightarrow \langle J_B M_B, s_b m_b|V|J_A M_A, s_a m_a\rangle$$

where s_a and s_b are spins of projectiles, and J_A and J_B are those of the initial and final states of the nucleus.

The rest of the development of the DWBA theory for direct inelastic scattering consists of arriving at analytical expressions for the transition amplitude. This involves two stages of multipole expansions, namely

1) The multipole expansion for the above matrix element into the transferred angular momenta (ℓ,s,j) representations. In analogy to Wigner-Eckart theorem, the transition amplitude is expanded in terms of "reduced" amplitude $\beta^{\ell m m_a m_b}_{sj}$.
2) The partial wave expansion for the distorted waves χ to obtain explicit expressions for the reduced amplitude.

These expansion treatments put the DW theory on a formal and elegant mathematical foundation. Detailed discussions have been given in previous references (Sa 64).

4.1.1 $Ca^{40}(p,p')$ in Collective Model

For the $Ca^{40}(p,p')$ reaction, simplified expressions for the form factor can be obtained via several approximations. The interaction considered here is assumed to be

1) local, therefore the "zero-range" condition is satisfied automatically.

2) static (no time dependence) and central, each term of the multipole expansion of

$$\bar{V}(\vec{r},aA)=\sum_{\ell sj,\mu}(-1)^{j-\mu}\bar{V}_{\ell sj,\mu}(A,r)T_{\ell sj,-\mu}(\Omega,a) \qquad (4\text{-}4)$$

being a scalar product, where A, a denote the internal coordinates of target nucleus A and projectile a respectively.

The spin of the ground state of Ca^{40}, J_A, is zero, so $j=J_B$. The spin 1/2 of the proton allows the transfer spin s to be 0 or 1, thus

$$\vec{J}_B=\vec{L}, \qquad \text{or } \vec{J}_B=\vec{L}+\vec{I}.$$

One also finds that in a given transition, possible values of ℓ, s, j are limited. To take $j^{\pi}=3^-$, for example, there are only two multipole components, (303) and (313). For the special case s=0, the form factor $G_{\ell sj}$ becomes

$$G_{\ell}(r)=\sqrt{2s_a+1}\ \langle L||\bar{V}_{\ell}(r)||0\rangle \qquad (4\text{-}5)$$

which is used in the following collective model studies. The microscopic model descriptions for the scattering from the odd parity states follow different approaches as presented in Chapter VI.

4.1.2 Vibrational Collective Model

It is well known that the nuclear collective model has been very successful in explaining the strong transition observed in inelastic scattering. This model assumes a non-spherical potential well $\bar{V}$ which induces inelastic scattering to low-lying collective vibrational or rotational states. The nuclear deformations modify the average field on a macroscopic scale as felt by the projectile due to the short range nature of the nuclear force. The deviations of the average nuclear field from spherical symmetry are described by the theory of Bohr and Mottelson. A treatment of this potential in the framework of DW theory has been formulated by Bassel et al. (Ba 62).

The spherical potential is just the optical potenial, hence the deviations from spherical symmetry can be obtained by expanding the potential in a Taylor series about $R=R_o$

$$U=U(r-R_o)-\delta R\frac{d}{dr}U(r-R_o) + \ldots$$

Retaining terms to 1st order in δR, one finds that

$$\bar{V}= -\delta R\frac{d}{dr}U(r-R_o).$$

In the vibrational model, the nuclear surface deformations are defined by

$$\delta R(\theta,\phi) = R_o \sum_{L,M} \alpha^{*}_{LM} Y^{M}_{L}(\theta,\phi)$$

The distortion parameters α_{LM} are assumed dynamical and capable of creating or annihilating phonons of angular momentum L with z-component M. The nuclear potential $\bar{V}$ is now

$$\bar{V}=R_o\left[\frac{d}{dr}\,U(r-R_o)\right]\sum_{L,M}\alpha_{LM}Y_L^M(\theta,\phi)$$

The multipole component $\bar{V}_{LM}$ is then

$$\bar{V}_{LM}=i^{\ell}R_o\left[\frac{d}{dr}\,U(r-R_o)\right]\alpha^*_{LM}.$$

The dynamical deformation parameters α^*_{LM} can be expressed in terms of usual boson creation and annihilation operators b^*_{LM} and b_{LM} for 2^L-pole oscillation

$$\alpha^*_{LM}=\left(\frac{\hbar\omega_L}{2C_L}\right)^{1/2}\left[b^*_{LM}+(-1)^M\,b_{LM}\right]$$

where $\hbar\omega_L$ is the energy of each phonon and C_L is the restoring-force parameters. For an even-even target, $J_A=0$ and no initial phonon exists, then

$$\langle L||\alpha^*_L||0\rangle=\left(\frac{\hbar\omega_L}{2C_L}\right)^{1/2}.$$

If no spin-orbit potential is included in the optical potential $U(r-R_o)$, then

$$\langle J_B=L|\bar{V}_{LM}|J_A=0\rangle=-i^L R_o\left[\frac{d}{dr}\,U(r-R_o)\right]\beta_{\ell}^{vib} \qquad (4\text{-}6)$$

where

$$\beta_L^{vib}=\left[(2L+1)\frac{\hbar\omega_L}{2C_L}\right]^{1/2}.$$

It can be seen that the form factor $<|V|>$ has the same radial shape as $\frac{d}{dr} U(r-R_o)$. This means that in this simplified model, the detailed nature of the nuclear structure is ignored and the total effective interactions are limited into a few standard types of form factors with the interaction strength to be extracted by comparison with the observed inelastic cross section.

4.1.3 Vibrational Model Parameters and Reduced Transition Probability

The Hamiltonian of a vibrator having dynamical parameter α_{LM} is

$$H_L=\sum_M (-1)^M (B_L \alpha_{LM}\alpha_{L,-M}+C_L \alpha_{LM}\alpha_{L,-M}).$$

where B_L is the "mass transport parameters" and C_L previously defined as the "restoring force parameter". In terms of the "observables" excitation energy E_L and the "model dependent" deformation $\delta_L=\beta_L R_o$, B_L and C_L can be found by

$$(B_L/\hbar^2)=1/2(2L+1)(R_o^2/\delta_L^2)(1/E_L).$$

$$C_L=1/2(2L+1)(R_o^2/\delta_L^2)E_L. \qquad (4\text{-}7)$$

The reduced transition probability for electric excitation of a 2^L-pole vibration in an even-even nucleus is given (Ow 64) by

$$B(pp';0\to L)=\left\{\frac{Ze(2L+1)}{4\pi R_o^{L-2}}\langle r^{2L-2}\rangle\right\}^2\frac{\delta_L^2}{R_o^2}. \qquad (4\text{-}8)$$

The results of calculated B(pp') are often compared with the single-particle estimate in Weisskopf unit, i.e.,

$$C_{sp}=B(pp';0\to L)/B_{sp}(EL;0\to L)$$

where

$$B_{sp}(pp';0\to L)=[(2L+1)/4\pi]e^2\langle r^L\rangle^2,$$

and $\langle r^L\rangle^2$ is calculated using a uniform change distribution. The value of G_{sp} measures in some sense the "collective strength" of the state. It is also of general interest to compare the B(pp')'s with two sum rules. The first is the non-energy-weighted sum rule (La 60).

$$NEWSR=\sum_n B_n(pp';0\to L)=(e^2Z/4\pi)\langle r^{2L}\rangle,$$

where the sum is over all states with same spin L. The second sum rule is the energy-weighted sum rule (Na 65).

$$EWSR=\sum_n(E_n-E_o)B(pp';L\to 0)$$

$$=\frac{Z^2e^2L\hbar^2}{8\pi AM}(2L+1)^2\langle r^{2L+2}\rangle.$$

where AM is the mass of the nucleus.

The results of calculations for these vibrational parameters, B(pp')'s and quantities of comparisons are presented in Section 4.5.2.

4.2 Optical Model Analysis

In order to obtain parameters for the calculation for the distorted wave χ, the angular distributions of elastic scattering were analyzed. The optical potential used in this work was as follows:

$$U(r)=U_c(r)-V_0 f(x)+\left(\frac{h}{M_\pi c}\right)^2 V_{SO}(\vec{\sigma}\cdot\vec{\ell})\frac{1}{r}\frac{d}{dr}f(X_{SO})$$

$$-i\left(W_0-4W_D\frac{d}{dX'}\right)f(x')$$

where $U_c(r)$ is the Coulomb potential due to a uniformly charged sphere of radius $R_c=1.25\ A^{1/3}$ and

$$U_c=\frac{Ze^2}{r}, \qquad r\geq R_c$$

$$=\frac{Ze^2}{2R_c}\left(3-\frac{r^2}{R_c^2}\right), \qquad r\leq R_c.$$

The factor $f(x)$ is of the usual Wood-Saxon shape

$$f(x)=(1+e^x)^{-1} \quad \text{where } x=\frac{r-R_0A^{1/3}}{a}.$$

The parameters which enter the DWBA calculations were determined by fitting the calculated cross sections from this potential to the observed elastic data. The search code GIBELUMP* was used to vary the parameters. The criterion for a fit was to minimize the quantity,

---

*Unpublished FORTRAN-IV computer code written by F. G. Perey and modified by R. M. Haybron at Oak Ridge National Laboratory.

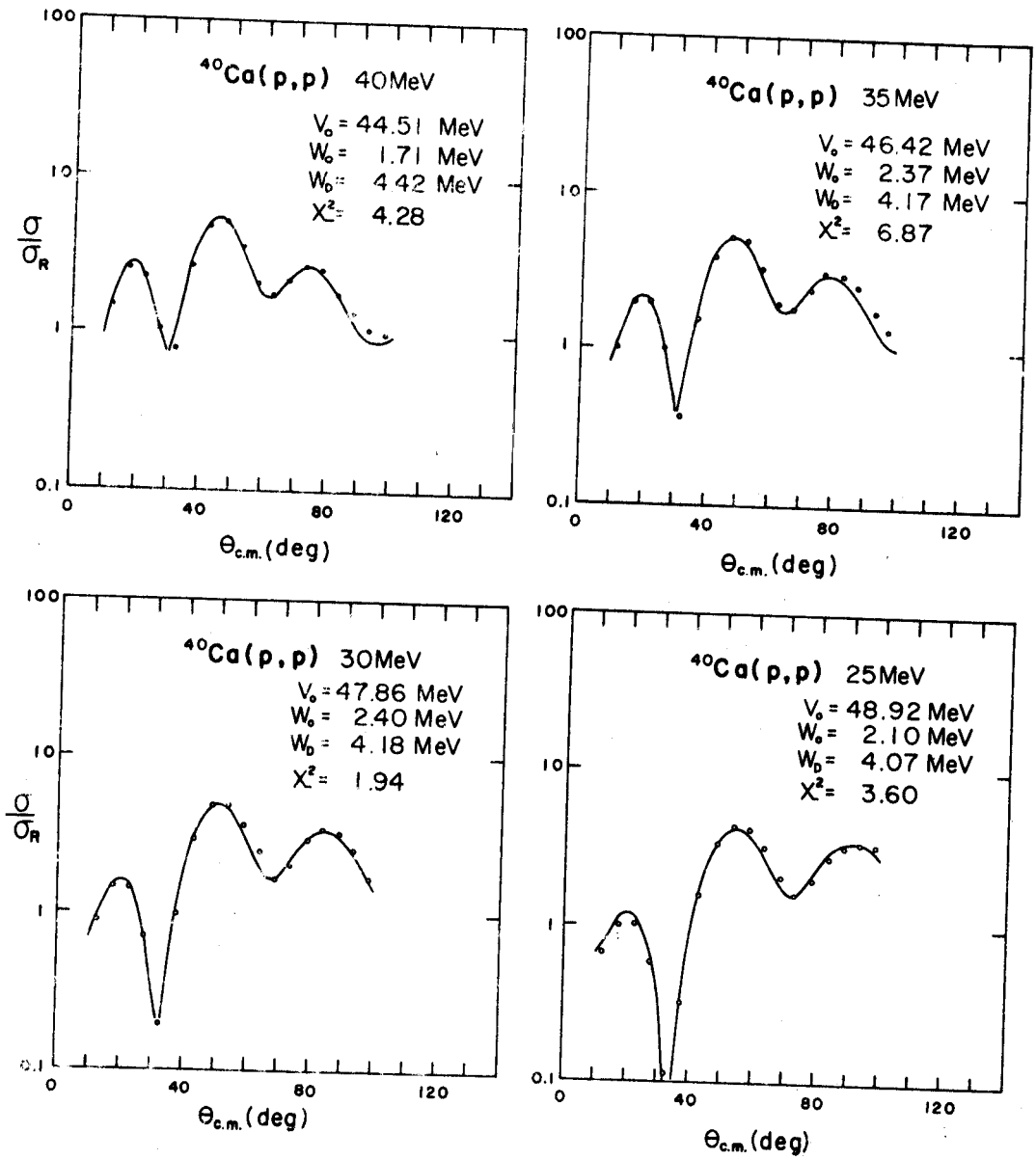

Figure 4.1.--Optical model fits to the experimental elastic scattering results at E_p=25 to 40 MeV.

$$\chi^2 = \frac{1}{N} \sum_{i=1}^{N} \left[\frac{\sigma_{ex}(\theta_i) - \sigma_{th}(\theta_i)}{\Delta\sigma_{ex}(\theta_i)} \right]^2$$

where N is the number of data points, $\sigma_{ex}(\theta_i)$ is the observed differential cross section at the center-of-mass angle θ_i and $\sigma_{th}(\theta_i)$ is the theoretical value at θ_i. The relative uncertainty $\Delta\sigma_{ex}(\theta_i)$ was taken to be 3% of $\sigma_{ex}(\theta_i)$ for all data points.

The geometrical parameters (r_0 and a) for various components of the optical potential and the average spin-orbit strength (V_{SO}) were taken from the analysis of elastic scattering and polarization measurements for 40 MeV protons on eleven nuclei from ^{12}C to ^{208}Pb. (Fr 67). The remaining parameters searched were V_0, W_0 and W_D. The results are listed in Table IV-1. These parameters were used for the DW calculations presented in this study.

The elastic data, in ratio to Rutherford scattering, and the final optical model calculation are shown in Fig. 4-1.

4.3 DWBA Calculations

The DW calculations were made using a FORTRAN-IV version of the Oak Ridge computer code JULIE (OR 62, 67). The program has been adapted onto the XDS, Σ-7 computer*

*Unpublished Sigma-7 program description on JULIE, Cyclotron Laboratory, Michigan State University.

TABLE IV-1.--Optical Parameters.

r_R = 1.16 F,	a_R = 0.75 F
r_I = 1.37 F,	a_I = 0.63 F
r_{SO} = 1.064 F	a_{SO} = 0.738 F
V_{SO} = 6.04 MeV	

E_p (MeV)	V_0 (MeV)	W_0 (MeV)	W_D (MeV)	χ^2
25	48.92	2.10	4.07	3.60
30	47.86	2.40	4.18	1.90
35	46.42	2.37	4.17	6.87
40	44.51	1.71	4.42	4.28

and stored in the computer's file under the timesharing Janus system. Typical running time was about 1 to 2 minutes per case depending on the scope of calculation involved.

The input consists of three major parts corresponding to the elements in the integral of the transition amplitude (Eq. 4.2) namely, the form factor, the entrance channel (incoming DW) and the exit channel (outgoing DW). The form factors used for collective model were complex. The real part was calculated by JULIE whereas the imaginary part was external numerical input. Options 2 and 3 as in SALLY (pp. 64, OR 62) were used for ℓ=2 and ℓ=3 respectively. For ℓ larger than 3, the value of b_ℓ (pp. 42, OR 62) was set to zero, i.e., no Coulomb potential was included. Since

the spin-orbit potential for form factor calculations was not provided by JULIE, only $G_{\ell o \ell}$ was computed. In other words, spin flip was not taken into account. The imaginary potential was just the first derivative of the imaginary part of the optical potential with respect to r. The input deck for JULIE was provided by the program DEFABSORB written by B. Preedom and K. Thompson.

The input for the entrance channel was essentially the set of optical model parameters listed in Table IV-1 plus controls over the option of potential used and the maximum angular momentum of the partial waves included. The optical parameters for the exit channel used depend on whether the Q-value effect was considered or not. Fig. 4.2 is shown to summarize the general results of the calculations for ℓ=2 to ℓ=8 and for energy dependence as well as the Q-value effect. For ℓ=8, spin-orbit term in optical potential can not be included unless j=ℓ (Table 1, OR 66). In order to see the effect of the spin-orbit potential on the distribution, calculations were made with and without this term in both entrance and exit channels for the case of ℓ=6. It was found that the effect is small except for 25 MeV as illustrated.

The normalization between the output of JULIE and the experimental distribution, for (p,p') and complex collective model using options F6=2 or 3, is

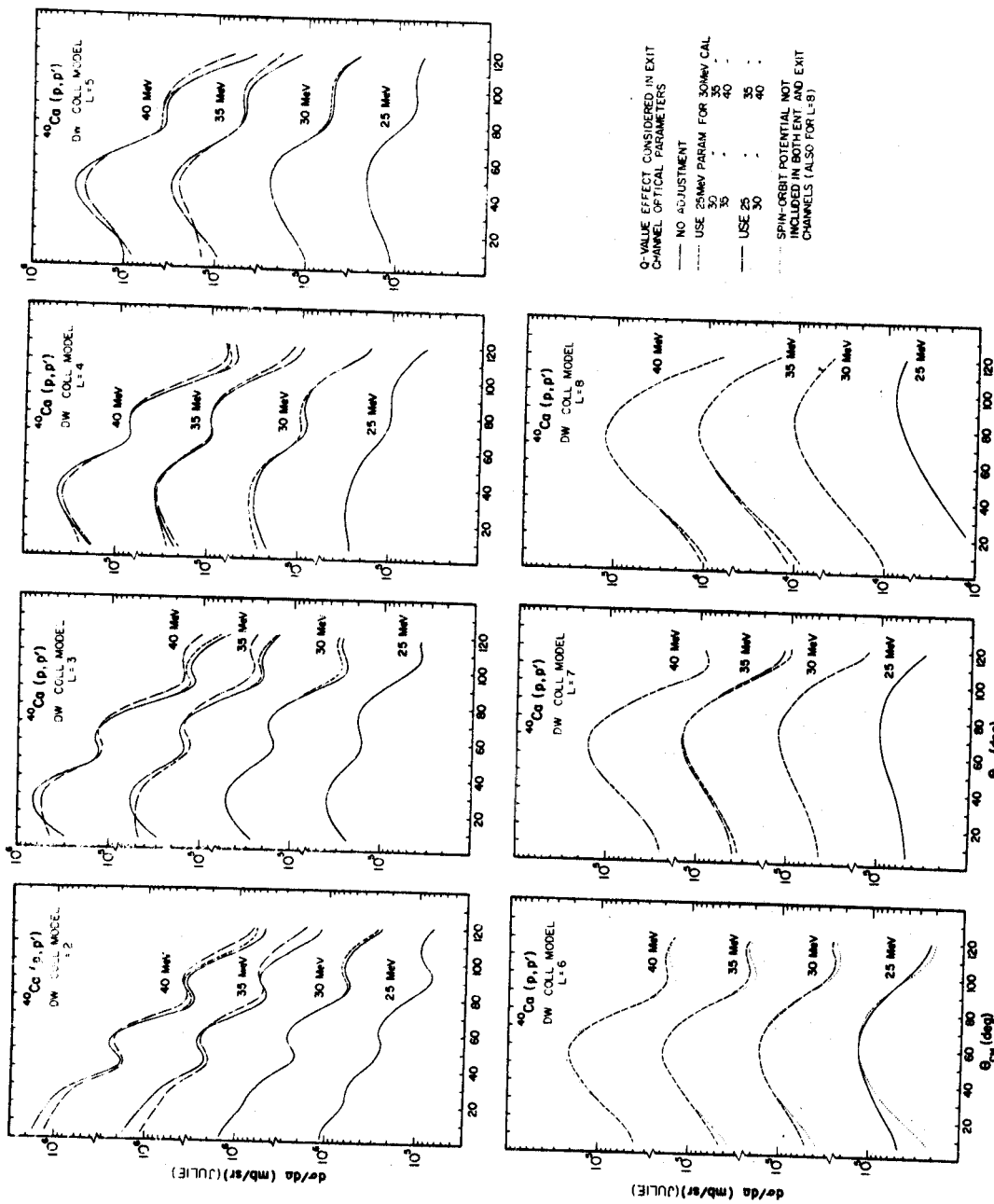

Figure 4.2.--Summary of the DWBA calculations using collective model F.F. for ℓ=2 to ℓ=8 at E_p=25 to 40 MeV.

$$\sigma(\text{exp}) = \frac{1}{5014} \cdot \frac{1}{2L+1} \frac{2J_B+1}{2J_A+1} \beta_L^2 \sigma_L \text{ (JULIE)}$$

where L is the tranferred orbital angular momentum. For an even-even target J_B=L and J_A=0, the above equation becomes

$$\sigma(\text{exp}) = \frac{\beta_L^2}{5014} \sigma_L \text{ (JULIE)}$$

The differential cross section scales in Fig. 4.2 were taken directly from the JULIE calculation so that consistency was maintained throughout.

To extract the deformation parameters β_L, program SIGTOTE (Th 69) was used. This program compares the total cross sections σ(exp) and σ_L(JULIE) within the angular range of this experiment according to the equation

$$\sigma(\text{exp})\Big|_{\theta_i}^{\theta_f} = 2\pi \int_{\theta_i}^{\theta_f} \frac{d\sigma}{d\theta}(\text{exp}) \sin\theta \, d\theta$$

and then calculates the β_L. The code also commands a computer routine to plot the collective model fit on 4-cycle semi-log graph. The deformation δ_L is defined as $\beta_L R_0$ where R_0 is the real radius of the target nucleus $r_R A^{1/3}$. For ^{40}Ca, R_0 = 3.96 fm was used throughout.

4.4 Representative Results of Collective Model Fit

Fig. 4.3 shows the results of the representative 2^+(3.900 MeV), 3^-(3.732 and 6.281 MeV), 4^+(6.502 MeV) and

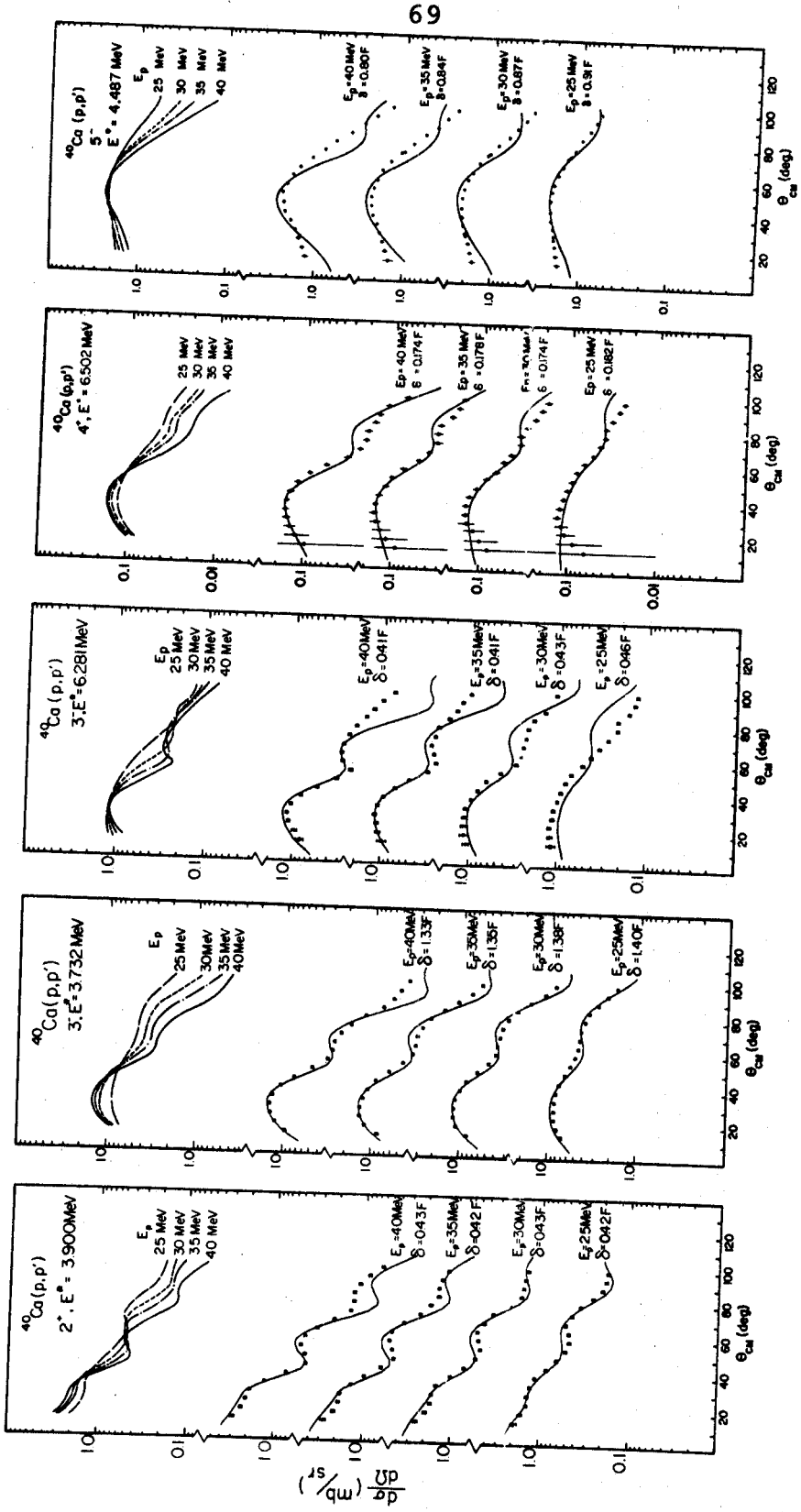

Figure 4.3.--Typical results of experimental distributions and collective model fits (solid curves). The upper parts show the variation of shape of the experimental distribution with respect to beam energy.

5^-(4.487 MeV) states. Except for the 6.502 level all other four are strongly excited. At the top of each column of Fig. 4.3, the energy dependence of the shape of the angular distributions are illustrated. It is seen that the structure of the distribution becomes more pronounced as the beam energy increases. At E_p=30 to 40 MeV the shapes of angular distributions with different L-transfer are quite distinctive one from the other. The lower part of the column indicates the comparisons between data and collective model calculations. The results of individual states are discussed in the following paragraphs.

2^+(3.900 MeV): The angular distributions of this state have a unique shape. The differential cross sections peak at small angle and dropping off somewhat slower up to about 30° than they do past 30°. A flat region occurs at around 50 degree at E_p=40 MeV and moving out steadily to around 70 degree at 25 MeV. Following that are a fast descent and another flat region again. This feature distinguishes the 2^+ from 3^- and 1^- and provides a positive method for identifying the spin of this state. The collective model predictions are very good specially at 25 and 30 MeV. At 35 and 40 MeV good agreements are still achieved except at large angles. The success of the model in this case is that not only the shape of the empirical distributions at four energies are reproduced, but also the relative magnitude as well, as revealed by the constant of δ_2's.

3^-(3.732 MeV): Similar to the case of 2^+, the shape of the angular distribution changes smoothly as the beam energy varies. A maximum occurs at about 25 degree, but its magnitude decreases almost 40% as E_p drops from 40 to 25 MeV. The quality of the collective model fit for this state is comparable to that for 2^+ state. The deformation δ_3 (1.35 fm) varies only about 5% among the four proton energies. Again the energy dependence patterns of the calculation coincide with those of the experimental observations.

3^-(6.281 MeV): As can be seen from Fig. 4.3, the shapes of the angular distributions of this state appear somewhat different from those of the 3.732 MeV state. The maximum is also at about 25 degree but here the magnitudes are approximately constant. At E_p=40 MeV there is a second maximum located at about 62 degree which is washed out as the beam energy drops to 25 MeV. Consequently the energy dependence looks dissimilar to the 3.732 MeV state. Sizable discrepancies between the calculations and the data at large forward angles can be seen. However, the relative ratios of the total cross sections under the angular range of the experiment do not differ appreciably between the results of theory and experiment as indicated by the small variations of δ (only 13%).

4^+(6.502 MeV): The angular distributions are similar to those of 3.732 MeV state except that the maximum is shifted to about 35 degree. At 25 MeV, the distribution of this state is not clearly distinguishable from that of either 3^- or 5^-. The spin identification has to be made by using every piece of evidence available, namely the consistency in the angular positions of maxima, the collective model fits and the comparisons with the results of 3^- and 5^- at every beam energy. Again the deformations obtained flutuate only a few percent.

5^-(4.487 MeV): The dominant characteristic of the experimental distributions of this state is the lack of structure as a function of angle. The collective model calculations underestimate the cross sections at both small and some large angles but overshoot around the maximum at about 45°. The predicted increment of the magnitude of the maximum is more than 70% from E_p=25 MeV to 40 MeV, whereas the data show less than 10%. On the other hand, the deformation decreases only 10% as for the case of second 3^-(6.281 MeV).

4.5 General Results of Collective Model Analysis

In this section the general results of the experimental and the collective model analysis are summarized in terms of the L transfer assignment, nuclear deformation and reduced transition probabilities. Comparisons with other experiments will be presented in Chapter V.

4.5.1 L Transfer Assignments and Nuclear Deformations

The representative angular distributions discussed in the last section were used heavily as standards to assist in the determinations of the L-transfers to other states. It was found that most of the angular distributions with the same L at the same energy resemble each other in shape. Distributions revealing possible differences in microscopic structure and reaction mechanism were also noted. Since there are four distributions for each state to be compared with the standards, the ambiguities in determining the L-transfer for a given state were minimized.

The L assignments to the components of a doublet were obtained from the decomposition method (see Section 3.8). The high spin states having L=6 or L=7 were identified by finding the best fit to the experimental distributions with those from calculation using L=5, 6, 7 and 8.

Distorted wave collective model calculations were done for every state with appropriate adjustments for the Q-value effects in exit channels. Nuclear deformations were then extracted using program SIGTOTE (Section 4.3). The L-value assigened and the deformation parameters along with other physical quantities are listed in Table IV-2 to IV-5. The experimental data, the collective model fits, and the standard distributions are shown in Fig. 4.4 to Fig. 4.8, where the solid curves are collective model calculations and the dashed curves show the shapes of the standard distributions.

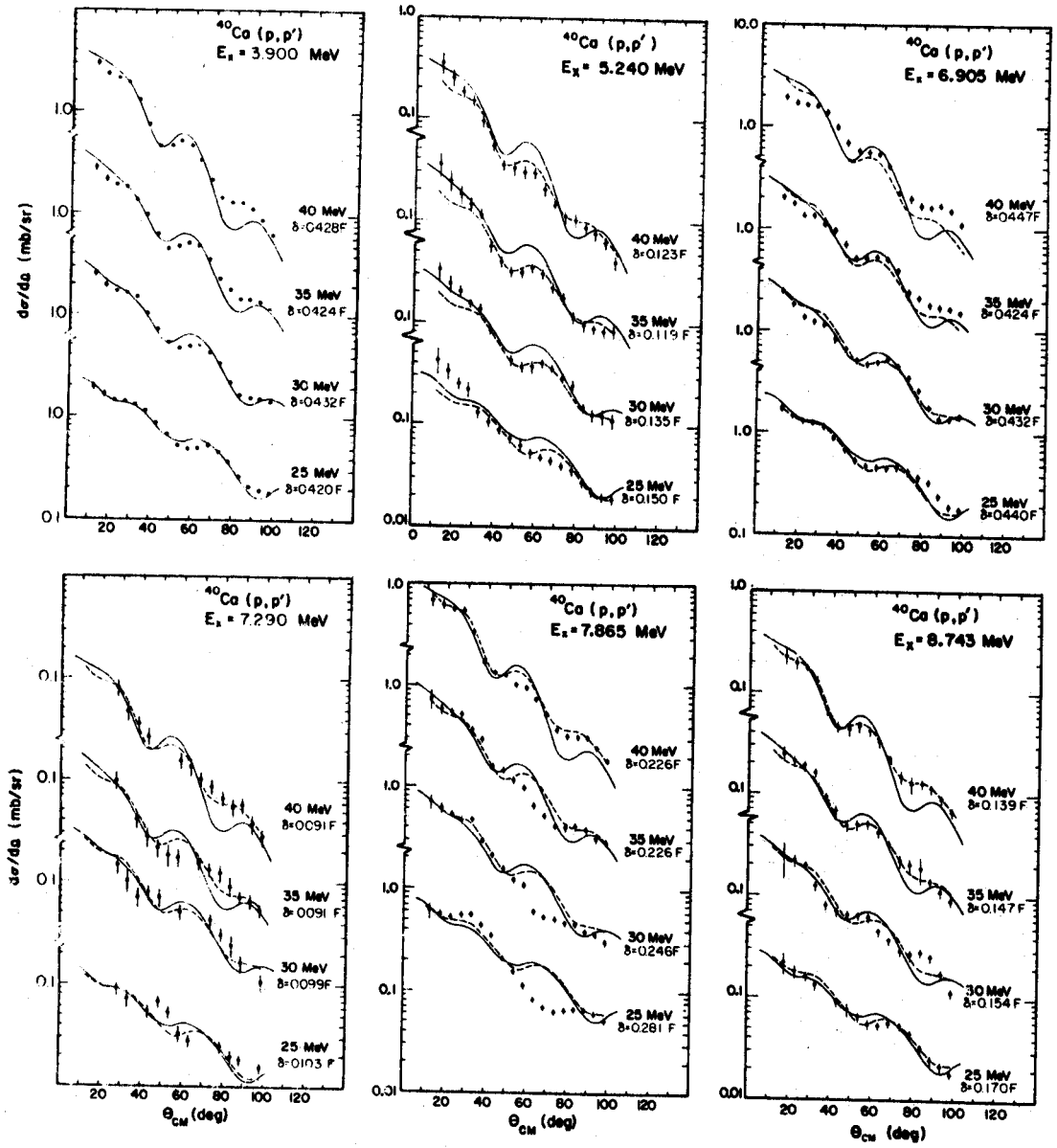

Figure 4.4.--Experimental distributions of ℓ=2 states and collective model fits (solid curves). The dash curves are those of 3.900 MeV state.

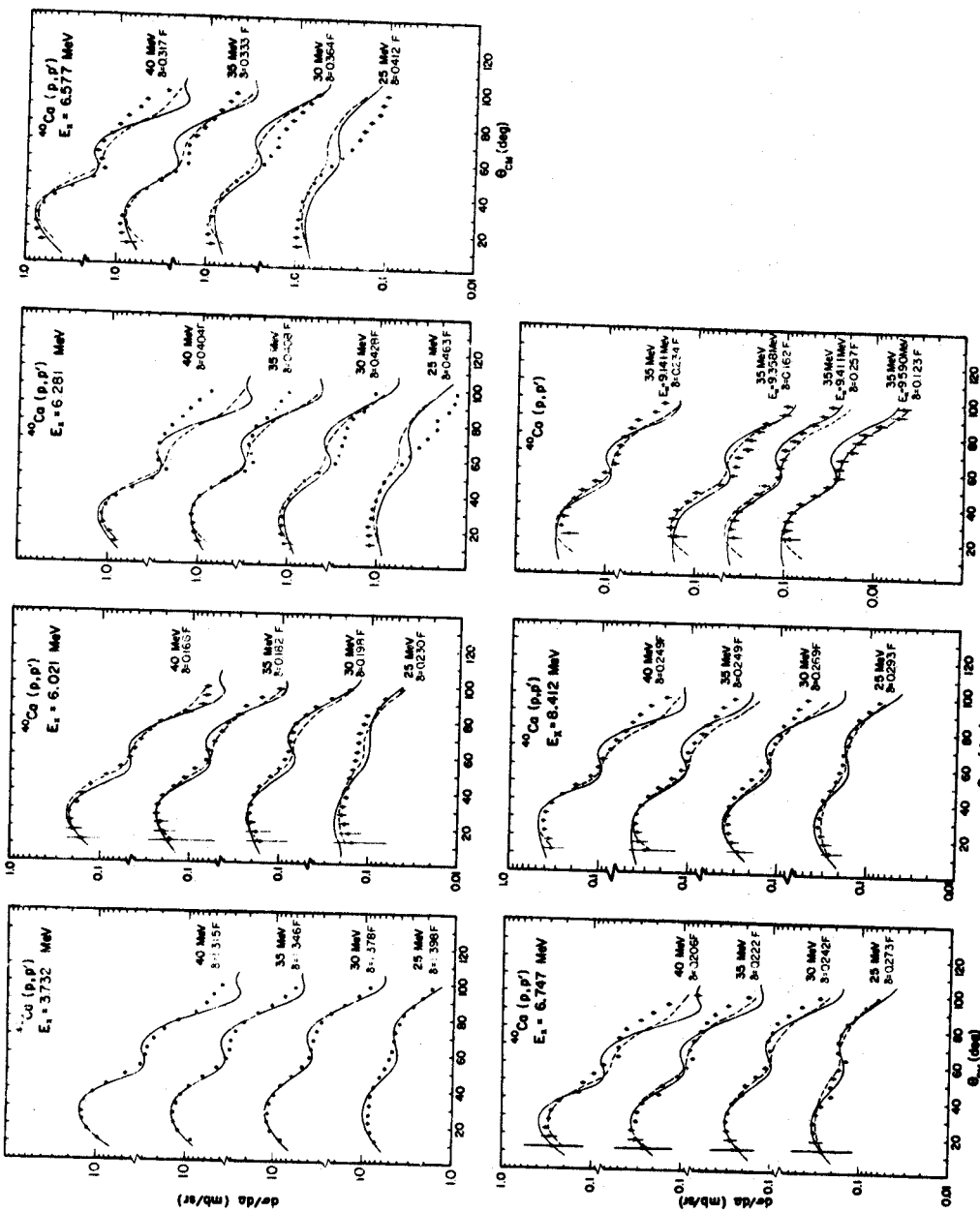

Figure 4.5.--Experimental distribution of ℓ=3 states and collective model fits (solid curves). The dash curves are those of 3.732 MeV state.

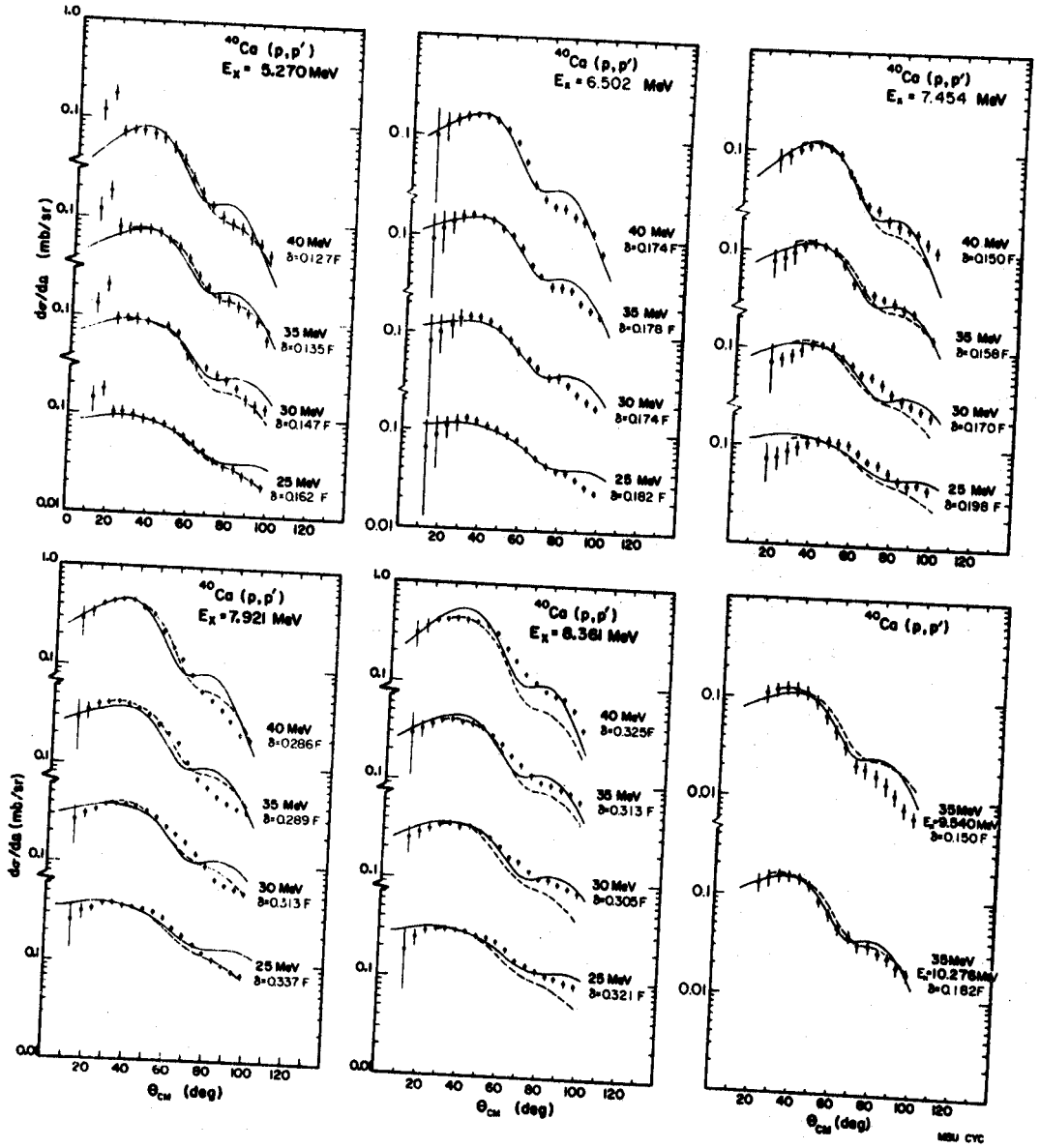

Figure 4.6.--Experimental distributions of L=4 states. Solid curves are collective model fits. Dash curves are those of 6.502 state.

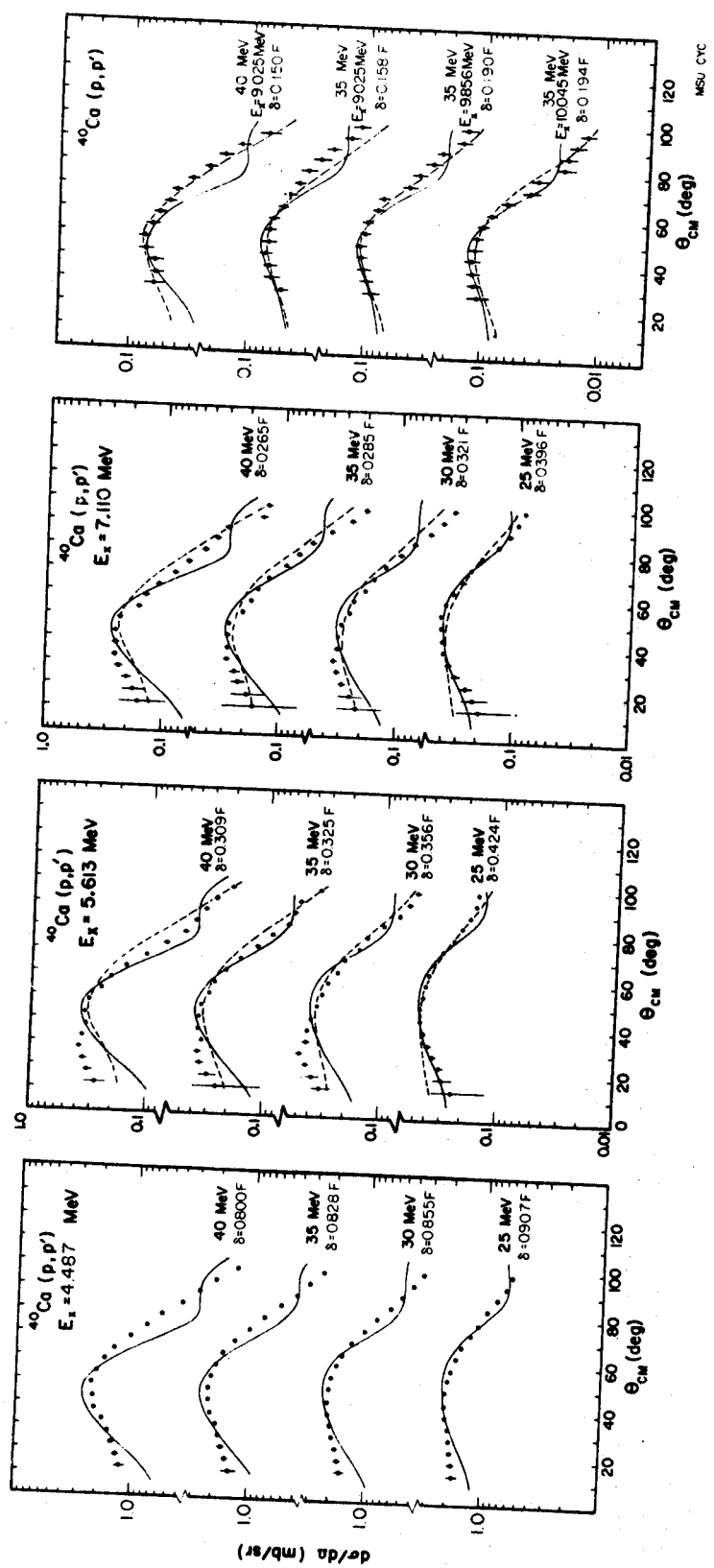

Figure 4.7.--Experimental distribution of ℓ=5 states and collective model fits (solid curves). The dash curves are those of 4.487 MeV state.

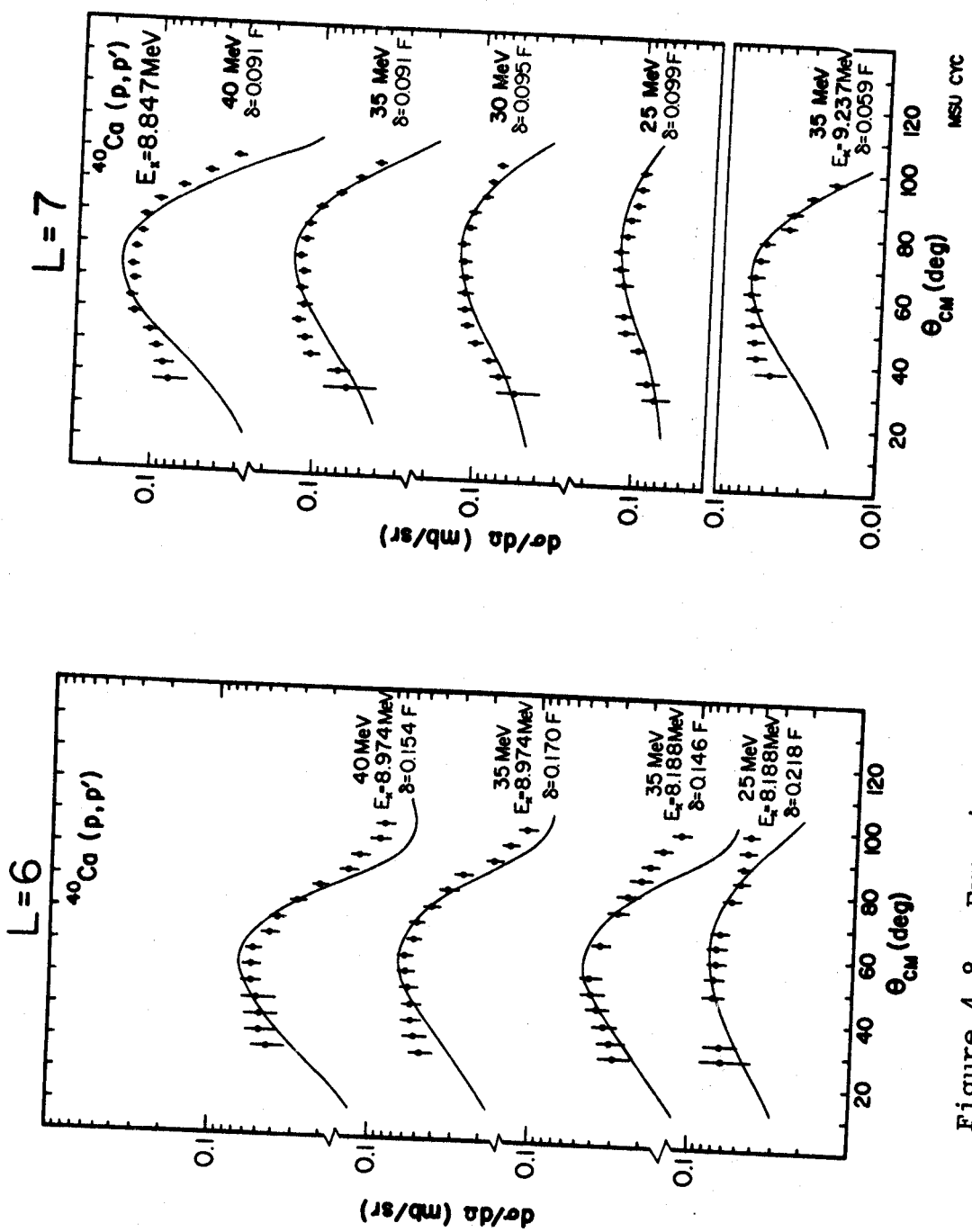

Figure 4.8.--Experimental distributions of ℓ=6 and ℓ=7 states, and collective model fits (solid curves).

4.5.2 Reduced Transition Probabilities

Having made the L-assignments to all excited states and extracted the corresponding nuclear deformation parameters β_L, one can then make the calculations for the reduced transition probabilities B(pp'; O→L).

The values of B(pp') obtained from this method are model-and parameter-dependent, namely on the quantities $\langle r^{2L-2} \rangle$, β_L and R_0. Assuming that for a given excited state its angular distribution is well fitted by a collective model calculation, then the deformation parameter β_L extracted will not be subject to high uncertainty except in its model dependence. The remaining factor which is in question is $\langle r^{2L-2} \rangle$ because of its strong dependence on the transition density $\rho(\vec{r})$ and consequently on the parameters within. Gruhn et al. (Gr 69) have investigated the sensitivity of the $B(EL)_{(p,p')}$ results to the parameters of the transition density for ^{58}Ni. They also compared the calculated $B(EL)_{(p,p')}$ using three different models of the density function. Their finding is that when the non-uniform density distributions determined by electron elastic scattering are used, the result of a calculation for (p,p')B(EL)'s are most inconsistent with the (EM)B(EL)'s for the high multipolarity transitions. Gruhn et al. suggested that if a uniform-density distribution having a radius equal to the Fermi "equivalent" uniform-charge-density radius be used, qualitative agreement with the (EM)B(EL)'s was recovered.

It is for this reason that this prescription was used for this thesis to calculate the (p,p')B(EL)'s for Ca^{40}. Indeed, very good agreement was found when the results were compared with those of (e,e') and (p,p'γ) experiments (see Section 5.3).

The quantities B(EL)'s, G(sp)'s, B_L/h^2 and C_L were calculated using the program VIPAR written by C. Gruhn and K. Thompson. A Fermi equivalent uniform-density distribution with r_0=1.33 Fm (R_0=4.55 fm for Ca^{40}) was used. The results are listed in Table IV-2 to IV-5.

TABLE IV-2.--Collective Vibrational Parameters, $Ca^{40}(p,p')$,Ep=40 MeV.

E_x (MeV)	L	β_L	δ_L (F)	B(pp') (F^{2L})	GU(Sp)	$B_L/\hbar^2$ $(MeV)^{-1}$	C_L (MeV)	$(B_L)_{Hyd}/B_L$	B(pp';0→L) NEWSR
3.732	3	0.308	1.315	0.243E+06	25.36	0.112E+02	0.156E+03	0.211	0.513
3.900	2	0.100	0.428	0.124E+03	2.13	0.724E+02	0.110E+04	0.033	0.059
4.487	5	0.187	0.800	0.385E+07	16.02	0.396E+02	0.798E+03	0.060	0.175
5.240	2	0.029	0.123	0.103E+02	0.18	0.652E+03	0.179E+05	0.004	0.005
5.270	4	0.030	0.127	0.469E+04	0.31	0.110E+04	0.304E+05	0.002	0.005
5.613	5	0.072	0.309	0.574E+06	2.39	0.212E+03	0.569E+04	0.011	0.026
6.021	3	0.039	0.166	0.387E+03	0.40	0.436E+03	0.158E+05	0.005	0.008
6.281	3	0.095	0.404	0.229E+04	2.39	0.706E+02	0.279E+04	0.034	0.048
6.502	4	0.041	0.174	0.880E+04	0.58	0.473E+03	0.200E+05	0.005	0.009
6.577	3	0.074	0.317	0.141E+04	1.47	0.110E+03	0.474E+04	0.022	0.030
6.747	3	0.048	0.206	0.596E+03	0.62	0.253E+03	0.115E+05	0.009	0.013
6.905	2	0.105	0.447	0.136E+03	2.32	0.375E+02	0.179E+04	0.063	0.065
7.110	5	0.062	0.265	0.422E+06	1.76	0.228E+03	0.115E+05	0.010	0.019
7.290	2	0.021	0.091	0.562E+01	0.10	0.857E+03	0.455E+05	0.003	0.003
7.454	4	0.035	0.150	0.654E+04	0.43	0.555E+03	0.308E+05	0.004	0.006
7.531	3	0.035	0.150	0.316E+03	0.33	0.427E+03	0.242E+05	0.006	0.007
7.558	4	0.044	0.186	0.101E+05	0.66	0.356E+03	0.203E+05	0.007	0.010
7.865	2	0.053	0.226	0.347E+02	0.59	0.129E+03	0.796E+04	0.018	0.017
7.921	4	0.067	0.286	0.236E+05	1.55	0.145E+03	0.908E+04	0.016	0.023
8.090	2	0.037	0.158	0.170E+02	0.29	0.256E+03	0.168E+05	0.009	0.008
8.110	3	0.035	0.150	0.316E+03	0.33	0.397E+03	0.261E+05	0.006	0.007
8.361	4	0.076	0.325	0.307E+05	2.01	0.105E+03	0.737E+04	0.022	0.030
8.412	3	0.058	0.249	0.871E+03	0.91	0.139E+03	0.982E+04	0.017	0.018
8.535	5	0.043	0.182	0.199E+06	0.83	0.402E+03	0.293E+05	0.006	0.009
8.578	2	0.040	0.170	0.196E+02	0.34	0.209E+03	0.154E+05	0.011	0.009
8.743	2	0.033	0.139	0.131E+02	0.22	0.306E+03	0.234E+05	0.008	0.006
8.847	7	0.021	0.091	0.213E+08	0.36	0.212E+04	0.166E+06	0.001	0.002
8.974	6	0.036	0.154	0.295E+07	0.78	0.632E+03	0.509E+05	0.004	0.006
9.025	5	0.035	0.150	0.135E+06	0.56	0.560E+03	0.456E+05	0.004	0.006

TABLE IV-3.--Collective Vibrational Parameters, $Ca^{40}(p,p')$, Ep=35 MeV.

E_x (MeV)	L	β_L	δ_L (F)	B(pp') (F^{2L})	GU(Sp)	$B_L/\hbar^2$ $(MeV)^{-1}$	C_L (MeV)	$(B_L)_{Hyd}/B_L$	B(pp';0→L) NEWSR
3.732	3	0.215	1.346	0.255E+05	26.57	0.107E+02	0.149E+03	0.221	0.538
3.930	2	0.099	0.424	0.122E+03	2.09	0.738E+02	0.112E+04	0.032	0.058
4.487	5	0.104	0.528	0.413E+07	17.17	0.370E+02	0.745E+03	0.064	0.187
5.240	2	0.028	0.119	0.268E+01	0.16	0.697E+03	0.191E+05	0.003	0.005
5.272	4	0.030	0.138	0.830E+04	0.85	0.969E+03	0.269E+05	0.002	0.005
5.613	5	0.074	0.325	0.635E+06	2.64	0.132E+03	0.505E+04	0.012	0.029
6.021	3	0.043	0.180	0.465E+03	0.49	0.363E+03	0.132E+05	0.007	0.010
6.281	3	0.095	0.404	0.234E+04	2.44	0.693E+02	0.273E+04	0.034	0.049
6.502	4	0.042	0.178	0.921E+04	0.60	0.452E+03	0.191E+05	0.005	0.009
6.577	3	0.079	0.333	0.156E+04	1.63	0.993E+02	0.429E+04	0.024	0.033
6.747	3	0.052	0.220	0.693E+03	0.72	0.814E+03	0.391E+04	0.011	0.015
6.905	2	0.029	0.124	0.122E+03	2.09	0.417E+02	0.199E+04	0.057	0.058
7.110	5	0.067	0.285	0.488E+06	2.03	0.107E+03	0.996E+04	0.018	0.022
7.200	2	0.021	0.091	0.562E+01	0.10	0.557E+03	0.456E+05	0.003	0.003
7.454	4	0.037	0.158	0.726E+04	0.46	0.500E+03	0.278E+05	0.005	0.007
7.541	3	0.039	0.164	0.387E+03	0.40	0.340E+03	0.198E+05	0.007	0.008
7.598	4	0.046	0.198	0.114E+05	0.75	0.814E+03	0.179E+05	0.008	0.011
7.665	2	0.053	0.226	0.347E+02	0.59	0.129E+03	0.796E+04	0.018	0.017
7.921	4	0.069	0.293	0.248E+05	1.59	0.141E+03	0.883E+04	0.017	0.024
8.000	2	0.030	0.166	0.187E+02	0.32	0.232E+03	0.152E+05	0.010	0.009
8.110	3	0.037	0.158	0.351E+03	0.37	0.358E+03	0.235E+05	0.007	0.007
8.188	5	0.034	0.144	0.265E+07	0.70	0.770E+03	0.517E+05	0.008	0.006
8.361	4	0.072	0.313	0.285E+05	1.87	0.114E+03	0.795E+04	0.021	0.028
8.412	3	0.059	0.249	0.871E+03	0.91	0.139E+03	0.982E+04	0.017	0.018
8.536	5	0.044	0.184	0.208E+06	0.87	0.385E+03	0.281E+05	0.006	0.009
8.678	2	0.038	0.164	0.187E+02	0.32	0.219E+03	0.161E+05	0.011	0.009
8.743	2	0.034	0.147	0.147E+02	0.25	0.274E+03	0.209E+05	0.009	0.007
8.847	7	0.021	0.091	0.213E+08	0.36	0.212E+04	0.166E+06	0.001	0.002
8.974	6	0.040	0.170	0.860E+07	0.95	0.519E+03	0.418E+05	0.005	0.008
9.025	5	0.037	0.158	0.150E+06	0.63	0.505E+03	0.411E+05	0.005	0.007
9.141	3	0.055	0.234	0.769E+03	0.80	0.145E+03	0.121E+05	0.016	0.016
9.237	7	0.014	0.059	0.896E+07	0.15	0.483E+04	0.412E+06	0.000	0.001
9.358	3	0.038	0.162	0.369E+03	0.38	0.295E+03	0.258E+05	0.008	0.008
9.411	3	0.060	0.257	0.928E+03	0.97	0.116E+03	0.103E+05	0.020	0.020
9.540	4	0.035	0.150	0.654E+04	0.43	0.434E+03	0.395E+05	0.005	0.006
9.590	3	0.029	0.123	0.213E+03	0.22	0.439E+03	0.459E+05	0.005	0.004
9.856	5	0.044	0.190	0.217E+06	0.90	0.320E+03	0.311E+05	0.007	0.010
0.045	5	0.045	0.194	0.226E+06	0.94	0.301E+03	0.304E+05	0.008	0.010
0.276	4	0.043	0.182	0.963E+04	0.63	0.274E+03	0.289E+05	0.009	0.009

TABLE IV-4.--Collective Vibrational Parameters, $Ca^{40}(p,p')$, Ep=30 MeV.

E_x (MeV)	L	β_L	δ_L (F)	B(pp') (F^{2L})	GU(Sp)	$B_L/\hbar^2$ $(MeV)^{-1}$	C_L (MeV)	$(B_L)_{Hyd}/B_L$	B(pp';0→L) NEWSR
3.732	3	0.322	1.378	0.267E+05	27.85	0.102E+02	0.142E+03	0.232	0.563
3.900	2	0.101	0.432	0.127E+03	2.17	0.711E+02	0.108E+04	0.033	0.060
4.487	5	0.200	0.855	0.440E+07	18.30	0.347E+02	0.698E+03	0.068	0.199
5.240	2	0.032	0.135	0.124E+02	0.21	0.542E+03	0.149E+05	0.004	0.006
5.270	4	0.034	0.147	0.628E+04	0.41	0.518E+03	0.227E+05	0.003	0.006
5.613	5	0.083	0.354	0.752E+05	3.17	0.160E+03	0.504E+04	0.015	0.035
6.021	3	0.046	0.198	0.551E+03	0.58	0.307E+03	0.111E+05	0.008	0.012
6.281	3	0.100	0.428	0.257E+04	2.69	0.629E+02	0.248E+04	0.038	0.054
6.502	4	0.041	0.174	0.880E+04	0.58	0.473E+03	0.200E+05	0.005	0.009
6.577	3	0.085	0.364	0.186E+04	1.94	0.831E+02	0.359E+04	0.029	0.039
6.747	3	0.057	0.242	0.823E+03	0.86	0.183E+03	0.834E+04	0.013	0.017
6.905	2	0.101	0.432	0.127E+03	2.17	0.401E+02	0.191E+04	0.059	0.060
7.110	5	0.075	0.321	0.620E+05	2.58	0.155E+03	0.785E+04	0.015	0.028
7.290	2	0.023	0.099	0.666E+01	0.11	0.724E+03	0.385E+05	0.003	0.003
7.454	4	0.040	0.170	0.840E+04	0.55	0.432E+03	0.240E+05	0.005	0.008
7.531	3	0.039	0.166	0.387E+03	0.40	0.349E+03	0.198E+05	0.007	0.008
7.558	4	0.046	0.198	0.114E+05	0.75	0.314E+03	0.179E+05	0.008	0.011
7.865	2	0.058	0.246	0.411E+02	0.70	0.109E+03	0.672E+04	0.022	0.020
7.921	4	0.073	0.313	0.285E+05	1.87	0.120E+03	0.753E+04	0.020	0.028
8.090	2	0.041	0.174	0.206E+02	0.35	0.211E+03	0.138E+05	0.011	0.010
8.110	3	0.040	0.170	0.406E+03	0.42	0.309E+03	0.203E+05	0.008	0.009
8.361	4	0.071	0.305	0.270E+05	1.77	0.120E+03	0.837E+04	0.020	0.026
8.412	3	0.063	0.269	0.102E+04	1.06	0.119E+03	0.842E+04	0.020	0.021
8.535	5	0.046	0.198	0.236E+06	0.98	0.340E+03	0.248E+05	0.007	0.011
8.578	2	0.040	0.170	0.196E+02	0.34	0.209E+03	0.154E+05	0.011	0.009
8.743	2	0.036	0.154	0.161E+02	0.28	0.249E+03	0.191E+05	0.010	0.008
8.847	7	0.022	0.095	0.232E+08	0.39	0.194E+04	0.152E+06	0.001	0.002

TABLE IV-5.--Collective Vibrational Parameters, $Ca^{40}(p,p')$, Ep=25 MeV.

E_x (MeV)	L	β_L	δ_L (F)	B(pp') (F^{2L})	GU(Sp)	$B_L/\hbar^2$ $(MeV)^{-1}$	C_L (MeV)	$(B_L)_{Hyd}/B_L$	B(pp';0→L) NEWSR
3.732	3	0.327	1.398	0.275E+05	28.67	0.933E+01	0.138E+03	0.239	0.580
3.900	2	0.098	0.420	0.120E+03	2.05	0.752E+02	0.114E+04	0.032	0.057
4.487	5	0.212	0.907	0.435E+07	20.60	0.308E+02	0.621E+03	0.077	0.224
5.240	2	0.035	0.150	0.153E+02	0.26	0.439E+03	0.120E+05	0.005	0.007
5.270	4	0.038	0.162	0.763E+04	0.50	0.673E+03	0.187E+05	0.004	0.007
5.613	5	0.099	0.424	0.108E+07	4.50	0.113E+03	0.355E+04	0.021	0.049
6.021	3	0.054	0.230	0.743E+03	0.78	0.227E+03	0.624E+04	0.010	0.016
6.281	3	0.109	0.463	0.301E+04	3.14	0.538E+02	0.212E+04	0.044	0.064
6.502	4	0.043	0.182	0.963E+04	0.63	0.432E+03	0.183E+05	0.005	0.009
6.577	3	0.096	0.412	0.239E+04	2.49	0.649E+02	0.281E+04	0.037	0.050
6.747	3	0.064	0.273	0.105E+04	1.09	0.144E+03	0.656E+04	0.016	0.022
6.905	2	0.103	0.440	0.131E+03	2.25	0.387E+02	0.184E+04	0.061	0.063
7.110	5	0.093	0.396	0.943E+06	3.93	0.102E+03	0.516E+04	0.023	0.043
7.290	2	0.024	0.103	0.721E+01	0.12	0.669E+03	0.355E+05	0.004	0.003
7.454	4	0.046	0.198	0.114E+05	0.75	0.319E+03	0.177E+05	0.007	0.011
7.531	3	0.044	0.190	0.507E+03	0.53	0.266E+03	0.151E+05	0.009	0.011
7.558	4	0.053	0.226	0.148E+05	0.97	0.241E+03	0.138E+05	0.010	0.014
7.865	2	0.066	0.281	0.536E+02	0.92	0.833E+02	0.515E+04	0.028	0.026
7.921	4	0.079	0.337	0.330E+05	2.17	0.103E+03	0.649E+04	0.023	0.032
8.090	2	0.043	0.183	0.225E+02	0.38	0.193E+03	0.126E+05	0.012	0.011
8.110	3	0.045	0.194	0.529E+03	0.55	0.237E+03	0.156E+05	0.010	0.011
8.188	6	0.051	0.218	0.591E+07	1.57	0.346E+03	0.232E+05	0.007	0.013
8.361	4	0.075	0.321	0.300E+05	1.97	0.108E+03	0.755E+04	0.022	0.029
8.412	3	0.069	0.293	0.121E+04	1.26	0.100E+03	0.710E+04	0.024	0.025
8.535	5	0.053	0.226	0.307E+06	1.28	0.261E+03	0.190E+05	0.009	0.014
8.578	2	0.042	0.178	0.215E+02	0.37	0.190E+03	0.140E+05	0.012	0.010
8.743	2	0.040	0.170	0.196E+02	0.34	0.205E+03	0.156E+05	0.012	0.009
8.847	7	0.023	0.099	0.252E+08	0.42	0.179E+04	0.140E+06	0.001	0.003

4.6 L=1 States

Figure 4.9 shows the experimental cross sections obtained for three ℓ=1 states at 5.899, 6.944 and 8.270 MeV. The solid curves drawn against the data of 5.899 MeV are the results of collective model calculations. It is seen that the fits are very poor, therefore deformation parameters were not obtained for ℓ=1 states. This is because that under the incompressibility constraint, the ℓ=1 vibration corresponds to the oscillation of the center of mass of the nucleus, which of course is not the excitation observed. A microscopic description which accounts for the 1st and 2nd 1^- states is given in Chapter VI.

4.7 First Excited 0^+ State

The collective model using only an R-vibration also failed to reproduce the shapes of the distributions for the first excited 0^+ state (3.35 MeV). Calculations for this state based on a generalized collective vibrational model have been carried out by Satchler (Sa 66a, Sa 67) but no data were available at the time those calculations were made. These calculations were redone by the author of this thesis. The potential U(V,R,a,r) was assumed to undergo oscillations of the form:

$$U=\delta R\left(\frac{\partial U}{\partial V}\right)+\delta V\left(\frac{\partial U}{\partial V}\right)+\delta a\left(\frac{\partial U}{\partial a}\right)$$

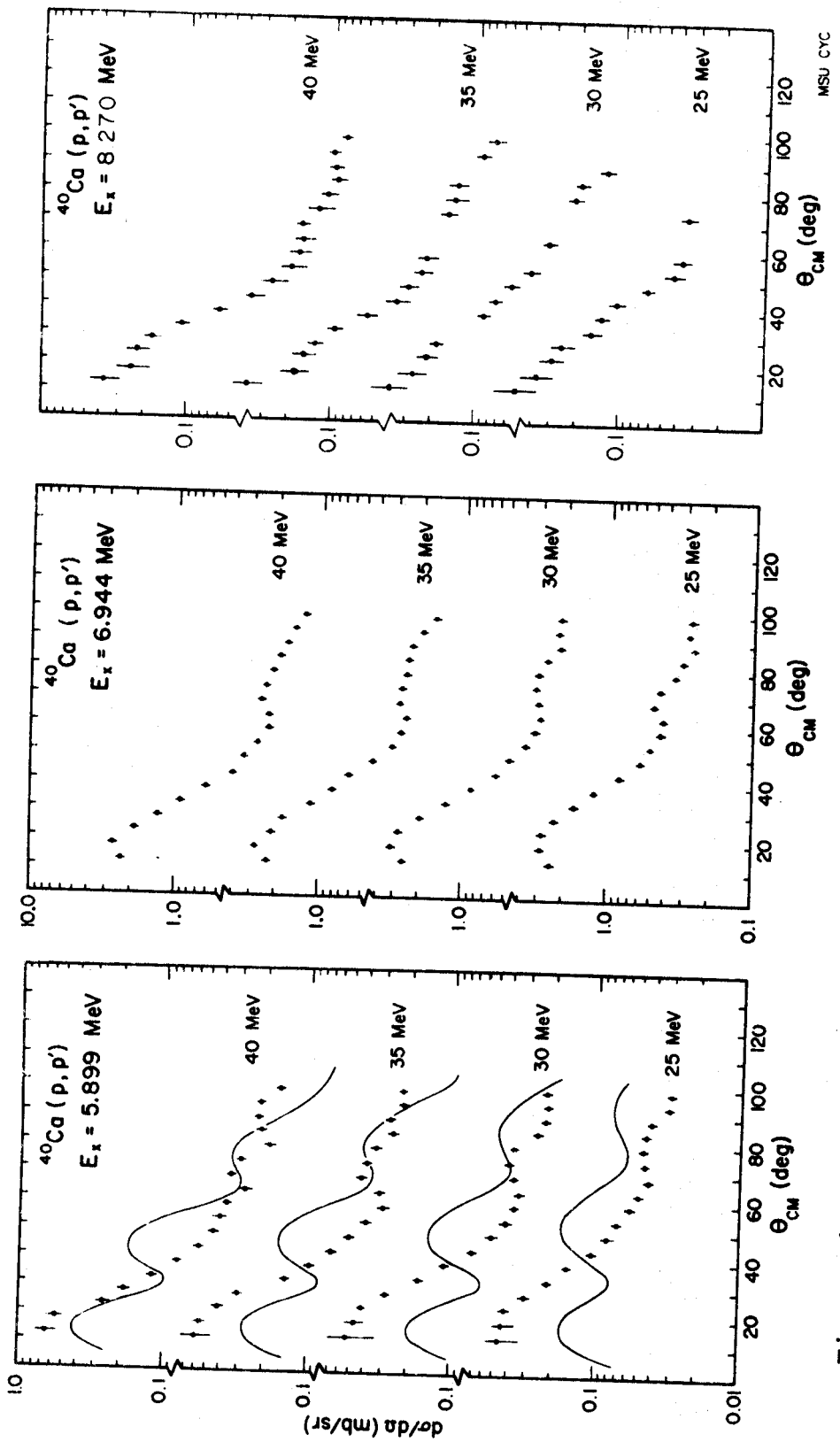

Figure 4.9.--Experimental distributions of ℓ=1 states. The solid curves show the poor collective model predictions.

with the constraint:

$$(3R^2+\pi^2a^2)\frac{\delta R}{R}+(R^2+\pi^2a^2)\frac{\delta V}{V}+2\pi^2a^2\frac{\delta a}{a}=0$$

where $U(r)=-Vf(x)$, $\chi=\frac{r-R}{a}$, $f(x)=(e^x+1)^{-1}$.

Five vibration modes were tried. They are:

(1)

Breathing mode, $\delta a = 0$

$$\Delta U_1(r)=[R\frac{V}{a}\frac{df(x)}{dx} + BVf(x)]\frac{\delta R}{R}$$

(2)

a-vibration, $\delta V = 0$

$$\Delta U_2(r)=\frac{RV}{a}\frac{df(x)}{dx}[1-c(\frac{r-R}{R})]\frac{\delta R}{R}$$

(3)

a-vibration, $\delta R = 0$

$$\Delta U_3(r)=V[\frac{df(x)}{dx}(\frac{r-R}{a}) + Df(x)]\frac{\delta a}{a}$$

(4)

a-vibration, $\delta R = 0$, $\delta V = 0$

$$\Delta U_4(r)=[V(\frac{r-R}{R})\frac{df(x)}{dx}]\frac{\delta a}{a}$$

(5)

all vibrations

$$\Delta U_5(r)=\Delta U_1(r)+\Delta U_3(r)$$

$$B=\frac{3R^2+\pi^2a^2}{R^2+\pi^2a^2},\quad C=\frac{3R^2+\pi^2a^2}{2\pi^2a^2},\quad D=B/C$$

A computer program was written to generate the form factors corresponding to the potentials described above. These form factors were obtained using the prescription discussed in Section 4.1.2. The parameters of the potentials are the same as those used in other calculations. Form factor decks adaptable to the JULIE code were part of the output of the program. Fig. 4.10 shows the results of these calculations at E_p=25 MeV and a comparison with the data at the same energy. The fit to the data is seen to be poor. Also note that the calculations are out of phase with the data. On the other hand, previous calculations by Satchler were reproduced indicating that the program is correct. Calculations were also done at 30, 35, and 40 MeV with similar results. Also calculated were the angular distributions in which the parameters V, R, and a were varied on a grid-like basis. In addition, complex form factors within the framework of the a-vibration theory were tried. No fit was found.

Next an empirical form factor of the following form was assumed

$$F(r)=A\left[e^{-\frac{(r-R+a)^2}{a}}-Be^{-\frac{(r-R-a)^2}{a}}\right]$$

After searching on R, a, and B it was found that the data could be fitted using the form factor shown in Fig. 4.11.

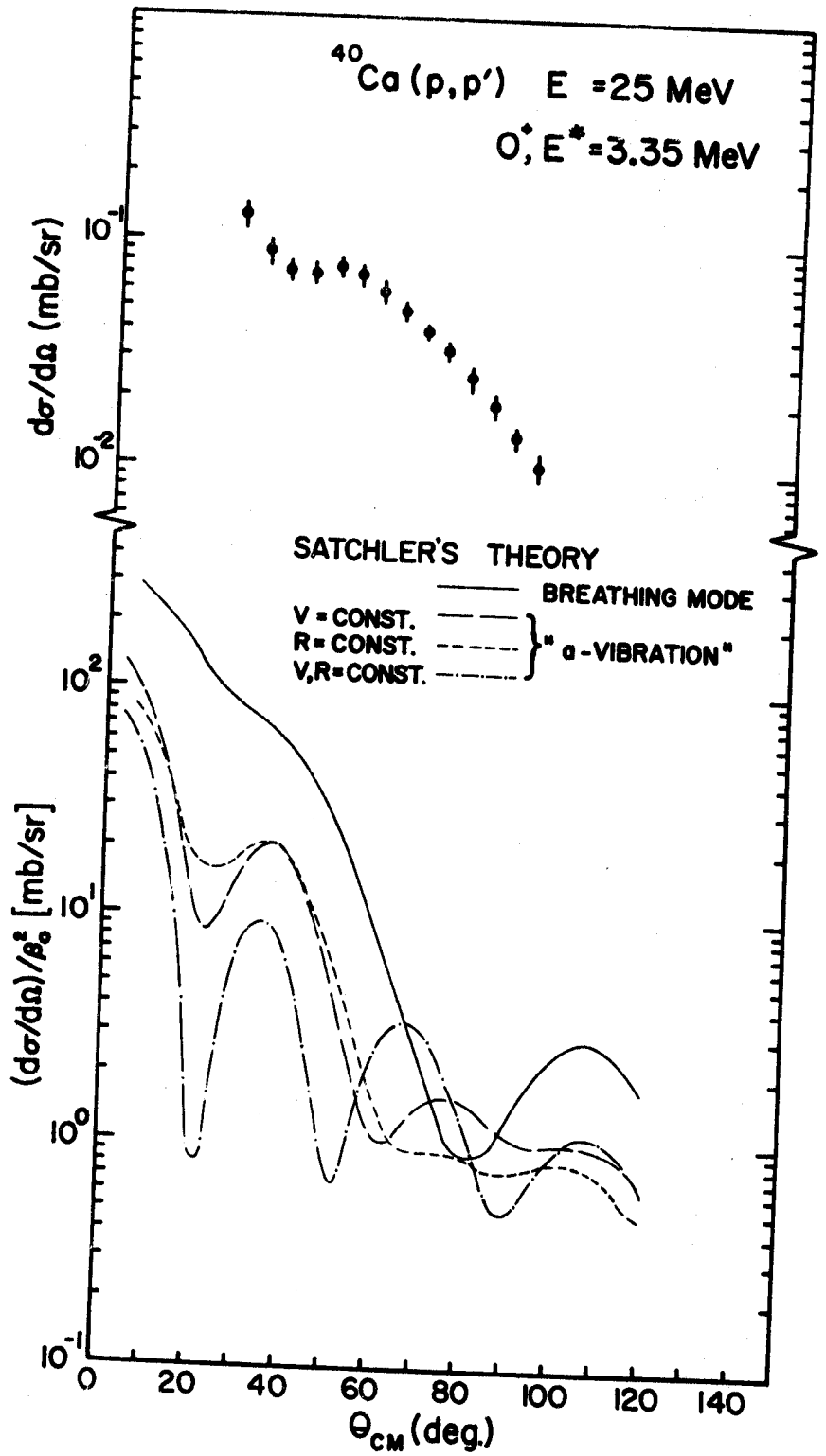

Figure 4.10.--Results of generalized collective model calculations based on Satchler's theory.

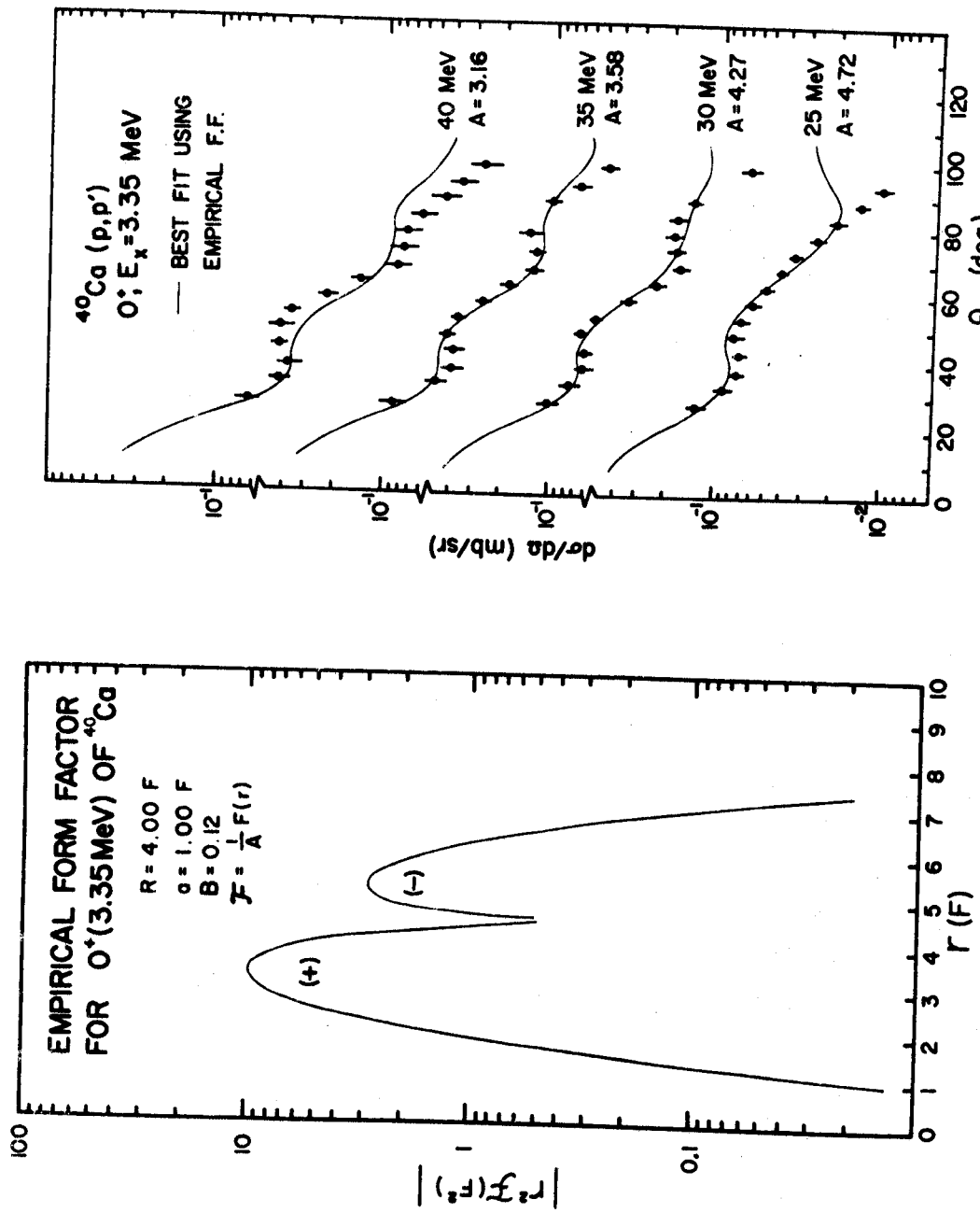

Figure 4.11.--Experimental distribution of the first 0^+ state and empirical F.F. fits.

A comparison of the data with the calculated cross sections using this form factor is also shown. The main difference between this form factor and the a-vibration form factor is in the relative size of the oscillation in the surface. Possibly if one were to relax the constraint, the a-vibration f.f. would be more similar to the empirical f.f. However, if one postulates that the ground state and the excited 0^+ state are mixture of spherical and deformed components then one may expect a form factor similar to the empirical f.f.

In order to confine the discussion to the domain of collective model analysis, alternate explanations are presented in Chapter VI.

CHAPTER V

COMPARISONS WITH OTHER EXPERIMENTS

5.1 Energy Levels

Fig. 5.1 shows the levels seen in this (p,p') experiment and those observed in other types of reactions. Only representative results are shown. The energies of the low lying levels have been determined with high precision by high resolution (p,p') (Ma66, Gr 66) and γ-ray measurements (Do 68, Po 69). The energies given in this work were obtained by a calibration which used Grace and Poletti's results.

As can be seen from Fig. 5.1, good agreement hold between the results of the present experiment and that of Grace and Poletti from 3.731 MeV to 8.847 MeV excitation energy. A constant shift of 4 to 5 KeV lower was observed when the level energies of the present work were compared with those measured in γ-decay experiments. The 5.21 MeV and 6.54 MeV states were too weakly excited to be seen in this experiment. Above 7 MeV, the (α,α') experiment recorded only a few levels due to limitation of their detection system.

Above 9 MeV the present experiment observed many levels previously seen in (p,γ) work (Le 66), but no attempt was made at comparing those results with this experiment.

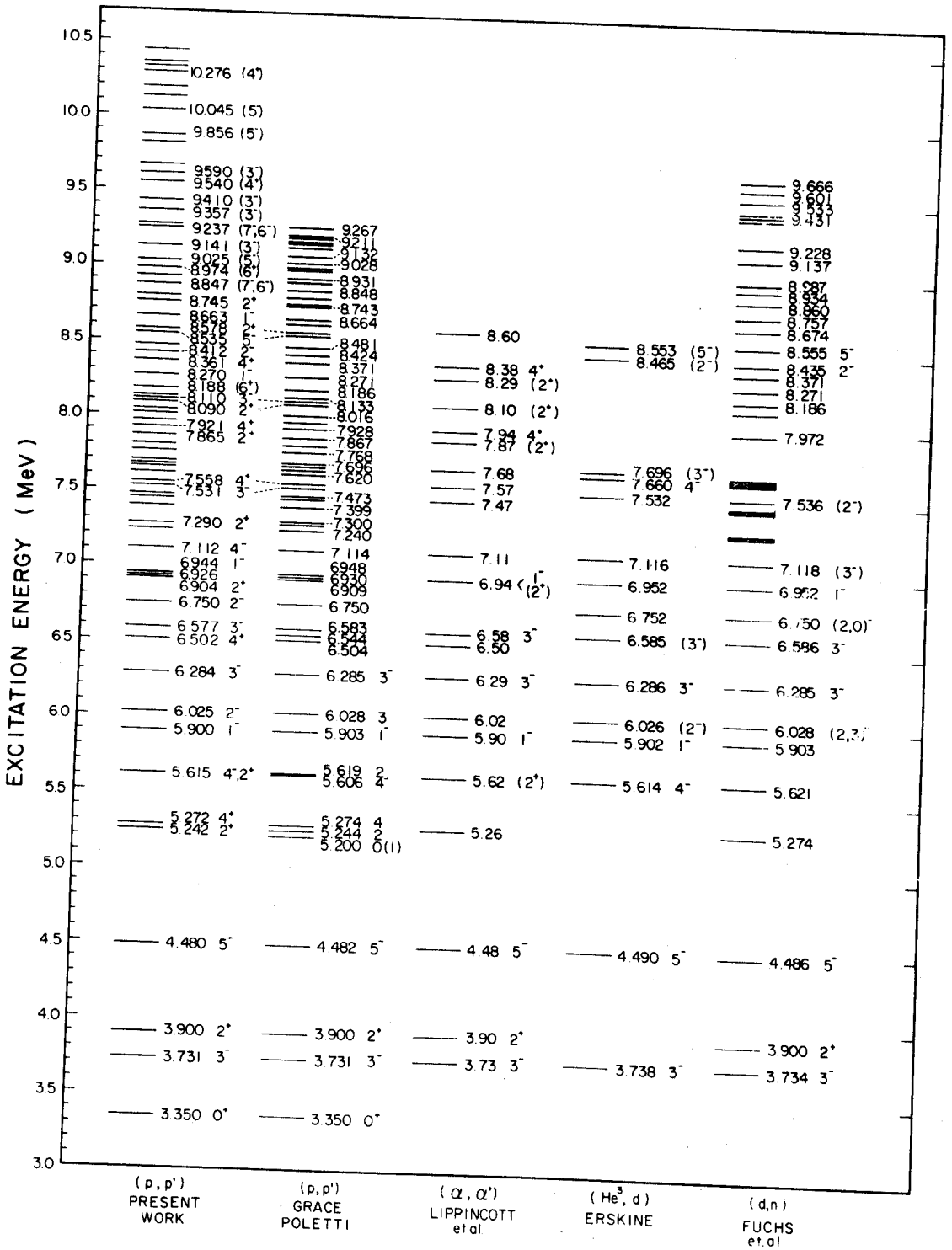

Figure 5.1.--Energy levels of ^{40}Ca observed by various experiments.

5.2 Spin Identification

The J^{π} assignments of the excited states of Ca^{40} obtained from various experimental sources are summarized in Table V-1. Some of this information has been reported by Seth et al. (Se 67). Since then many new results on spin assignments for the excited levels of Ca^{40} including those from this experiment have become available.

Generally speaking, the inelastic scattering method is not in a position to give definite spin and parity assignments, but rather, only the L transfer values. It has been concluded in Chapter IV that even the L-values determined by low energy (<30 MeV) (p,p') experiment are subject to rather high uncertainty.

The (He^3,d) and (d,n) stripping reactions to Ca^{40}, on the other hand select primarily the odd parity states. In these cases, the inelastic scattering findings complement the stripping experiments.

The normal even-parity states can positively be determined by the evidences of apparent L-transfer observed by inelastic scatterings, of the discriminating nature of stripping reactions and by γ-ray decay schemes, since the even-parity states predominately favor the transitions to other even-parity states.

TABLE V-1.--Spin and Parity Assignments of States in Ca^{40}.

Ref. 3		(p,p') 25-40 MeV THIS WORK		(p,p') 55MeV Ref. 5	(p,p') 17 MeV Ref. 4	(α,α') 51 MeV Ref. 7	(α,α') 31 MeV Ref. 8	(e,e') 20220 MeV Ref. 10	(e,e') 20-60 MeV Ref. 11	(^{3}He,d) 12 MeV Ref. 12	(^{3}He,d) 14 MeV Ref. 13	(d,n) 6 MeV Ref. 14	(p,γ) Ref. 15, 16	(p,γ) Ref. 17, 18	(p,p'γ) 7.5-9.6 MeV Ref. 3	(p,p'γ) 9 MeV Ref. 19	(p,p'γ) 8-10 MeV Ref. 20, 21	γ-Res. Ref. 24	Summary
No.	E_x	Lp	J^π	Lp	Lp														
1	3.350		0^+																0^+
2	3.737	3	3^-	3	3	3^-	3^-	3^-	3^-	3^-	3^-	3^-	3^-	3^-	3^-	3^-	3^-		3^-
3	3.904	2	2^+		2	2^+	2^+	2^+	2^+				2^+	2^+	2^+	2^+	2^+		2^+
4	4.492	5	5^-	5		5^-	5^-	5^-		5^-	5^-	5^-	5^-	5^-	5^-	5^-	5^-		5^-
5	5.212																		
6	5.249	2	2^+			} ( )$^-$									0,(1)	0^+	0^+		0^+
7	5.279	4	4^+										2	2	2	2^+	2^+		2^+
8	5.615	5	4^-										4^+	4^+	4	4^+	4^+		4^+
9	5.627	2	2^+			} ( )$^-$	} (2^+)			4^-	4^-	4^-	4^-	4^-	$4^{(-)}$	4^-	4^-		4^-
10	5.900	1	1^-											2	2	2^+	2^+		2^+
11	6.025	3	2^-			3^-	1^-			1^-	1^-	1^-			1^-	1^-	1^-		1^-
	6.029							} 3^-		(2$^-$)	(2$^-$)	(2,3)$^-$			3,(2)	2^-	2^-		2^-
12	6.285	3	3^-		3	3^-	3^-									3^+	3^+2^-		(3^+)
13	6.509	4	4^+		} 3					3^-	3^-	3^-	$3^{(-)}$		3^-	3^-	3^-		3^-
14	6.544																4^+		4^+
15	6.585	3	3^-			3^-	3^-										4^+		4^+
16	6.750	3	(2,3)$^-$							(3$^-$)	3^-	3^-					3^-		3^-
17	6.909	2	2^+							( )$^-$	(2,0)$^-$	2^-			3^-				2^-
18	6.930	>3	(>3)	} 2+3	} 2	2^+3^-	(2^+)	} (2$^+$3)	} (2$^+$3)				} (1,2)					2^+	2^+
19	6.948	1	1^-			2^+1^-	1^-												(>3)
20	7.114	5	4^-		3					( )$^-$	1^-	1^-						1^-	1
22	7.280	2	$(0,2)^+$							( )$^-$	(3)$^-$	(3)$^-$							4^-
23	7.300																		
26	7.455	4											0						
27	7.473													2					
28	7.531	3	(2,3)$^-$																
29	7.558	4	4^+							( )	(2)$^-$	(2)$^-$							2^-
31	7.655													<5					4^+
32	7.676	(≥6)								4^-	4^-								4^-
33	7.696																		(>6)
36	7.867	2	2^+				(2$^+$)			(3)$^-$	3^-								3^-
37	7.928	4	4^+			4^+	4^+												2^+
40	8.092	2	2^+																4^+
41	8.113	3	(2,3)$^-$			} 2^+	} (2^+)												2^+
43	8.186	(6)	(6^+)																(2,3)$^-$
44	8.271	1	$(0,1)^-$				(2$^+$)												(6$^+$)
46	8.371	4	4^+			4^+	4^+												$(0,1)^-$
47	8.424	3	2^-																4^+
49	8.535	5	5^-							(2$^-$)	2^-	2^-							2^-
50	8.578	2	2^+			} 2^+		} 5^-		(5$^-$)	5^-	5^-							5^-
52	8.664	1	$(0,1)^-$																2^+
53	8.743	2	2^+																$(0,1)^-$
56	8.848	7	$(6,7)^-$																2^+
59	8.977	6	(6^+)																$(6,7)^-$
60	8.993																		
61	9.028	5	(5^-)																
63	9.132	3	$(2,3)^-$																
64	9.158																		
	9.237	(7)	$(6,7)^-$																
	9.358	3	$(2,3)^-$																
	9.411	3	$(2,3)^-$																
	9.540	4	(4^+)																
	9.590	3	$(2,3)^-$																
	9.637	2+5																	
	9.856	5	(5^-)																
	10.045	5	(5^-)																
	10.274	4	(4^+)																

(d,n)		$(p,\gamma)_{15\,16}$	
9.404	(3)$^-$	9.41	2
9.408	(2)$^-$	9.61	3^+
9.435	(1)$^-$	9.65	2^-
9.540	(1)$^-$	9.79	3
9.608	(2)$^-$	9.87	1
10.040	(0)$^-$	9.96	4^+
		10.33	1

Ref. 5 (Ya 64); Ref. 4 (Gr 65); Ref. 7 (Sp 65); Ref. 8 (Li 67); Ref. 10 (Bl 63); Ref. 11 (Ei 69); Ref. 12 (Er 66); Ref. 13 (Se 67); Ref. 14 (Fu 69); Ref. 15 (Le 66); Ref. 16 (Le 67); Ref. 17 (Li 68); Ref. 18 (Do 68); Ref. 19 (Po 69); Ref. 20 (An 69); Ref. 21 (Ma 68); Ref. 24 (Me 68).

5.2.1 States Below 6.585 MeV

The spins and parities of low-lying levels below 6.585 MeV have been well determined. The most complete set of spin assignments was given by Anderson et al. (An 69) who have done extremely precise $(p,p'\gamma)$ measurements. A summary of the previous assignments has been discussed by Seth et al. (Se 67). The spins and parities of $3.350(0^+)$, $3,373(3^-)$, $3.904(2^+)$, $4.492(5^-)$, $5.615(4^-)$, $5.900(1^-)$, $6.025(2^-)$, $6.285(3^-)$ and $6.585(3^-)$ MeV excited states are consensus assignments. Of the triplet at 5.21-5.25-5.28 MeV the 5.21 MeV state, which was not seen in this experiment, has been identified as 0^+ by all of the most recent $(p,p'\gamma)$ works (Po 69, An 69, Ma 68).

Individual angular distributions for the 5.25 and 5.28 MeV states were obtained (see Fig. 4.4 and Fig. 4.6) and are assigned 2^+ and 4^+. The assignments are in agreement with results of (p,γ) and $(p,p'\gamma)$ experiments (Le 66, Le 67, Li 68).

The 5.627 MeV component of the 5.62 MeV doublet has been identified as 2^+ by many γ-decay experiments. In this work, the angular distributions of this doublet permit some mixture of L=2 to L=5. The upper limit of the L=2 contribution was determined to be ($\delta_2 \sim 0.09 \pm 0.02$ fm). The value of B(E2) in Weisskopf units, i.e., G(sp), based on this estimated deformation is in qualitative agreement with other electromagnetic transition measurements. On the other hand, the (α,α') experiment by Lippincott et al. (Li 67) observed

only the 2^+ component indicating that this state is observed in both types of inelastic scattering.

The 6.029 MeV level of the 6.025-6.029 MeV doublet was discovered by the Oxford group. It is assigned as having $J^\pi=3^+$, but 2^- was not entirely ruled out according to Anderson et al. In the present experiment, this doublet was observed to be an L=3 transfer as a whole.

Anderson et al. are the only group who identify the 6.540 MeV level as 4^+. In the present experiment the 6.510 MeV level was well resolved from the 6.580 MeV state (see Fig. 2.4) and found to be a 4^+ state. However, the 6.540 MeV level was not seen at all. It may be the case that this state was weakly excited with respect to the 6.51 MeV level and because it is also a 4^+, the analyzed group may actually be a 4^+-4^+ doublet.

5.2.2 States Between 6.750 and 7.558 MeV Excitation Energy

Extensive gamma-ray studies on the energy levels and their spins and parities of Ca^{40} stopped at 6.58 MeV. Above 6.75 MeV, existing J^π assignments to some levels are firm whereas others are debatable. The results of this experiment resolved some of these ambiguities.

The 6.750 MeV level: This state has been preferably assigned as 0^- over 2^- by Seth et al. in their $^{39}(He^3,d)$ experiment (Se 67). Comprehensive explanations for their assignment were also given by these authors. However,

Fuchs et al., who have done the $^{39}K(d,n)$ experiment (Fu 69) to unfold the problem of the missing 2^- strength of the T=0 quartets of the $[d_{3/2}^{-1}f_{7/2}]$ and $[d_{3/2}^{-1}P_{3/2}]$ configurations, found that this 6.75 MeV should be assigned as 2^- based on an observed L_p=3 transition, as opposite to the L_p=1 assignment obtained by Seth et al. This means that the (d,n) reaction saw this state as the 2^- component of the $[d_{3/2}^{-1}f_{7/2}]$ quartet but the (He^3,d) work suggested that it be the 0^- of the $[d_{3/2}^{-1}P_{3/2}]$ quartet. In this (p,p') experiment, the 6.75 MeV level was observed excited by a L=3 transfer indicating that the (p,p') reaction favors the 2^- assignment or possibly 3^- (see Fig. 4.5). Resolution for the discrepancy between the contradictory results of the (d,n) and (He^3,d) reactions can be found partly from Gerace and Green's calculations (Ge 68) based on the mixing of $\overline{3p\text{-}3h}$ deformed states with shell model states of T. T. S. Kuo.

The wavefunction of the second 2^- state, from Gerace et al. calculations, shows that it contains about 29% of $|\overline{3p\text{-}3h}\rangle$, and 69% of ψ_1^{2-} (KUO), in which $[d_{3/2}^{-1}f_{7/2}]$ is the largest component (Ku 66). Hence the theoretical configuration proposed for the second 2^- state are deformed plus the $[d_{3/2}^{-1}f_{7/2}]$. The predicted energies for the first and second 2^- states are 6.4 and 6.85 MeV which closely agree with the experimental values of 6.02 and 6.75 MeV if the

latter is assigned to 2^-. The agreement between theory, (d,n) and this (p,p') experiment suggests that the 2^- assignment is favored. It has been pointed out by Seth et al. that appreciable L=3 transition can be mixed with L_p=1 without affecting the quality of L_p=1 fits but the inverse is just the opposite. It was also found that in their data the smallest angles of observation for this 6.75 MeV state stopped at about 30°, where the maxima of L_p=3 distributions occur. Their proposed L_p=1 peaking at about 10°, without comparison with data, may result in their overestimating the $G_{\ell=1}$ strength.

The 6.91-6.93-6.95 MeV triplet: individual angular distributions for 6.91 and 6.95 MeV states were obtained and their J^π-values are positively assigned as 2^+ and 1^- (see Fig. 4.4 and Fig. 4.9). Metzger, using γ-resonance techniques (Me 68) has concentrated his effort on this 6.91-6.93-6.95 MeV triplet, and he was able to identify the first and third members as 2^+ and 1^-, in agreement with this (p,p') finding. The 6.95 MeV level has also been assigned 1^- by proton stripping reactions. As has been mentioned in Section 3.9, where the analysis of this triplet was discussed in detail, the middle level of 6.93 MeV may be a high spin state ($\geq$3).

The 7.114 level: The spin and parity of this state has been tentatively assigned $(3)^-$ by many authors of previous works. This assignment was first given by Gray et al. in their (p,p') experiment using relatively low proton beam energy. This level was also observed by the

(α,α') reaction (Li 67) although no spin identification was made. An L_p=1 transition observed for this state in (He^3,d) (Er 66, Seth 67, Fo 70) and (d,n) (Fu 69) reactions leads to the $(3)^-$ assignments by these authors.

A contradictory result was found in this (p,p') experiment. The angular distributions of this state resemble those having L=5 transfer and are very similar to those of the 5.62 MeV state (see Fig. 4.7). At E_p=25 MeV, the distributions of these two levels agree very well with the L=5 collective model prediction. At E_p=40 MeV, the distributions are intermediate between L=5 and L=4. In any case, the angular distributions of the 5.62 and 7.11 MeV states are remote from those of L=3 transfer. Other evidences of similarity between these two levels can be seen from the $^{39}K(p,\gamma)$ experiment performed by Lindeman et al. (Li 68). The gamma-ray branchings of both the 5.62 and 7.11 MeV levels were found about the same, namely 70% to 3.74 MeV level and 30% to 4.49 MeV level.

The forementioned calculations by Gerace and Green suggest that the second 4^- state is essentially a collective state with over 80% of $\overline{3p\text{-}1h}$ strength. The predicted energy is 7.65 MeV. Thus it is believed that the 7.11 MeV level corresponds to the second 4^- of Gerace and Green's scheme. The L_p=1 (in stripping) transition property of this state cannot, perhaps, be interpreted by the simple particle-hole picture of the shell model.

It appeared that the present data on the 7.11 MeV state are most consistent with a 4^- assignment.

The 7.53 MeV level: This state has been observed in (He^3,d) and (d,n) experiments and tentatively assigned as $(2)^-$, based on the shell model. In the present experiment, this and the 7.56 MeV levels are not separated and analyzed by decomposition method (Section 3.8). The 7.53 MeV level is found to be excited by a L=3 transfer in agreement with the results of proton stripping reactions. The 7.56 MeV state is identified as 4^+. The 7.57 MeV level observed in the (α,α') experiment (Li 67) may correspond to this state.

5.2.3 T=1 Analog States

The T=1 analog states of ^{40}K have been assigned by Erskine at $7.660(4^-)$, $7.696(3^-)$, $8.465(2^-)$ and $8.553(5^-)$ MeV. His proposal was based on the results of his (He^3,d) data and on Enge's (d,p) experiments (Er 66, En 59) and of the observation of the lowest T=1 state in Ca^{40} by Rickey et al. (Ri 65, Ka 68). Also these experimental results agree with the calculated excitation for the lowest K^{40} analog states in Ca^{40} in $[d_{3/2}^{-1}f_{7/2}]$ configuration. Experimentally, this has been further investigated by Seth et al. and Fuchs et al. Both groups have confirmed Erskine's identification. Fuchs et al. even extended this technique to identify the T=1, $[d_{3/2}^{-1}p_{3/2}]$ quartet.

In the present experiment, the 7.660, 7.676, 7.696 MeV triplet was not resolved and the J^{π}-values of the 7.660 and 7.696 MeV states are taken from the results of authors mentioned above. The 8.424 and 8.535 MeV levels are observed to be L=3 and 5 transitions respectively, consistent with results of the stripping reaction experiments. The $[d_{3/2}^{-1}p_{3/2}]$ T=1 quartet was proposed by Fuchs et al. to consist of the $10.040(0^-)$, $9.435(1^-)$, $9.408(2^-)$ and $9.404(3^-)$ MeV levels. At E_p=35 MeV, a level at 10.045 MeV was seen having L=5 transfer. It is suspected that this may not be the same level observed by Fuchs et al. No angular distribution for the 9.435 MeV state was obtained here. A doublet at 9.411 MeV with an L=3 transfer angular distribution was observed which may correspond to the 2^- and 3^- levels at 9.408 and 9.404 MeV.

5.2.4 States Between 7.6 and 8.8 MeV

Aside from the T=1 analog states discussed in the last section, there are a few even-parity states which lie in this region. The 7.867, 8.092, 8.578 and 8.743 MeV levels were identified as 2^+ and the 7.928, 8.371 MeV levels as 4^+, in agreement with the results of (α,α') experiments. It is interesting to observe from the Table V-1 that the (α,α') experiments missed all the T=1 states as expected from the selection rule $\Delta T=0$ for the inelastic scattering of Alpha particles.

There are two L=1 states observed in this region. The 8.271 MeV level (see Fig. 4.9) is tentatively assigned

$(0,1)^-$. The possibility of 0^- was assumed since the angular distributions of unnatural parity states are not distinguishable from those of natural parity states with spin just one unit higher. The 0^- component of the T=0 $[d_{3/2}^{-1}p_{3/2}]$ quartet was tentatively assigned by Fuchs et al. to be one of the 8.271 or 8.371 or 8.931 MeV levels. In the present experiment the 8.93 MeV level was very weakly excited (about 30±10 μb/sr at 30° and 8±4 μb/sr at 60° at E_p=25 MeV) and no angular distribution could be obtained. The 8.371 MeV level has been identified as 4^+ in this and two (α,α') experiments. As in the case of the 7.114 MeV level, the nature of L_p=1 transition observed in (d,n) reaction for the 8.371 MeV state is open to further investigation. Another L=1 state is the 8.664 level which was also weakly excited in this experiment.

The 8.113 MeV level is assumed to be $(2,3)^-$.

5.2.5 The High L Transfer States and Levels Above 9 MeV

Several states having spins possibly equal to 6 or greater were observed. The characteristics associated with high L transfer in the (p,p') reaction is that the angular distributions of such excited states are isotropic at low proton beam energy, as can be seen in Fig. 4.8. The 8.186 and 8.974 MeV levels are observed with L=6 transfer, and their J^π-values are tentatively assigned as 6^+. The L=7 transfer to the 8.848 MeV state and its angular distributions show systematic agreement with the collective model predictions at four beam energies. This state is tentatively

assigned $J^{\pi}=(6^-,7^-)$. The same assignment is given to the 9.237 MeV level but with less confidence, for there is only one angular distribution analyzed and compared with theory.

It is believed that these high spin states in the Ca^{40} nucleus have been observed and identified in this experiment for the first time. Extreme care has been taken in the analysis of these states. However, further investigations by other types of reactions are needed to confirm these findings.

Finally, the spins and parities of a few levels above 9 MeV excitation energy are tentatively assigned from their apparent L-transfers, as listed in Table V-1. Due to the fact that the density of states is very high above 9 MeV (see Fig. 5.1), one to one correspondences with the results of Fuchs et al. and Leenhouts et al. was not made.

5.3 Comparisons of δ_L's and G's

Table V-2 summarizes the experimental nuclear deformations, δ_L, we obtained, and includes the present and previously reported experiments. Only comparable results are listed here. It can be seen that for the 3.73 MeV(3^-) state the energy dependence of δ_L on the incident proton energy is not obvious. For six beam energies and three independent experiments, the deformation was found to be more or less a constant 1.4 fm. The observations of two (α,α') measurements are consistent with each other and incidentally very

TABLE V-2.--Comparison of Nuclear Deformations, δ_L (F).

E_x (MeV)	L	(p,p')[a] This Exp. 40 MeV	(p,p') This Exp. 25 MeV	(p,p') Ref. 4 17 MeV	(p,p') Ref. 5 55 MeV	(α,α') Ref. 7 50 MeV	(α,α') Ref. 8 31 MeV	(e,e') Ref. 10 120-220 MeV
3.737	3	1.32	1.40	1.44	1.32	0.85	0.96	0.84
3.904	2	0.43	0.42	0.40		0.34	0.40	0.48
4.492	5	0.80	0.91		0.68	0.35	0.52	0.40
6.285	3	0.40	0.46	0.52		0.40	0.48	0.23
6.585	3	0.32	0.41	0.60		0.31	0.36	
7.114	5	0.27	0.40	0.68*				
7.867	2	0.23	0.28				0.32	
7.928	4	0.29	0.34			0.29	0.36	0.40
8.371	4	0.32	0.32			0.24	0.32	
8.535	5	0.18	0.23					0.31
8.578	2	0.14	0.17			0.19		

Ref. 4 (Gr 65)
Ref. 5 (Ya 64)
Ref. 7 (Sp 65)
Ref. 8 (Li 67)
Ref. 10 (Bl 63)
*L=3 was used

close to the (e,e') result, but only 2/3 of those obtained from (p,p').

The deformation of 3.90 MeV(2^+) state is independent of proton energy as well as of the type of scattering particle. Other even-parity states show about the same trend. For the 4.49 MeV(5^-) state, the (p,p') deformation is again about twice as large as the (α,α') findings. The results for the 6.28 MeV states are quite consistent in every case. The qualitative agreement between (α,α') and (p,p') experiments on 6.58 state can also be noted, except for the 17 MeV (p,p') work.

Statistically one finds that the deformations extracted at higher energy are consistently smaller than those at lower energies in both (p,p') and (, ') experiments. This trend of energy dependence may result from the model and analysis procedure used.

A comparison of the reduced transition probabilities with (e,e') and γ-decay experiments is made in Table V-3. The entries for the present experiments were from the calculations described in Chapter IV. Only those transitions with 100% to ground state branching, i.e., B(EL;O→L) are compared. As can be seen from the table the G values obtained in this experiment agree very well with the majority of all other results, especially those of Eisenstein et al. (Ei 69). It has been pointed out by these authors that their findings are relatively parameter-or model-dependent.

TABLE V-3.--Comparisons of Reduced Transition Probabilities, G(sp) in Weisskopk Single Particle Units.

Transition (100% or ~100%)		(p,p')[c] Present 40 MeV	(e,e') Ref. 11	(e,e') Ref. 10	Ref. 18[a] Ref. 24[b]	(p,p'γ) Ref. 19	(p,p'γ) Ref. 20	(p,p'γ) Ref. 21
3^-(3.737)	0^+(g.s.)	28.7±2.0	31.7	7.4±0.8		20.7±5.1		
2^+(3.904)→	"	2.05±0.2	2.0	2.4±0.75	4±1.3[a]	2.47±0.82	1.6±0.5	1.7
2^+(5.249)→	"	0.26±0.05				0.12±0.02		1.1
2^+(5.627)→	"	0.13±0.05				0.22±0.06	0.2±0.08	0.23±0.08
2^+(6.909)→	"	2.25±0.23	1.7	2.7±0.3	1.7[b]		1.7±0.15	4

Ref. 11 (Ei 69), Ref. 10 (Bl 63), Ref. 18 (Do 68), Ref. 24 (Me 68)
Ref. 19 (Po 69), Ref. 20 (An 69), Ref. 21 (Ma 68).

[c]Fermi equivalent, uniform charge distribution with Γ_0=1.33F, also see Section 4.1 and (Gr 69).

The striking agreement between this (p,p') and Eisenstein's (e,e') experiments indicate that the prescription proposed by Gruhn et al. (Gr 69), for the (p,p')B(EL)'s calculation allows the (p,p') results to be scaled against the (e,e') data reliably.

A comparison of $B(pp';\ 0\rightarrow L)$ and $B(\alpha\alpha';\ 0\rightarrow L)$ is shown in Table V-4.

TABLE V-4.--Comparisons of Reduced Transition Probabilities Between (p,p') and (α,α').

E_x	L	G_L (p,p') this work	G_L (α,α') (Li 67)*
3.90	2	2.05±0.20	2.9±0.5
5.62	2	0.13±0.05	0.7±0.2
7.87	2	0.92±0.15	1.8±0.4
8.10	2	0.38±0.06	2.1±0.3
3.73	3	28.7 ±3.0	23.6±3.5
6.29	3	3.1 ±0.3	6.6±1.0
6.58	3	2.5 ±0.3	3.8±0.6
7.94	4	2.2 ±0.2	5.6±0.8
8.38	4	2.0 ±0.2	4.3±0.6
4.48	5	20.6 ±2.1	17.7±2.7

*Also A. Bernstein, in Advances in Nuclear Physics, edited by M. Baranger and E. Vogt (Plenum Press, Inc. New York), Vol. III.

CHAPTER VI

MICROSCOPIC DESCRIPTION

A great deal of work, both theoretical and experimental, has been directed towards the understanding of the energy level scheme and transition rates in Ca^{40} in terms of the shell-model and its extensions (Gi 64, 67; Ku 66; Ge 68; Le 67; Di 68; etc.). The properties of the negative parity states in Ca^{40} have been most vigorously investigated. The RPA seems to give a reasonably good description of the salient features of these states which are formed predominately, although not entirely, from single particle-hole excitations. Positive-parity states are likely to contain large admixtures of many particle-many hole excitations, i.e. deformed components, and are not so easily described.

Recently some progress has been made in describing the (p,p') reaction in terms of a direct interaction between the projectile and target nucleons through an effective force. The properties of the effective force are largely dictated by the empirical two-nucleon potential. In particular, it has been shown by direct calculation that the bound state reaction matrix ("bare" effective force between bound nucleons) is a good guess at the "bare effective force in

the inelastic scattering process when the laboratory energy of the projectile is in the range from 15-70 MeV (Am 67; Sc 69; Pe 69; etc.). This is based on the studies of strong, normal parity inelastic transition and the real well of the optical potential which mainly test the strong central, iso-scalar component of the force. In these studies it was found that exchange effects are important, as was originally pointed out by Amos, Madsen, and collaborators.

In the present work, microscopic distorted wave approximation calculations are performed for some of the negative parity states of Ca^{40} and comparisons made with our (p,p') data. Random-phase-approximation state vectors of T. T. S. Kuo (Ku 66a) are used for the states of ^{40}Ca in the calculation and exchange effects are included approximately in the DW calculations. The Kallio-Kolltveit (K-K) force and the central part of the Hamada-Johnston (H-J) force are used for the projectile-target interaction. The latter is basically the same force which has been used in the RPA calculation.

6.1 Theory

The antisymmetrized distorted-wave transition amplitude for the spin-dependent nucleon-nucleus scattering reaction is given by

$$T_{DW} = \sum_{p,r} \langle B|a_p^+ a_r|A\rangle x$$

$$\langle \chi_b^{(-)}(0)\phi_p(1)|t(0,1)|\chi_a^{(+)}(0)\phi_r(1) - \chi_a^{(+)}(1)\phi_r(0)\rangle$$

where

$t(0,1)$ denotes the particle-target interaction, the

χ's are the distorted waves mentioned in Sec. 4.1

a_p^+, a_r are shell-model state creation or annihilation operators,

$|A\rangle, |B\rangle$ refers to the nuclear states, and

$|\phi\rangle$ is the single-particle shell-model state.

The first term in T_{DW} is the usual direct matrix element, the second is the exchange term which arises automatically from the antisymmetrization. Details concerning both the effective interaction and the nuclear wave functions used in this thesis are discussed in the following subsections. The procedures used to reduce the transition amplitude to partial matrix elements $\langle V\rangle$ using the nucleon-nucleon interaction

$$t(01) = \sum_{\substack{st \\ \lambda Y}} (-1)^{\lambda+Y} t_{st}(\vec{r}_{01}) \sigma_\lambda^s(0) \sigma_{-\lambda}^s(1) \tau_Y^T(0) \tau_Y^T(1)$$

have been given in detail by McManus and Petrovich (Pe 70). This program permits the separation of the details of the interaction model and the nuclear structure from the distorted wave calculation. With the approximate antisymmetrization the nuclear wave function and the radial form of

the interaction are further separated. The main features of their formulation are:

1) The form factor $\tilde{F}^{LSJ,T}$ is related to the transition density $F^{LSJ,T}$ by the expression

$$\tilde{F}^{LSJ,T}(r_0) = i^L \int r_1^2 dr_1 v_{STL}(r_0;r_1) F^{LSJ,T}(r_1)$$

The transition density $F^{LSJ,T}(r_1)$ contains all of the information on the nuclear wave functions and their coupling scheme. The function v_{STL} represents the radial form of the interaction including the exchange effects. Its explicit expression is

$$v_{STL}(r_0;r_1) = [t_{ST}(r_{01}) + A^{(1)}(\lambda_0^2)]\frac{\delta(r_0-r_1)}{r_0^2}$$

where the first term is related to the direct inelastic scattering and the second is the exchange.

2) The quantity $A^{(1)}(\lambda_0^2)$ is the first term of the Taylor expansion of the Fourier transformation of t_{ST}^E; they are related by

$$t_{ST}^E = \sum_{S'T'} A_{ST}^{S'T'} t_{ST}$$

$$A(\lambda^2) = \int e^{-i\bar{\lambda}\cdot\bar{r}_{01}} t_{ST}^E(r_{01}) d^3r_{01}$$

$$= A^{(1)}(\lambda_0^2) + (\lambda^2-\lambda_0^2)\frac{dA}{d\lambda^2}\Big|_{\lambda^2=\lambda_0^2} + \cdots$$

This is used to reduce the form of the exchange component of the partial matrix element to that of the direct component, so that the above expression for $\tilde{F}$ can be achieved. The simplest approximation for treating the exchange component is done by making

$$A(\lambda^2) \rightarrow A^{(1)}(\lambda_0^2),$$

where λ_0^2 is defined as

$$\lambda_0^2 = k_{LAB}^2 = 2ME_{LAB}/\hbar^2,$$

hence $A^{(1)}(\lambda_0^2)$ is energy dependent. This approximation is treated for the K-K and other effective range forces.

6.1.1 Effective Interaction

In analogy to the shell-model calculations using the G-matrix, the two-body interaction to be used in nucleon-nucleus scattering calculations is given by

$$t = v - v \frac{Q}{e - i\varepsilon} t, \quad t\phi = v\Psi$$

where v is the "bare" nucleon-nucleon potential, and Q is the Pauli operator which excludes all the occupied states. The energy denominator e is defined in accord with the conventions of Kuo and Brown (Kuo 66), but is appropriate for the scattering problem (see the appendix of (Sa 67)). The effective interaction used in this work was assumed to be

$$\bar{V}_{eff} = \sum_i t(i,a)$$

where the summation is over all active nucleons. It was also assumed that the two-body interaction t is local, state independent, and a scalar separately in spin, isospin and coordinate space. It has the form given by Kerman, McManus, and Thaler (Ke 59), i.e.,

$$t(i,a) = t_{00}(r_{ia}) + V_{10}(r_{ia})\vec{\sigma}_i\cdot\vec{\sigma}_a + t_{01}(r_{ia})\vec{\tau}_i\cdot\vec{\tau}_a + t_{11}(r_{ia})\vec{\sigma}_i\cdot\vec{\sigma}_a\vec{\tau}_i\cdot\vec{\tau}_a$$

In the above relations the double subscript on t is to be read as ST, referring to the multipole components of the force in spin and isospin space respectively.

Approximations which under certain conditions give simplified expressions for t(ia) have been given. This can be written, if the imaginary part of t is small, as

$$t \simeq t_B - i\pi t_B Q\delta(e) t_B$$

where t_B is real and satisfies the relationship

$$t_B = v - v\frac{Q}{e}t_B.$$

Using the Scott-Moskowski separation method and taking the Hamada-Johnston potential (Ha 62) for the nucleon-nucleon potential v, Kuo and Brown have shown that the attractive even component of t_B can be represented by

$$t_B \simeq v - v_\ell \frac{Q}{e} v_\ell$$

$$\simeq v_\ell - v_{T\ell} \frac{Q}{e} v_{T\ell} \qquad \text{(attractive, even)}$$

where T denotes the tensor component of the long range part of v_ℓ of the H-J potential. It has been shown that (Ku 67, Pe 70) if the average effect of the odd state interaction is small, then near the target

$$t^{Even} = t_B^E - i\pi t_B^E Q\delta(e) t_B^E$$

$$t^{Odd} \simeq 0$$

and

$$t_B^E = v_\ell^{TE} - \frac{8}{\langle e \rangle} V_{T\ell}^2 + \frac{2S_{12}V_{T\ell}^2}{\langle e \rangle} \qquad \text{(triplet, even)}$$

$$= v_\ell^{SE} \qquad \text{(singlet, even)}$$

where S_{12} is the tensor operator.

The two-body interaction t used in the present calculations was further simplified such that

1) the imaginary part of t was neglected,
2) the tensor part of potential was not included.

One might expect that the calculations so performed for certain states would be quite inadequate for comparison with the corresponding experimental results. They were still used, partly because the existing program was not in readiness to include the tensor and imaginary parts of t

and partly because the effects of neglecting the tensor force was one aspect of the study.

The types of interactions under investigation are discussed briefly in the following:

A. The Kallio-Kolltveit force: In using this force t was approximated by

$$t \simeq V^{TE}(V^{SE})$$

The S-state condition was relaxed and the interaction was allowed to act only on even states. It was pointed out by Petrovich, McManus, and collaborators (Pe 69) that this requirement may lead to errors of up to 20% in the strength of the interaction. The explicit form of the interaction (Ka 64) is the following:

$$V^{KK}_{T,S}(r) = +\infty \qquad r \leq 0.4F$$

$$= -A_{T,S} e^{-\alpha_{T,S}(r-0.4)} \qquad r > 0.4F$$

where $A_T = 475.0$ MeV, $\alpha_T = 2.5214F^{-1}$

$A_S = 330.8$ MeV, $\alpha_S = 2.4021F^{-1}$

The above parameters were determined by fitting the potential to the scattering length and the binding energy of the deuteron.

B. The Kuo-Brown Force: given by ref. (Ha 62, Ku 67). The t was approximated by taking only the central force

$$t \simeq V_{\ell}^{TE} - \frac{8}{\langle e \rangle} V_{T\ell}^{2}.$$

C. Yukawa Force: A real 1F range Yukawa "equivalent" to the K-K force was used

$$V(r) = V_0 e^{-mr}/mr, \qquad m = 1.0F.$$

The strength V_0 was determined by a normalization procedure similar to that used for deformation parameters (see Sec. 4.3).

6.1.2 Wave Functions

Extensive calculations for the ground state and the odd parity states of Ca^{40} in terms of particle-hole configurations using the RPA method, have been carried out by Gillet and Sanderson (Gi 64, 67), Kuo (Ku 66), Leenhouts (Le 67), Dieperink et al. (Di 68) and Perez (Pe 69a). Effects of spherical and deformed state mixing between the odd parity states have also been reported by Gerace and Green (Ge 68). Moreover the simple shell-model picture for this nucleus was given by Erskine (Er 66), Seth et al. (Se 67) and Fuchs et al. (Fu 69).

Gillet and Sanderson predict the results of the diagonalization of the matrix elements of the effective two-body force taken between the single particle-hole shell-model states. The unperturbed energy of a particle-hole configuration is the appropriate value determined by experiments. The energies for proton particle-hole states are taken from those of Sc^{41} and K^{39} with $\Delta E(d_{3/2}^{-1}f_{7/2})$ equal to 6.71 MeV, whereas for neutron states are from Ca^{41} and Ca^{39} with $\Delta E'(d_{3/2}^{-1}f_{7/2}) = 7.37$ MeV. The difference in ΔE and $\Delta E'$ is accounted for by the average Coulomb energy shift. The effective force parameter of the spin and iso-spin dependent Gaussian potential (Calcium force) is 40~45 MeV and the oscillator parameter is 0.53. Isospin was not considered a good quantum number thus their results showed strong T mixing. States with calculated level energies below 10 MeV are shown in Fig. 6.1 along with the results of other investigations. However, Seth et al. and Fuchs et al. found from their proton stripping experiments that the odd parity excited states of Ca^{40} can be explained rather well by a predominantly simple shell-model and that T-mixing of low-lying states was much less than predicted. A summary of "configuration, spin and isospin" assignments to the Ca^{40} negative parity states in terms of $[d_{3/2}^{-1}f_{7/2}]$ and $[d_{3/2}^{-1}p_{3/2}]$ shell-model states has been given by Fuchs et al.

In his pure RPA treatment of the odd parity spectrum of Ca^{40}, Kuo used a G-matrix derived from the H-J potential

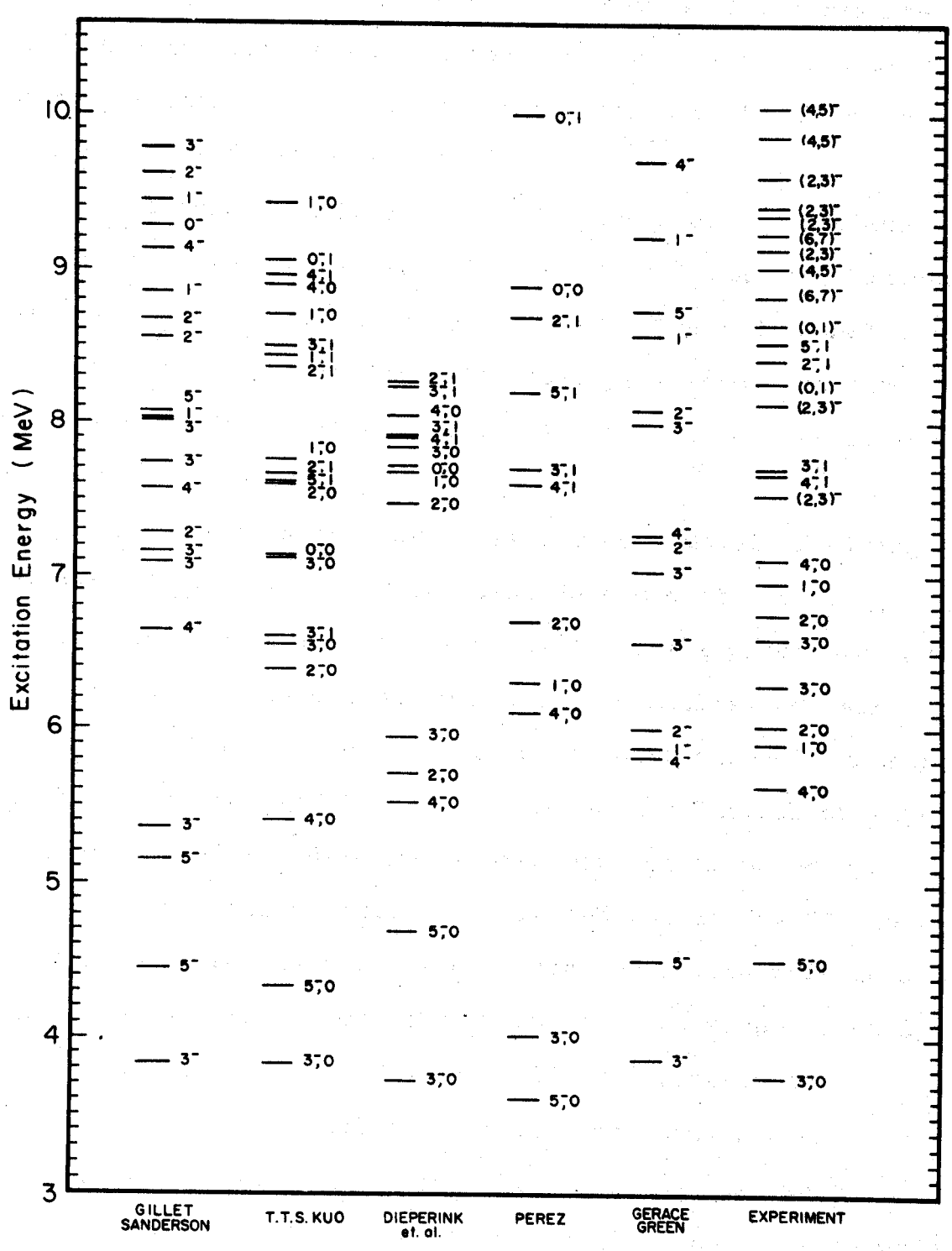

Figure 6.1.--Theoretical and experimental energy levels for negative parity states of ^{40}Ca.

for diagonalization. His spectrum is shown in the second column of Fig. 6.1 for the comparison with Gillet's results. Both RPA calculations encountered the difficulty of putting too much strength into the octupole transition to the ground state from the first 3^- state.

Dieperink's calculations used the modified surface delta interaction (MSDI) in both the RPA and TDA formulations, using a $[d^{-1}_{3/2}f_{7/2}]$ splitting of 7.3 MeV. Their diagonalized wave functions are very close to the unperturbed particle-hole states. The positions of the first four T=1 states were successfully predicted.

Gerace and Green have constructed a model of mixing shell-model 1p-1h states with 3p-3h deformed states to describe the odd parity states of Ca^{40}. Their procedure was to start with RPA wave functions which were obtained using $\Delta E(d^{-1}_{3/2}f_{7/2})$=5.4 MeV and SPE II. Kuo's particle-hole matrix elements were used and the effects of core polarization were included. The 3p-3h deformed states were constructed by first coupling Nilsson orbits no. 14 and no. 11 (Ge 67) to obtain a 1p-1h K=1 wave function, then recoupling this to a 2p-2h wave function to get the 3p-3h wave function. Finally matrix elements of the H-J potential taken between the $\langle$1p-1h$|_J$ and $|$3p-3h$\rangle_J$ deformed states were obtained and the diagonalization was carried out. The diagonalized wave functions contain RPA wavefunctions and deformed |3p-3h> wave functions as illustrated in their paper. Their calculated

spectrum is in good agreement with the experimental one below 8 MeV.

Fuchs et al. have derived the spectroscopic factors for their (d,n) work using Gerace and Green's wave functions and assuming the K^{39} ground state to be a pure $d_{3/2}$ hole. They found that the theory agreed with experiment very well except a few discrepancies. Goode (Go 70) has calculated several E2 decays for the low-lying T=0 odd parity states of Ca^{40}. It was shown that a pure RPA description of these decays was not satisfactory, whereas Gerace and Green's picture provides a consistent explanation of the B(E2) values. In the comparison with the results of this thesis, several predictions of Gerace and Green were supported. For example, the deformed nature of the first 1^- state at 5.90 MeV and the predicted existence of the level sequence 3^-, 2^-, 4^- around 7 MeV are confirmed.

The purpose of this section is to summarize some of the current theoretical descriptions for the wave functions of the odd parity states of Ca^{40}, so that one can estimate the uncertainties in the DWBA calculations due to the wave functions used. In this thesis T. T. S. Kuo's wave functions were used. It seems to be clear that Gerace and Green's wave function should have been used, but the existing program did not include the code to treat their wave functions.

6.2 The Calculations

The procedure used in the distorted wave calculation for the microscopic model is the same as that for the collective model as described in Section 4.3. An external real form factor is input into JULIE. The optical model parameters used are the same as those for collective model studies. To obtain the external form factor, two separate programs NUCFAC and FBART were used. Both were written by F. Petrovich.

6.2.1 Transition Density

NUCFAC calculates the transition density $F^{LSJ,T}$ which uses nuclear wave functions as input. When harmonic oscillator wave functions are used, F^{LSJ} can always be written in the following form

$$F^{LSJ}(r) = \sum_{N_a}^{N_b} C_N^{LSJ} \alpha^{N+3} r^N e^{-\alpha^2 r^2}$$

where $N_a = (\ell'+\ell)_{min}$

$N_b = (\ell+\ell'+2n+2n'-4)_{max}$

$\alpha = 0.498\ F^{-1}$ (in this work)

The explicit expressions for the oscillator wave functions and for the transition density can be found in Petrovich's thesis.

The wave functions used were given by Kuo (Ku 66a). For the convenience of future reference, they are listed

in Table VI-1. The resulting transition density functions are given in Table VI-2.

6.2.2 Form Factors

The form factor $\tilde{F}^{LSJ,T}$ was calculated using program FBART which performed the integration over the integrand $v(r_0,r_1)F(r_1)$. As mentioned in Section 6.1, v consists of two terms, a direct and an exchange. Form factor outputs can be obtained for direct only, or exchange only, or total.

For the K-K force, the separation distances were d_s=1.025F, and d_T=0.925F respectively. The Fourier transformation amplitude $A^{(1)}(\lambda_0^2)$ is given in Table VI-3.

For the K-B force, the separation distances were $d_s=d_T$=1.025F. The Fourier transformation amplitude $A^{(1)}(\lambda_0^2)$ is shown in Table VI-4.

6.3 Results and Discussions

Calculations for the lst 1^-, T=0 state; lst 2^-, T=0,1 states; lst, 2nd and 3rd 3^-, T=0 states; lst 3^-, T=1 state; lst 4^-, T=0,1 states; lst 5^-, T=0,1 states; and 6^-, T=0,1 states were performed. The lst 3^-, T=0; and lst 5^-, T=0 states have also been investigated by Schaeffer and Petrovich. Comparison with the results of these authors and discussion on the calculations in this thesis will be presented in the following subsections.

TABLE VI-1.--RPA Wave Functions Used (Given by T. T. S. Kuo).

J^π,T	E_{th} (MeV)		$1f_{7/2}\ 1d_{5/2}^{-1}$	$1f_{7/2}\ 2s_{1/2}^{-1}$	$1f_{7/2}\ 1d_{3/2}^{-1}$	$2p_{3/2}\ 1d_{5/2}^{-1}$	$2p_{3/2}\ 2s_{1/2}^{-1}$	$2p_{3/2}\ 1d_{3/2}^{-1}$	$1f_{5/2}\ 1d_{5/2}^{-1}$	$1f_{5/2}\ 2s_{1/2}^{-1}$	$1f_{5/2}\ 1d_{3/2}^{-1}$	$2p_{1/2}\ 1d_{5/2}^{-1}$	$2p_{1/2}\ 2s_{1/2}^{-1}$	$2p_{1/2}\ 1d_{3/2}^{-1}$
$0^-,0$	7.144							1.013	-0.042				-0.040	
$0^-,1$	9.052							0.987	0.031				0.170	
$1^-,0$	7.767		-0.187			0.440	0.005	0.715	-0.009		-0.024		0.021	0.516
$1^-,0$	8.449		0.065			-0.066	0.024	-0.948	-0.003		-0.035		0.002	0.306
$2^-,0$	6.393		0.219		0.896	-0.005	0.088	-0.361	0.061	0.043	0.068	0.026		0.100
$2^-,1$	7.672		0.336		0.121	0.080	-0.891	-0.051	0.051	-0.040	-0.015	0.023		0.255
$3^-,0$	3.826	X	-0.378	-0.538	-0.736	-0.126		-0.215	0.199	0.233	-0.285	0.146		
		Y	-0.201	-0.236	-0.222	-0.085		-0.130	0.107	0.129	-0.163	0.087		
	6.558	X	0.019	-0.509	0.569	-0.138		-0.617	0.015	0.120	-0.017	0.139		
		Y	-0.012	-0.072	-0.031	-0.030		-0.060	0.028	0.051	-0.026	0.045		
	7.118	X	0.044	0.625	-0.255	-0.107		-0.720	0.001	-0.078	-0.001	0.091		
		Y	0.015	-0.034	0.001	-0.008		0.016	-0.013	0.003	0.024	0.000		
$3^-,1$	6.567		0.052	0.198	-0.963	-0.013		0.166	0.035	0.044	0.041	0.012		
$4^-,0$	5.407		0.147	0.053	0.980	0.014			-0.007		0.131			
$4^-,1$	6.521		0.018	0.146	0.990	0.010			0.025		0.025			
$5^-,0$	4.323		-0.153		-1.005				0.215					
$5^-,1$	7.610		-0.186		0.984				-0.029					
$6^-,0$	12.730		1.000											
$6^-,1$	12.309		1.000											

TABLE VI-2.--Transition Density Function

$$F^{LSJ}(r) = \sum_{N_a}^{N} b_{\alpha N+3} r^{N} e^{-\alpha r^2}$$

J ,T	E_{th} (MeV)	LSJ,T	C_N^{LSJ} N=1	N=3	N=5
0^-,0	7.144	110,0	-1.140	1.841	-0.737
0^-,1	9.052	110,1	0.484	1.159	-0.527
1^-,0	7.767	101,0	-0.023	-1.373	0.484
1^-,1	8.449	101,1	0.053	0.146	-0.055
2^-,0	6.393	112,0	0.251	-0.441	-0.103
2^-,1	7.672	112,1	0.586	-0.714	-0.065
3^-,0	3.826	303,0		-1.128	0.909
		313,0		-0.231	0.264
3^-,0	6.558	303,0		-1.180	0.512
		313,0		-0.625	0.175
3^-,0	7.118	303,0		-0.457	0.114
		313,0		-0.393	0.153
3^-,1	6.567	303,1		0.198	-0.003
4^-,0	5.407	314,0		0.051	0.082
4^-,1	6.521	314,1		0.104	0.072
5^-,0	4.323	505,0			-0.265
		515,0			-0.175
5^-,1	7.610	505,1			0.178
		515,1			0.204
6^-,0					0.316
6^-,1					0.316

TABLE VI-3.--$A^{(1)}(\lambda_0^2)$ for the K-K force.

Ep (MeV)	A_{00}	A_{10}	A_{01}	A_{11}
25	-206.0	40.0	97.0	68.0
30	-180.0	33.9	26.3	60.1
35	-159.0	28.8	77.7	53.0
40	-138.0	23.7	68.2	45.9

TABLE VI-4.--$A^{(1)}(\lambda_0^2)$ for the K-B force.

Ep (MeV)	A_{00}	A_{10}	A_{01}	A_{11}
25	-166.5	31.5	79.5	55.5
30	-146.0	26.6	67.7	48.6
35	-127.5	22.6	62.5	42.5
40	-112.0	19.1	55.5	97.3

6.3.1 The 1^-, T=0 State:

The major p-h components of the wave functions for this RPA 1st 1^- state are $[2p_{3/2}d_{5/2}^{-1}]$, $[2p_{3/2}d_{3/2}^{-1}]$ and $[f_{5/2}d_{5/2}^{-1}]$. The calculated angular distributions at 40 and 25 MeV are best fitted by the distributions of the 2nd experimental 1^- (6.944 MeV) state. Figure 6.2 shows good agreement both in shape and magnitude between theory and experiment if so assigned. The magnitude of the distribution at 5.900 MeV is about 10 times smaller than that theoretically predicted. Gerace and Green's (GG) calculations show that the 1st 1^- state is strongly deformed whereas the 2nd 1^- is a very pure RPA 1st 1^- state. Thus the assignment of the RPA 1st 1^- state to the 2nd experimental 1^- state is supported by Gerace and Green's theory. In other words, the microscopic DW calculations, the angular distributions obtained in this experiment, are in agreement with Gerace and Green's deformed model.

6.3.2 The 1st 3^-, T=0 State:

The antisymmetrized DW calculations for the lowest 3^- state have been previously reported by Petrovich and McManus (Pe 69), and Schaeffer (Sc 69). The results of the present calculations are shown in Fig. 6.3. For this 3^- state the magnitudes and positions of the maxima are well reproduced at each beam energy. The overall shapes of the experimental distributions are also qualitatively fitted indicating that the energy dependence of the exchange effects

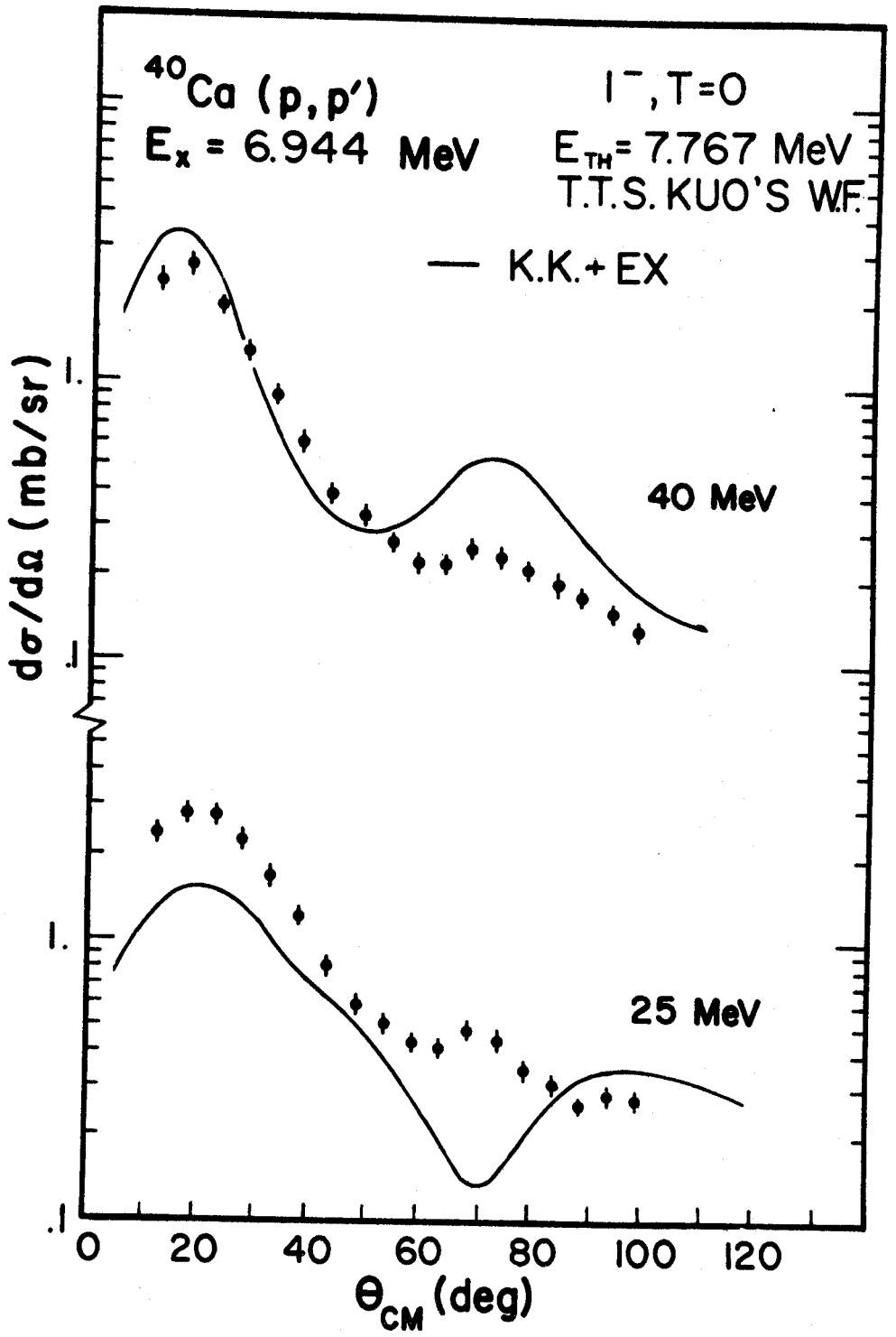

Figure 6.2.--Microscopic DW calculations for the 1^-, T=0 state.

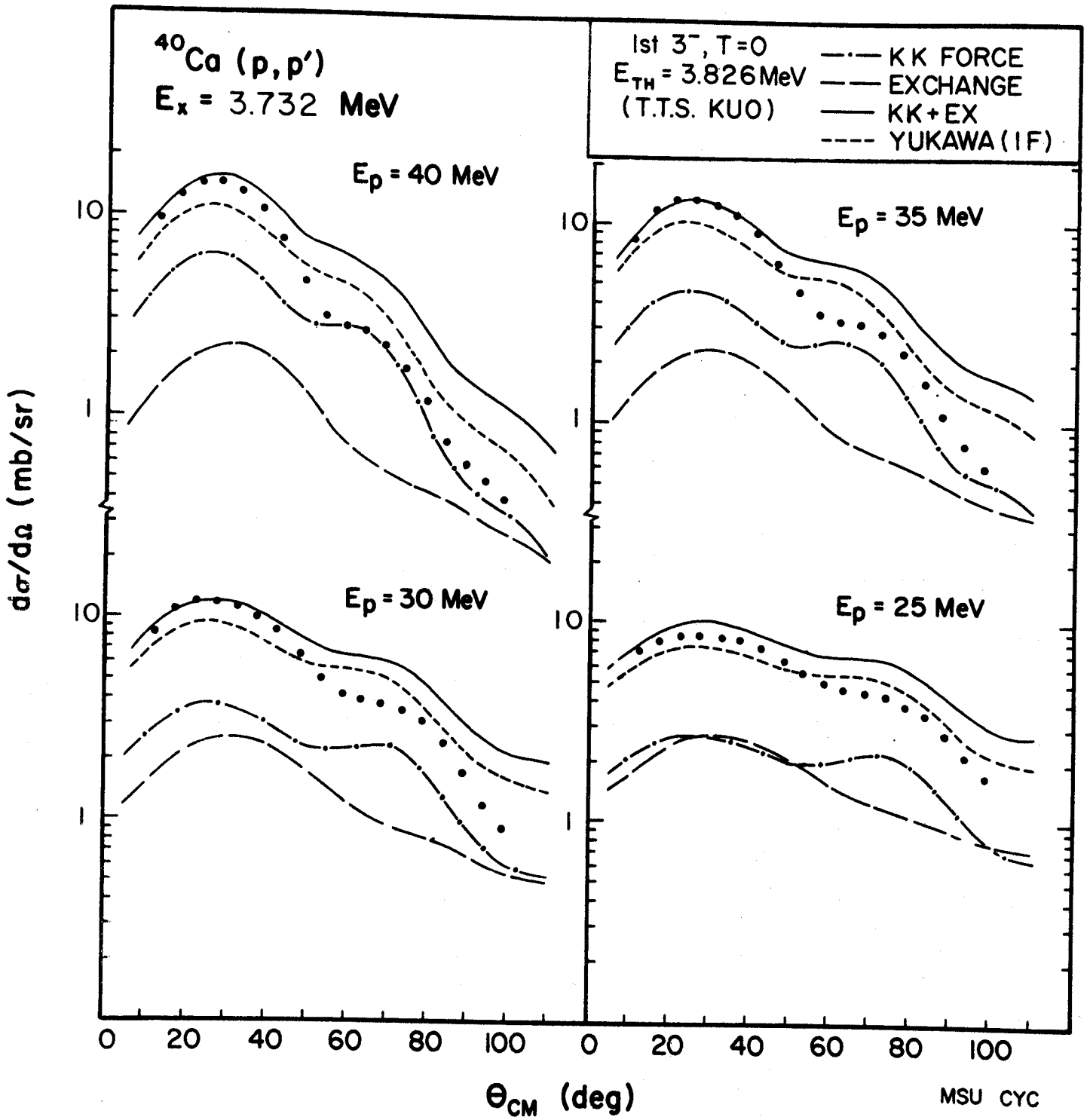

Figure 6.3.--Microscopic DW calculations for the 1st 3^-, T=0 state.

has been correctly accounted for. It can be seen from Fig. 6.3 that the contributions from exchange become increasingly important at the lower energy.

The calculations using 1 fm range "KK equivalent" Yukawa force are also illustrated in Fig. 6.3. The distributions are very similar to those obtained by using KK+EX forces. The results of KB+EX forces are not shown because the shapes of the calculated distributions (in direct, exchange and total) were found identical to those using KK+EX forces, except that the predicted magnitudes were found to be about 25% lower. This similarity applies to the calculations for the 2nd 3^- (6.285 MeV) and the 5^- (4.487 MeV) states.

Schaeffer has also performed similar calculations for Ca^{40} with proton energies from 17.3 to 55 MeV. He used the Blatt-Jackson potential and Gillet and Sanderson's wave functions. The dependence of exchange effects upon the energy was investigated by examining the ratio of the total cross section $\sigma[D+E]$ to the direct cross section $\sigma[D]$. A comparison of the results of his calculations with those obtained in this work are given in Table VI-5.

TABLE VI-5.--Ratio of total cross sections $\sigma[D+E]/\sigma[D]$.

E_p (MeV	3^-		5^-	
	Schaeffer	This* Work	Schaeffer	This* Work
17.3	2.7		6.8	
20.3	3.3		7.9	
25.0		3.5		7.8
30.0	2.9	3.1	6.4	6.4
35.0		2.8		5.5
40.0	2.5	2.5	4.6	4.8
50.0	2.3		3.6	

6.3.3 The 2nd and 3rd 3^-, T=0 States

Figure 6.4 shows the results of the calculations for the 6.285 MeV state using direct, exchange and a direct plus exchange force. The experimental cross sections are again well reproduced except at 40 MeV and at large angles where the exchange contributions are overestimated. The energy dependence of the exchange effects with respect to the direct term can easily be seen as in the case of the 1st 3^- T=0 state.

A comparison of the experimental angular distributions between this 3^- and the 1st 3^- states reveals some differences which may be attributed to the nuclear wave functions or to the mechanism of the interaction or both. The agreement between the antisymmetrized distorted wave (ADW) calculations

*Both KK and KB forces give the same results.

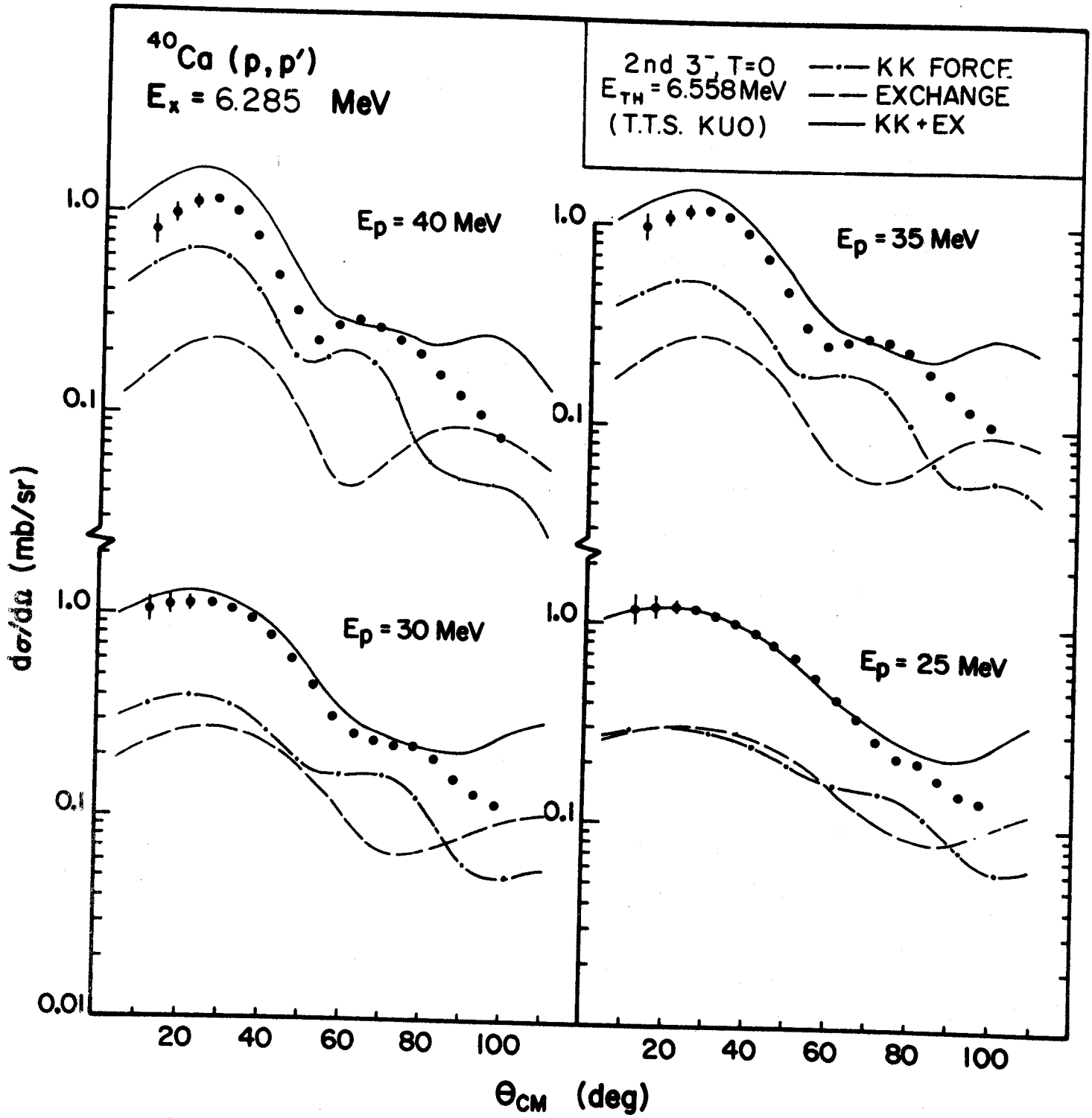

Figure 6.4.--Microscopic DW calculations for the 2nd 3^-, T=0 state.

and the experimental results seems to suggest that the RPA descriptions for this state are quite good. However, difficulties were encountered when the ADW calculations for the 3rd RPA 3^- state were compared with the distributions of the 3rd 3^- of the experimental spectrum. It was found that the calculated cross sections were 10 times too low, as can be seen in Fig. 6.7. On the other hand, the experimental distributions of the 2nd and 3rd 3^- look very similar not only in detailed variations but also in the absolute magnitude. It is possible that the calculations shown in Fig. 6.4 actually correspond to the 3rd experimental 3^-.

The extended shell-model calculations of Gerace and Green (Ge 68) show that the 3rd 3^- is made up entirely of the 2nd RPA 3^- and their 2nd 3^- is a mixture of the 3p-3h deformed state as well as the contributions from the 1st and the 2nd RPA 3^- states. The electric transition rates to the ground state from their 2nd and 3rd 3^- states were found about equal (1.9 vis 2.7) when SPE II was used. Gerace and Green's picture is in consistence with the excitation strength measured in this experiment (2.5 vis 1.7).

Thus a conclusion can be drawn that the 1st and 2nd RPA 3^- are good wavefunctions but the 3rd is not. The 2nd and 3rd experimental 3^- probably have similar microscopic structures either of which may be described by $\psi_2^{3^-}$ (RPA). Finally Gerace and Green's theory resolved the difficulties of RPA in giving satisfactory wavefunctions for the 3rd 3^- state.

6.3.4 The 5^-, T=0,1 States

The ADW calculations for the 5^-, T=0 (4.48 MeV) state are shown in Fig. 6.5. The exchange term dominates the contribution to give the correct magnitudes of the differential cross sections but overshoots somewhat at large angles. The contributions from the direct term are small as can be seen from Fig. 6.5 and the $\sigma[D+E]/\sigma[D]$ ratio in Table VI-5. The ADW calculations for this state demonstrate the extreme importance of the exchange effect in predicting the correct magnitude of the angular distributions.

The results of the 1st 5^-, T=1 state are shown in Fig. 6.7. The distributions of the components LSJ=505 and 515 were found comparable in magnitude. The total distribution is the incoherent sum of these two components. The corresponding experimental results (see Fig. 3.2) show that the calculations predict the correct normalization.

The particle-hole configurations of these RPA 5^-, T=0,1 states are mainly $[f_{7/2}d_{3/2}^{-1}]$, in good agreement with the results of (He^3,d) and (d,n) measurements and the theory of Gerace and Green.

6.3.5 The Unnatural Parity States

The ADW calculations were done for the 2^-, T=0 state (6.025 MeV) at four energies, and for the 2^-, T=1 state (8.412 MeV) at 25 and 40 MeV. The results are illustrated in Fig. 6.6. At Ep=40 MeV, both T=0 and T=1 states are qualitatively reproduced. The calculations systematically

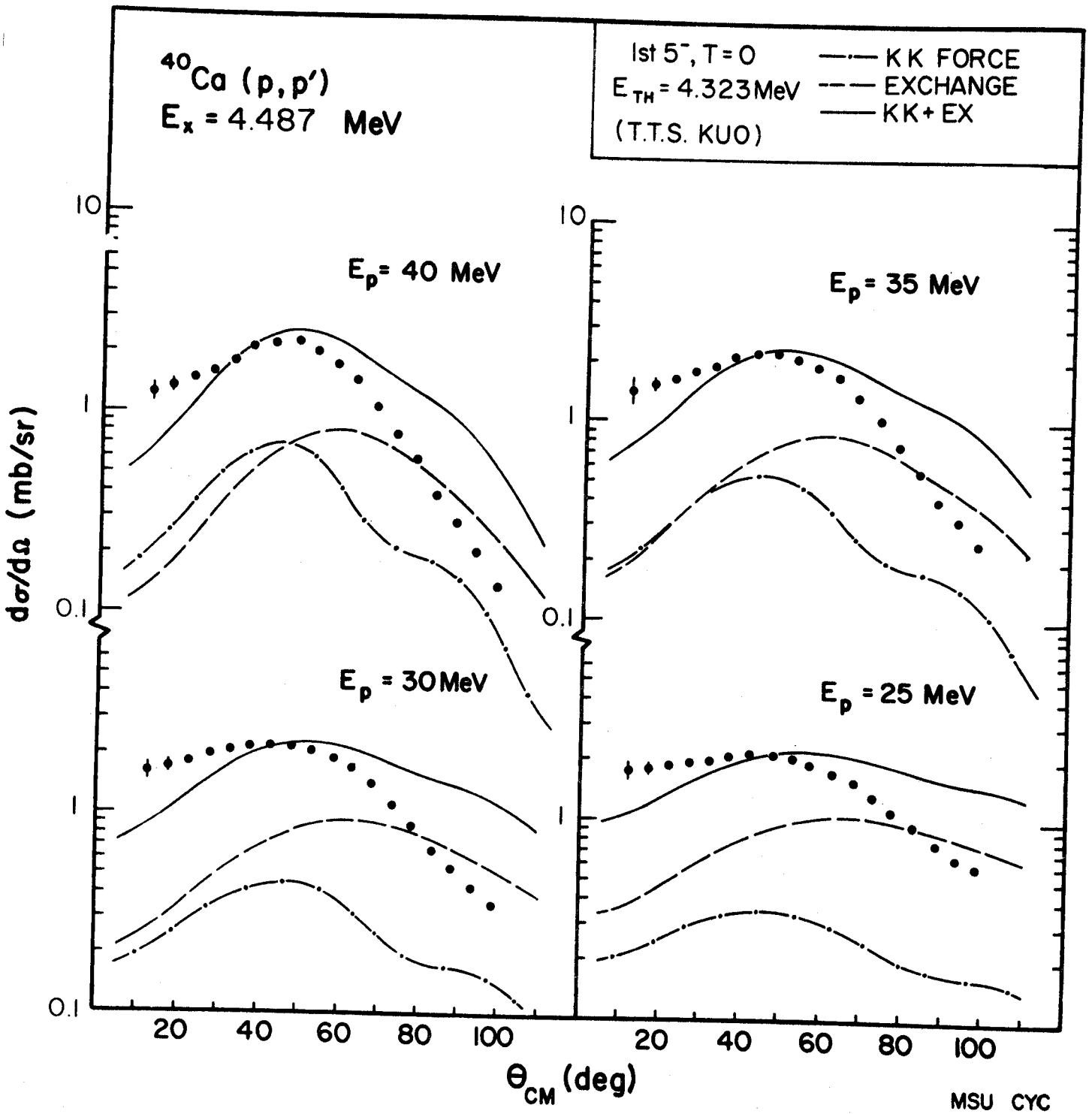

Figure 6.5.--Microscopic DW calculations for the 1st 5$^-$, T=0 state.

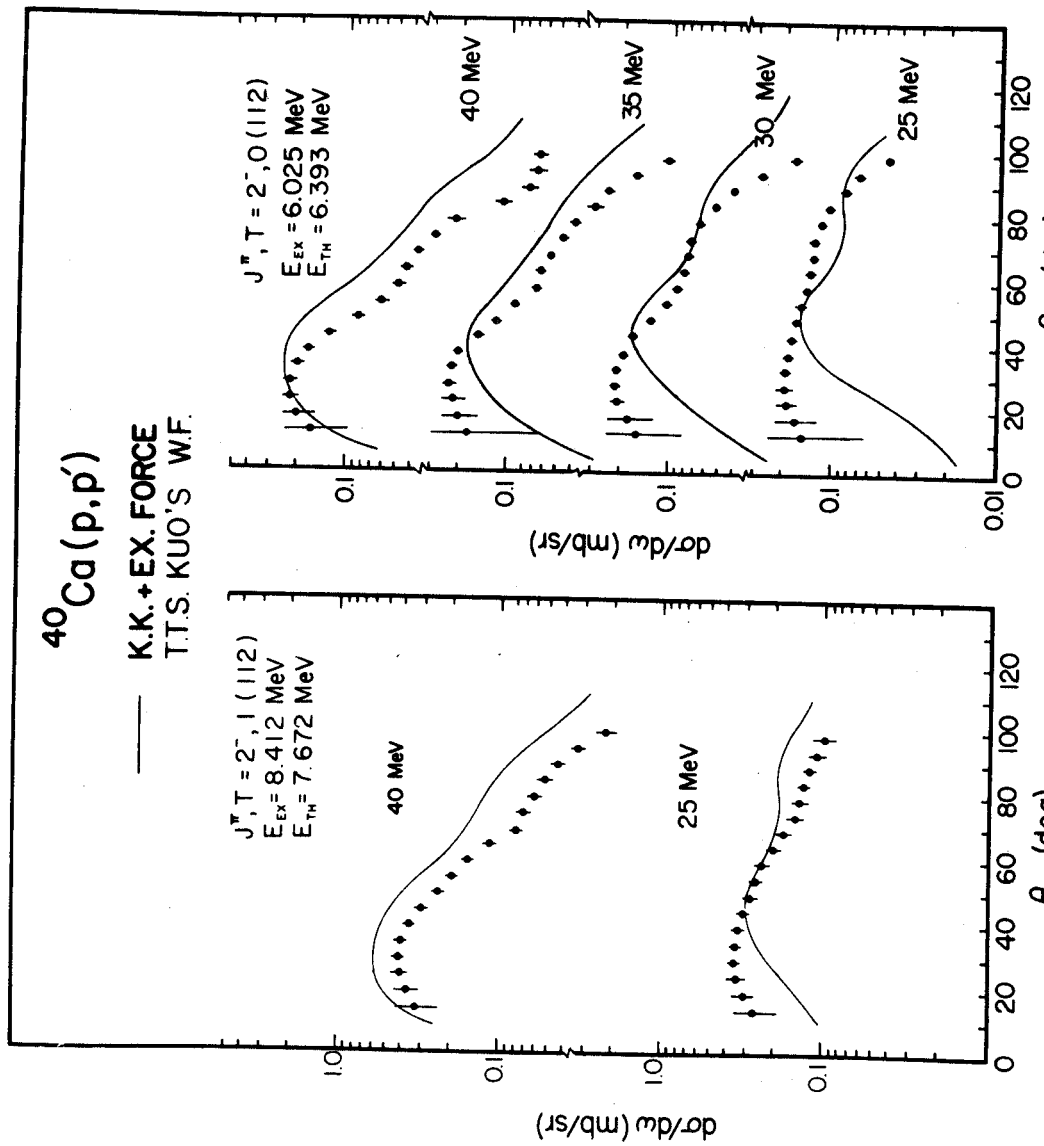

Figure 6.6.--Microscopic DW calculations for the 1st 2^-, T=0,1 states.

underestimate the differential cross sections at small angles.

The results for the first 4^-, T=0 and T=1 states are shown in Fig. 6.7. The predicted differential cross section for the 4^-, T=0 state is about 20 times lower than the experimental results of the 5.62 MeV state (see Fig. 4.7). This serious discrepancy has been carefully examined and was found not to be due to any error or mistake introduced in the procedure of calculation. On the other hand, this theoretical distribution resembles in shape to the experimental counterpart. For the 4^-, T=1 state, the predicted magnitude of the cross section is about 1/2 of the estimated experimental results (the 4^-, T=1 level at 7.660 MeV was not resolved, but a few clean spectra enabled the estimation of the cross section to be made). It was also noted that both calculated distributions of the 4^- T=0 and T=1 are similar.

Finally, results for the 6^-, T=0 and T=1 were also obtained as shown in Fig. 6.7. (Note that the labelings are correct.) The experimentally observed 6^- or 7^- level at 8.845 MeV may be assigned to the theoretical 6^-, T=1 state. The assignment of the 9.237 MeV level to the theoretical 6^-, T=0 state is also encouraging, because the predicted differential cross sections are close to those of the 9.237 MeV level.

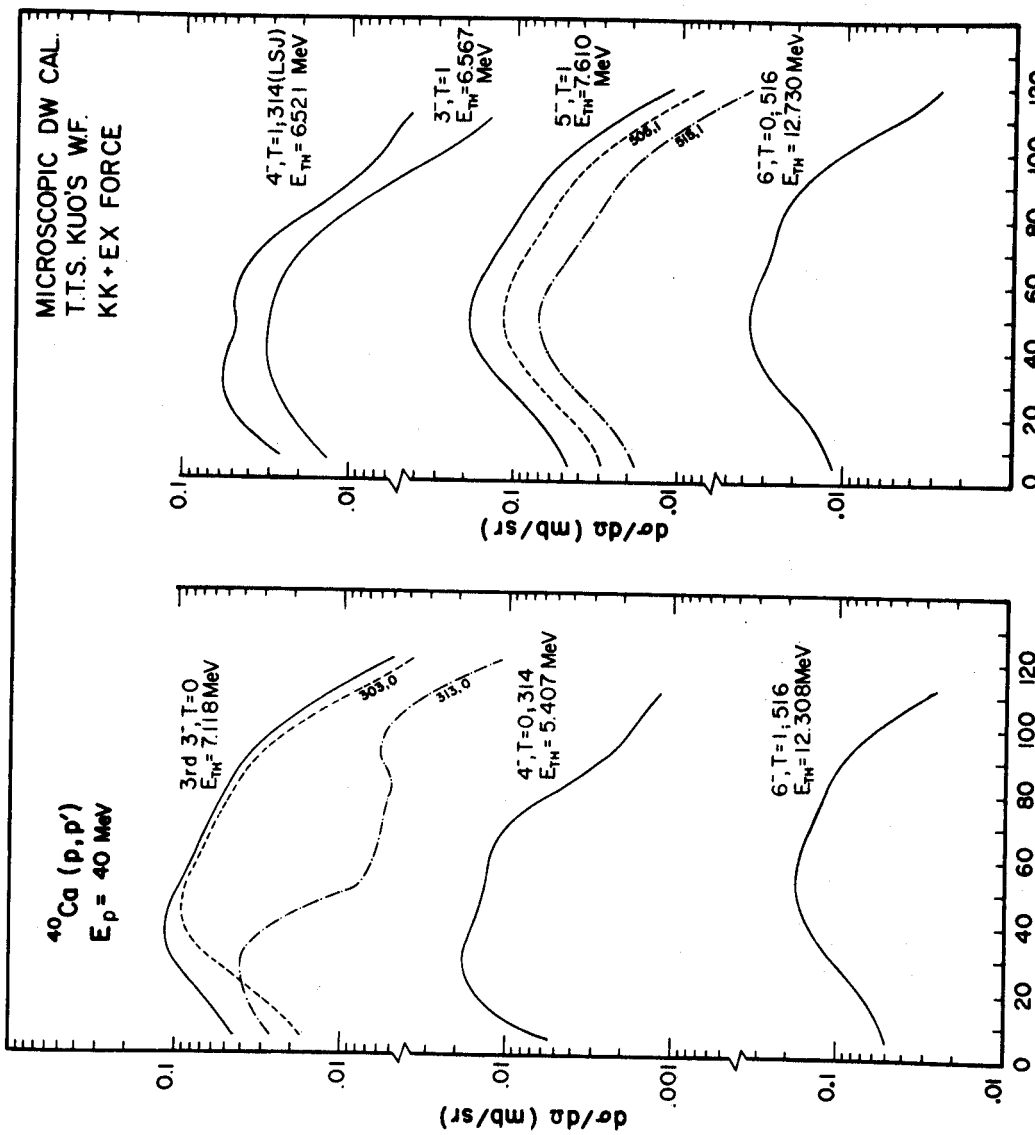

Figure 6.7.--Microscopic DW calculations for the 3rd 3^-, T=0; 1st 3^-, T=1; 1st 4^-, T=0,1; 6^-, T=0,1 states.

The RPA wave functions of these forementioned unnatural parity states are more or less pure single particle-hole states (see Table VI-1). They are

RPA 1st 2^-, T=0 $\sim f_{7/2} d_{3/2}^{-1}$

RPA 1st 2^-, T=1 $\sim 2p_{3/2} 2S_{1/2}^{-1}$

RPA 1st 4^-, T=0,1 $\sim f_{7/2} d_{3/2}^{-1}$

RPA 6^-, T=0,1 $= f_{7/2} d_{5/2}^{-1}$

The similarities in the wavefunctions of the 4^- and 6^- states, as well as the differences between the 2^-, T=0 and 2^-, T=1 states are also reflected by the calculated distributions as expected. Gerace and Green's deformed model agrees with the RPA in presenting the wave functions for the 1st 4^- state. This $[f_{7/2} d_{3/2}^{-1}]$ configuration has been confirmed by Erskine, Seth et al. and Fuchs et al. in their $[He^3,d]$ and [d,n] experiments respectively. Thus the wavefunctions of this state are believed to be well understood. The failure of ADW calculation for this particular state must be due to the effective force used. Perhaps the tensor force will play an important role in regaining the correct normalization.

6.4 Discussions on Even-Parity States

6.4.1 Systematics

Fig. 6.8 shows all the even parity states observed in this experiment. The spacing between the vertical lines is in accord with a J(J+1) relationship for the energy of these states so that a graphical inspection for this relationship can be made. The length of the horizontal lines is proportional to the transition strength. The open circles are for those states observed in other experiments (see Table V-1).

The low-lying even parity states of Ca^{40} have been described in terms of multiparticle-multihole configurations by Gerace and Green (Ge 67; Ge 69) and by Federman and Pittel (Fe 69; Fe 69b).

In their earlier paper (Ge 67), Gerace and Green considered some of the low-lying states as mixtures of the double closed 2s-1d shell model state (j=0) with two intrinsic deformed states (containing components with even angular momenta) formed by raising 2 and 4 particles from the $1d_{3/2}$ shell into the 2p-1f shell. They calculated the matrix elements of the Hamada-Johnston nucleon-nucleon force between the unperturbed deformed states and diagonalized the matrix to find the wave functions of the final perturbed states which are mixtures of 0p-0h, 2p-2h, 4p-4h configurations. The unperturbed energies of the 2^+ levels were

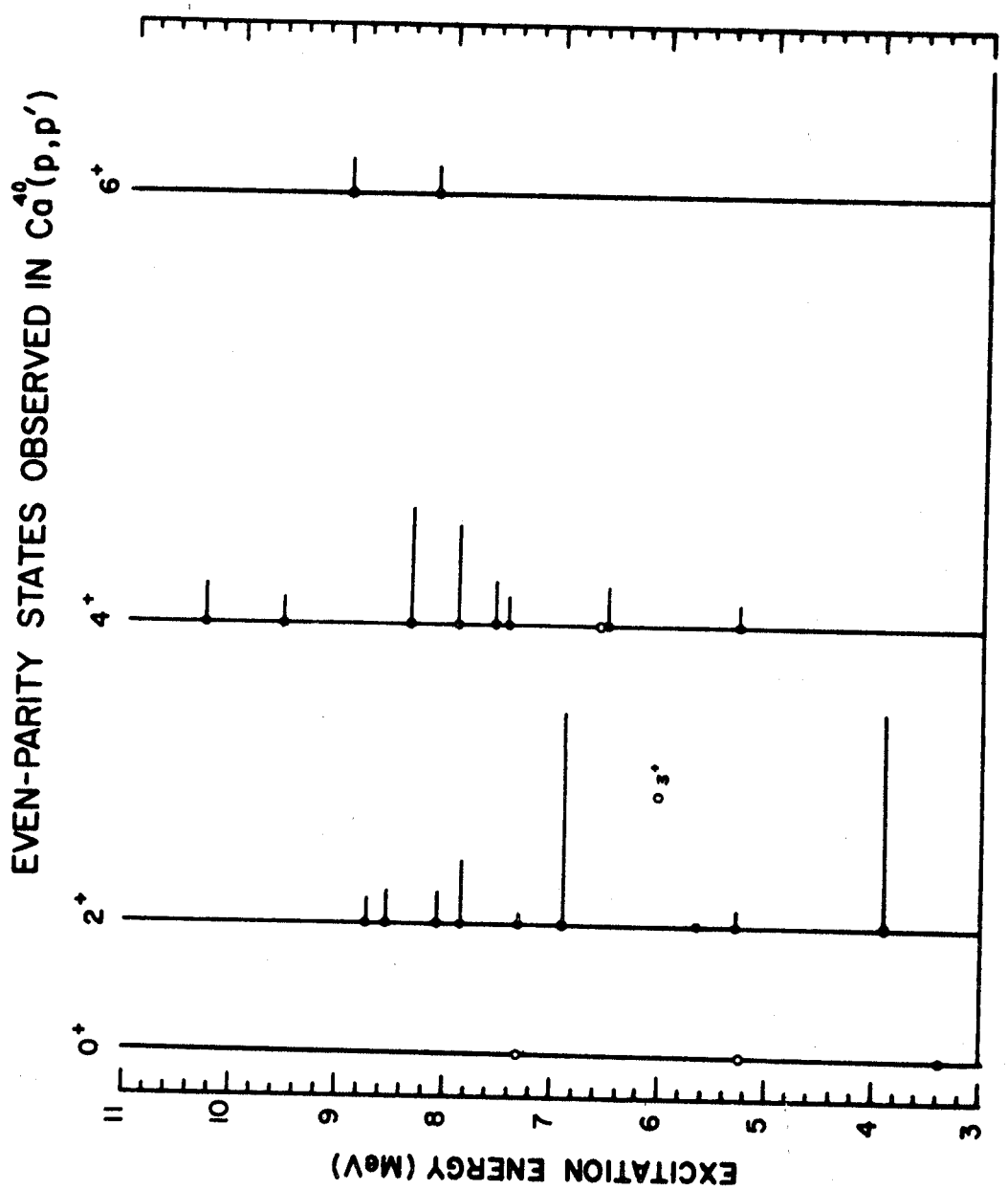

Figure 6.8.--Systematics of the even-parity states in Ca^{40} observed in this experiment. Open circles are those from other experiments.

adjusted to fit the perturbed energies of the same to those of the observed levels. The unperturbed energies of J=0 and J=4 levels were determined by the $\frac{\hbar^2}{2I}(J+1)J$ relationship with $\frac{\hbar^2}{2I} \simeq 0.1$. Their results are:

Main Configuration	0^+	2^+	4^+
4p-4h (mixed with 2p-2h)	3.55 MeV	3.90	5.25
2p-2h (mixed with 4p-4h)	7.33 MeV	6.90	8.00

where the two 0^+ states are further mixed with the $(0p\text{-}0h)^{J=0}$ configurations. The first sequence corresponds to the experimentally observed $3.35(0^+)$, $3.90(2^+)$ and $5.28(4^+)$ states which seem to form a perfect rotational band (see Fig. 6.8). For the second sequence, the 8.00 MeV level may be either the observed 7.92 or 8.10 MeV level. This 2p-2h sequence does not follow the J(J+1) relationship and no explanation on this aspect was given. Gerace and Green (Ge 69) also used their deformed model and mixing technique to account for the 5.20 MeV (0^+) and 5.24 MeV (2^+) states of Ca^{40}. K-band mixing and 6p-6h, 8p-8h deformed rotational bands were included. Their previous calculations (Ge 67) were modified to allow all-out mixing between 0p-0h, 2p-2h, 4p-4h, 6p-6h and 8p-8h configurations. Anderson et al. (An 69) compared their $(p,p'\gamma)$ results with Gerace and Green's picture. A k=2, 4p-4h band for $5.25(2^+)$, $6.03(3^+)$

and 6.51(4^+) MeV levels, and a k=0, 8p-8h band for 5.21(0^+), 5.63(2^+) and 6.54(4^+) MeV levels were constructed based on the enhancement of the in-band transitions. The former band does not obey the J(J+1) law whereas the latter does (see Fig. 6.8). Anderson et al. found that there was a general agreement between the experimental reduced matrix elements and the theoretical values for the 4p-4h and 8p-8h states. But they also pointed out a few discrepancies which demand further discussion.

Federman and Pittel (Fe 69), on the other hand, showed that an alternative description for the low-lying 0^+ levels of Ca^{40} is possible which does not require a 6p-6p or 8p-8h state. They proposed a weak coupling model in which the energies of the known 0^+ levels in Ca^{40} can be accurately reproduced. This model includes only 0p-0h, 2p-2h and 4p-4h configurations, but allows all possible intermediate spins and isospins. The calculated energies for the lst 3 0^+ states are 3.29, 5.22, 7.62 MeV, in excellent agreement with the experimental results. The same model was applied to the 2^+ states of Ca^{40} (Fe 69b). Again all 8 2^+ states are well reproduced by the calculated spectrum. It is realized that Gerace and Green's model attempted to retain the band structure of the deformed even-parity states, whereas Federman and Pittel's model emphasized only the configurations of the spectrum of a given even J, thus no calculation was made for 4^+ states.

These two models have enjoyed success in different areas and a comparison between them can only be made by an experiment on electromagnetic transitions between those states covered by both areas of studies.

So far, all the observed 0^+, 2^+ states and those 4^+ states below 7 MeV have been theoretically investigated. However, the 6^+ states and the 4^+ states above 7 MeV observed in this experiment may bring new information out of the band structures of the even-parity states in Ca^{40}. Further theoretical and experimental studies on this aspect are desired.

6.4.2 The 1st Excited 0^+ State

There is a general agreement between Gerace and Green (GG)'s and Federman and Pittel (FP)'s models that the 3.35 MeV level in Ca^{40} is mainly a 4p-4h deformed state. The 4p-4h strength predicted is about 70% by GG model and is about 83% by FP model. The $Ca^{42}(p,t)Ca^{40}$ experiment (Sm 69) showed that if the ground state is assumed to be a pure 0p-0h (shell-model) state, the 3.35 MeV 0^+ state is certainly not a pure 2p-2h state. This evidence complements GG's and FP's results.

The configuration of the ground state of Ca^{40} is described mainly by 0p-0h (~82%) mixed with 2p-2h (~17%). This mixture has been supported by $Ca^{40}(p,d)$, $Ca^{40}(He^3,He^4)$ reactions (Gl 65) and also by $K^{39}(He^3,d)$ experiment (Se 67). If one compares the wave functions of the ground state and

those of the 1st excited 0^+ state predicted by GG's model, such as

Ground	state:	0p-0h(0.91);	2p-2h(0.41)
3.35 MeV	state:	4p-4h(-0.83)	6p-6h(-0.45)

one finds that the 3.35 MeV state might be predominantly a 4p-4h excitation from the ground state as a whole.

In Section 4.7, it was mentioned that the (p,p') data obtained in this experiment could be fitted using an empirical form factor shown in Fig. 4.11, and that the fit is very sensitive to the relative size of the oscillation in the surface. If a form factor--calculated by using 4p-4h wave functions and appropriate effective interaction--could be obtained, it would be interesting to see the comparison between this theoretical form factor with the empirical one.

The decay modes of this state have recently been summarized by Harihar et al. (Ha 70). They concluded that the branching ratio of double γ emission with respect to internal pair emission is in the order of 4×10^{-4}. The probability for the decay of this 0^+ state by conversion electrons is also negligible.

CHAPTER VII

SUMMARY AND CONCLUSION

The angular distributions for protons inelastically scattered from various excited states of Ca^{40} have been measured at incident proton energies of 25,30,35 and 40 MeV. Data of about 50 states have been analyzed and the systematical and consistent variations of the distributions with respect to the proton beam energy were observed. The L-transfer quantum numbers for most of the observed states have been obtained and compared with the results of other experiments. Good agreements were obtained in general and some ambiguities that existed in previous experiments were clarified. It is concluded that the (p,p') experiment, performed at higher as well as various proton energies with a good detection system, enables one to determine the L-value with less uncertainty. States with spin-transfer larger than 5 have been observed and identified.

The DWBA collective model analysis has been carried out and the deformations δ_L's were extracted. It was found that the collective model was successful in predicting angular distributions in agreement with this experiment,

except for the cases of L=0 and L=1, where it is known to be incorrect description. Generally speaking, the collective DWBA distributions follow the same energy dependence patterns as those of the experimental observations. It also appeared that the overall shape and magnitude of the experimental angular distributions of a given L are roughly independent of beam energy and excitation energy. Therefore, the δ's extracted are more or less energy independent. However, this statement does not apply to every excited state. For example, the individual distributions of the 6.767 MeV state coincide in shape with those of the 3.732 MeV state, but the relative magnitudes in going from one energy to the next do not. Thus the observed energy dependent of δ for this 6.747 MeV state may be real and interpretations for this pehnomenon are to be desired.

The reduced transition probabilities B(EL) scaled for the (p,p') experiment were obtained using Fermi equivalent uniform-density-distributions.

Finally, the antisymmetrized distorted wave calculations have been performed for some negative parity states, using the K-K force and T. T. S. Kuo's R.P.A. wave functions. The particle-hole configurations of these states were investigated by examining the overall results of these ADW calculations and by comparing them with other theoretical and experimental results. The nature of the states under study were fairly well understood. It was also found that the central force used in the ADW calculations is adequate

in predicting the distributions of the normal parity states, but a tensor force may be essential to reproduce those of the unnatural parity states.

Considering the (p,p') reaction in conjunction with other types of experiments as a probe to study the nuclear structure of ^{40}Ca, one finds that the achievement of previously reported ^{40}Ca (p,p') experiments was limited. With the completion of this work, the accomplishments of the Ca^{40} (p,p') reaction have been much improved and its capabilities enhanced. The probability of further advancement may be high too. A (p,p') experiment performed at beam energy higher than 40 MeV with a resolution less than 10 KeV may be very fruitful.

REFERENCES

REFERENCES

(Ag 68) D. Agassi and R. Schaeffer, Phys. Letters 26B (1968)703.

(Ag 69) D. Agassi, V. Gillet, A. Lumbroso, Nucl. Phys. A130(1969)129.

(Am 67) K. A. Amos, V. A. Madsen, and I. E. McCarthy, Nucl. Phys. A94(1967)103.

(An 69) R. Anderson, A. G. Robertson, D. F. H. Start, L. E. Carlson, and M. A. Grace, Nucl. Phys. A131(1969)113.

(Ar 68) A. J. Armini, J. W. Sunier, and J. R. Richardson, Phys. Rev. 165(1968)1194.

(Ba 62) R. H. Bassel, G. R. Satchler, R. M. Drisko, and E. Rost, Phys. Rev. 128(1962)2693.

(Ba 65) R. W. Bauer, A. M. Bertsein, G. Heymann, E. P. Lippincott and N. S. Wall, Phys. Letters 14 (1965)129.

(Be 68) W. Benenson, R. deForest, W. P. Johnson, E. Kashy, Nuclear Inst. and Methods 64(1968)40.

(Bl 61) H. G. Blosser, Communication and Electronics, (January 1961).

(Bl 66) H. G. Blosser and A. I. Galonsky, IEEE Trans. on Nuclear Science, NS-13 No. 4, 466(1966).

(Bl 63) D. Blum, P. Barreau, and J. Bellieard, Phys. Letters 4(1963)109.

(Bl 66a) L. N. Blumberg, E. E. Gross, A. van der Woude, A. Zucker and R. H. Bassel, Phys. Rev. 147 (1966)812.

(Ca 67) J. M. Cameron, Technical Report P-80 University of California, Los Angeles, California (1967); Phys. Rev. 167(1968)908.

(Ca 69) T. R. Canada, R. S. Cox, J. S. Duval, C. H. Sinex and C. M. Class, Phys. Rev. 188(1969)1741.

(Di 68) A. E. L. Dieperink, H. P. Leenhouts, and P. J. Brussaard, Nucl. Phys. A116(1968)555.

(Do 68) K. W. Dolan and D. K. McDaniels, Phys. Rev. 175 (1968)1446.

(Ei 69) R. A. Eisenstein, D. W. Madsen, H. Theissen, L. S. Cardman and C. K. Bockelman, Phys. Rev. 188 (1969)1815.

(En 67) P. M. Endt and C. van der Leun, Nucl. Phys. A105 (1967)313.

(Er 66) J. R. Erskine, Phys. Rev. 149(1966)854.

(Fe 69) P. Federman and S. Pittel, Nucl. Phys. A139(1969) 108.

(Fe 69a) P. Federman, Nucl. Phys. A124(1969)363.

(Fe 69b) P. Federman and S. Pittel, Phys. Rev. 186(1969) 1106.

(Fo 70) J. S. Forster, K. Bearpark, J. L. Hutton and J. F. Sharpey-Schafer, Nucl. Phys. A150(1970) 30.

(Fr 67) M. P. Fricke, E. E. Gross, B. J. Morton, and A. Zucker, Phys. Rev. 156(1967)1207.

(Fu 69) H. Fuchs, K. Grabisch and G. Röschert, Nucl. Phys. A129(1969)545.

(Fu 68) S. A. Fulling, and G. R. Satchler, Nucl. Phys. A111(1968)81.

(Ge 67) W. J. Gerace and A. M. Green, Nucl. Phys. A93 (1967)110.

(Ge 68) W. J. Gerace and A. M. Green, Nucl. Phys. A113 (1968)641.

(Ge 69) W. J. Gerace and A. M. Green, Nucl. Phys. A123 (1969)241.

(Gi 64) V. Gillet and E. A. Sanderson, Nucl. Phys. 54 (1964)472.

(Gi 67) V. Gillet and E. A. Sanderson, Nucl. Phys. A91 (1967)292.

(Gl 65) C. Glashausser, M. Kondo, M. E. Rickey and E. Rost, Phys. Letters 14(1965)113.

(Go 70) P. Goode, Nucl. Phys. A140(1970)481.

(Go 68) M. M. Gordon, R. E. Berg, and H. G. Blosser, Nuclear Instr. and Methods 58, 327(1968).

(Gr 66) M. A. Grace and A. R. Poletti, Nucl. Phys. 78 (1966)273.

(Gr 65) W. S. Gray, R. A. Kenefick and J. J. Kraushaar, Nucl. Phys. 67(1965)542.

(Gr 69) C. R. Gruhn, B. M. Preedom, and K. Thompson, Phys. Rev. Letters 23(1969)1175(c).

(Gr 67) C. R. Gruhn, T. Y. T. Kuo, K. Thompson, and J. Frank, Bull. APS 12(1967)585.

(Ha 62) T. Hamada, and I. E. Johnston, Nucl. Phys. 34 (1962)382.

(Ha 70) P. Harihar, J. D. Ullman, and C. S. Wu, Phys. Rev. C2(1970)462.

(Ja 66) J. F. Janni, Air Force Weapons Laboratory Report AFWL-TK-65-150 (1966).

(Jo 58) L. H. Johnston and D. A. Swenson, Phys. Rev. 111 (1958)212.

(Ka 64) A. Kallio and K. Kolltveit, Nucl. Phys. 53(1964) 87.

(Ka 68) E. Kashy and J. L. Snelgrove, Phys. Rev. 172 (1968)1124.

(Ko 68) W. J. Kossler, Phys. Rev. 165(1968)1209.

(Ku 68a) T. T. S. Kuo, Private communication with H. McManus (1966).

(Ku 66) T. T. S. Kuo and G. E. Brown, Nucl. Phys. 85(1966) 40.

(Ku 67) T. T. S. Kuo, Nucl. Phys. A103(1967)71.

(Ku 68) T. T. S. Kuo and G. E. Brown, Nucl. Phys. A114 (1968)241.

(La 60) A. M. Lane and E. Pendelbury, Nucl. Phys. 15 (1960)39.

(La 68) D. Larner, S. A. Williams, Nucl. Phys. A107(1968) 354.

(Le 68) C. M. Lederer, J. M. Hollander and I. Perlman, Table of Isotopes, 6th edition (1968).

(Le 66) H. P. Leenhouts, and P. M. Endt, Physica 32 (1966)322.

(Le 67) H. P. Leenhouts, Physica 35(1967)290.

(Li 68) H. Lindeman, G. A. P. Engelbertink, M. W. Ockeleon and H. S. Pruys, Nucl. Phys. A122(1968)373.

(Li 67) E. P. Lippincott, and A. M. Bernstein, Phys. Rev. 163(1967)1170; E. P. Lippincott, Thesis (1967), MIT.

(Lo 67) W. G. Love, and G. R. Satchler, Nucl. Phys. A101 (1967)424.

(Lo 68) W. G. Love, Thesis, University of Tennessee (1968).

(Ma 68) J. R. MacDonald, D. F. H. Start, R. Anderson, A. G. Robertson and M. A. Grace, Nucl. Phys. A108 (1968)6.

(Ma 67) Mackenzie, G. H., E. Kashy, M. M. Gordon, and H. G. Blosser, IEEE Trans. on Nuclear Science, NS-14 No. 3, 450(1967).

(Ma 70) C. Maggiore, Ph.D. Thesis, Michigan State University, (1970).

(Ma 66) A. Marinov and J. R. Erskine, Phys. Rev. 147(1966) 826.

(Mc 64) H. McManus, Les Mecanismes des Reactions Nucleaires (1964)289.

(Me 68) F. R. Metzger, Phys. Rev. 165(1968)1245.

(Na 65) O. Nathan and S. G. Nilsson in Alpha-, Beta-, Gamma-ray Spectroscopy, edited by K. Siegbahn (North Holland Publishing Company, Amsterdam, The Netherlands, 1965), Chap. X.

(Or 62) (Or 67) R. H. Bassel, R. M. Drisko, and G. R. Satchler, Oak Ridge National Laboratory Report No. ORNL-3240, 1962 (unpublished); and Oak Ridge National Laboratory Memrandum to the Users of the Code JULIE, 1966 (Unpublished).

(Ow 64) L. W. Owen, and G. R. Satchler, Nucl. Phys. 51 (1964)155.

(Pe 69a) S. M. Perez, Nucl. Phys. A136(1969)599.

(Pe 69) F. Petrovich, H. McManus, V. A. Madsen and J. Atkinson, Phys. Rev. Letters 22(1969)895.

(Pe 70) F. Petrovich, Ph.D. Thesis, Michigan State University, (1970).

(Po 69) A. R. Poletti, A. D. W. Jones, J. A. Becker and R. E. McDonald, Phys. Rev. 181(1969)1606.

(Ri 64) B. W. Ridley and J. F. Turner, Nucl. Phys. 58 (1964)497.

(Sa 64) G. R. Satchler, Nucl. Phys. 55(1964)1.

(Sa 66a) G. R. Satchler, Private communication with C. R. Gruhn, 1966.

(Sa 66) G. R. Satchler, Nucl. Phys. 77(1966)481.

(Sa 67) G. R. Satchler, Nucl. Phys. A100(1967)481.

(Sa 67a) G. R. Satchler, Nucl. Phys. A95(1967)1.

(Sc 69) R. Schaeffer, Nucl. Phys. A132(1969)186.

(Se 67) K. K. Seth, J. A. Biggerstaff, P. D. Miller and G. R. Satchler, Phys. Rev. 164(1967)1450.

(Sm 69) S. M. Smith, and A. M. Bernstein, Nucl. Phys. A125 (1969)339.

(Sn 67) J. L. Snelgrove, and E. Kashy, Nucl. Inst. and Methods 52(1967)153.

(Sp 65) A. Springer and B. G. Harvey, Phys. Letters 14 (1965)116.

(Th 69) K. Thompson, Ph.D. Thesis, Michigan State University, (1969).

(Wi 67) C. William, Private communication.

(Ya 64) K. Yagi et al., Phys. Letters 10(1964)186.

APPENDICES

APPENDIX I

PLOTTED ANGULAR DISTRIBUTIONS

The following pages contain plots of the experimental center-of-mass angular distributions. All of the plots are shown on the same scale and in the same arrangement so that a direct graphical comparison of the collective theoretical results and experimental data can be made.

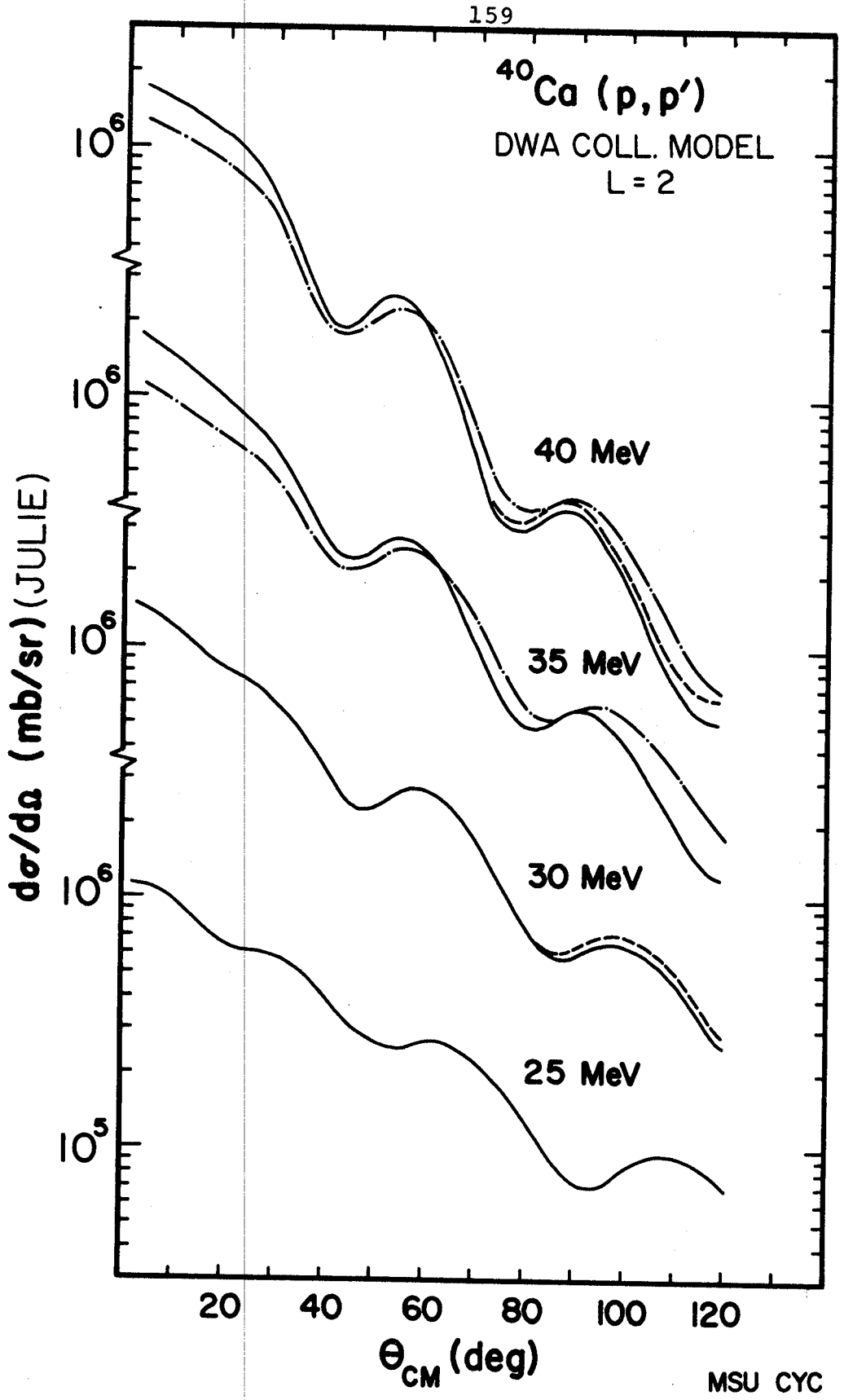
^{40}Ca (p, p')
DWA COLL. MODEL
L = 2
40 MeV
35 MeV
30 MeV
25 MeV
10^6
10^6
10^6
10^6
10^5
dσ/dΩ (mb/sr) (JULIE)
20
40
60
80
100
120
θ_{CM} (deg)
MSU CYC

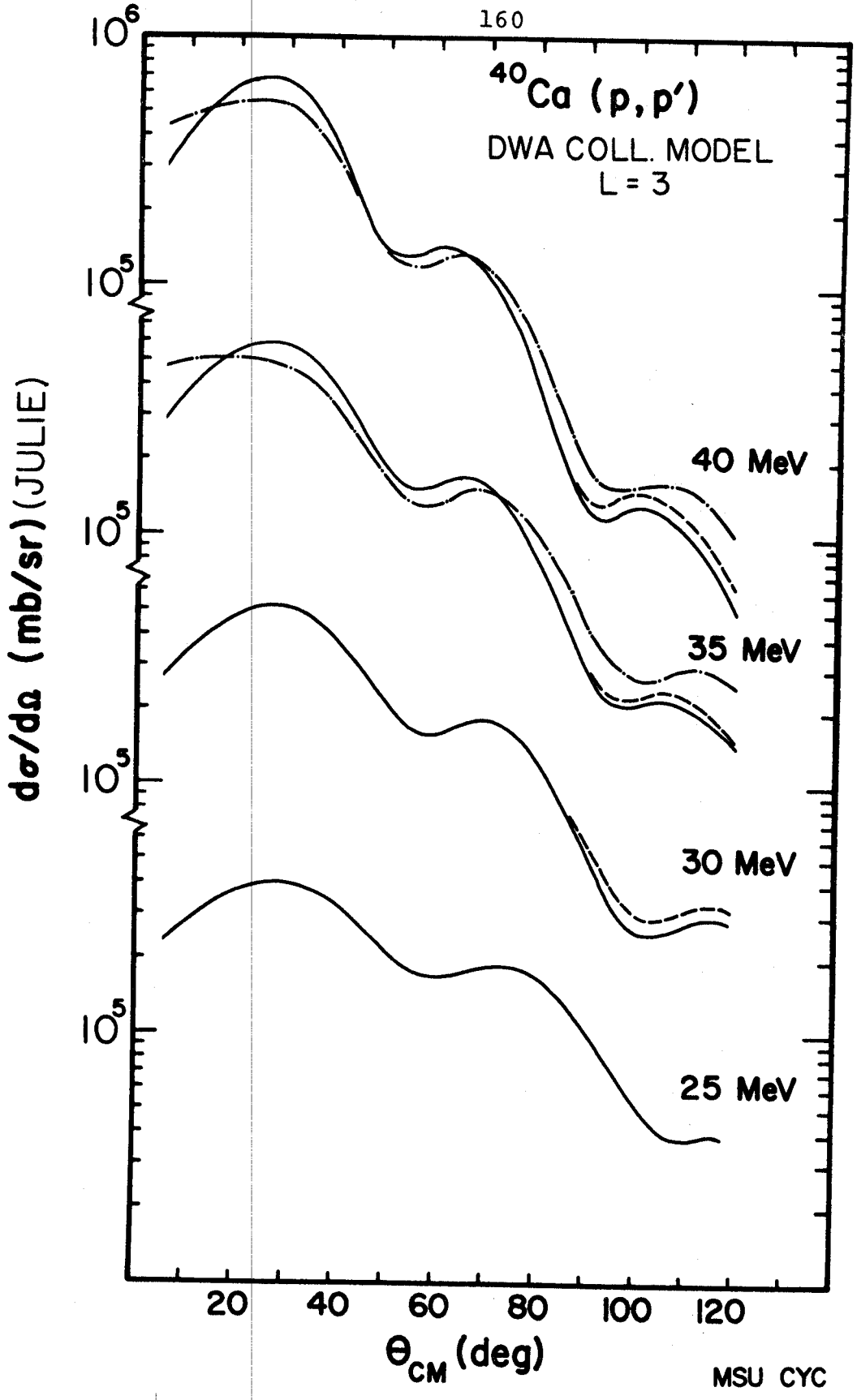
^{40}Ca (p, p')
DWA COLL. MODEL
L = 3
40 MeV
35 MeV
30 MeV
25 MeV
10^6
10^5
10^5
10^5
10^5
dσ/dΩ (mb/sr) (JULIE)
20
40
60
80
100
120
Θ_{CM} (deg)
MSU CYC

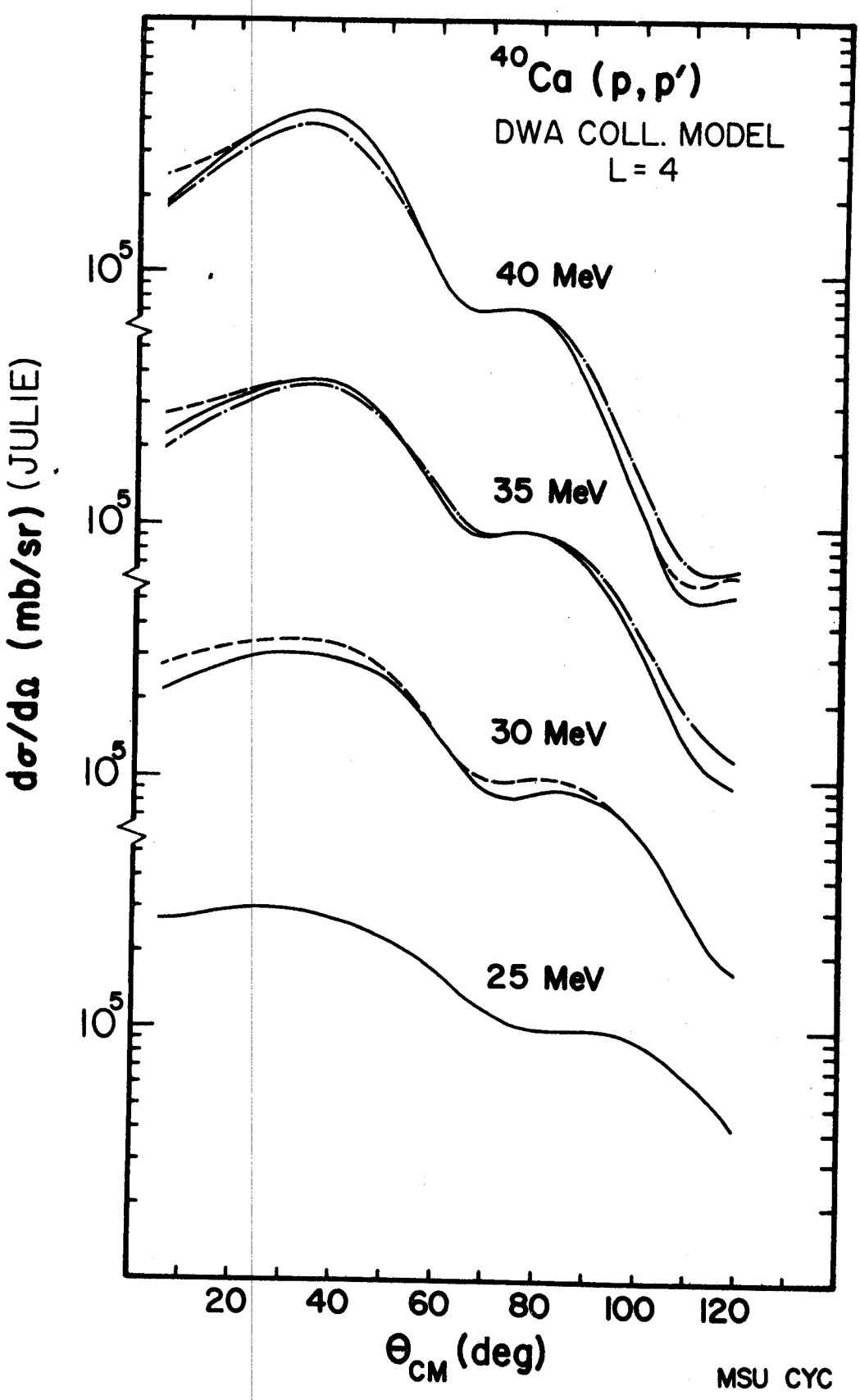
^{40}Ca (p, p′)
DWA COLL. MODEL
L = 4
40 MeV
35 MeV
30 MeV
25 MeV
10^5
10^5
10^5
10^5
dσ/dΩ (mb/sr) (JULIE)
20
40
60
80
100
120
Θ_{CM} (deg)
MSU CYC

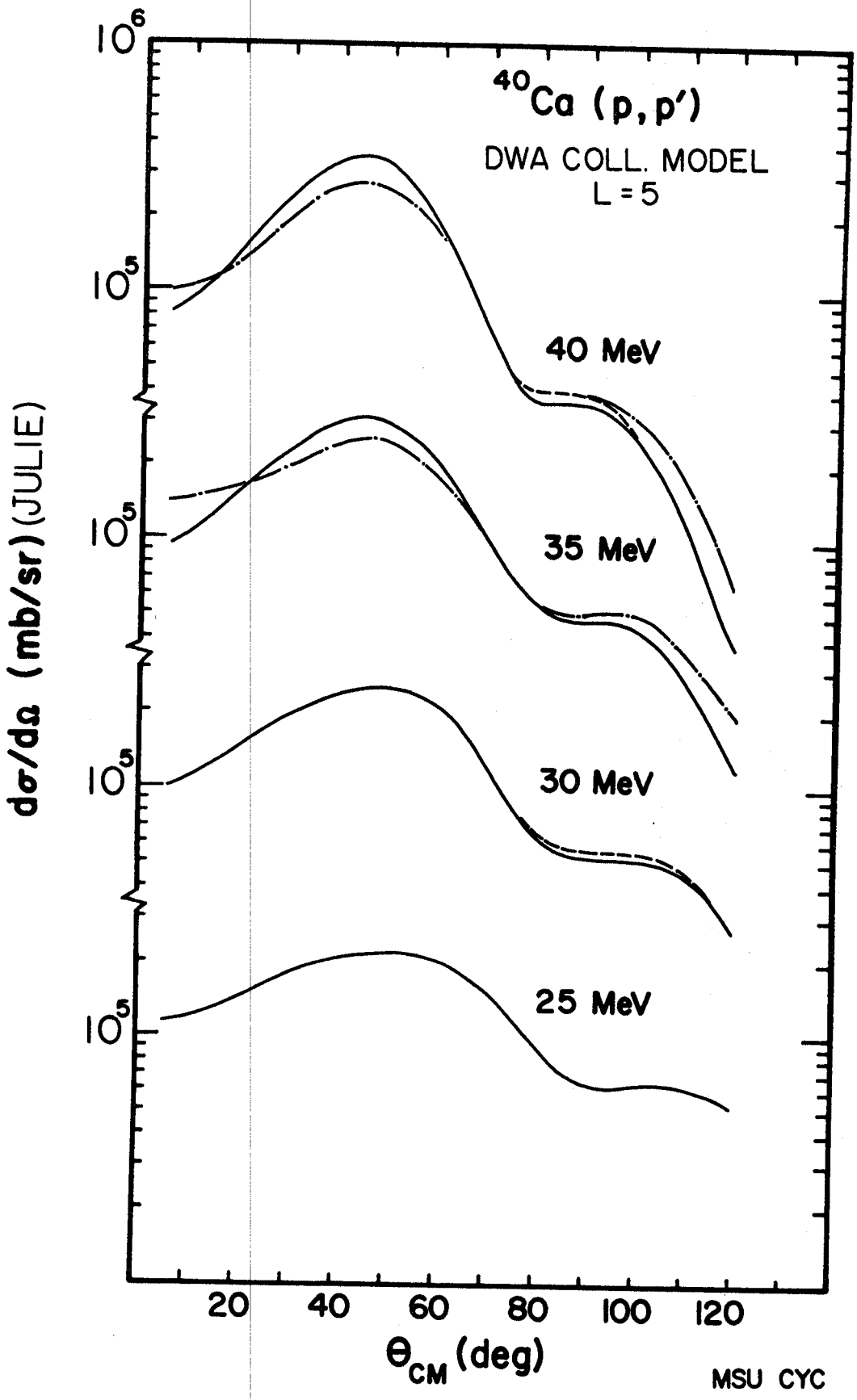
^{40}Ca (p, p')
DWA COLL. MODEL
L = 5
40 MeV
35 MeV
30 MeV
25 MeV
10^6
10^5
10^5
10^5
10^5
dσ/dΩ (mb/sr) (JULIE)
20
40
60
80
100
120
θ_{CM} (deg)
MSU CYC

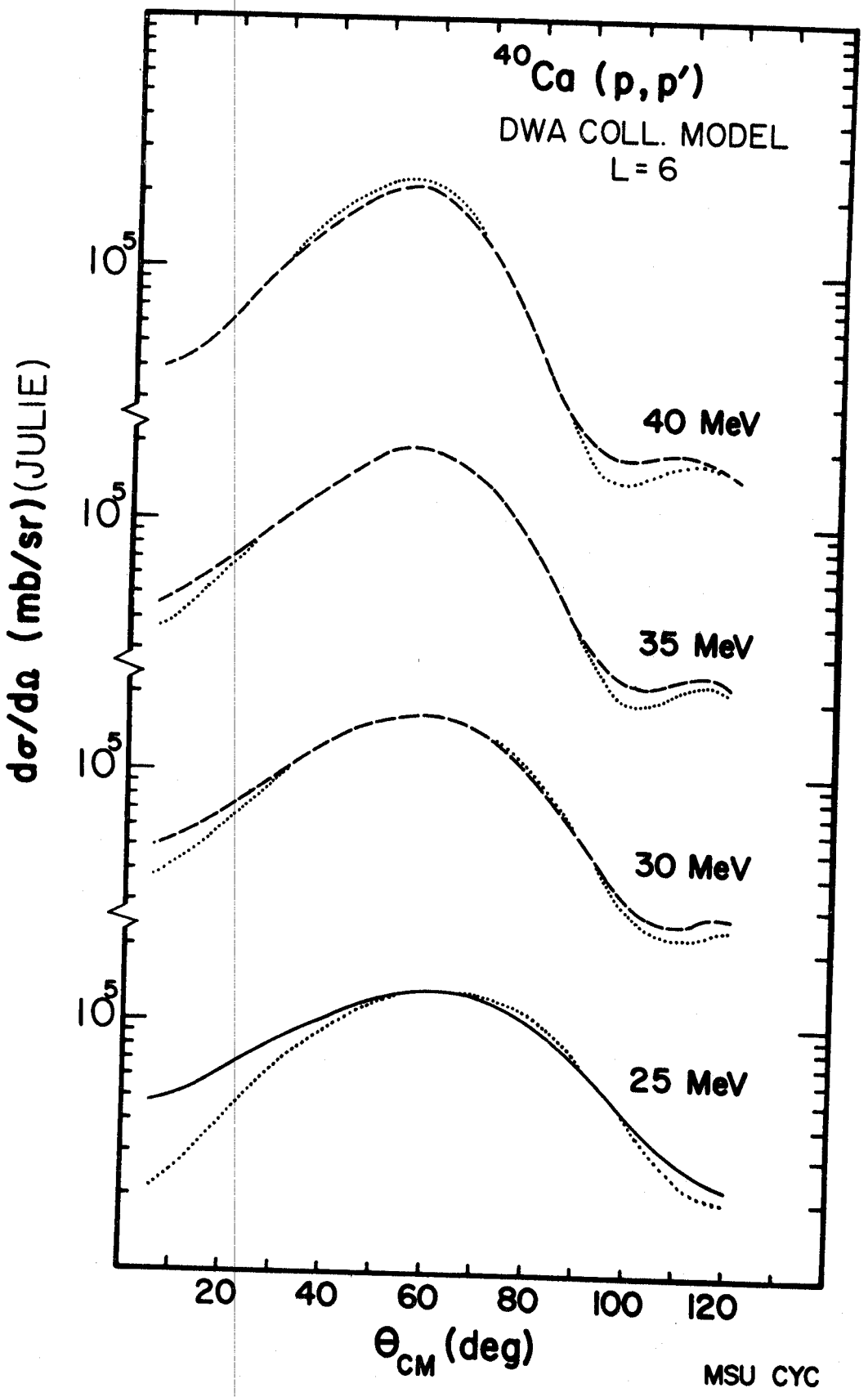
^{40}Ca (p, p')
DWA COLL. MODEL
L = 6
40 MeV
35 MeV
30 MeV
25 MeV
10^5
10^5
10^5
10^5
dσ/dΩ (mb/sr) (JULIE)
20
40
60
80
100
120
θ_{CM} (deg)
MSU CYC

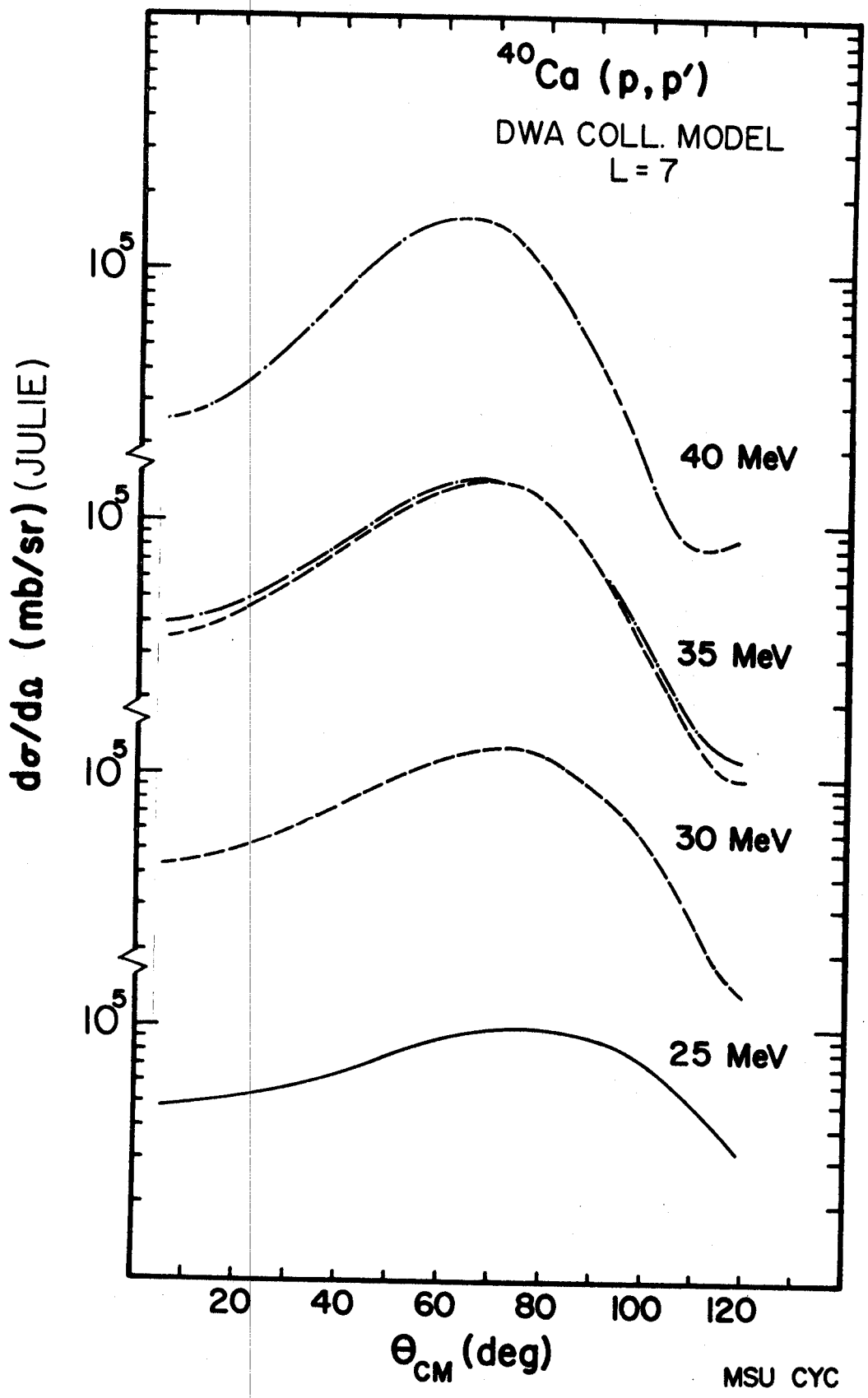
^{40}Ca (p, p')
DWA COLL. MODEL
L = 7
40 MeV
35 MeV
30 MeV
25 MeV
10^5
10^5
10^5
10^5
dσ/dΩ (mb/sr) (JULIE)
20
40
60
80
100
120
θ_{CM} (deg)
MSU CYC

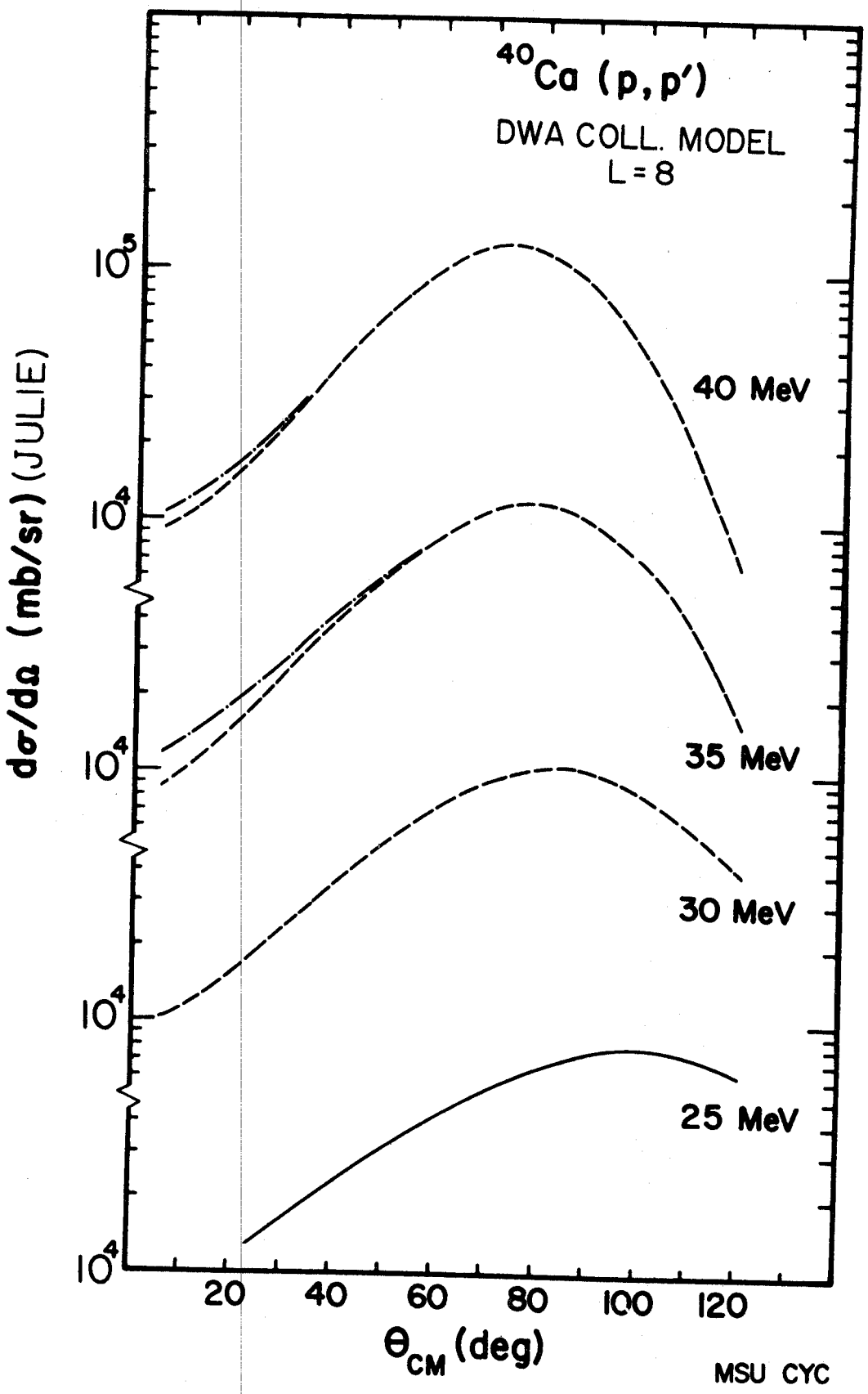
^{40}Ca (p, p′)
DWA COLL. MODEL
L = 8
40 MeV
35 MeV
30 MeV
25 MeV
dσ/dΩ (mb/sr) (JULIE)
10^5
10^4
10^4
10^4
10^4
20
40
60
80
100
120
θ_{CM} (deg)
MSU CYC

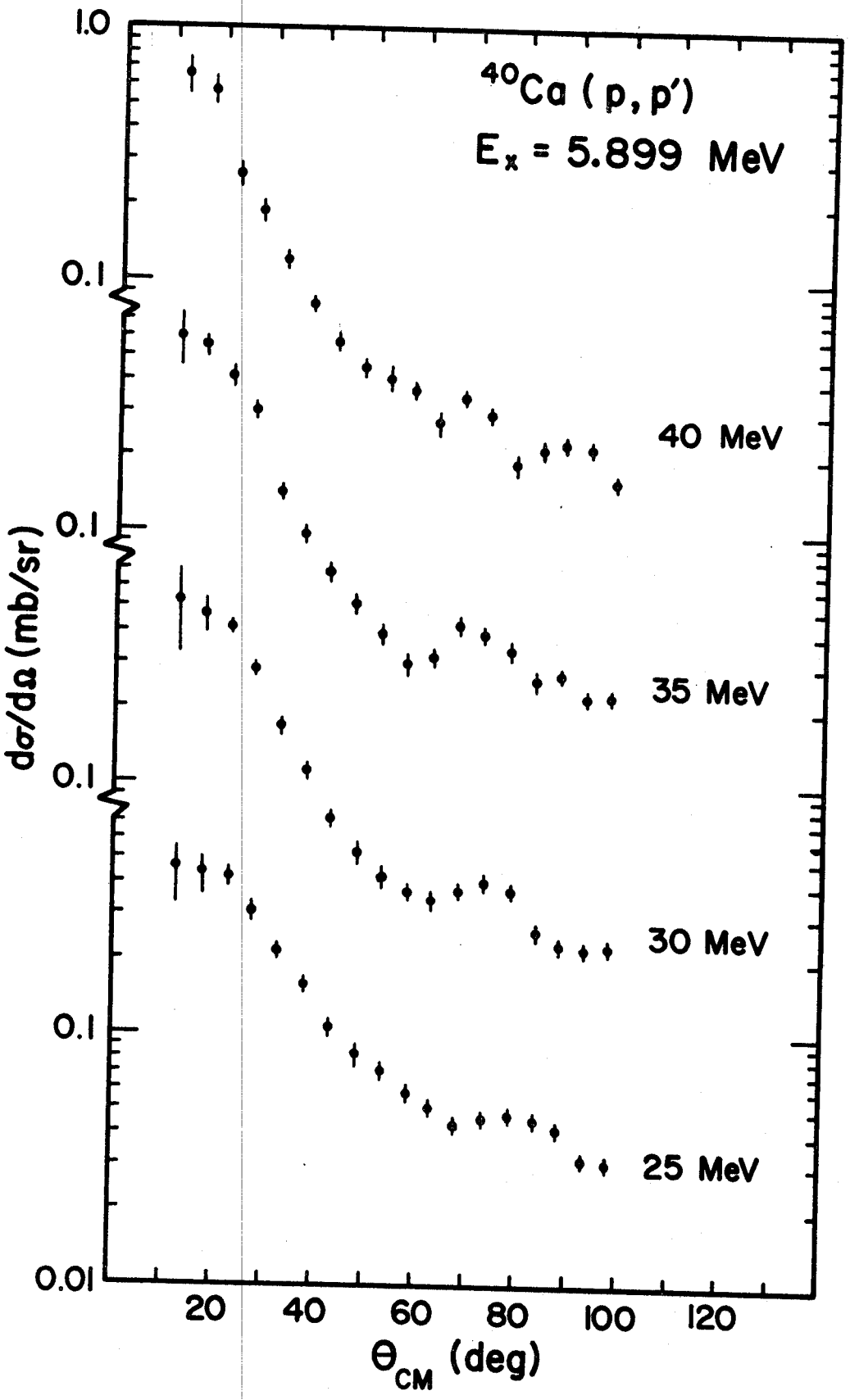
^{40}Ca (p, p')
E_x = 5.899 MeV
40 MeV
35 MeV
30 MeV
25 MeV
dσ/dΩ (mb/sr)
1.0
0.1
0.1
0.1
0.1
0.01
20
40
60
80
100
120
Θ_{CM} (deg)

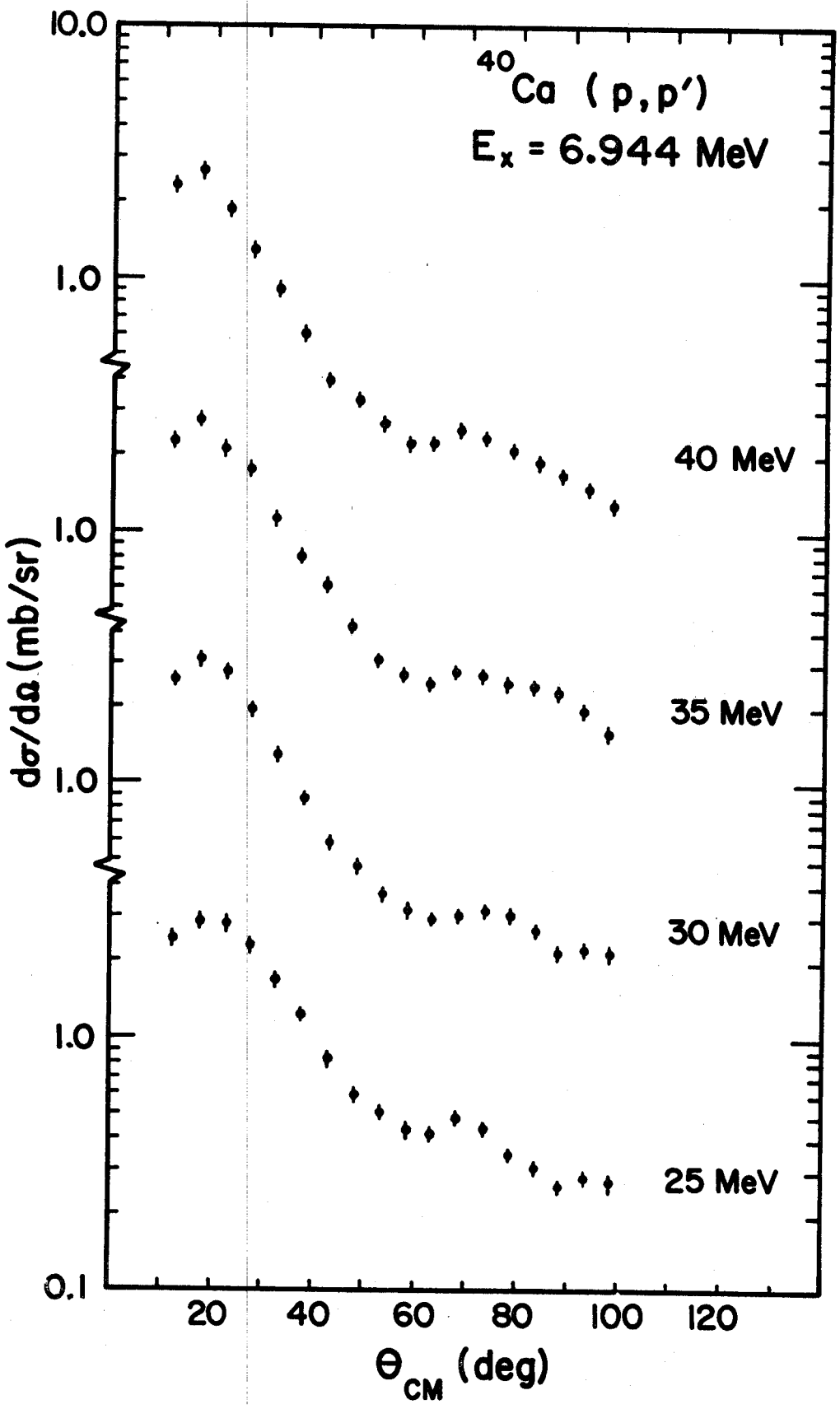
^{40}Ca (p,p')
E_x = 6.944 MeV
40 MeV
35 MeV
30 MeV
25 MeV
10.0
1.0
1.0
1.0
1.0
0.1
dσ/dΩ (mb/sr)
20
40
60
80
100
120
Θ_{CM} (deg)

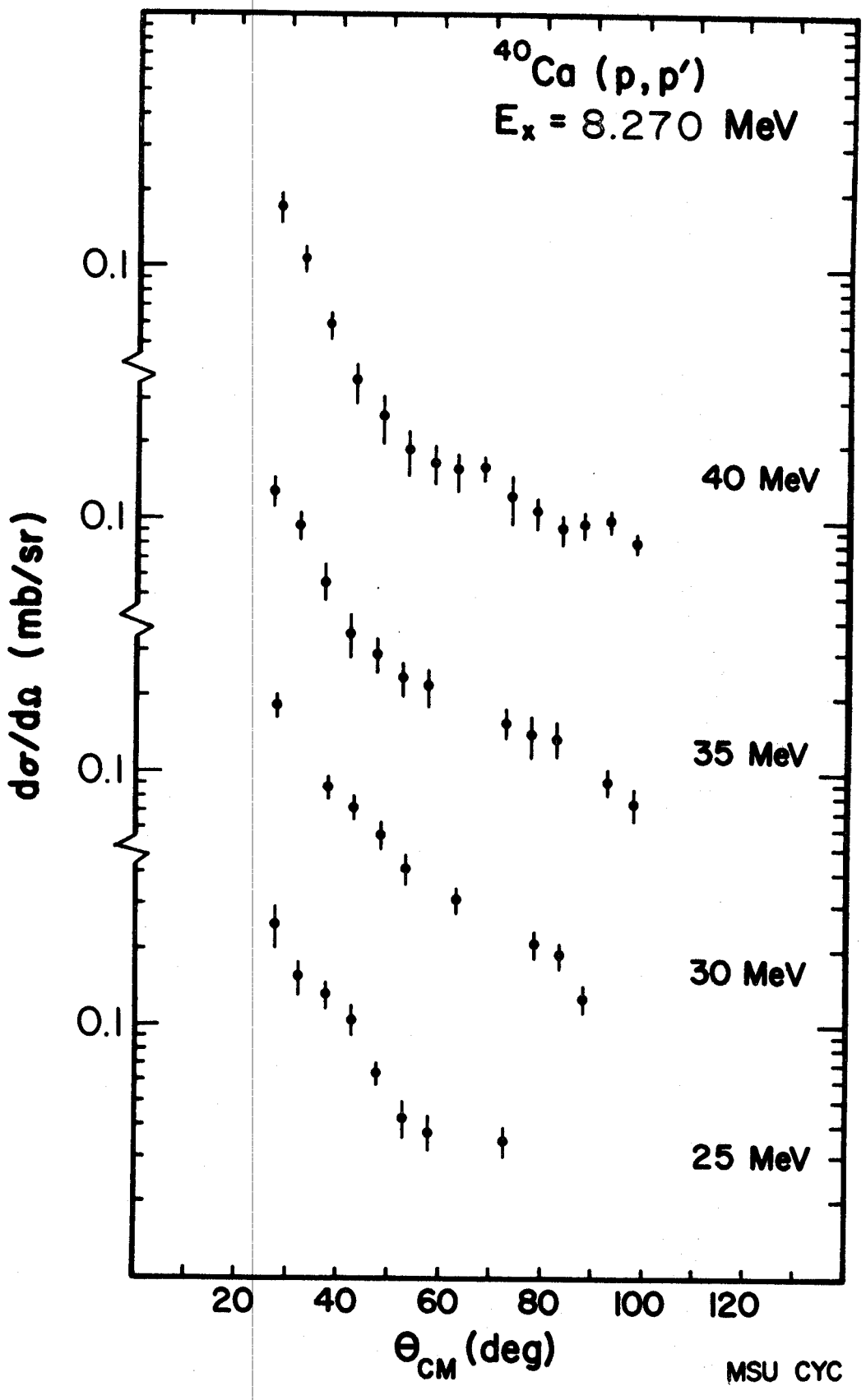
^{40}Ca (p, p')
E_x = 8.270 MeV
40 MeV
35 MeV
30 MeV
25 MeV
0.1
0.1
0.1
dσ/dΩ (mb/sr)
20
40
60
80
100
120
Θ_{CM} (deg)
MSU CYC

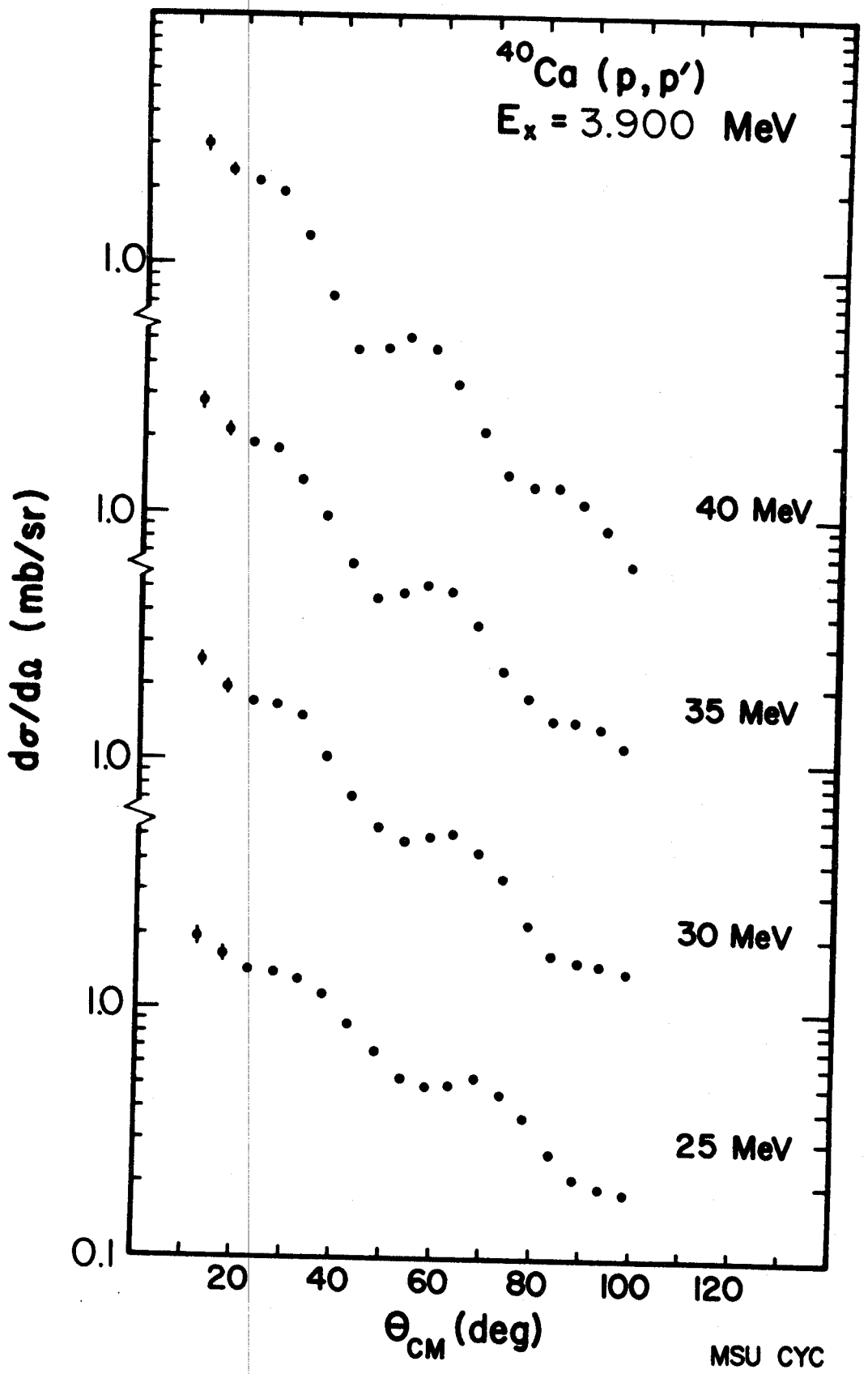
^{40}Ca (p, p')
E_x = 3.900 MeV
40 MeV
35 MeV
30 MeV
25 MeV
dσ/dΩ (mb/sr)
1.0
1.0
1.0
0.1
20
40
60
80
100
120
Θ_{CM} (deg)
MSU CYC

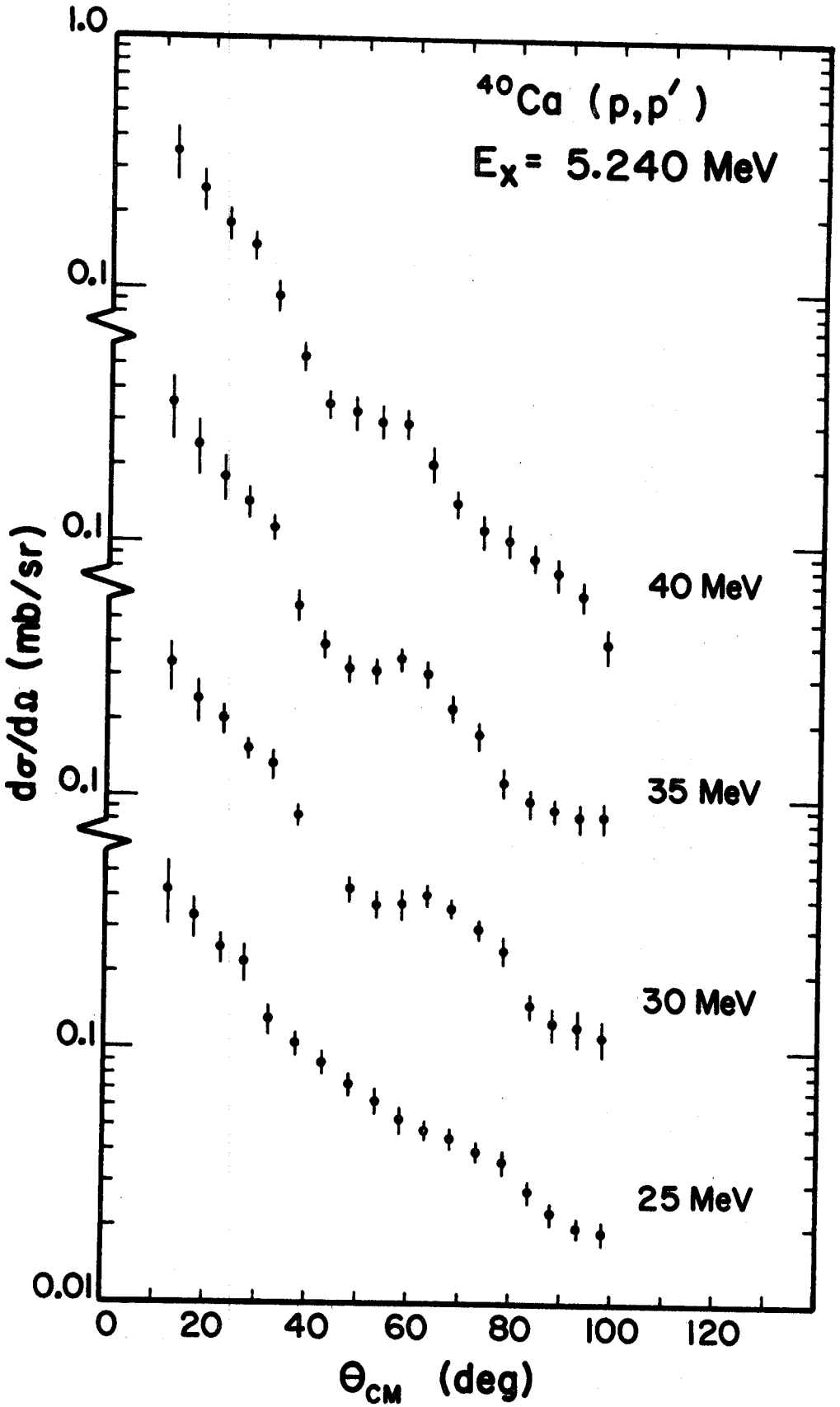
^{40}Ca (p,p′)
E_x = 5.240 MeV
40 MeV
35 MeV
30 MeV
25 MeV
dσ/dΩ (mb/sr)
1.0
0.1
0.1
0.1
0.01
0
20
40
60
80
100
120
Θ_{CM} (deg)

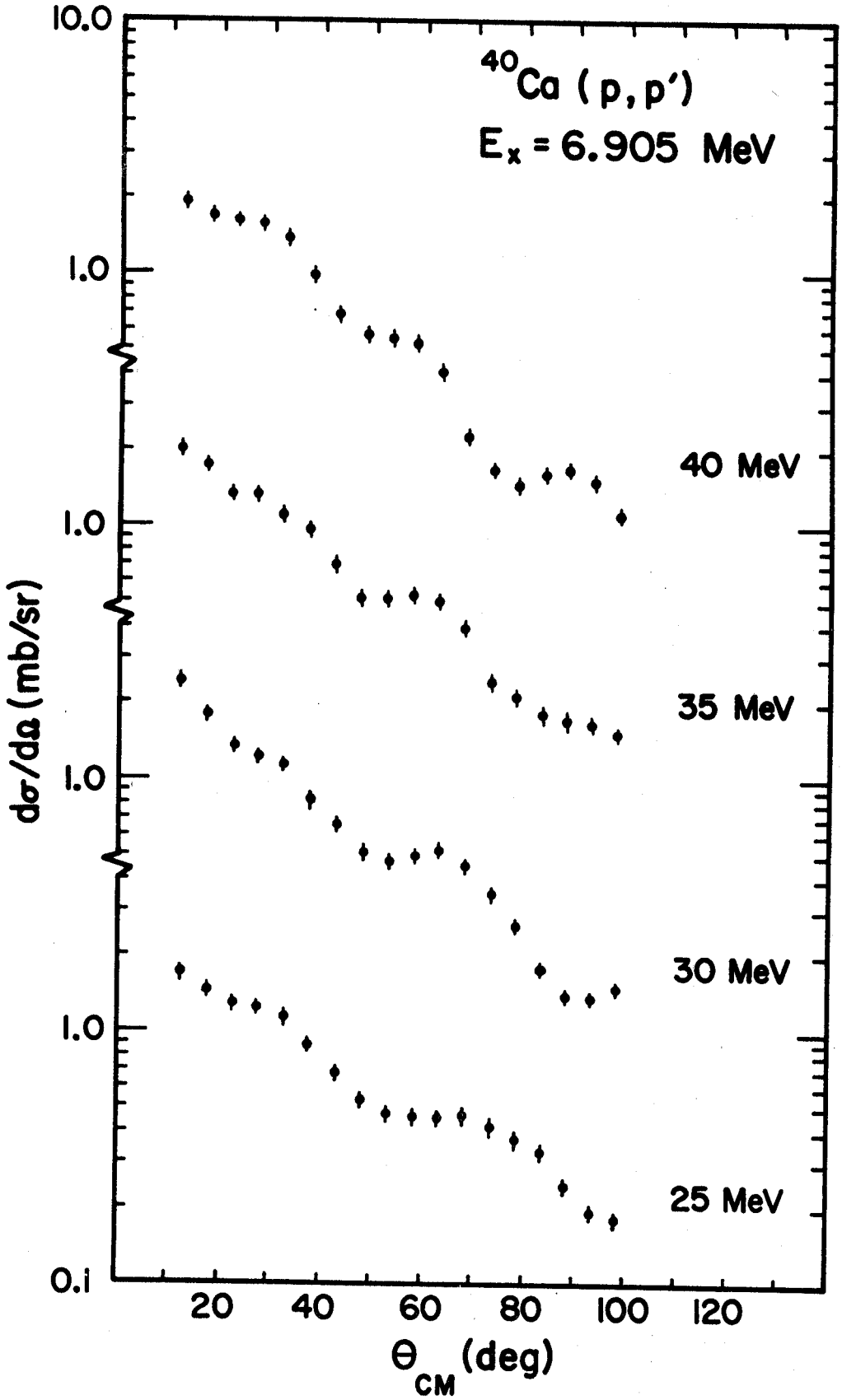
^{40}Ca (p, p')
E_x = 6.905 MeV
40 MeV
35 MeV
30 MeV
25 MeV
dσ/dΩ (mb/sr)
10.0
1.0
1.0
1.0
1.0
0.1
20
40
60
80
100
120
Θ_{CM} (deg)

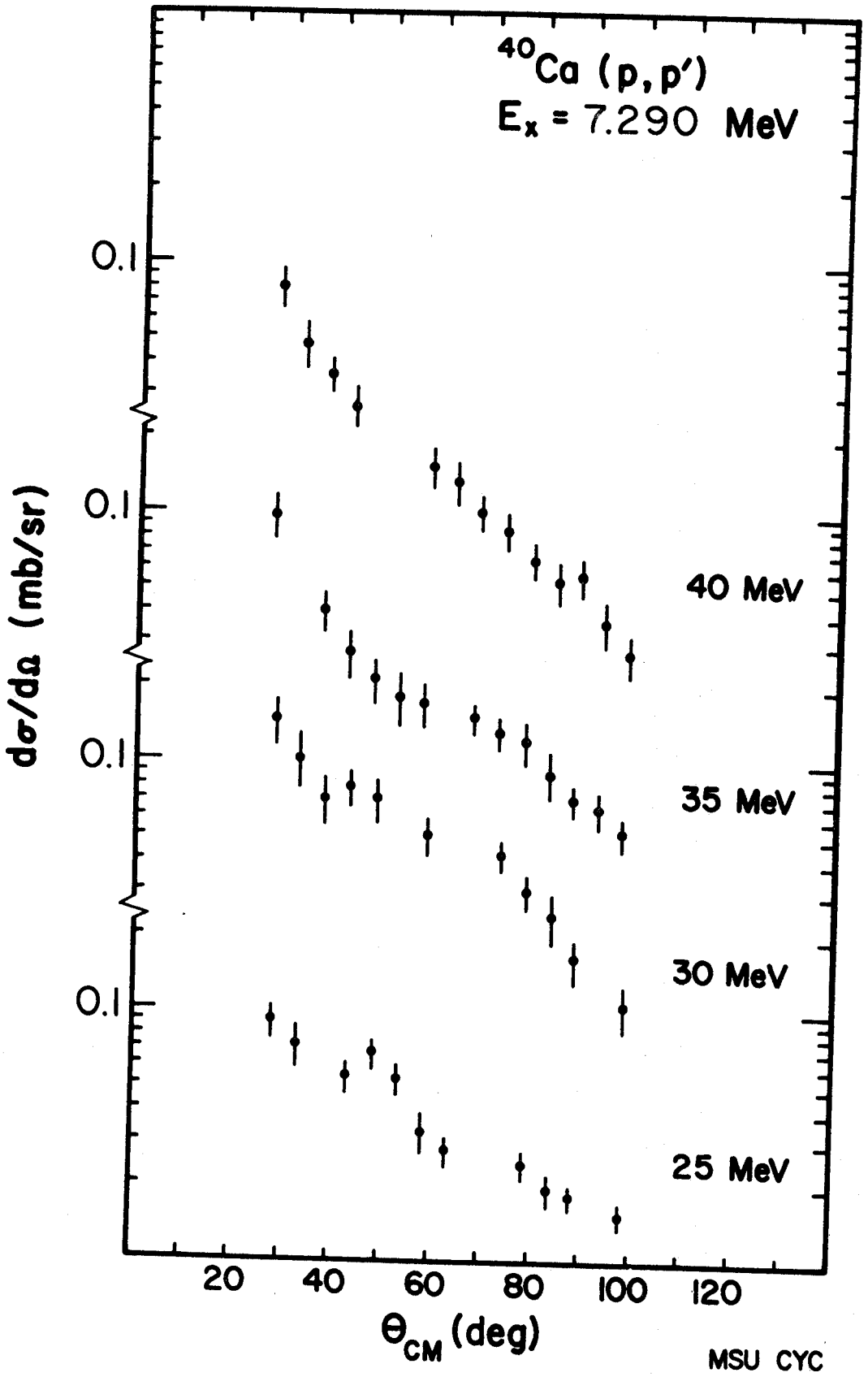
^{40}Ca (p, p′)
E_x = 7.290 MeV
0.1
0.1
0.1
0.1
40 MeV
35 MeV
30 MeV
25 MeV
dσ/dΩ (mb/sr)
20
40
60
80
100
120
θ_{CM} (deg)
MSU CYC

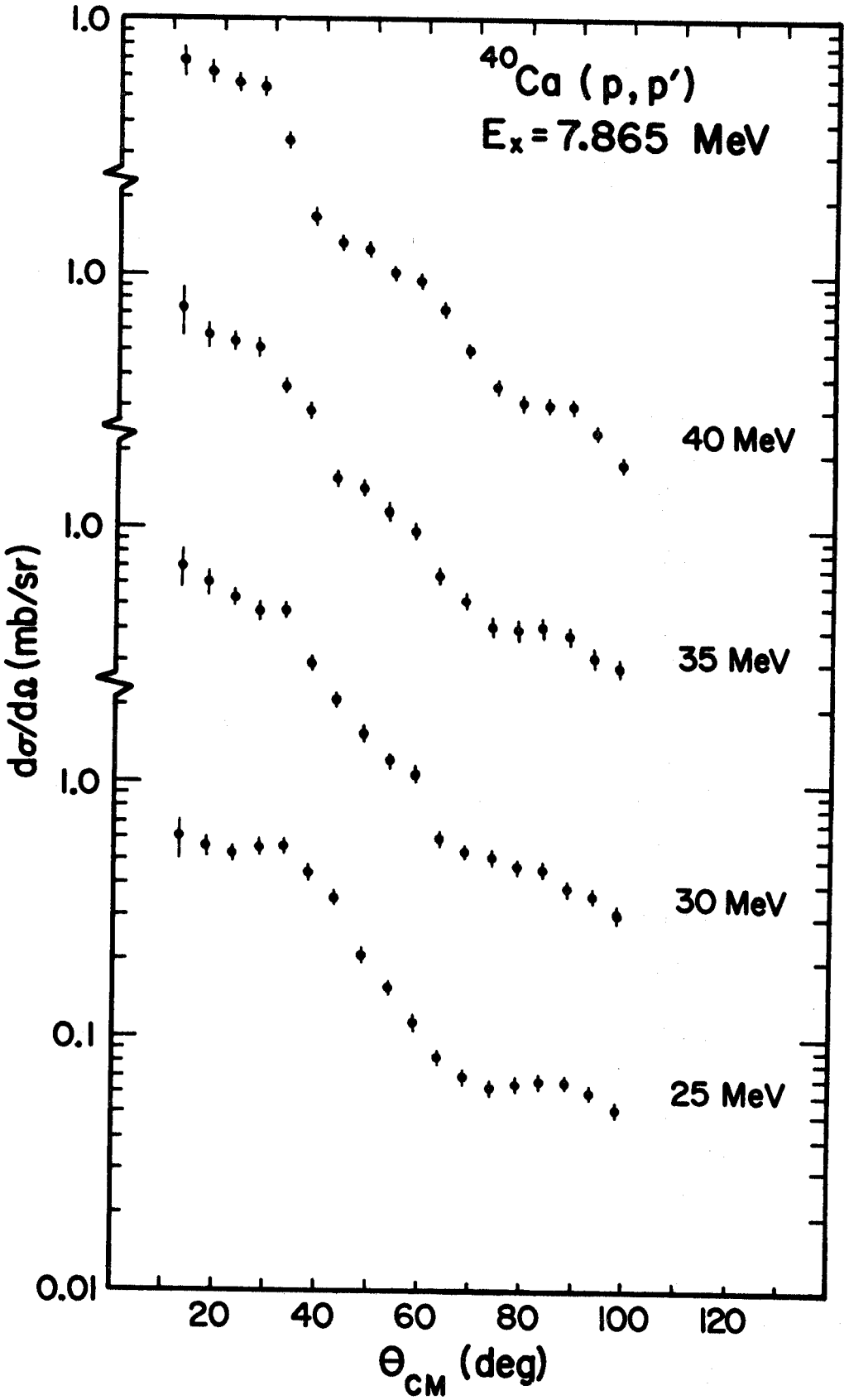
^{40}Ca (p, p')
E_x = 7.865 MeV
40 MeV
35 MeV
30 MeV
25 MeV
dσ/dΩ (mb/sr)
1.0
1.0
1.0
0.1
0.01
20
40
60
80
100
120
Θ_{CM} (deg)

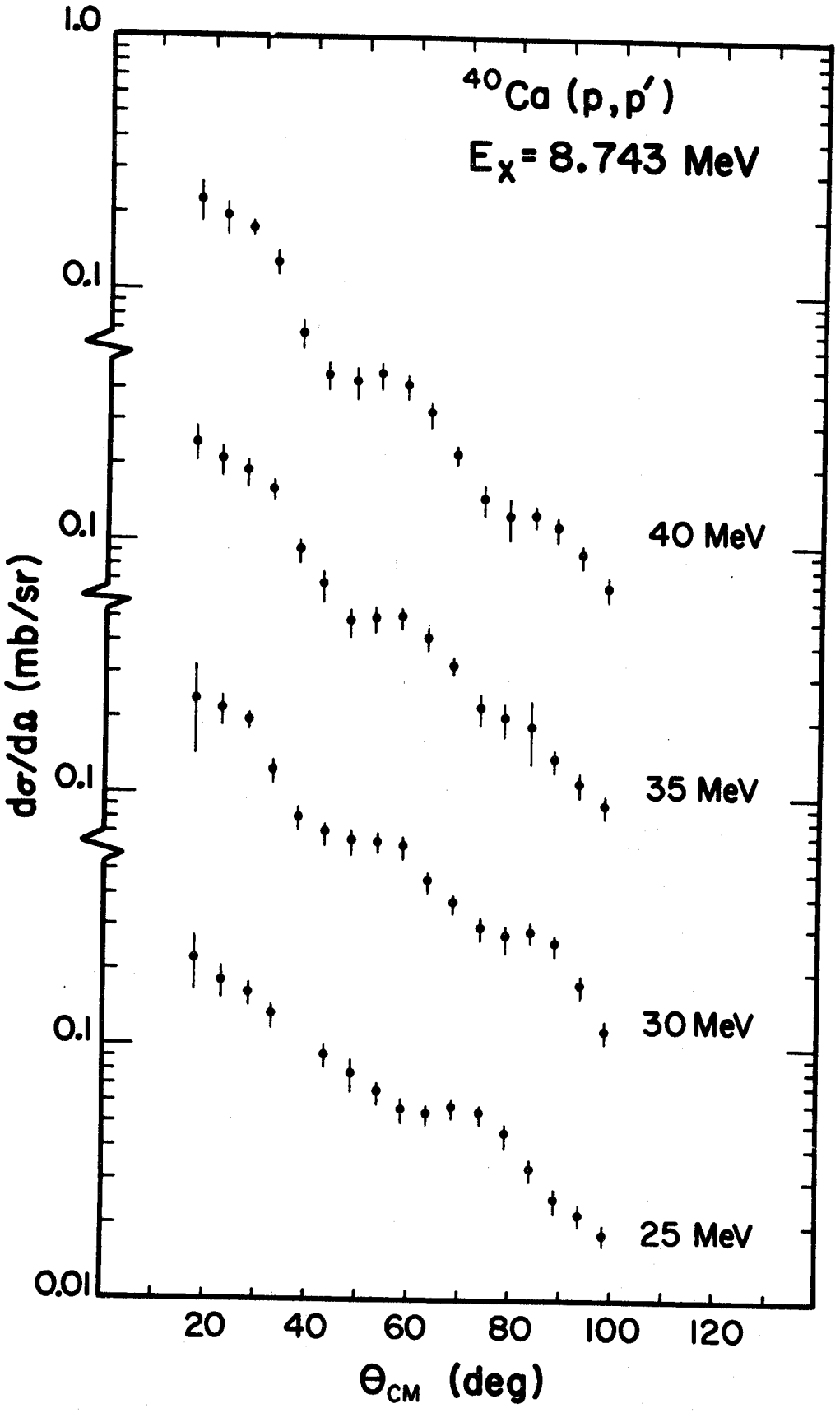
^{40}Ca (p,p′)
E_x = 8.743 MeV
40 MeV
35 MeV
30 MeV
25 MeV
dσ/dΩ (mb/sr)
1.0
0.1
0.1
0.1
0.01
20
40
60
80
100
120
Θ_{CM} (deg)

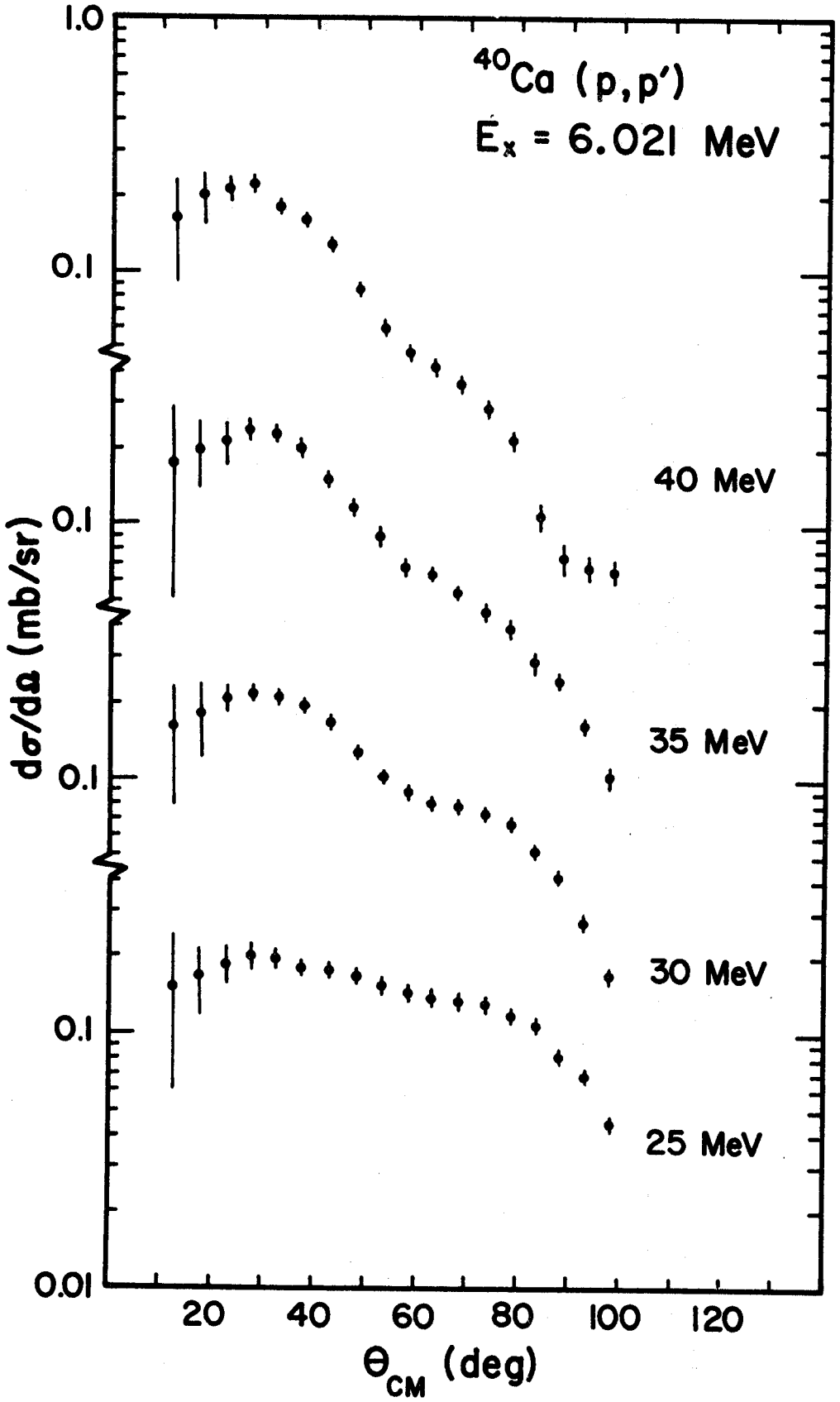
^{40}Ca (p,p')
E_x = 6.021 MeV
40 MeV
35 MeV
30 MeV
25 MeV
dσ/dΩ (mb/sr)
1.0
0.1
0.1
0.1
0.01
20
40
60
80
100
120
Θ_{CM} (deg)

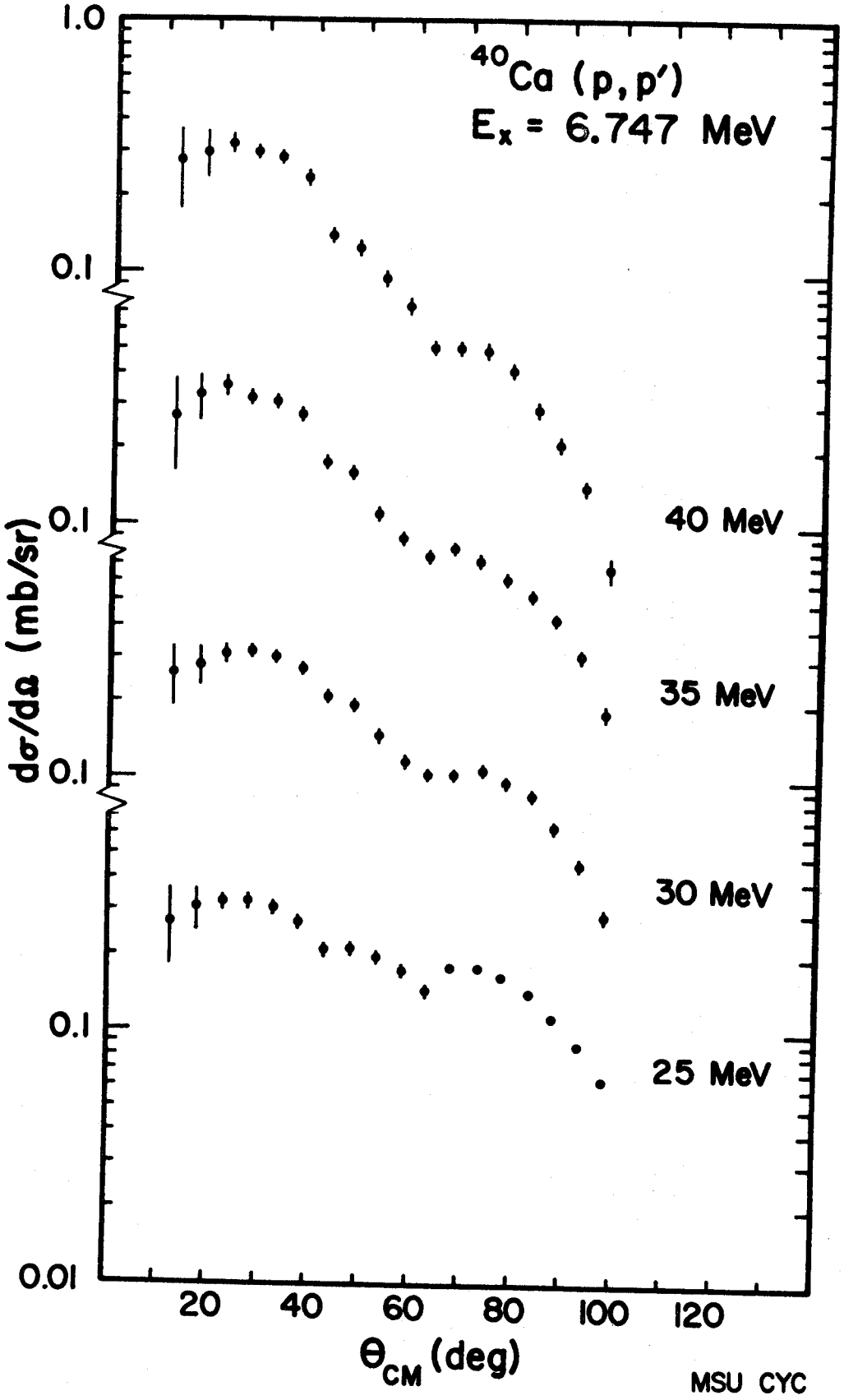
^{40}Ca (p, p′)
E_x = 6.747 MeV
40 MeV
35 MeV
30 MeV
25 MeV
dσ/dΩ (mb/sr)
1.0
0.1
0.1
0.1
0.01
20
40
60
80
100
120
Θ_{CM} (deg)
MSU CYC

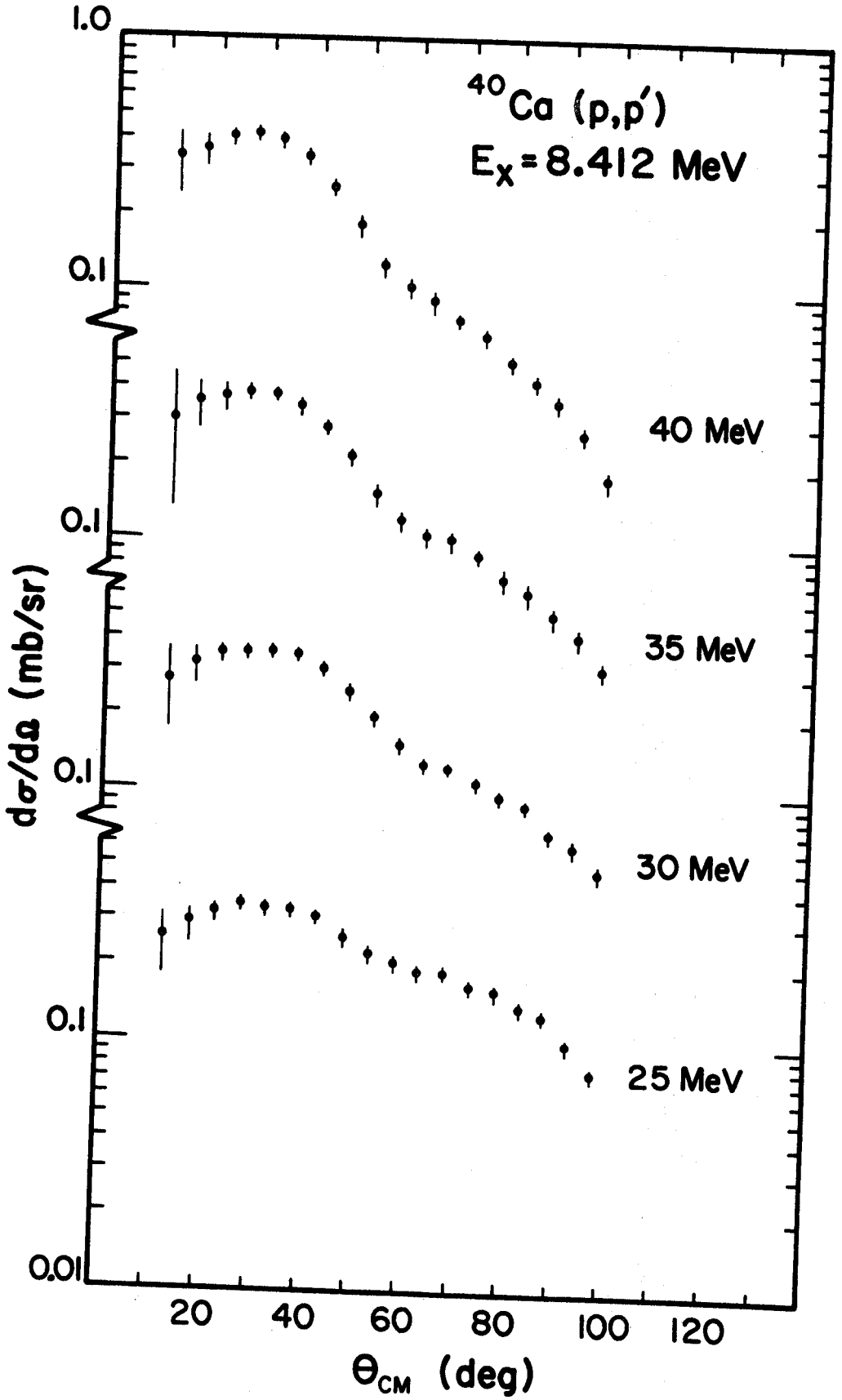
^{40}Ca (p,p′)
E_x = 8.412 MeV
40 MeV
35 MeV
30 MeV
25 MeV
dσ/dΩ (mb/sr)
1.0
0.1
0.1
0.1
0.01
20
40
60
80
100
120
Θ_{CM} (deg)

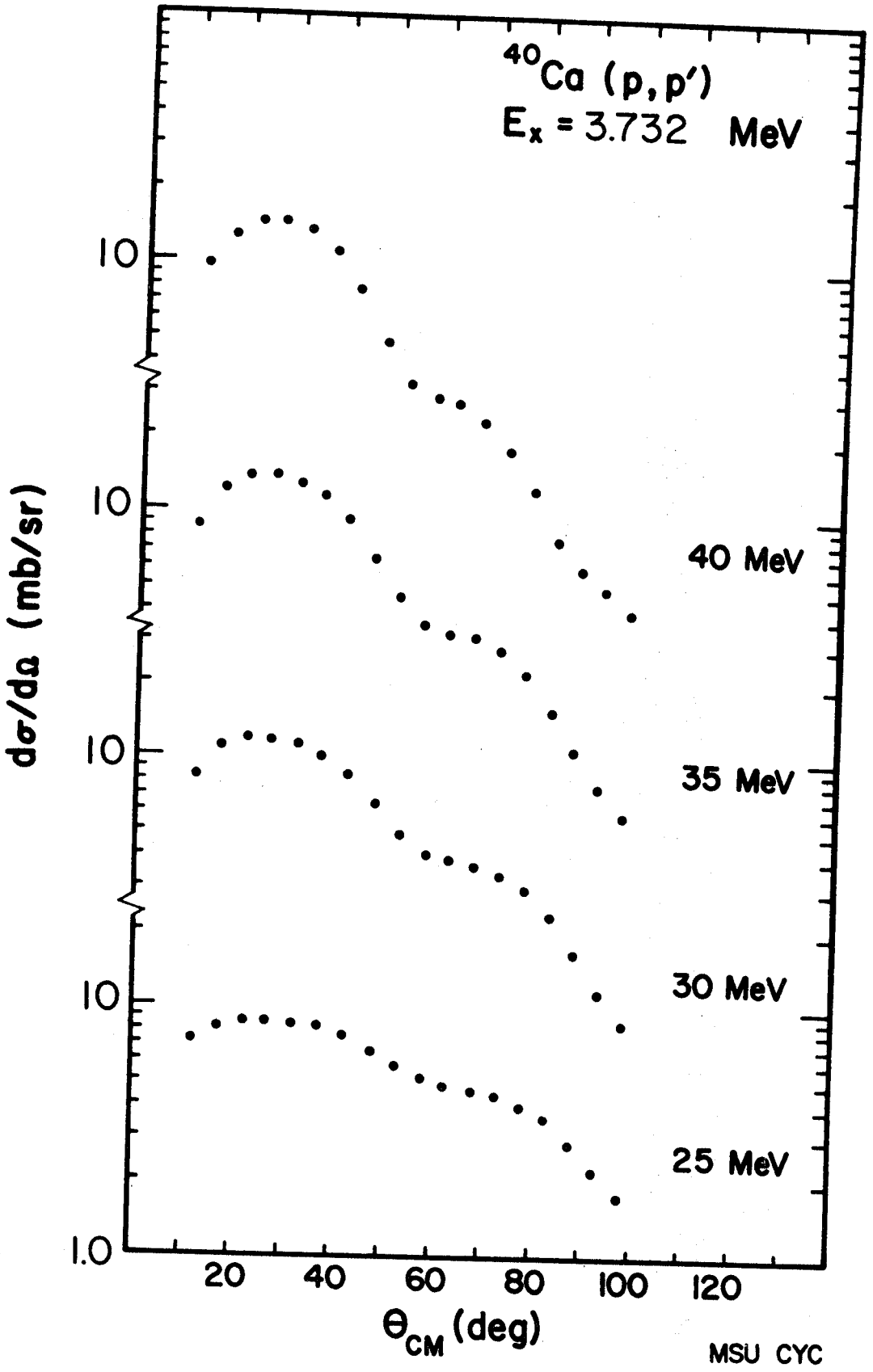
^{40}Ca (p, p′)
E_x = 3.732 MeV
40 MeV
35 MeV
30 MeV
25 MeV
dσ/dΩ (mb/sr)
10
10
10
1.0
20
40
60
80
100
120
θ_{CM} (deg)
MSU CYC

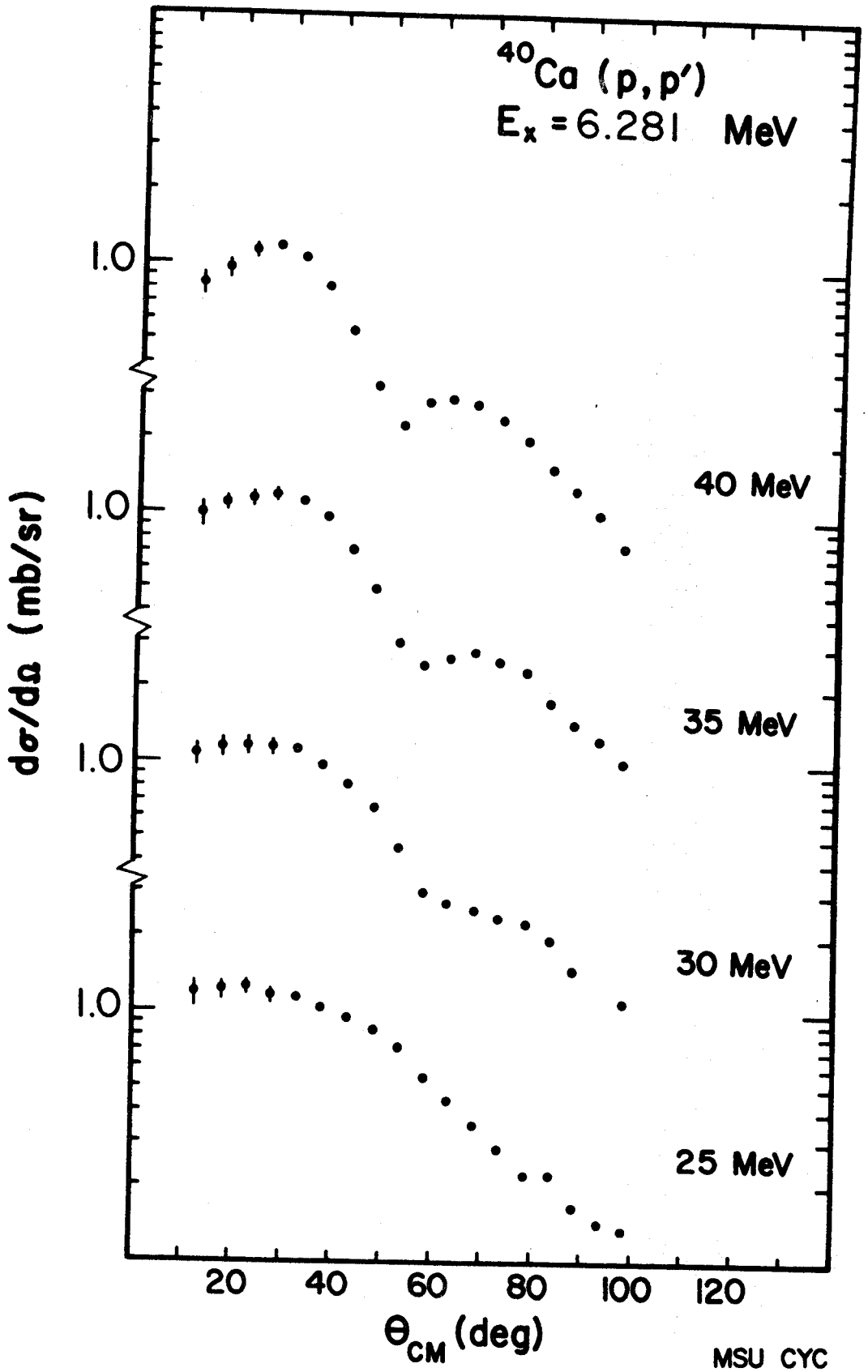
^{40}Ca (p, p′)
E_x = 6.281 MeV
40 MeV
35 MeV
30 MeV
25 MeV
1.0
1.0
1.0
dσ/dΩ (mb/sr)
20
40
60
80
100
120
θ_{CM} (deg)
MSU CYC

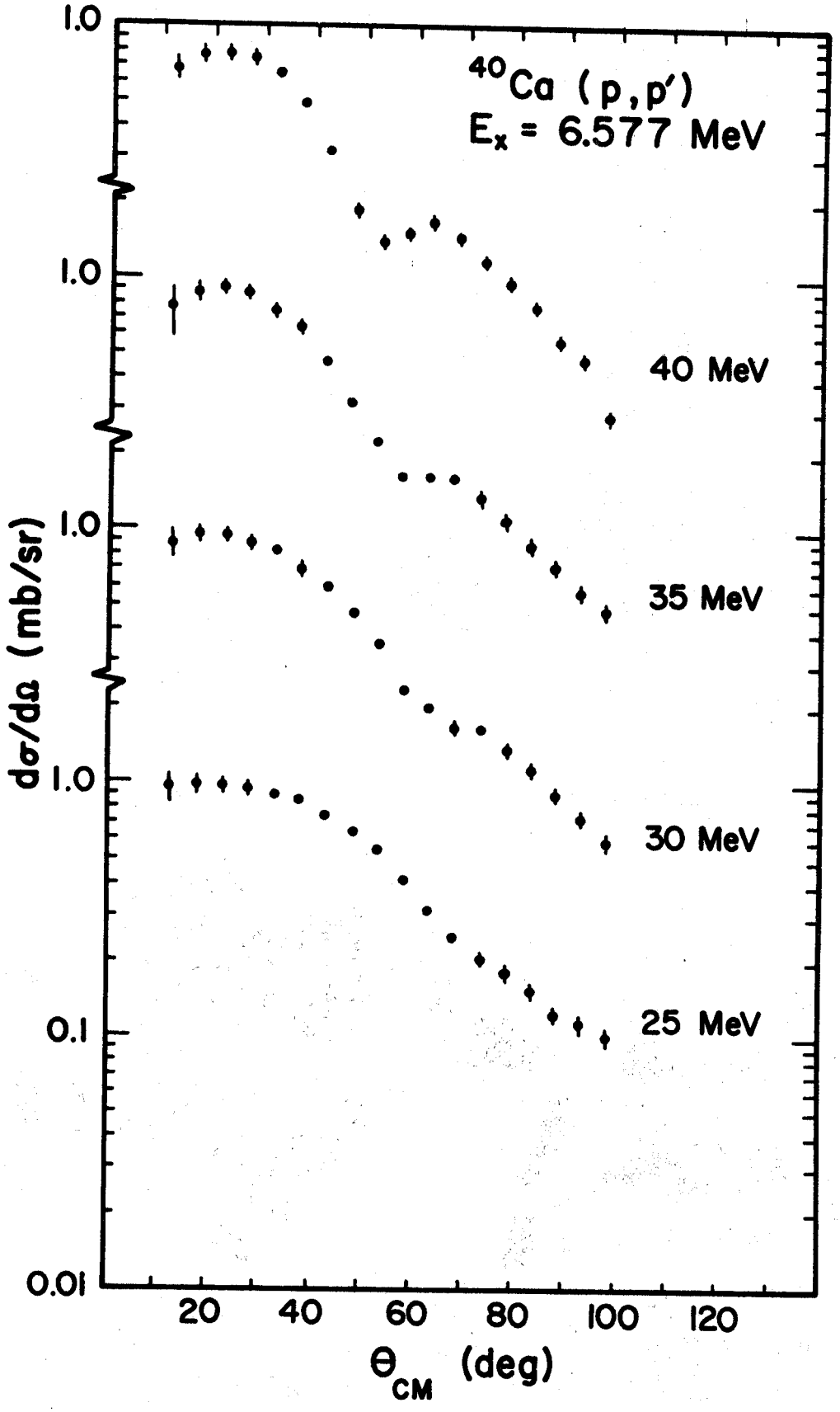
^{40}Ca (p,p')
E_x = 6.577 MeV
40 MeV
35 MeV
30 MeV
25 MeV
dσ/dΩ (mb/sr)
1.0
1.0
1.0
1.0
0.1
0.01
20
40
60
80
100
120
Θ_{CM} (deg)

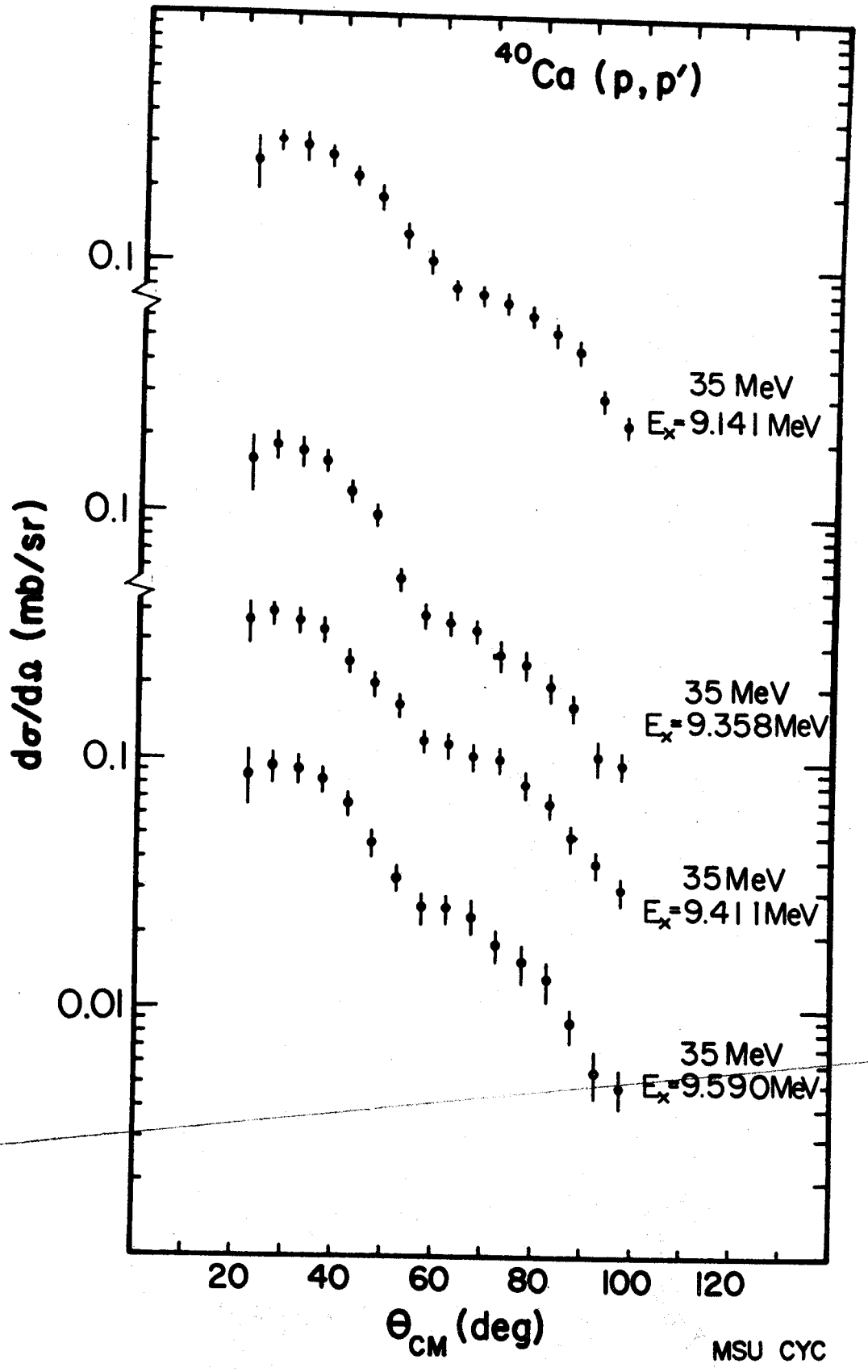
40Ca (p, p')
35 MeV
Ex=9.141 MeV
35 MeV
Ex=9.358MeV
35MeV
Ex=9.411MeV
35 MeV
Ex=9.590MeV
0.1
0.1
0.1
0.01
dσ/dΩ (mb/sr)
20
40
60
80
100
120
θCM (deg)
MSU CYC

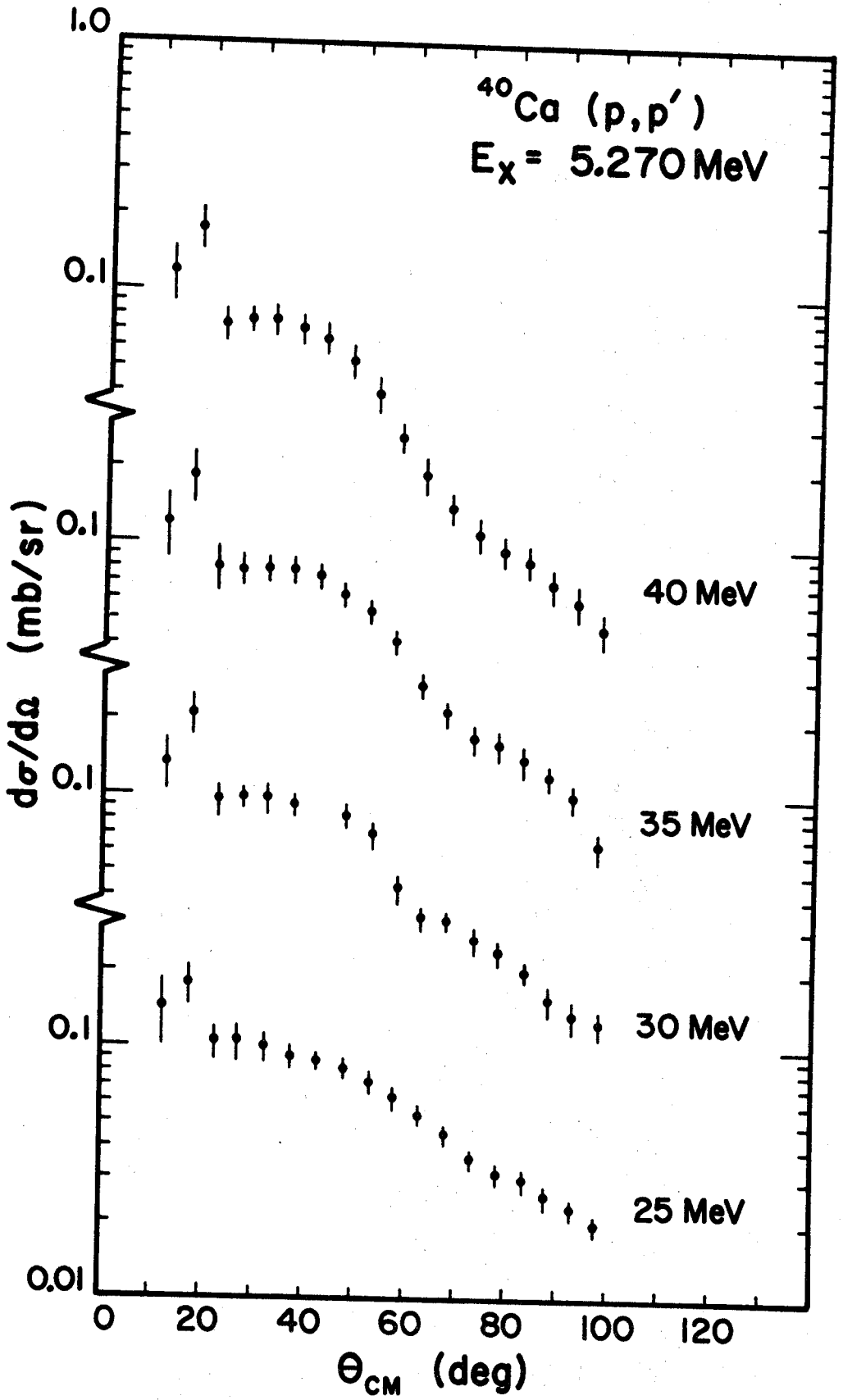
^{40}Ca (p,p′)
E_x = 5.270 MeV
40 MeV
35 MeV
30 MeV
25 MeV
dσ/dΩ (mb/sr)
1.0
0.1
0.1
0.1
0.01
0
20
40
60
80
100
120
θ_{CM} (deg)

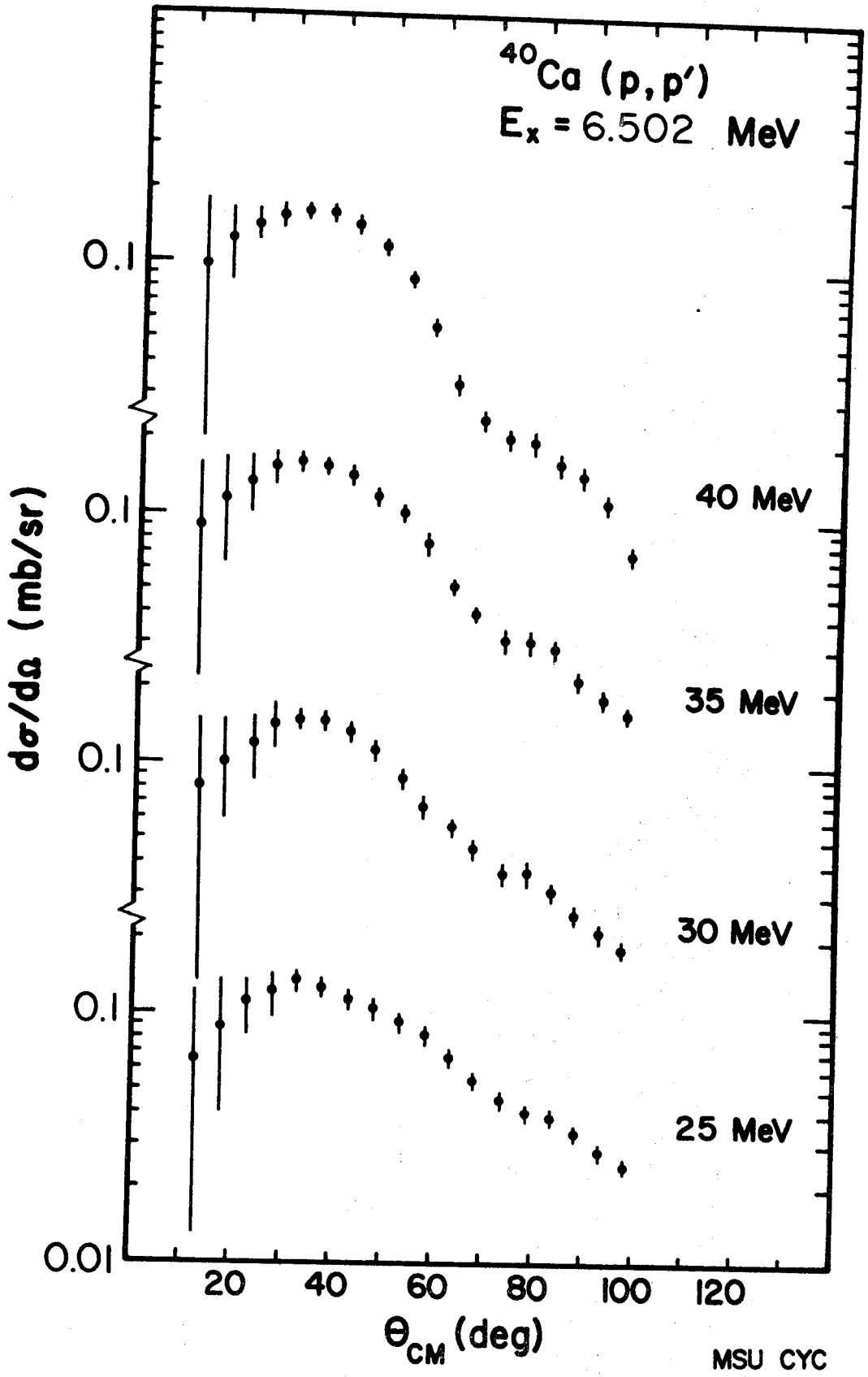
^{40}Ca (p, p')
E_x = 6.502 MeV
40 MeV
35 MeV
30 MeV
25 MeV
0.1
0.1
0.1
0.01
dσ/dΩ (mb/sr)
20
40
60
80
100
120
θ_{CM} (deg)
MSU CYC

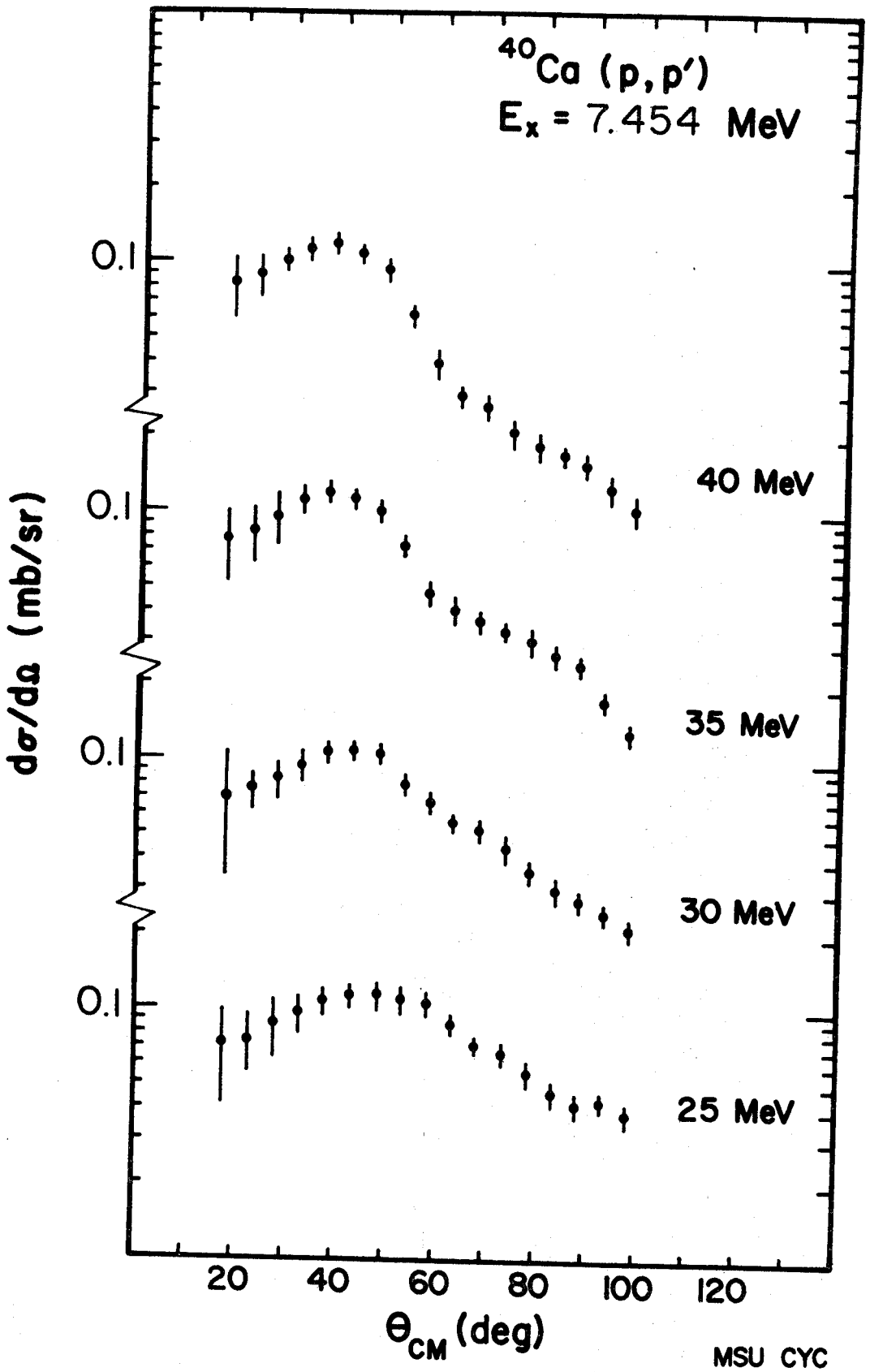
^{40}Ca (p, p′)
E_x = 7.454 MeV
40 MeV
35 MeV
30 MeV
25 MeV
0.1
0.1
0.1
dσ/dΩ (mb/sr)
20
40
60
80
100
120
θ_{CM} (deg)
MSU CYC

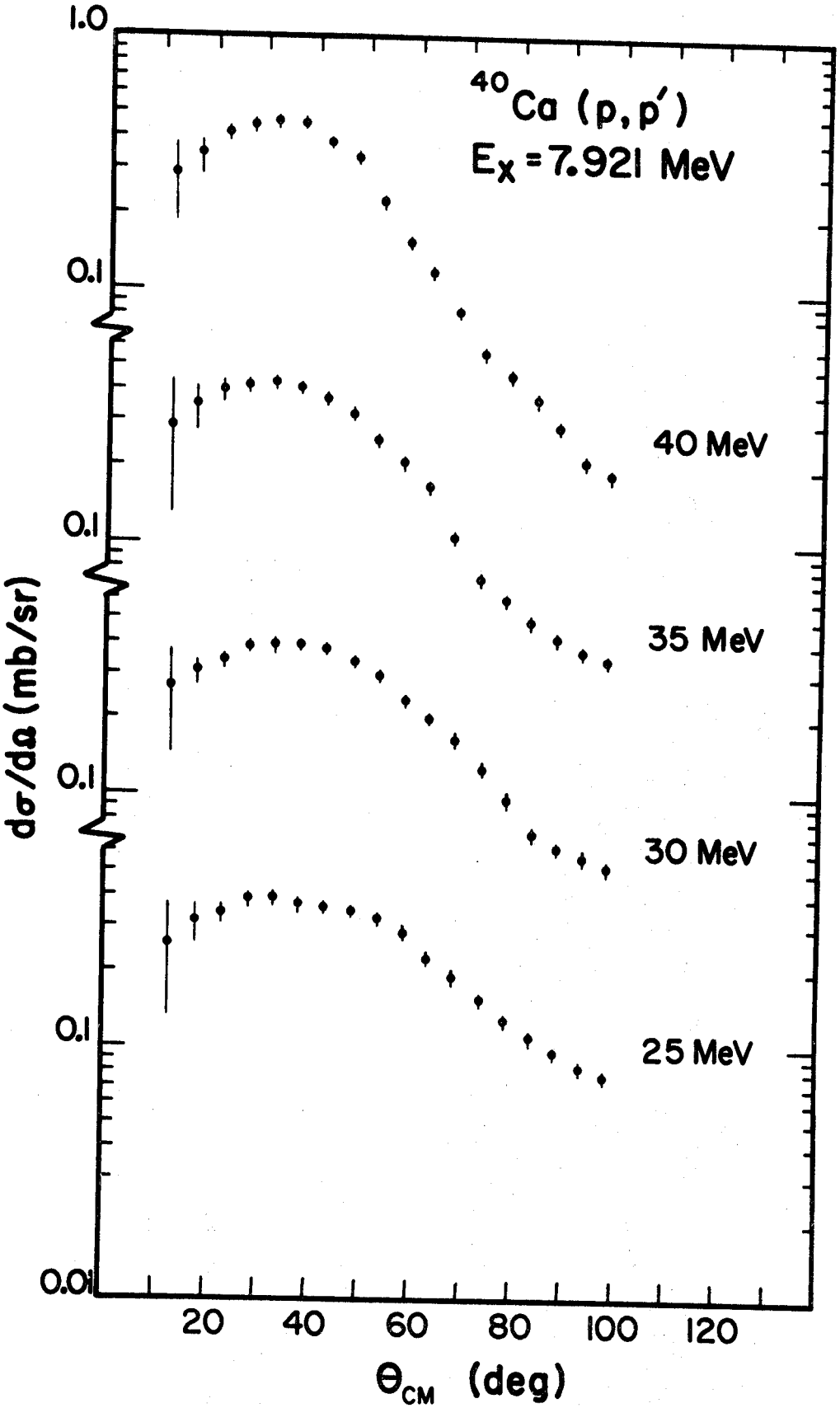
1.0
0.1
0.1
0.1
0.1
0.01
^{40}Ca (p, p′)
E_x = 7.921 MeV
40 MeV
35 MeV
30 MeV
25 MeV
dσ/dΩ (mb/sr)
20
40
60
80
100
120
Θ_{CM} (deg)

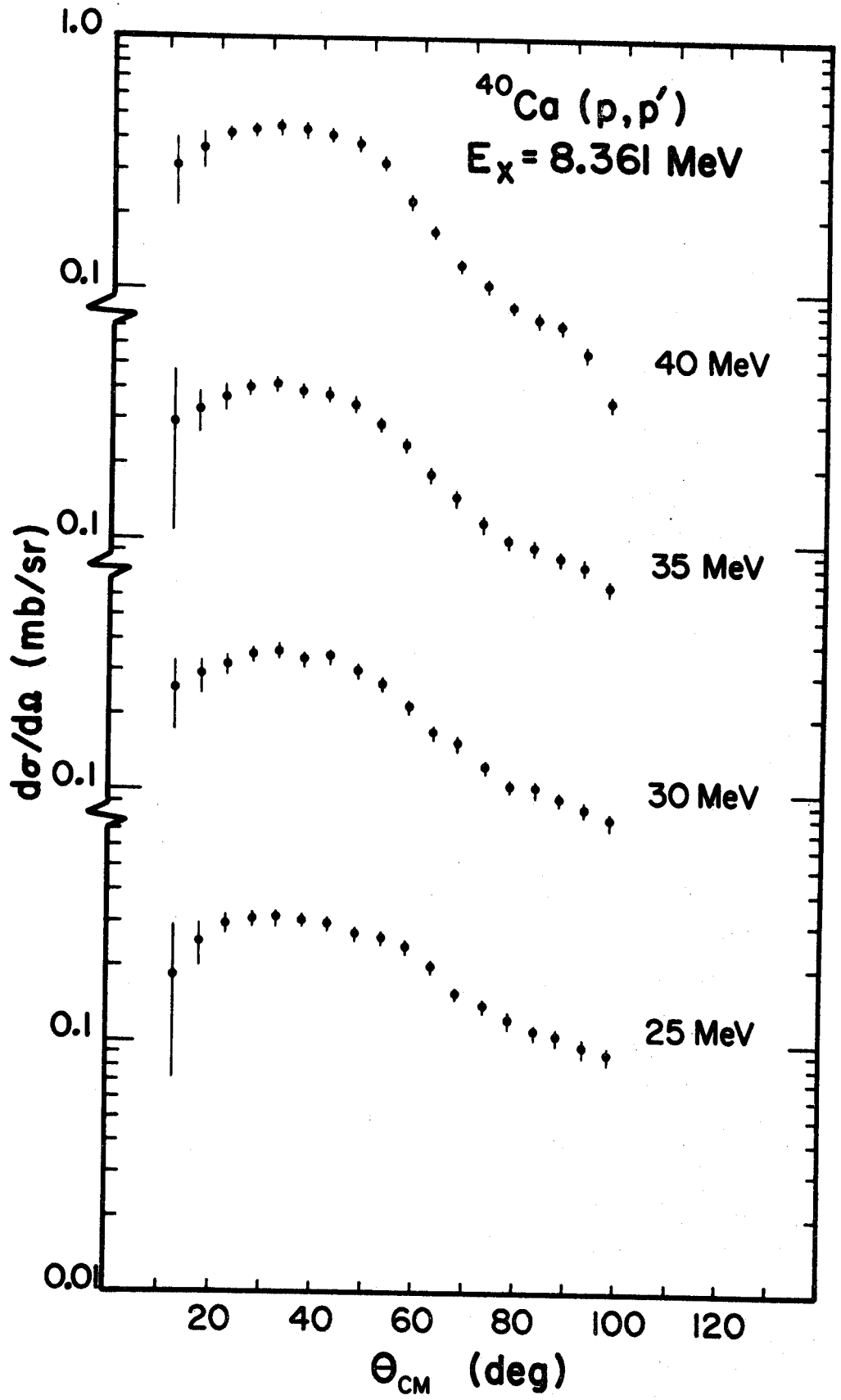
^{40}Ca (p,p′)
E_x = 8.361 MeV
40 MeV
35 MeV
30 MeV
25 MeV
dσ/dΩ (mb/sr)
1.0
0.1
0.1
0.1
0.01
20
40
60
80
100
120
Θ_{CM} (deg)

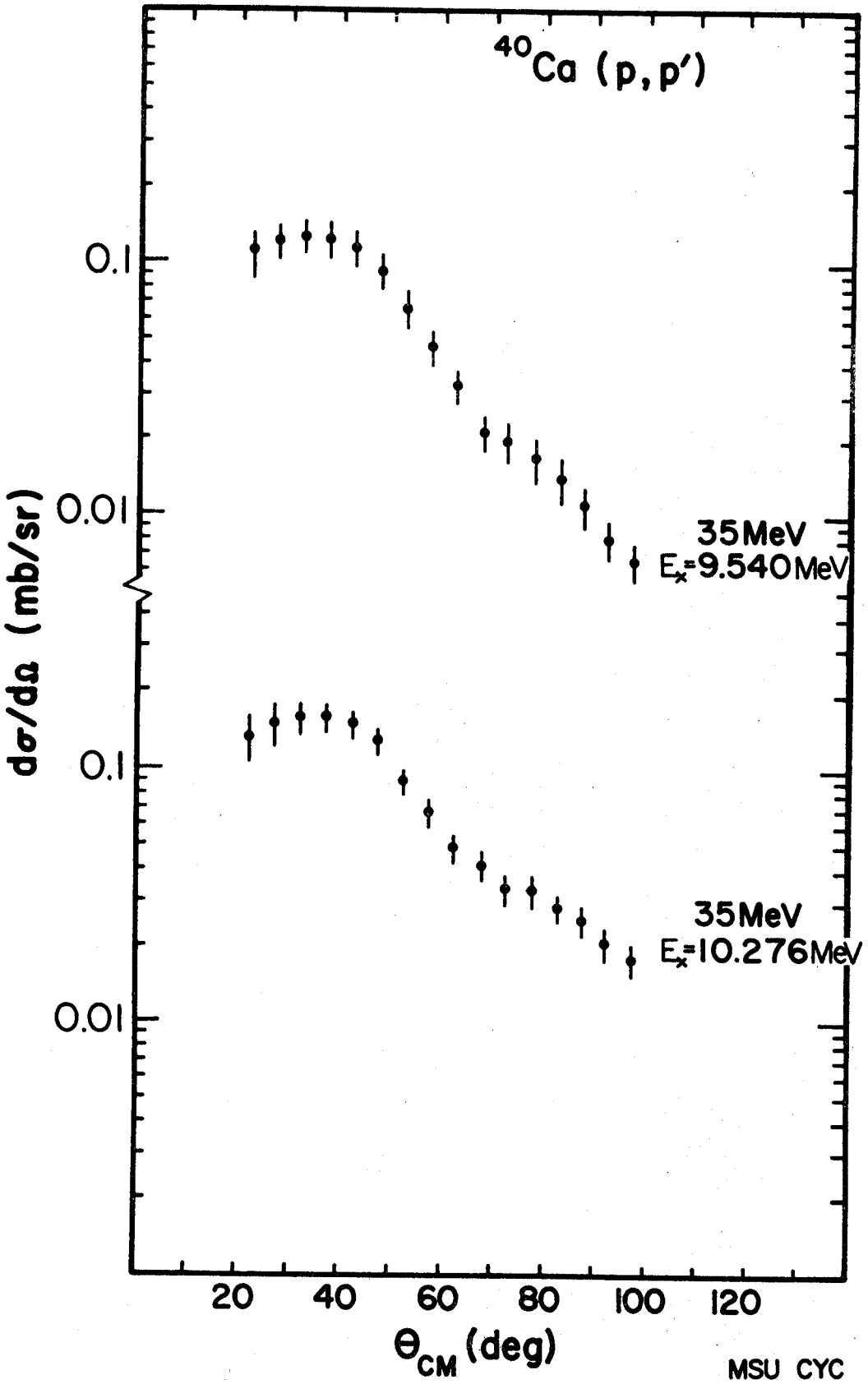
^{40}Ca (p, p′)
0.1
0.01
35MeV
E_x=9.540MeV
0.1
35MeV
E_x=10.276MeV
0.01
dσ/dΩ (mb/sr)
20
40
60
80
100
120
Θ_{CM} (deg)
MSU CYC

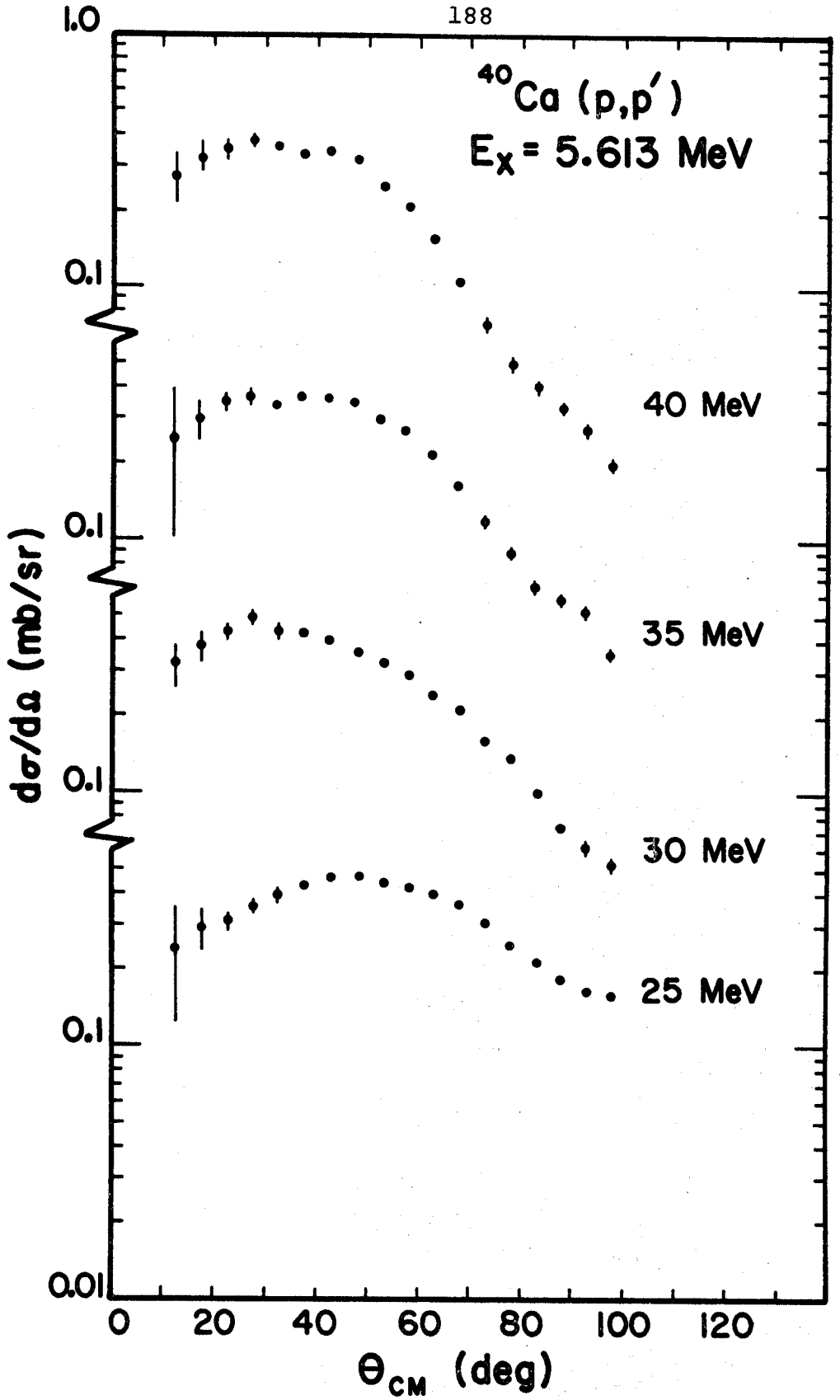
^{40}Ca (p,p′)
E_x = 5.613 MeV
40 MeV
35 MeV
30 MeV
25 MeV
dσ/dΩ (mb/sr)
1.0
0.1
0.1
0.1
0.01
0
20
40
60
80
100
120
Θ_{CM} (deg)

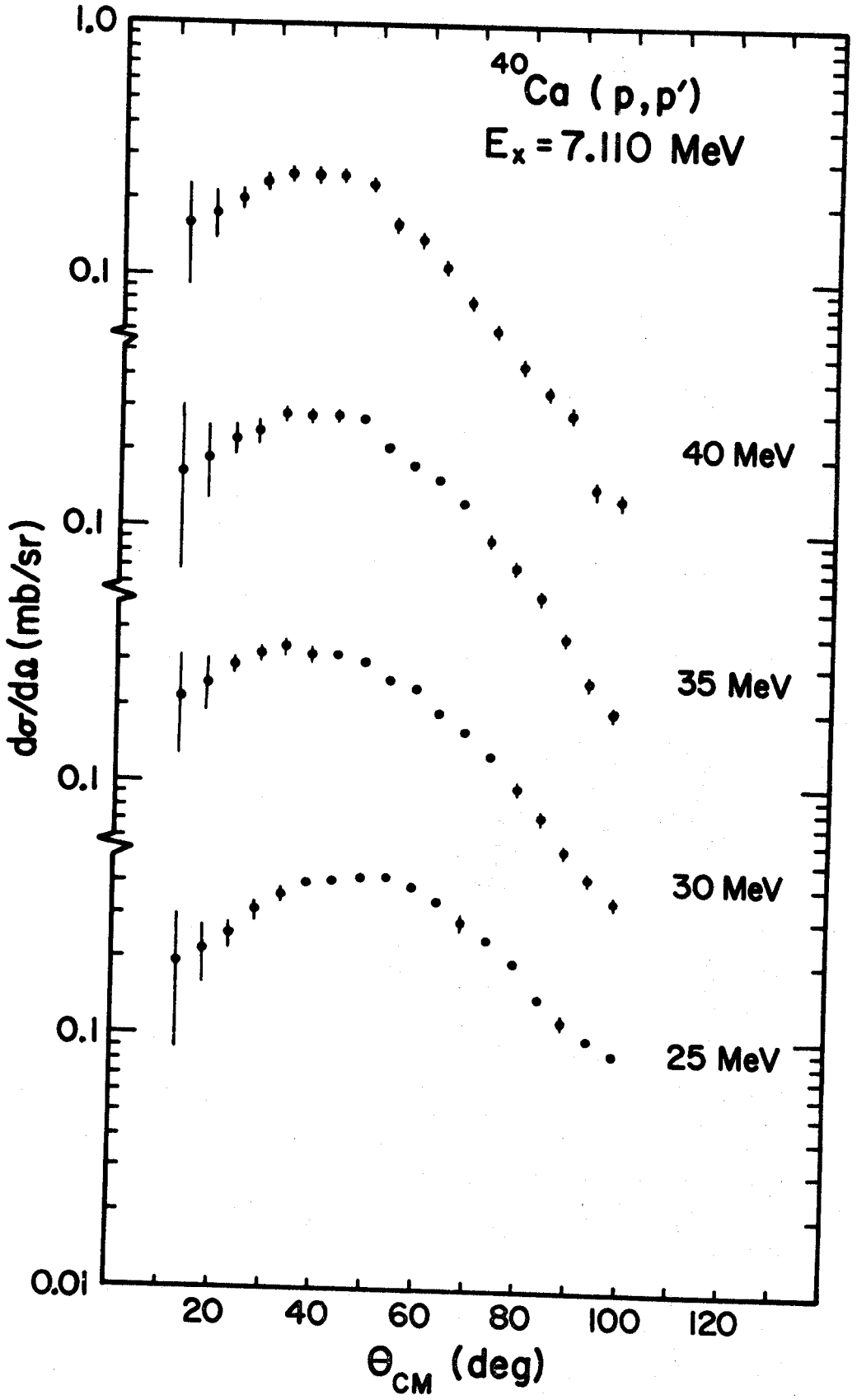
^{40}Ca (p,p')
E_x = 7.110 MeV
40 MeV
35 MeV
30 MeV
25 MeV
dσ/dΩ (mb/sr)
1.0
0.1
0.1
0.1
0.01
20
40
60
80
100
120
Θ_{CM} (deg)

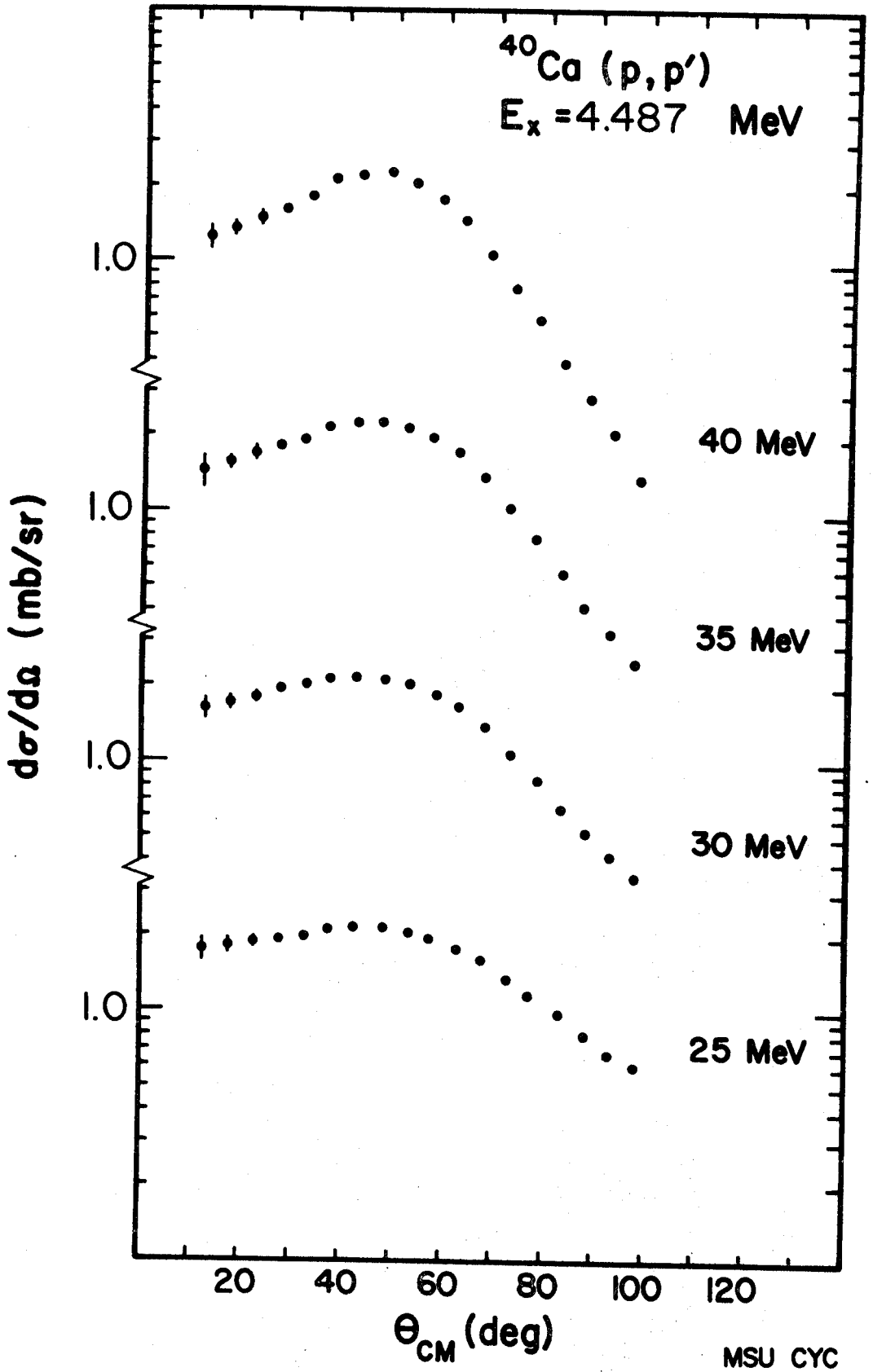
^{40}Ca (p, p′)
E_x = 4.487 MeV
40 MeV
35 MeV
30 MeV
25 MeV
1.0
1.0
1.0
dσ/dΩ (mb/sr)
20
40
60
80
100
120
θ_{CM} (deg)
MSU CYC

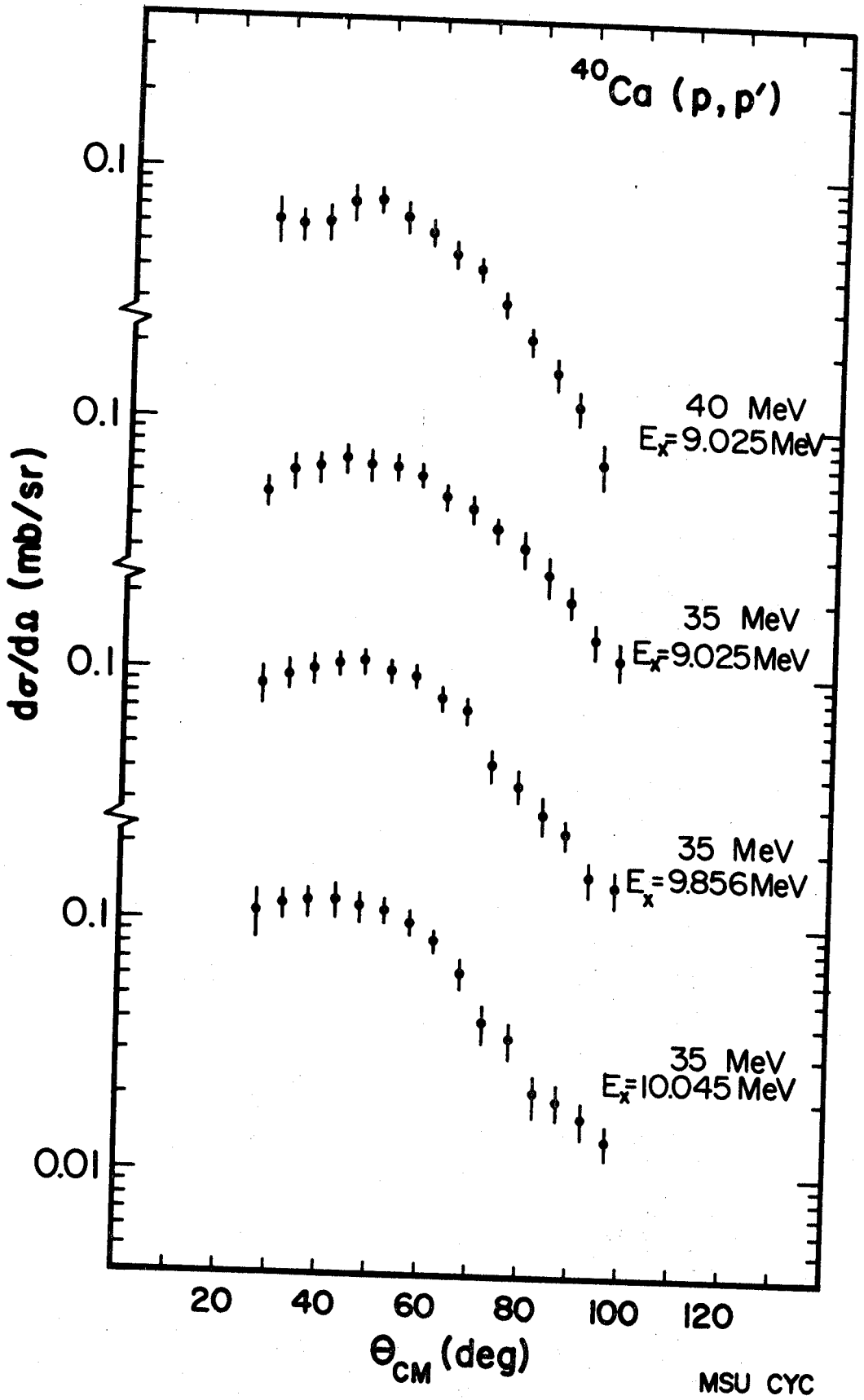
^{40}Ca (p, p′)
0.1
0.1
0.1
0.1
0.01
dσ/dΩ (mb/sr)
40 MeV
E$_x$=9.025MeV
35 MeV
E$_x$=9.025MeV
35 MeV
E$_x$=9.856MeV
35 MeV
E$_x$=10.045 MeV
20
40
60
80
100
120
Θ$_{CM}$ (deg)
MSU CYC

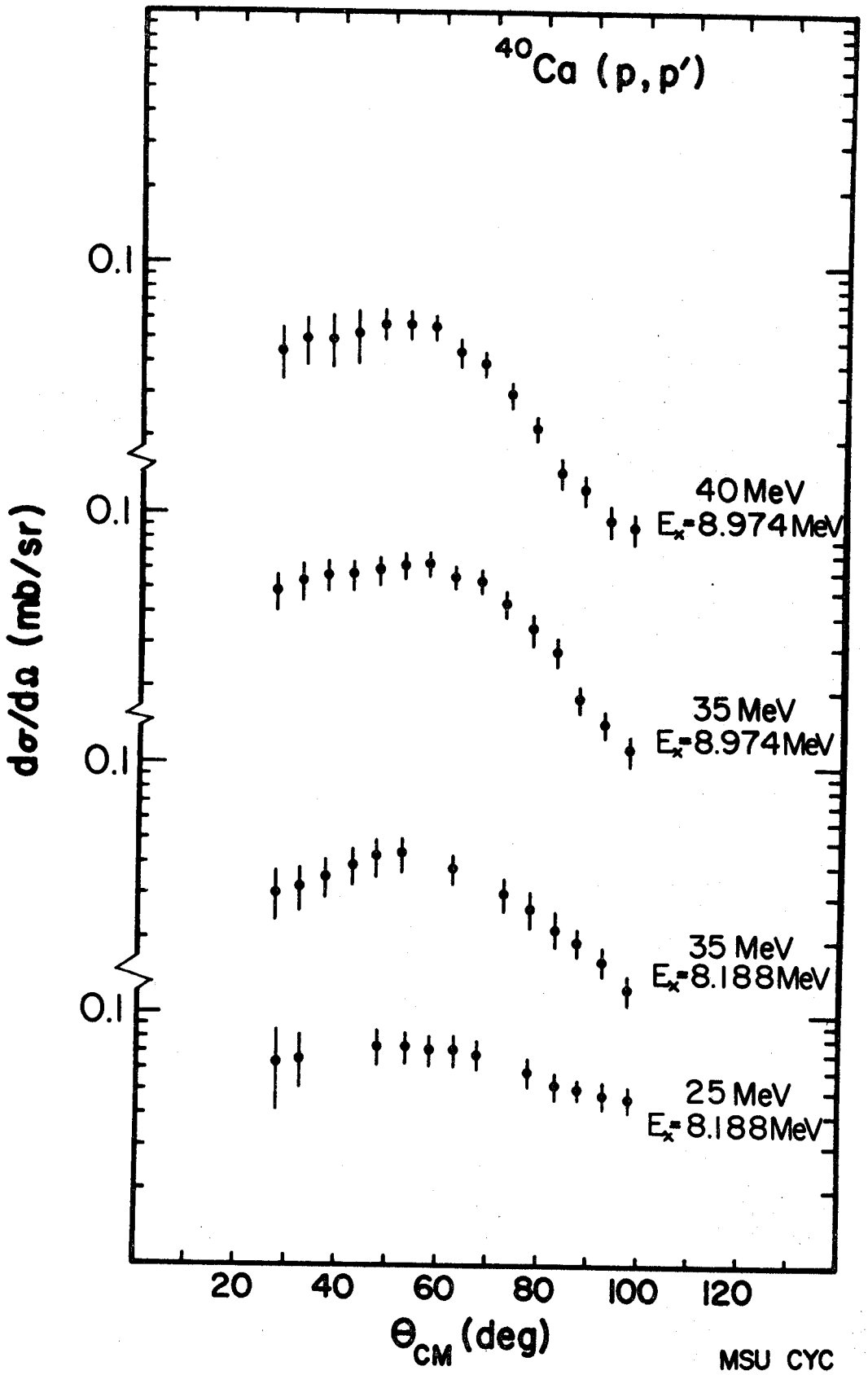
^{40}Ca (p, p′)
0.1
0.1
0.1
0.1
40 MeV
E_x=8.974 MeV
35 MeV
E_x=8.974 MeV
35 MeV
E_x=8.188 MeV
25 MeV
E_x=8.188 MeV
dσ/dΩ (mb/sr)
20
40
60
80
100
120
Θ_{CM} (deg)
MSU CYC

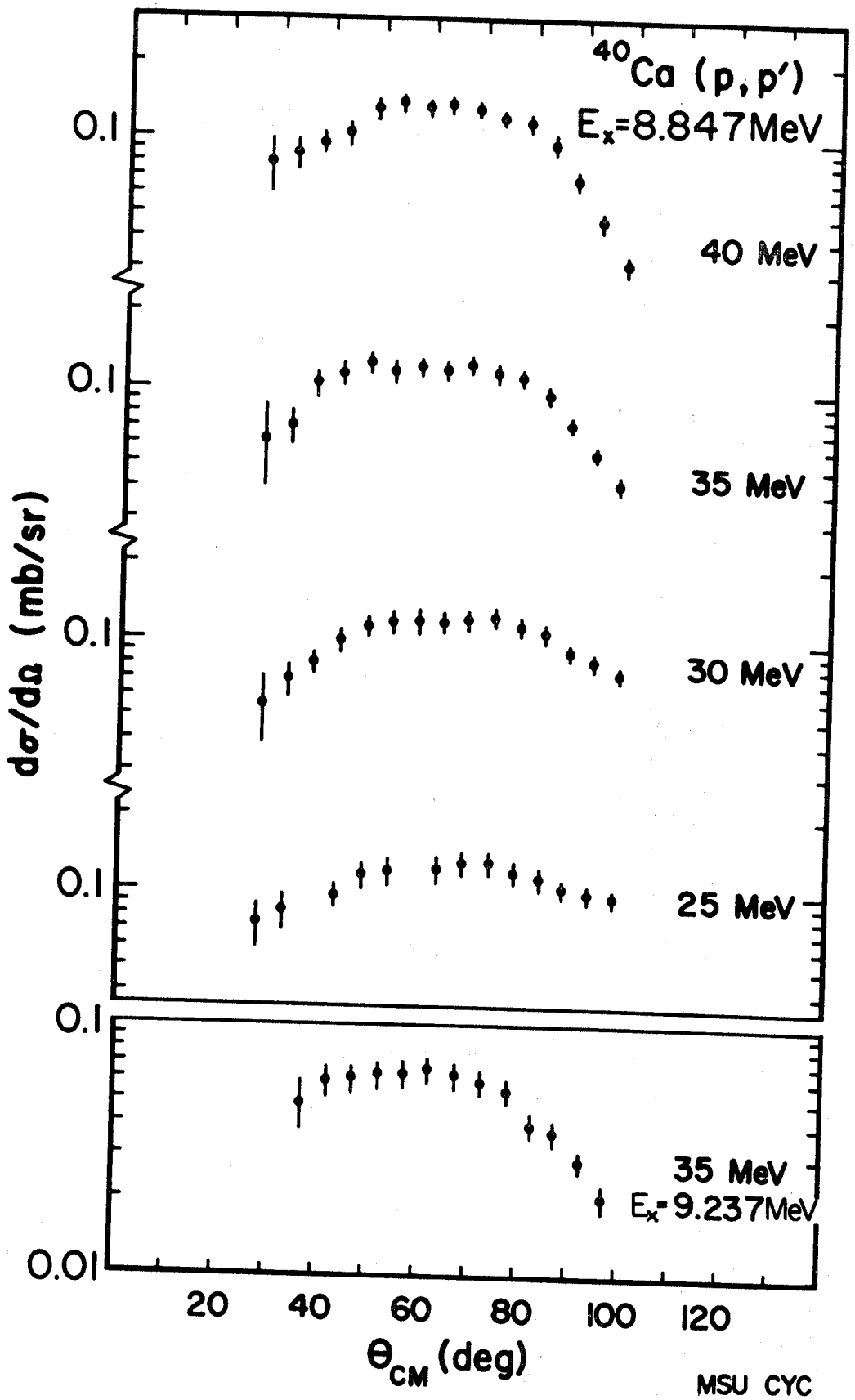
^{40}Ca (p, p')
E_x=8.847MeV
40 MeV
35 MeV
30 MeV
25 MeV
35 MeV
E_x=9.237MeV
0.1
0.1
0.1
0.1
0.1
0.01
dσ/dΩ (mb/sr)
20
40
60
80
100
120
θ_{CM} (deg)
MSU CYC

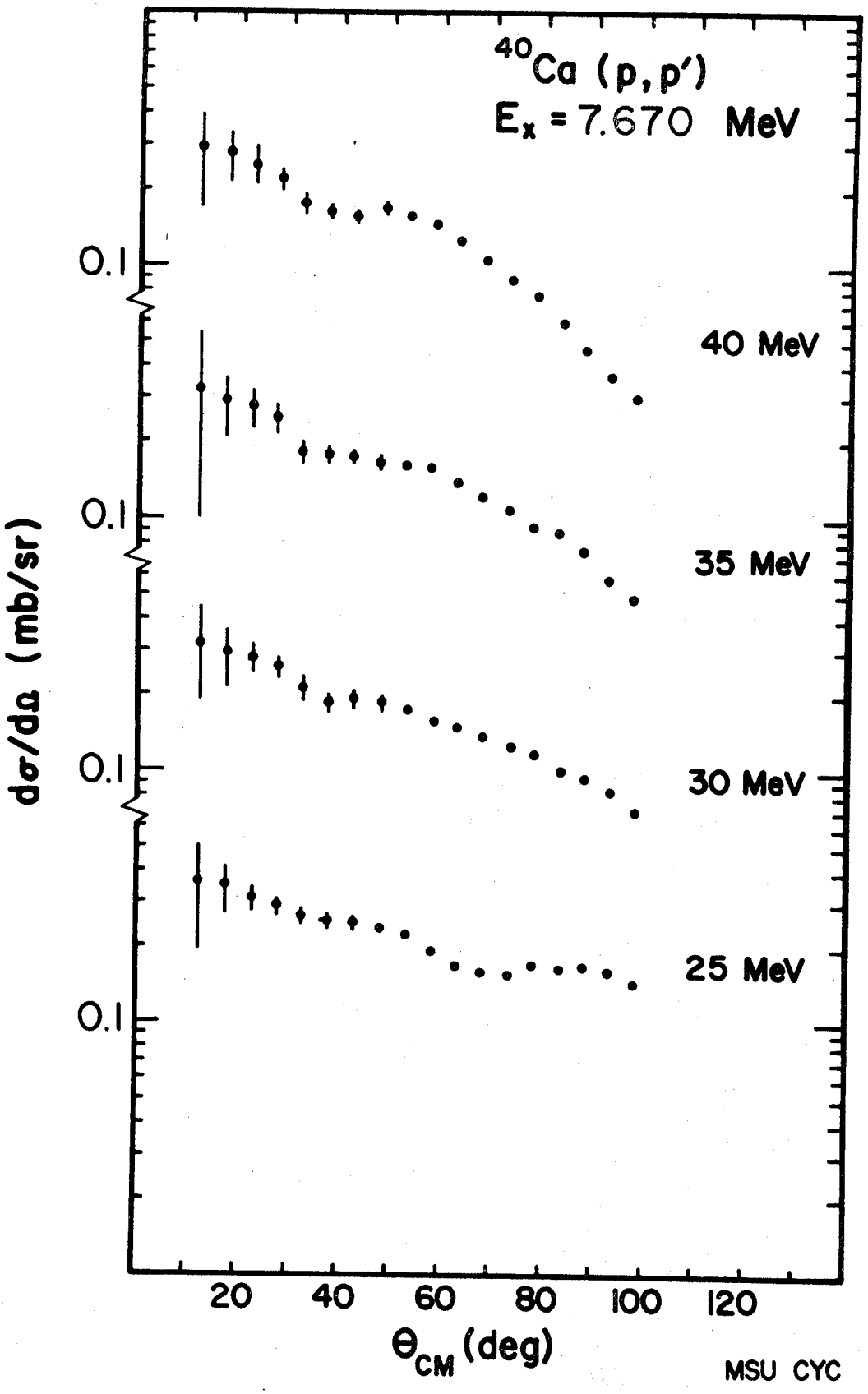
^{40}Ca (p, p′)
E_x = 7.670 MeV
40 MeV
35 MeV
30 MeV
25 MeV
0.1
0.1
0.1
0.1
dσ/dΩ (mb/sr)
20
40
60
80
100
120
Θ_{CM} (deg)
MSU CYC

APPENDIX II

TABULATED ANGULAR DISTRIBUTIONS

CA4C PROTON ELASTIC SCATTERING AT 24.926 MEV

ANG(CM) (DEG)	Dσ/DΩ (MB/SR)	ERROR (%)	ANG(L.) (DEG)	Dσ/DΩ (MB/SR)
12.31	4457.5000	0.083	12.00	4685.8008
17.43	1671.2000	0.105	17.00	1754.9744
22.56	609.2798	0.120	22.00	638.9622
27.37	163.2200	0.322	26.70	170.8404
27.67	146.2300	0.242	27.00	153.4668
32.48	15.9640	0.805	31.70	16.6738
37.58	26.1810	0.434	36.70	27.2669
42.69	78.6640	0.254	41.70	81.7283
47.78	106.3900	0.202	47.00	110.1534
53.17	95.5310	0.204	52.00	98.5710
58.24	64.3040	0.228	57.00	66.1162
63.31	37.7150	0.256	61.70	38.6321
68.36	18.6260	0.349	66.70	18.9903
73.16	11.0850	0.415	71.70	11.2687
73.41	10.9380	0.444	72.00	11.0998
78.44	10.7740	0.423	77.00	10.9068
83.47	12.2740	0.378	82.00	12.3546
88.15	12.0890	0.320	86.70	12.1133
93.19	10.6850	0.322	91.70	10.6655
98.77	8.7471	0.339	96.70	8.6868

CA4C PROTON ELASTIC SCATTERING AT 30.044 MEV

ANG(CM) (DEG)	Dσ/DΩ (MB/SR)	ERROR (%)	ANG(L.) (DEG)	Dσ/DΩ (MB/SR)
12.31	4033.2996	0.085	12.00	4241.0781
17.44	1691.5000	0.118	17.00	1776.6917
22.56	588.7698	0.114	22.00	617.1724
27.36	136.1900	0.341	26.70	142.5841
27.67	120.3800	0.194	27.00	126.0068
32.48	19.3430	0.821	31.70	20.1968
37.58	55.4510	0.275	36.70	57.7913
42.69	101.8000	0.160	41.70	105.7859
47.78	106.1500	0.159	47.00	109.9363
53.17	72.3900	0.175	52.00	74.7065
58.25	38.9460	0.251	57.00	40.0558
63.31	19.9890	0.275	61.70	20.4864
68.37	10.0980	0.353	66.70	10.3035
73.11	9.6520	0.381	71.70	9.7968
73.42	9.7582	0.413	72.00	9.9174
78.45	11.1090	0.349	77.00	11.2446
83.48	10.6920	0.383	82.00	10.7620
88.19	8.4576	0.337	86.70	8.4696
93.19	5.5789	0.373	91.70	5.5740
98.19	3.1466	0.535	96.70	3.1369

CA40 PROTON ELASTIC SCATTERING AT 34.775 MEV

ANG(CM) (DEG)	Dσ/DΩ (MB/SR)	ERROR (%)	ANG(L.) (DEG)	Dσ/DΩ (MB/SR)
11.80	4073.3997	0.112	11.50	4284.5156
16.93	1904.0999	0.092	16.50	2000.6177
22.05	669.3699	0.136	21.50	702.4241
26.86	155.8800	0.329	26.20	163.3601
31.98	28.9800	0.431	31.20	30.2831
37.08	67.7570	0.268	36.20	70.6285
42.19	104.8900	0.173	41.20	109.0434
47.28	94.0350	0.153	46.20	97.4852
52.37	59.3360	0.174	51.20	61.2902
57.44	27.7500	0.251	56.20	28.5458
62.51	12.2340	0.357	61.20	12.5235
67.57	8.6144	0.389	66.20	8.7833
72.62	8.9522	0.296	71.20	9.0970
72.92	9.0077	0.506	71.50	9.1453
77.96	8.9908	0.520	76.50	9.0970
82.98	7.1135	0.530	81.50	7.1666
87.69	4.8260	0.387	86.20	4.8501
92.70	2.9197	0.515	91.20	2.9197
97.69	1.9197	0.617	96.20	1.6650

CA40 PROTON ELASTIC SCATTERING AT 39.828 MEV

ANG(CM) (DEG)	Dσ/DΩ (MB/SR)	ERROR (%)	ANG(L.) (DEG)	Dσ/DΩ (MB/SR)
12.31	3859.5999	0.069	12.00	4060.5928
17.44	1662.8997	0.090	17.00	1747.4944
22.56	526.0298	0.116	22.00	551.9248
27.38	115.7500	0.286	26.70	121.2291
27.68	95.3860	0.218	27.00	99.8982
32.49	44.1820	0.404	31.70	46.1848
37.60	84.7930	0.216	36.70	88.3882
42.70	93.8900	0.165	41.70	97.6058
48.10	63.7760	0.255	47.00	66.0679
53.19	30.3310	0.287	52.00	31.3207
58.26	12.6680	0.412	57.00	13.0302
63.02	8.0040	0.543	61.70	8.2042
68.08	7.6440	0.430	66.70	7.7940
73.13	7.2940	0.409	71.70	7.4079
73.43	7.2460	0.548	72.00	7.3596
78.47	5.6000	0.534	77.00	5.6705
83.49	3.1560	0.576	82.00	3.1852
88.20	2.0080	0.785	86.70	2.0028
93.20	1.3200	0.828	91.70	1.3271
98.20	1.0620	0.748	96.70	1.0617

CA40(P,P')CA40* EX= 3.350 MEV

EP= 24.926 MEV

ANG(CM) (DEG)	Dσ/DΩ (MB/SR)	ERRΘR (%)
27.42	0.1350	13.70
32.54	0.0905	13.59
37.65	0.0740	10.14
42.76	0.0729	11.80
48.16	0.0788	13.20
53.26	0.0710	12.82
58.34	0.0600	12.17
63.09	0.0502	9.36
68.21	0.0410	9.27
73.21	0.0343	9.33
78.55	0.0253	13.83
83.59	0.0193	14.51
88.29	0.0140	13.57
93.29	0.0104	14.42

EP= 30.044 MEV

ANG(CM) (DEG)	Dσ/DΩ (MB/SR)	ERRΘR (%)
27.41	0.1000	16.00
32.53	0.0760	15.53
37.65	0.0635	11.18
42.76	0.0625	10.08
48.16	0.0692	10.40
53.24	0.0520	10.38
58.32	0.0336	12.50
63.08	0.0229	11.79
68.14	0.0166	12.05
73.19	0.0176	13.07
78.54	0.0200	12.00
83.56	0.0176	13.64
88.27	0.0140	11.43
98.27	0.0065	15.38

EP= 34.775 MEV

ANG(CM) (DEG)	Dσ/DΩ (MB/SR)	ERRΘR (%)
26.90	0.0894	20.81
32.02	0.0484	11.98
37.13	0.0396	17.42
42.24	0.0383	14.83
47.33	0.0420	12.14
52.22	0.0362	10.22
57.51	0.0256	11.72
62.58	0.0180	12.22
67.64	0.0128	13.28
72.69	0.0121	11.57
78.03	0.0134	20.15
87.77	0.0099	12.12
92.77	0.0068	14.71
97.76	0.0046	15.22

EP= 39.828 MEV

ANG(CM) (DEG)	Dσ/DΩ (MB/SR)	ERRΘR (%)
27.41	0.0678	16.52
32.53	0.0396	16.41
37.64	0.0372	15.86
42.75	0.0439	11.16
48.15	0.0415	18.07
53.24	0.0369	12.20
58.32	0.0227	14.10
63.08	0.0140	15.00
68.14	0.0075	18.67
73.18	0.0080	20.00
78.53	0.0075	21.33
83.55	0.0060	20.00
88.27	0.0044	22.73
93.27	0.0035	20.00
98.26	0.0026	23.08

CA40(P,P')CA40* EX= 3.732 MEV

EP= 24.926 MEV

ANG(CM) (DEG)	Dσ/DΩ (MB/SR)	ERRθR (%)
12.33	7.1300	3.00
17.47	8.1290	1.78
22.60	8.6400	1.01
27.42	8.6390	1.40
27.73	8.6390	1.02
32.54	8.5640	1.10
37.66	8.2790	0.79
42.77	7.6440	0.82
48.18	6.6120	0.83
53.27	5.7530	0.85
58.35	5.1230	0.82
63.11	4.7580	0.73
68.18	4.5650	0.69
73.26	4.3840	0.62
73.53	4.4690	0.70
78.57	4.0300	0.70
83.59	3.6270	0.71
88.30	2.8740	0.66
93.31	2.2440	0.70
98.30	1.7810	0.76

EP= 30.044 MEV

ANG(CM) (DEG)	Dσ/DΩ (MB/SR)	ERRθR (%)
12.33	8.3030	2.60
17.47	10.9910	1.70
22.60	11.8650	0.86
27.42	11.7610	1.16
27.72	11.7390	0.62
32.54	11.4060	1.06
37.65	10.0450	0.65
42.76	8.5470	0.56
48.16	6.4840	0.64
53.25	4.8890	0.67
58.33	4.0630	0.78
63.10	3.9330	0.62
68.16	3.6800	0.59
73.21	3.4390	0.64
73.51	3.4340	0.69
78.55	2.9940	0.67
83.57	2.3550	0.83
88.29	1.6820	0.75
93.29	1.1560	0.83
98.28	0.8760	0.99

EP= 34.775 MEV

ANG(CM) (DEG)	Dσ/DΩ (MB/SR)	ERRθR (%)
11.52	8.6100	3.70
16.95	12.0650	1.44
22.08	13.6310	1.06
26.90	13.5080	1.12
32.02	12.6060	0.68
37.13	11.1980	0.66
42.24	9.0920	0.59
47.34	6.4600	0.59
52.43	4.5390	0.63
57.52	3.5350	0.71
62.59	3.2870	0.69
67.65	3.1730	0.64
72.70	2.8000	0.53
73.00	2.6930	0.92
78.04	2.2390	1.05
83.06	1.5680	1.13
87.78	1.0360	0.82
92.78	0.7670	1.00
97.77	0.5940	1.05

EP= 39.828 MEV

ANG(CM) (DEG)	Dσ/DΩ (MB/SR)	ERRθR (%)
12.33	9.6300	1.87
17.46	12.5700	1.24
22.59	14.2300	0.75
27.41	14.3720	0.78
27.72	14.3940	0.55
32.53	13.4110	0.73
37.64	10.9000	0.60
42.75	7.6900	0.57
48.15	4.8380	0.92
53.24	3.2600	0.86
58.32	2.8860	0.87
63.09	2.7440	0.73
68.15	2.3090	0.78
73.20	1.7900	0.83
73.50	1.8030	1.10
78.54	1.2260	1.14
83.56	0.7750	1.16
88.27	0.5940	1.44
93.28	0.4970	1.36

CA40(P,P')CA40* EX= 3.900 MEV

EP= 24.926 MEV

ANG(CM) (DEG)	Dσ/DΩ (MB/SR)	ERRθR (%)
12.34	1.9640	8.70
17.47	1.6700	5.50
22.60	1.4330	3.40
27.43	1.4210	3.60
32.55	1.3100	2.80
37.66	1.1530	2.20
42.77	0.8590	2.60
48.18	0.6640	2.90
53.27	0.5240	3.10
58.35	0.4800	3.00
63.12	0.4870	2.70
68.18	0.5260	2.20
73.23	0.4560	2.10
73.53	0.4460	2.30
78.57	0.3620	2.40
83.60	0.2630	2.70
88.31	0.2070	2.60
93.31	0.1890	2.70
98.30	0.1820	2.90

EP= 30.044 MEV

ANG(CM) (DEG)	Dσ/DΩ (MB/SR)	ERRθR (%)
12.33	2.5170	5.50
17.47	1.9700	4.60
22.60	1.7230	2.70
27.42	1.6700	3.20
27.72	1.6740	1.80
32.54	1.4960	3.10
37.65	1.0330	2.10
42.76	0.7240	2.50
48.17	0.5410	2.80
53.26	0.4780	3.10
58.34	0.5040	2.60
63.10	0.5160	2.10
68.17	0.4320	2.10
73.21	0.3500	2.10
73.52	0.3330	2.50
78.55	0.2200	2.80
83.58	0.1670	3.50
88.29	0.1570	2.90
93.29	0.1500	2.50
98.28	0.1400	2.70

EP= 34.775 MEV

ANG(CM) (DEG)	Dσ/DΩ (MB/SR)	ERRθR (%)
11.32	2.7440	6.60
16.95	2.1200	4.50
22.08	1.8800	3.35
26.90	1.5270	3.25
32.02	1.3710	2.08
37.14	0.9750	2.50
42.25	0.6300	2.57
47.35	0.4560	2.78
52.44	0.4780	2.45
57.52	0.5140	2.10
62.59	0.4830	1.93
67.65	0.3550	2.04
72.70	0.2340	2.14
73.00	0.2270	3.65
78.04	0.1790	4.20
83.07	0.1460	4.20
87.78	0.1450	2.45
92.79	0.1340	2.85
97.77	0.1150	2.55

EP= 39.828 MEV

ANG(CM) (DEG)	Dσ/DΩ (MB/SR)	ERRθR (%)
12.33	2.9700	4.70
17.46	2.3820	3.40
22.59	2.1330	3.15
27.41	1.9210	2.27
32.53	1.3000	2.50
37.65	0.7430	2.50
42.75	0.4510	2.80
48.16	0.4610	3.60
53.25	0.5120	2.50
58.33	0.4560	2.33
63.09	0.3330	2.80
68.15	0.2150	2.67
73.20	0.1450	3.10
73.50	0.1320	4.40
78.54	0.1300	3.75
83.57	0.1290	3.05
88.28	0.1110	3.54
93.28	0.0870	3.37
98.27	0.0620	3.20

CA40(P,P')CA40* EX= 4.487 MEV

EP= 24.926 MEV

ANG(CM) (DEG)	Dσ/DΩ (MB/SR)	ERRθR (%)
12.33	1.7390	8.80
17.47	1.7860	4.70
22.60	1.8570	3.00
27.42	1.9070	3.00
27.72	1.9140	2.26
32.54	1.9980	2.50
37.65	2.1010	1.56
42.76	2.1430	1.60
48.17	2.1100	1.54
53.26	2.0510	1.40
58.34	1.9190	1.37
63.10	1.7680	1.20
68.16	1.5950	1.22
73.21	1.3640	1.20
73.52	1.3240	1.31
78.55	1.1440	1.31
83.58	0.9660	1.39
88.29	0.7910	1.26
93.29	0.6700	1.31
98.28	0.6000	1.30

EP= 30.044 MEV

ANG(CM) (DEG)	Dσ/DΩ (MB/SR)	ERRθR (%)
12.33	1.6010	0.00
17.47	1.6950	5.50
22.60	1.7990	2.60
27.42	1.9420	3.00
27.72	1.9570	1.55
32.54	2.0490	2.52
37.65	2.1360	1.40
42.76	2.1770	1.11
48.17	2.1380	1.12
53.26	2.0650	1.06
58.34	1.8710	1.16
63.10	1.6800	0.93
68.16	1.3930	0.94
73.21	1.1030	1.14
73.52	1.0440	1.25
78.55	0.8580	1.25
83.58	0.6570	1.53
88.29	0.5170	1.33
93.29	0.4260	1.33
98.28	0.3470	1.61

EP= 34.775 MEV

ANG(CM) (DEG)	Dσ/DΩ (MB/SR)	ERRθR (%)
11.82	1.4410	5.00
16.96	1.5560	5.70
22.09	1.6580	4.00
26.91	1.8090	3.20
32.03	1.9110	1.80
37.15	2.1720	1.60
42.26	2.2590	1.20
47.36	2.2590	1.10
52.45	2.1260	0.93
57.53	1.9550	1.00
62.60	1.7200	0.97
67.67	1.3870	1.00
72.72	1.0470	0.90
73.02	0.9990	1.60
78.06	0.7750	1.90
83.08	0.5740	1.90
87.80	0.4150	1.40
92.80	0.3310	1.60
97.79	0.2510	1.60

EP= 39.828 MEV

ANG(CM) (DEG)	Dσ/DΩ (MB/SR)	ERRθR (%)
12.33	1.2470	0.40
17.47	1.3500	5.60
22.60	1.4900	3.00
27.42	1.6080	2.60
27.72	1.6310	1.90
32.54	1.8160	2.10
37.65	2.1560	1.50
42.76	2.2130	1.12
48.17	2.2950	1.46
53.26	2.0440	1.14
58.34	1.7720	1.12
63.10	1.4810	1.30
68.16	1.0780	1.16
73.21	0.7900	1.28
73.52	0.7900	1.72
78.55	0.5860	1.72
83.58	0.3960	1.68
88.29	0.2860	2.15
93.29	0.2080	2.15
98.28	0.1370	2.15

CA40(P,P')CA40* EX= 5.240 MEV

EP= 24.926 MEV

ANG(CM) (DEG)	DσΩ/DΩ (MB/SR)	ERRθR (%)
12.35	0.4200	30.00
17.50	0.3300	20.00
22.63	0.2500	15.00
27.45	0.2200	17.60
32.58	0.1300	14.40
37.70	0.1050	11.00
42.81	0.0880	11.20
48.22	0.0720	10.50
53.31	0.0620	12.40
58.40	0.0530	12.00
63.17	0.0480	10.80
68.23	0.0450	9.50
73.58	0.0400	10.80
78.62	0.0360	10.80
83.65	0.0280	12.20
88.36	0.0230	12.00
93.36	0.0200	10.30
98.35	0.0190	10.30

EP= 30.044 MEV

ANG(CM) (DEG)	DσΩ/DΩ (MB/SR)	ERRθR (%)
12.35	0.3300	25.00
17.48	0.2450	20.00
22.61	0.2000	15.00
27.74	0.1550	9.80
32.56	0.1350	14.80
37.68	0.0840	11.40
48.20	0.0430	12.60
53.29	0.0370	12.70
58.37	0.0380	13.80
63.14	0.0410	11.40
68.20	0.0360	9.30
73.56	0.0300	11.00
78.59	0.0250	12.90
83.62	0.0150	12.00
88.33	0.0130	16.00
93.33	0.0125	17.00
98.33	0.0115	15.60

EP= 34.775 MEV

ANG(CM) (DEG)	DσΩ/DΩ (MB/SR)	ERRθR (%)
11.82	0.3500	30.00
16.96	0.2400	25.00
22.10	0.1800	22.00
26.92	0.1450	15.00
32.04	0.1150	12.00
37.16	0.0560	14.00
42.24	0.0400	13.40
47.37	0.0320	12.40
52.46	0.0315	12.00
57.55	0.0350	11.50
62.62	0.0310	12.00
67.68	0.0225	12.00
73.04	0.0180	14.50
78.08	0.0115	15.00
83.10	0.0097	15.00
87.82	0.0090	12.00
92.82	0.0084	14.00
97.81	0.0086	15.40

EP= 39.828 MEV

ANG(CM) (DEG)	DσΩ/DΩ (MB/SR)	ERRθR (%)
12.33	0.3500	25.60
17.47	0.2500	20.90
22.60	0.1850	16.20
27.73	0.1500	12.50
32.55	0.0940	14.60
37.66	0.0540	14.00
42.70	0.0350	15.50
48.18	0.0330	16.80
53.27	0.0300	16.80
58.35	0.0300	14.00
63.12	0.0210	17.60
68.18	0.0145	14.60
73.53	0.0115	17.20
78.57	0.0105	15.00
83.59	0.0090	14.60
88.31	0.0078	16.00
93.31	0.0064	15.50
98.31	0.0041	17.60

CA40(P,P')CA40* EX= 5.270 MEV

EP= 24.926 MEV

ANG(CM) (DEG)	Dσ/DΩ (MB/SR)	ERRθR (%)
12.35	0.1450	30.00
17.50	0.1800	20.00
22.63	0.1050	15.00
27.45	0.1050	17.60
32.58	0.1000	14.40
37.70	0.0920	11.00
42.81	0.0880	11.20
48.22	0.0820	10.40
53.31	0.0730	12.40
58.40	0.0630	12.00
63.17	0.0540	10.80
68.23	0.0450	9.50
73.58	0.0360	10.80
78.62	0.0320	10.80
83.65	0.0300	12.20
88.36	0.0260	12.20
93.36	0.0230	10.30
98.35	0.0200	10.30

EP= 30.044 MEV

ANG(CM) (DEG)	Dσ/DΩ (MB/SR)	ERRθR (%)
12.35	0.1350	25.00
17.48	0.2100	20.00
22.61	0.0960	15.00
27.74	0.0980	9.80
32.56	0.0970	14.80
37.68	0.0920	11.40
48.20	0.0830	12.60
53.29	0.0700	12.70
58.37	0.0430	13.80
63.14	0.0330	11.40
68.20	0.0320	9.30
73.56	0.0270	11.00
78.59	0.0240	12.90
83.62	0.0200	12.00
88.33	0.0155	16.00
93.33	0.0135	17.00
98.33	0.0125	14.60

EP= 34.775 MEV

ANG(CM) (DEG)	Dσ/DΩ (MB/SR)	ERRθR (%)
11.82	0.1200	30.00
16.96	0.1850	25.00
22.10	0.0800	22.00
26.92	0.0780	15.00
32.04	0.0790	12.00
37.16	0.0780	14.00
42.27	0.0740	13.40
47.37	0.0630	12.40
52.46	0.0540	12.00
57.55	0.0410	11.50
62.62	0.0275	12.00
67.68	0.0215	12.00
73.04	0.0170	14.50
78.08	0.0160	15.00
83.10	0.0140	15.00
87.82	0.0120	12.00
92.82	0.0100	14.00
97.81	0.0064	15.40

EP= 39.828 MEV

ANG(CM) (DEG)	Dσ/DΩ (MB/SR)	ERRθR (%)
12.33	0.1200	25.00
17.45	0.1800	20.90
22.60	0.0750	16.20
27.73	0.0780	12.50
32.55	0.0780	14.60
37.66	0.0720	14.00
42.77	0.0660	15.50
48.18	0.0540	16.80
53.27	0.0400	16.80
58.35	0.0270	14.00
63.12	0.0190	17.60
68.18	0.0140	14.90
73.53	0.0110	17.20
78.57	0.0095	15.00
83.59	0.0087	14.60
88.31	0.0070	16.00
93.31	0.0060	15.50
98.31	0.0047	17.60

CA40(P,P')CA40* EX= 5.613 MEV

EP= 24.926 MEV

ANG(CM) (DEG)	Dσ/DΩ (MB/SR)	ERRθR (%)
12.35	0.2370	50.00
17.50	0.2880	20.60
22.63	0.3050	9.75
27.46	0.3514	9.03
27.76	0.3538	6.42
32.58	0.3850	5.47
37.71	0.4220	3.62
42.82	0.4540	3.62
48.23	0.4572	3.63
53.33	0.4395	3.43
58.41	0.4215	2.92
63.18	0.3910	2.71
68.25	0.3570	2.60
73.30	0.2892	2.70
73.60	0.3026	2.82
78.64	0.2451	3.00
83.67	0.2122	3.11
88.38	0.1809	2.77
93.38	0.1612	2.79
98.37	0.1556	2.54

EP= 30.044 MEV

ANG(CM) (DEG)	Dσ/DΩ (MB/SR)	ERRθR (%)
12.34	0.3200	21.50
17.48	0.3800	14.70
22.62	0.4300	6.64
27.44	0.4836	6.13
32.57	0.4291	5.50
37.59	0.4193	3.38
42.80	0.4005	2.92
48.21	0.3566	3.31
53.30	0.3226	3.06
58.38	0.2880	3.34
63.15	0.2430	2.65
68.21	0.2090	2.51
73.27	0.1610	3.15
73.57	0.1710	3.32
78.61	0.1370	3.37
83.63	0.0996	4.43
88.35	0.0735	4.06
93.35	0.0610	4.36
98.34	0.0522	4.64

EP= 34.775 MEV

ANG(CM) (DEG)	Dσ/DΩ (MB/SR)	ERRθR (%)
11.82	0.2500	60.00
16.96	0.3000	19.00
22.10	0.3450	10.00
26.92	0.3655	7.94
32.05	0.3380	4.41
37.16	0.3676	4.07
42.27	0.3635	3.33
47.38	0.3500	2.80
52.47	0.2983	2.80
57.56	0.2707	2.75
62.63	0.2190	2.84
67.69	0.1626	3.07
72.74	0.1225	2.73
73.05	0.1188	4.83
78.09	0.0882	5.93
83.11	0.0650	6.22
87.83	0.0583	3.74
92.83	0.0512	4.25
97.82	0.0354	4.61

EP= 39.828 MEV

ANG(CM) (DEG)	Dσ/DΩ (MB/SR)	ERRθR (%)
12.34	0.2750	22.85
17.47	0.3280	14.35
22.50	0.3500	10.00
27.43	0.3790	5.60
27.74	0.3755	4.24
32.55	0.3567	4.93
37.67	0.3353	3.90
42.78	0.3406	3.30
48.18	0.3170	4.11
53.28	0.2529	3.58
58.36	0.2053	3.51
63.13	0.1550	4.30
68.19	0.1054	3.98
73.24	0.0704	4.58
73.54	0.0731	6.13
78.58	0.0498	6.55
83.60	0.0402	5.75
88.32	0.0330	6.60
93.32	0.0268	6.28
98.31	0.0198	5.90

CA40(P,P')CA40* EX= 5.900 MEV

EP= 24.926 MEV

ANG(CM) (DEG)	Dσ/DΩ (MB/SR)	ERRθR (%)
12.35	0.4500	28.00
17.50	0.4300	18.20
22.64	0.4150	8.35
27.46	0.3040	10.25
27.77	0.3220	6.40
32.59	0.2110	7.63
37.71	0.1568	6.34
42.83	0.1057	8.52
48.24	0.0825	11.07
53.34	0.0713	10.22
58.42	0.0580	9.72
63.19	0.0508	9.60
68.26	0.0431	9.05
73.31	0.0495	7.09
73.61	0.0461	8.46
78.65	0.0476	7.63
83.68	0.0457	7.78
88.39	0.0420	6.20
93.39	0.0318	7.00
98.38	0.0307	6.71

EP= 30.044 MEV

ANG(CM) (DEG)	Dσ/DΩ (MB/SR)	ERRθR (%)
12.35	0.5200	38.00
17.49	0.4600	15.80
22.62	0.4100	7.20
27.45	0.2790	7.94
27.75	0.2634	5.10
32.57	0.1684	8.77
37.69	0.1112	7.30
42.80	0.0724	8.60
48.21	0.0532	13.10
53.31	0.0426	12.23
58.39	0.0370	7.65
63.16	0.0341	9.72
68.22	0.0375	7.02
73.28	0.0405	7.92
73.58	0.0407	7.26
78.62	0.0373	7.14
83.64	0.0257	9.67
88.36	0.0227	8.16
93.36	0.0220	8.00
98.35	0.0224	7.75

EP= 34.775 MEV

ANG(CM) (DEG)	Dσ/DΩ (MB/SR)	ERRθR (%)
11.83	0.5900	23.80
16.97	0.5400	11.00
22.10	0.4100	10.50
26.92	0.2997	9.02
32.05	0.1425	7.30
37.17	0.0960	8.75
42.28	0.0680	9.50
47.38	0.0515	10.36
52.48	0.0388	8.84
57.56	0.0301	10.30
62.64	0.0321	8.57
67.70	0.0430	6.54
72.75	0.0398	5.35
73.05	0.0360	12.45
78.09	0.0342	10.35
83.12	0.0262	10.88
87.84	0.0273	5.70
92.84	0.0223	6.67
97.83	0.0227	5.95

EP= 39.828 MEV

ANG(CM) (DEG)	Dσ/DΩ (MB/SR)	ERRθR (%)
12.34	0.6500	17.60
17.48	0.5600	12.90
22.61	0.2650	9.28
27.43	0.1900	8.11
27.74	0.1860	6.64
32.55	0.1203	9.18
37.67	0.0810	7.11
42.78	0.0573	9.92
48.19	0.0460	9.66
53.28	0.0416	11.93
58.36	0.0370	7.28
63.13	0.0276	12.55
68.19	0.0344	7.44
73.24	0.0294	7.48
73.55	0.0277	11.92
78.58	0.0186	11.62
83.61	0.0215	8.27
88.32	0.0229	8.25
93.32	0.0220	7.00
98.31	0.0159	6.59

CA40(P,P')CA40* EX= 6.021 MEV

EP= 24.926 MEV

ANG(CM) (DEG)	Dσ/DΩ (MB/SR)	ERRθR (%)
12.35	0.1500	64.00
17.50	0.1650	30.60
22.64	0.1850	16.60
27.46	0.2004	13.00
27.77	0.1959	9.74
32.59	0.1914	7.97
37.72	0.1780	5.92
42.83	0.1750	6.30
48.24	0.1667	6.88
53.34	0.1516	6.77
58.43	0.1420	5.88
63.20	0.1370	5.05
68.26	0.1320	3.80
73.31	0.1305	4.25
73.62	0.1300	4.47
78.66	0.1160	4.51
83.68	0.1076	4.65
88.40	0.0823	4.24
93.40	0.0691	4.51
98.39	0.0452	5.24

EP= 30.044 MEV

ANG(CM) (DEG)	Dσ/DΩ (MB/SR)	ERRθR (%)
12.35	0.1590	51.40
17.45	0.1800	34.80
22.62	0.2060	10.50
27.76	0.2160	5.80
32.57	0.2103	7.67
37.69	0.1940	5.06
42.81	0.1670	4.61
48.22	0.1280	5.75
53.31	0.1020	5.83
58.40	0.0882	6.19
63.16	0.0809	5.36
68.23	0.0783	4.52
73.28	0.0734	5.15
73.58	0.0741	5.18
78.62	0.0665	5.13
83.65	0.0520	6.27
88.36	0.0413	5.62
93.36	0.0271	8.00
98.35	0.0168	9.00

EP= 34.775 MEV

ANG(CM) (DEG)	Dσ/DΩ (MB/SR)	ERRθR (%)
11.83	0.1750	70.00
16.97	0.1990	28.80
22.10	0.2150	17.00
26.93	0.2357	10.40
32.05	0.2287	5.56
37.17	0.2007	5.61
42.28	0.1505	5.72
47.39	0.1180	5.25
52.48	0.0900	5.45
57.57	0.0677	6.07
62.64	0.0643	5.42
67.70	0.0547	5.76
72.75	0.0475	4.75
73.26	0.0461	8.60
78.10	0.0394	9.60
83.12	0.0290	10.16
87.34	0.0243	6.13
92.84	0.0164	8.05
97.83	0.0104	9.76

EP= 39.828 MEV

ANG(CM) (DEG)	Dσ/DΩ (MB/SR)	ERRθR (%)
12.34	0.1620	45.50
17.48	0.2020	24.00
22.61	0.2130	12.45
27.43	0.2230	7.50
27.74	0.2320	5.78
32.56	0.1815	7.18
37.67	0.1607	5.62
42.78	0.1278	5.86
48.19	0.0842	8.06
53.28	0.0592	7.78
58.37	0.0476	8.18
63.13	0.0421	9.20
68.20	0.0362	7.20
73.25	0.0289	7.70
73.55	0.0291	11.00
78.59	0.0215	10.86
83.61	0.0109	12.95
88.33	0.0075	16.00
93.33	0.0068	12.86
98.32	0.0066	11.07

CA40(P,P')CA40* EX= 6.281 MEV

EP= 24.926 MEV

ANG(CM) (DEG)	Dσ/DΩ (MB/SR)	ERRθR (%)
12.36	1.1800	11.00
17.50	1.2100	5.50
22.64	1.2300	3.50
27.47	1.1473	4.16
32.60	1.1170	3.22
37.72	1.0057	2.31
42.84	0.9195	2.43
48.25	0.8175	2.57
53.35	0.7043	2.65
58.44	0.5301	2.78
63.21	0.4248	2.68
68.27	0.3431	2.70
73.33	0.2703	2.78
73.63	0.2780	2.94
78.67	0.2171	3.16
83.70	0.2154	3.04
88.41	0.1612	2.99
93.41	0.1395	3.03
98.40	0.1310	2.95

EP= 30.044 MEV

ANG(CM) (DEG)	Dσ/DΩ (MB/SR)	ERRθR (%)
12.36	1.0800	8.00
17.50	1.1500	11.00
22.64	1.1700	6.00
27.45	1.1506	4.91
32.58	1.1285	3.39
37.70	0.9686	2.18
42.81	0.8125	1.94
48.22	0.6508	2.37
53.32	0.4519	2.55
58.40	0.3008	3.10
63.17	0.2717	2.63
68.24	0.2537	2.35
73.29	0.2356	2.59
73.59	0.2361	2.90
78.63	0.2254	2.62
83.66	0.1949	2.99
88.37	0.1446	2.77
98.36	0.1084	3.04

EP= 34.775 MEV

ANG(CM) (DEG)	Dσ/DΩ (MB/SR)	ERRθR (%)
11.33	0.9600	12.00
16.97	1.0800	6.00
22.11	1.1200	4.25
26.93	1.1824	4.00
32.06	1.1020	2.40
37.17	0.9540	2.39
42.29	0.7104	2.28
47.39	0.4965	1.81
52.49	0.3075	2.76
57.57	0.2521	2.90
62.65	0.2669	2.55
67.71	0.2868	2.26
72.76	0.2600	1.82
73.06	0.2671	3.11
78.10	0.2419	3.39
83.13	0.1848	3.48
87.85	0.1514	2.25
92.85	0.1316	2.53
97.84	0.1074	2.54

EP= 39.828 MEV

ANG(CM) (DEG)	Dσ/DΩ (MB/SR)	ERRθR (%)
12.34	0.8052	9.41
17.48	0.9335	5.54
22.61	1.1081	3.34
27.43	1.1487	2.96
27.74	1.1678	2.18
32.56	1.0495	2.75
37.68	0.8085	2.33
42.79	0.5344	2.50
48.20	0.3260	4.02
53.29	0.2271	3.77
58.37	0.2841	2.94
63.14	0.2923	2.98
68.20	0.2760	2.35
73.25	0.2385	2.36
73.55	0.2443	3.14
78.59	0.2009	2.95
83.62	0.1568	2.71
88.33	0.1288	3.17
93.33	0.1032	3.04
98.32	0.0768	2.86

CA40(P,P')CA40* Ex= 6.502 MEV

EP= 24.926 MEV

ANG(CM) (DEG)	DσΩ/DΩ (MB/SR)	ERRθR (%)
12.38	0.0650	90.00
17.52	0.0880	54.00
22.66	0.1100	25.00
27.78	0.1220	18.24
32.61	0.1340	9.56
37.73	0.1260	8.12
42.86	0.1140	8.23
48.26	0.1040	9.97
53.36	0.0921	9.64
58.44	0.0824	7.72
63.22	0.0676	9.70
68.28	0.0544	6.90
73.64	0.0454	8.25
78.68	0.0401	8.38
83.71	0.0391	7.97
88.42	0.0338	7.19
93.42	0.0283	7.52
98.41	0.0247	7.62

EP= 30.044 MEV

ANG(CM) (DEG)	DσΩ/DΩ (MB/SR)	ERRθR (%)
12.36	0.0740	85.00
17.50	0.0980	50.00
22.64	0.1200	16.00
27.76	0.1426	14.00
32.58	0.1630	10.80
37.69	0.1450	14.00
42.82	0.1350	5.15
48.23	0.1160	6.37
53.32	0.0875	6.83
58.41	0.0726	7.63
63.18	0.0563	6.40
68.24	0.0450	6.38
73.60	0.0370	7.90
78.64	0.0368	7.30
83.66	0.0294	9.24
88.38	0.0245	9.05
93.38	0.0210	9.20
98.37	0.0180	9.10

EP= 34.775 MEV

ANG(CM) (DEG)	DσΩ/DΩ (MB/SR)	ERRθR (%)
11.83	0.0900	75.00
16.97	0.1150	45.00
22.01	0.1350	25.00
26.93	0.1530	14.00
32.06	0.1600	9.00
37.18	0.1550	6.34
42.29	0.1430	5.57
47.40	0.1200	5.60
52.49	0.1020	5.33
57.58	0.0759	5.80
62.65	0.0517	6.40
67.22	0.0402	6.76
73.07	0.0319	11.56
78.11	0.0318	10.77
83.14	0.0295	9.74
87.85	0.0219	6.48
92.86	0.0185	7.56
97.85	0.0160	7.07

EP= 39.828 MEV

ANG(CM) (DEG)	DσΩ/DΩ (MB/SR)	ERRθR (%)
12.34	0.0980	85.00
17.48	0.1250	33.00
22.62	0.1450	14.00
27.74	0.1570	7.95
32.57	0.1620	6.50
37.68	0.1590	5.77
42.79	0.1430	5.12
48.20	0.1190	6.33
53.79	0.0874	6.56
58.38	0.0562	7.10
63.14	0.0334	10.00
68.21	0.0240	9.50
73.56	0.0206	8.05
78.60	0.0196	10.40
83.62	0.0163	9.90
88.34	0.0148	9.90
93.34	0.0115	9.20
98.33	0.0071	9.20

CA40(P,P')CA40* EX= 6.577 MEV

EP= 24.926 MEV

ANG(CM) (DEG)	Dσ/DΩ (MB/SR)	ERRΘR (%)
12.36	0.9600	13.00
17.50	0.9900	7.60
22.65	0.9800	4.40
27.78	0.9397	4.75
32.61	0.9020	3.00
37.73	0.8592	2.49
42.85	0.7500	2.35
48.26	0.6400	2.73
53.36	0.5486	3.00
58.45	0.4165	3.12
63.22	0.3164	3.08
68.29	0.2486	3.15
73.64	0.2011	3.52
78.68	0.1774	3.58
83.71	0.1520	3.64
88.42	0.1214	3.44
93.43	0.1124	3.40
98.41	0.0996	3.48

EP= 30.044 MEV

ANG(CM) (DEG)	Dσ/DΩ (MB/SR)	ERRΘR (%)
12.36	0.8700	13.00
17.50	0.9500	7.40
22.64	0.9400	4.10
27.76	0.8812	4.72
32.58	0.8250	3.96
37.69	0.7010	6.10
42.82	0.5950	2.24
48.23	0.4740	2.77
53.33	0.3541	2.95
58.41	0.2320	3.70
63.18	0.1995	3.05
68.25	0.1655	3.00
73.60	0.1623	3.62
78.64	0.1350	3.44
83.67	0.1125	4.20
88.38	0.0903	3.68
93.38	0.0730	3.18
98.37	0.0581	4.28

EP= 34.775 MEV

ANG(CM) (DEG)	Dσ/DΩ (MB/SR)	ERRΘR (%)
11.83	0.7600	22.80
16.97	0.8700	8.00
22.01	0.9100	6.00
26.93	0.8752	4.84
32.06	0.7398	2.85
37.18	0.6480	2.63
42.29	0.4725	2.87
47.40	0.3228	2.95
52.49	0.2274	3.32
57.58	0.1653	3.48
62.65	0.1657	3.30
67.72	0.1641	3.00
73.07	0.1380	4.49
78.11	0.1110	4.82
83.14	0.0887	5.14
87.95	0.0735	3.26
92.86	0.0588	3.90
97.85	0.0494	3.81

EP= 39.828 MEV

ANG(CM) (DEG)	Dσ/DΩ (MB/SR)	ERRΘR (%)
12.34	0.6835	11.07
17.48	0.7668	7.60
22.62	0.7805	4.62
27.75	0.7555	3.74
32.57	0.6500	2.68
37.68	0.4942	3.00
42.79	0.3220	3.30
48.20	0.1876	5.50
53.29	0.1396	4.78
58.38	0.1515	4.13
63.15	0.1680	3.98
68.21	0.1454	3.34
73.56	0.1180	4.70
78.60	0.0975	4.37
83.63	0.0775	3.88
88.34	0.0568	4.85
93.34	0.0482	4.50
98.33	0.0286	4.74

CA40(P,P')CA40* EX= 6.747 MEV

EP= 24.926 MEV

ANG(CM) (DEG)	Dσ/DΩ (MB/SR)	ERRBR (%)
12.36	0.2700	33.00
17.51	0.3100	18.00
22.65	0.3200	6.95
27.79	0.3260	6.65
32.61	0.3104	5.34
37.74	0.2694	4.79
42.85	0.2091	5.78
48.27	0.2097	5.79
53.37	0.1950	3.87
58.45	0.1733	5.34
63.23	0.1435	5.09
68.29	0.1773	3.90
73.65	0.1783	3.78
78.69	0.1645	3.80
83.72	0.1430	3.98
88.43	0.1123	3.62
93.43	0.0886	4.07
98.42	0.0646	3.83

EP= 30.044 MEV

ANG(CM) (DEG)	Dσ/DΩ (MB/SR)	ERRBR (%)
12.35	0.2600	27.00
17.49	0.2800	18.00
22.63	0.3100	8.55
27.77	0.3158	4.65
32.59	0.3018	6.15
37.71	0.2717	4.55
42.82	0.2103	3.90
48.24	0.1950	4.40
53.33	0.1484	4.83
58.42	0.1160	5.78
63.19	0.1041	4.63
68.25	0.1047	3.85
73.61	0.1078	4.38
78.65	0.0965	4.34
83.67	0.0866	4.84
88.39	0.0653	4.45
93.39	0.0461	5.34
98.38	0.0290	6.35

EP= 34.775 MEV

ANG(CM) (DEG)	Dσ/DΩ (MB/SR)	ERRBR (%)
11.88	0.2720	40.00
16.97	0.3300	22.00
22.10	0.3630	8.00
26.93	0.3250	6.03
32.06	0.3152	4.53
37.18	0.2772	4.75
42.30	0.1779	3.48
47.40	0.1635	4.67
52.50	0.1120	5.36
57.58	0.0902	5.55
62.64	0.0769	5.10
67.72	0.0822	4.40
72.77	0.0743	3.76
78.12	0.0629	7.45
83.14	0.0541	6.62
87.96	0.0435	4.70
92.86	0.0312	5.76
97.85	0.0186	6.56

EP= 39.828 MEV

ANG(CM) (DEG)	Dσ/DΩ (MB/SR)	ERRBR (%)
12.34	0.2800	34.00
17.48	0.3000	21.00
22.62	0.3280	8.16
27.75	0.3022	4.60
32.57	0.2895	5.48
37.68	0.2420	3.80
42.80	0.1408	5.53
48.20	0.1270	7.01
53.30	0.0970	6.17
58.38	0.0758	6.46
63.15	0.0514	7.63
68.21	0.0517	6.06
73.57	0.0502	8.16
78.60	0.0417	7.10
83.63	0.0293	7.27
88.34	0.0215	8.41
93.34	0.0141	8.88
98.33	0.0068	10.82

CA40(P,P')CA40* EX= 6.905 MEV

EP= 24.926 MEV

ANG(CM) (DEG)	Dσ/DΩ (MB/SR)	ERRθR (%)
12.37	1.7200	5.00
17.51	1.4800	4.00
22.65	1.2900	3.00
27.48	1.2500	4.90
32.62	1.1500	4.80
37.74	0.8700	4.80
42.86	0.6800	5.70
48.27	0.5300	6.30
53.37	0.4700	6.30
58.46	0.4600	5.40
63.23	0.4500	4.80
68.30	0.4600	4.80
73.66	0.4200	4.60
78.70	0.3700	5.10
83.73	0.3300	5.20
88.44	0.2400	4.80
93.44	0.1900	4.70
98.43	0.1800	4.60

EP= 30.044 MEV

ANG(CM) (DEG)	Dσ/DΩ (MB/SR)	ERRθR (%)
12.35	2.4500	5.10
17.49	1.8300	3.80
22.63	1.3600	2.70
27.46	1.2400	3.60
32.59	1.1400	3.60
37.71	0.8100	3.20
42.83	0.6600	3.10
48.24	0.5100	4.50
53.34	0.4700	3.80
58.42	0.4950	3.60
63.19	0.5200	4.00
68.26	0.4500	3.40
73.61	0.3500	3.50
78.65	0.2650	4.30
83.68	0.1800	3.60
88.39	0.1400	4.00
93.39	0.1380	3.50
98.38	0.1500	3.20

EP= 34.775 MEV

ANG(CM) (DEG)	Dσ/DΩ (MB/SR)	ERRθR (%)
11.52	2.0200	5.80
16.97	1.7600	4.00
22.10	1.3400	3.70
26.94	1.3200	4.80
32.06	1.1000	4.80
37.19	0.9500	5.10
42.30	0.6900	5.00
47.40	0.5050	4.50
52.50	0.5100	4.70
57.59	0.5200	4.70
62.66	0.5000	4.50
67.73	0.3900	4.20
73.08	0.2380	6.30
78.12	0.2100	7.20
83.15	0.1800	6.60
87.86	0.1700	4.40
92.97	0.1650	4.50
97.86	0.1500	4.20

EP= 39.828 MEV

ANG(CM) (DEG)	Dσ/DΩ (MB/SR)	ERRθR (%)
12.34	1.9500	6.80
17.48	1.7200	4.80
22.62	1.6200	3.40
27.44	1.5800	5.40
32.57	1.3800	5.40
37.69	0.9700	4.80
42.80	0.6850	4.70
48.21	0.5740	6.70
53.30	0.5600	5.70
58.38	0.5400	5.40
63.15	0.4200	6.00
68.22	0.2300	5.40
73.27	0.1680	5.40
78.61	0.1450	6.30
83.63	0.1600	5.40
88.35	0.1690	6.00
93.35	0.1500	5.20
98.34	0.1100	4.80

CA40(P,P')CA40* EX= 6.944 MEV

EP= 24.926 MEV

ANG(CM) (DEG)	Dσ/DΩ (MB/SR)	ERRθR (%)
12.37	2.4600	5.00
17.51	2.9100	4.00
22.65	2.8500	3.00
27.48	2.3200	4.90
32.62	1.7200	4.80
37.74	1.2300	4.80
42.86	0.8100	5.70
48.27	0.5900	6.30
53.37	0.5100	6.30
58.46	0.4350	5.40
63.23	0.4150	4.80
68.30	0.4800	4.80
73.66	0.4400	4.60
78.70	0.3450	5.10
83.73	0.3050	5.20
88.44	0.2600	4.80
93.44	0.2800	4.70
98.43	0.2700	4.60

EP= 30.044 MEV

ANG(CM) (DEG)	Dσ/DΩ (MB/SR)	ERRθR (%)
12.35	2.6000	5.10
17.49	3.1300	3.80
22.63	2.7900	2.70
27.46	1.9600	3.60
32.59	1.3000	3.60
37.71	0.8700	3.20
42.83	0.5900	3.10
48.24	0.4700	4.50
53.34	0.3700	3.80
58.42	0.3200	3.60
63.19	0.2950	4.00
68.26	0.3050	3.40
73.61	0.3200	3.50
78.65	0.3100	4.30
83.68	0.2700	3.60
88.39	0.2200	4.00
93.39	0.2250	3.50
98.38	0.2150	3.20

EP= 34.775 MEV

ANG(CM) (DEG)	Dσ/DΩ (MB/SR)	ERRθR (%)
11.22	2.2900	5.80
16.97	2.7500	4.00
22.10	2.1400	3.70
26.94	1.8000	4.80
32.06	1.1400	4.80
37.19	0.8000	5.10
42.30	0.6100	5.00
47.40	0.4200	4.50
52.50	0.3100	4.70
57.59	0.2700	4.70
62.66	0.2500	4.50
67.73	0.2800	4.20
73.08	0.2700	6.30
78.12	0.2500	7.20
83.15	0.2450	6.60
87.86	0.2300	4.40
92.87	0.1950	4.50
97.86	0.1600	4.20

EP= 39.828 MEV

ANG(CM) (DEG)	Dσ/DΩ (MB/SR)	ERRθR (%)
12.34	2.3600	6.80
17.48	2.6900	4.80
22.62	1.9400	3.40
27.44	1.3400	5.40
32.57	0.9140	5.40
37.69	0.6100	4.80
42.80	0.4000	4.70
48.21	0.3350	6.70
53.30	0.2700	5.70
58.38	0.2250	5.40
63.15	0.2280	6.00
68.22	0.2560	5.40
73.27	0.2380	5.40
78.61	0.2140	6.30
83.63	0.1910	5.40
88.35	0.1720	6.00
93.35	0.1500	5.20
98.34	0.1300	4.80

CA40(P,P')CA40* EX= 7.110 MEV

EP= 24.926 MEV

ANG(CM) (DEG)	Dσ/DΩ (MB/SR)	ERRθR (%)
12.36	0.1900	54.00
17.51	0.2160	27.40
22.66	0.2500	12.90
27.80	0.3060	8.46
32.62	0.3545	6.33
37.75	0.3935	3.80
42.87	0.4000	4.02
48.28	0.4137	3.87
53.38	0.4158	3.57
58.47	0.3828	3.35
63.24	0.3372	3.00
68.31	0.2800	4.66
73.67	0.2385	3.24
78.71	0.1958	3.80
83.73	0.1416	3.96
88.45	0.1138	3.70
93.45	0.0974	3.75
98.44	0.0850	3.85

EP= 30.044 MEV

ANG(CM) (DEG)	Dσ/DΩ (MB/SR)	ERRθR (%)
12.35	0.2150	42.00
17.50	0.2450	24.00
22.64	0.2900	8.85
27.77	0.3240	4.40
32.59	0.3450	5.84
37.72	0.3214	4.16
42.83	0.3223	3.33
48.25	0.3040	3.50
53.34	0.2570	3.40
58.43	0.2420	3.58
63.20	0.1910	3.13
68.26	0.1620	3.12
73.32	0.1310	3.70
73.62	0.1307	3.94
78.66	0.0988	4.24
83.69	0.0745	4.70
88.40	0.0549	4.87
93.40	0.0425	5.40
98.39	0.0345	5.80

EP= 34.775 MEV

ANG(CM) (DEG)	Dσ/DΩ (MB/SR)	ERRθR (%)
11.83	0.1650	60.00
16.97	0.1900	32.00
22.01	0.2250	15.00
26.94	0.2422	10.76
32.07	0.2900	4.88
37.19	0.2847	4.48
42.30	0.2854	4.05
47.41	0.2770	3.28
52.51	0.2135	3.38
57.59	0.1815	3.41
62.67	0.1595	3.49
67.73	0.1297	3.52
72.78	0.0932	3.24
73.09	0.0918	5.90
78.13	0.0729	5.83
83.16	0.0551	6.87
87.87	0.0381	4.85
92.87	0.0258	6.36
97.86	0.0196	6.75

EP= 39.828 MEV

ANG(CM) (DEG)	Dσ/DΩ (MB/SR)	ERRθR (%)
12.34	0.1630	44.00
17.48	0.1800	22.52
22.62	0.2040	10.92
27.44	0.2412	7.10
27.75	0.2485	5.60
32.57	0.2590	5.90
37.69	0.2560	4.32
42.80	0.2570	3.77
48.21	0.2370	4.55
53.30	0.1638	4.49
58.39	0.1436	4.32
63.16	0.1114	5.04
68.22	0.0810	4.60
73.27	0.0642	4.70
73.57	0.0618	6.75
78.61	0.0448	6.83
83.64	0.0354	6.12
88.35	0.0287	7.08
93.35	0.0146	9.67
98.34	0.0132	7.26

CA40(P,P')CA40* EX= 7.290 MEV

EP= 24.926 MEV

ANG(CM) (DEG)	Dσ/DΩ (MB/SR)	ERRθR (%)
27.80	0.0890	14.50
32.62	0.0700	20.00
42.87	0.0530	15.00
48.28	0.0660	14.00
53.39	0.0520	16.00
58.47	0.0320	20.00
63.24	0.0270	15.50
78.71	0.0240	14.00
83.73	0.0190	17.00
88.45	0.0180	11.00
98.44	0.0150	12.50

EP= 30.044 MEV

ANG(CM) (DEG)	Dσ/DΩ (MB/SR)	ERRθR (%)
27.77	0.0720	21.00
32.59	0.0500	24.00
37.72	0.0350	22.00
42.83	0.0390	17.00
48.25	0.0350	21.00
58.43	0.0250	17.00
73.32	0.0210	13.00
78.66	0.0150	16.00
83.69	0.0120	22.00
88.40	0.0081	20.00
98.39	0.0052	21.00

EP= 34.775 MEV

ANG(CM) (DEG)	Dσ/DΩ (MB/SR)	ERRθR (%)
26.94	0.0950	20.00
37.19	0.0400	18.00
42.30	0.0270	22.00
47.41	0.0210	21.00
52.51	0.0180	23.00
57.59	0.0170	21.00
67.73	0.0150	13.00
72.78	0.0130	14.00
78.13	0.0120	20.00
83.16	0.0088	25.00
87.87	0.0071	14.00
92.87	0.0065	16.00
97.86	0.0052	16.00

EP= 39.828 MEV

ANG(CM) (DEG)	Dσ/DΩ (MB/SR)	ERRθR (%)
27.44	0.0790	17.00
32.57	0.0460	20.00
37.69	0.0350	15.00
42.80	0.0260	18.00
58.39	0.0150	18.00
63.16	0.0130	18.00
68.22	0.0100	16.00
73.27	0.0084	16.00
78.61	0.0064	16.00
83.64	0.0053	20.00
88.35	0.0056	17.00
93.35	0.0036	22.00
98.34	0.0027	20.00

CA40(P,P')CA40* EX= 7.454 MEV

EP= 24.926 MEV

ANG(CM) (DEG)	Dσ/DΩ (MB/SR)	ERRθR (%)
17.52	0.0708	40.00
22.66	0.0741	25.40
27.80	0.0865	26.30
32.62	0.0955	15.20
37.75	0.1070	10.00
42.87	0.1125	8.50
48.30	0.1130	8.90
53.40	0.1080	7.50
58.48	0.1050	7.40
63.26	0.0864	6.40
68.33	0.0717	6.80
73.68	0.0660	7.30
78.72	0.0552	7.80
83.75	0.0460	8.20
88.47	0.0415	6.90
93.47	0.0426	6.10
98.46	0.0381	6.50

EP= 30.044 MEV

ANG(CM) (DEG)	Dσ/DΩ (MB/SR)	ERRθR (%)
17.50	0.0700	50.00
22.64	0.0764	16.70
27.78	0.0840	16.20
32.59	0.0953	12.60
37.72	0.1080	8.50
42.82	0.1090	5.90
48.26	0.1060	7.10
53.35	0.0809	7.30
58.44	0.0684	8.10
63.20	0.0565	6.20
68.27	0.0530	5.50
73.63	0.0448	12.20
78.67	0.0360	7.40
83.70	0.0307	10.20
88.41	0.0280	7.20
93.42	0.0246	7.50
98.41	0.0213	7.40

EP= 34.775 MEV

ANG(CM) (DEG)	Dσ/DΩ (MB/SR)	ERRθR (%)
16.98	0.0760	31.40
22.11	0.0830	25.00
26.94	0.0942	22.90
32.07	0.1090	10.60
37.20	0.1180	8.50
42.31	0.1110	6.90
47.41	0.0996	6.70
52.51	0.0727	7.20
57.50	0.0473	9.10
62.67	0.0410	6.60
67.74	0.0365	6.60
72.80	0.0335	5.90
77.83	0.0305	11.20
82.86	0.0270	9.30
87.88	0.0248	6.40
92.88	0.0175	7.70
97.88	0.0132	8.10

EP= 39.828 MEV

ANG(CM) (DEG)	Dσ/DΩ (MB/SR)	ERRθR (%)
17.49	0.0810	27.00
22.62	0.0890	18.30
27.76	0.1010	8.10
32.58	0.1110	10.10
37.71	0.1170	8.00
42.82	0.1060	7.30
48.22	0.0930	8.50
53.31	0.0612	8.50
58.40	0.0391	13.30
63.17	0.0290	9.40
68.24	0.0265	9.50
73.58	0.0210	12.30
78.62	0.0184	11.30
83.65	0.0170	8.50
88.38	0.0157	10.00
93.36	0.0126	11.00
98.35	0.0102	9.30

CA40(P,P')CA40* EX= 7.539 MEV

EP= 24.926 MEV

ANG(CM) (DEG)	Dσ/DΩ (MB/SR)	ERRθR (%)
12.37	0.3000	32.84
17.52	0.3350	19.00
22.66	0.3420	9.74
27.80	0.3800	6.39
32.62	0.3700	7.60
37.75	0.3500	3.97
42.86	0.3340	3.96
48.30	0.3080	4.12
53.40	0.2850	3.89
58.48	0.2740	4.00
63.26	0.2480	3.55
68.33	0.2160	3.62
73.68	0.1800	3.71
78.72	0.1540	3.96
83.75	0.1320	3.48
88.47	0.1120	3.75
93.47	0.1007	3.74
98.46	0.0865	3.73

EP= 30.044 MEV

ANG(CM) (DEG)	Dσ/DΩ (MB/SR)	ERRθR (%)
12.36	0.2800	28.67
17.50	0.3140	19.30
22.64	0.3350	9.05
27.78	0.3420	4.66
32.59	0.3440	7.11
37.72	0.3260	4.12
42.82	0.2980	3.50
48.26	0.2620	3.98
53.35	0.2010	4.23
58.44	0.1580	4.68
63.20	0.1330	3.94
68.27	0.1030	4.04
73.63	0.0810	5.61
78.67	0.0680	5.10
83.70	0.0550	6.47
88.41	0.0451	7.07
93.42	0.0407	6.80
98.41	0.0309	6.28

EP= 34.775 MEV

ANG(CM) (DEG)	Dσ/DΩ (MB/SR)	ERRθR (%)
11.83	0.2800	57.14
16.98	0.3370	19.50
22.11	0.3510	12.96
26.94	0.3590	7.94
32.07	0.3600	4.38
37.20	0.3160	5.02
42.31	0.2510	2.92
47.41	0.1980	4.02
52.51	0.1630	4.40
57.50	0.1320	4.18
62.67	0.1050	4.09
67.74	0.0808	3.56
73.10	0.0612	7.72
77.83	0.0468	9.77
82.86	0.0371	6.66
87.88	0.0316	5.58
92.88	0.0263	6.25
97.88	0.0207	6.52

EP= 39.828 MEV

ANG(CM) (DEG)	Dσ/DΩ (MB/SR)	ERRθR (%)
12.35	0.2750	32.25
17.49	0.3100	19.58
22.62	0.3370	8.23
27.76	0.3500	4.72
32.58	0.3620	4.76
37.71	0.3050	4.13
42.82	0.2280	4.00
48.22	0.1860	5.60
53.31	0.1400	4.90
58.40	0.0960	5.52
63.17	0.0723	4.73
68.24	0.0605	5.48
73.58	0.0458	7.87
78.62	0.0355	7.30
83.65	0.0242	8.56
88.37	0.0182	9.59
93.36	0.0136	10.00
98.35	0.0083	10.56

CA40(P,P')CA40* EX= 7.670 MEV

EP= 24.926 MEV

ANG(CM) (DEG)	Dσ/DΩ (MB/SR)	ERRθR (%)
12.37	0.3600	45.00
17.52	0.3490	21.10
22.62	0.3130	10.30
27.80	0.2860	9.75
32.62	0.2640	6.90
37.75	0.2530	5.10
42.87	0.2470	5.75
48.30	0.2340	5.30
53.40	0.2220	5.00
58.48	0.1920	4.50
63.26	0.1660	4.75
68.33	0.1560	4.43
73.68	0.1530	4.20
78.70	0.1670	3.70
83.75	0.1600	3.90
88.47	0.1630	3.00
93.47	0.1570	3.00
98.46	0.1430	3.00

EP= 30.044 MEV

ANG(CM) (DEG)	Dσ/DΩ (MB/SR)	ERRθR (%)
12.36	0.3150	40.00
17.50	0.2920	25.00
22.64	0.2780	10.00
27.78	0.2560	6.20
32.59	0.2100	9.00
37.72	0.1850	6.40
42.82	0.1910	4.40
48.26	0.1840	5.30
53.35	0.1720	4.40
58.44	0.1560	4.80
63.20	0.1460	3.70
68.27	0.1350	3.50
73.63	0.1230	3.70
78.67	0.1140	3.50
83.70	0.0990	4.40
88.41	0.0913	3.50
93.42	0.0810	3.70
98.41	0.0675	3.90

EP= 34.775 MEV

ANG(CM) (DEG)	Dσ/DΩ (MB/SR)	ERRθR (%)
11.83	0.3090	69.00
16.98	0.2820	25.00
22.11	0.2680	17.50
26.94	0.2410	10.90
32.07	0.1780	6.50
37.20	0.1730	6.41
42.31	0.1710	4.80
47.41	0.1620	5.00
52.51	0.1580	4.30
57.50	0.1550	4.00
62.67	0.1360	3.95
67.74	0.1190	3.60
73.10	0.1050	6.10
77.83	0.0905	6.30
82.86	0.0857	5.65
87.88	0.0725	3.40
92.88	0.0557	4.20
97.87	0.0469	4.10

EP= 39.828 MEV

ANG(CM) (DEG)	Dσ/DΩ (MB/SR)	ERRθR (%)
12.35	0.2860	40.00
17.49	0.2750	21.60
22.62	0.2440	16.67
27.76	0.2160	7.38
32.58	0.1760	8.18
37.71	0.1640	5.00
42.82	0.1570	4.20
48.22	0.1680	5.96
53.31	0.1560	4.97
58.40	0.1450	5.36
63.17	0.1250	5.45
68.24	0.1050	4.53
73.58	0.0882	5.50
78.62	0.0753	4.84
83.65	0.0596	4.65
88.37	0.0462	5.37
93.36	0.0360	5.50
98.35	0.0294	4.85

CA40(P,P')CA40* EX= 7.865 MEV

EP= 24.926 MEV

ANG(CM) (DEG)	Dσ/DΩ (MB/SR)	ERRθR (%)
12.37	0.6020	18.60
17.53	0.5450	11.07
22.68	0.5130	4.46
27.82	0.5380	4.86
32.65	0.5470	4.55
37.78	0.4360	4.76
42.90	0.3420	4.32
48.34	0.2030	5.97
53.43	0.1540	5.87
58.53	0.1120	7.00
63.30	0.0814	6.90
68.37	0.0682	6.80
73.73	0.0622	6.83
78.78	0.0643	6.25
83.80	0.0660	5.34
88.51	0.0649	5.06
93.51	0.0595	5.17
98.50	0.0510	5.10

EP= 30.044 MEV

ANG(CM) (DEG)	Dσ/DΩ (MB/SR)	ERRθR (%)
12.36	0.6920	16.88
17.50	0.6030	12.00
22.65	0.5270	5.71
27.79	0.4650	3.58
32.61	0.4730	5.43
37.74	0.2920	4.18
42.85	0.2120	4.36
48.28	0.1560	6.00
53.29	0.1230	5.55
58.47	0.1080	5.77
63.23	0.0606	6.16
68.30	0.0537	6.07
73.66	0.0503	6.42
78.70	0.0469	7.34
83.73	0.0454	7.86
88.44	0.0386	6.08
93.44	0.0357	6.10
98.43	0.0303	6.17

EP= 34.775 MEV

ANG(CM) (DEG)	Dσ/DΩ (MB/SR)	ERRθR (%)
11.23	0.7250	22.70
16.97	0.5750	12.35
22.11	0.5370	9.38
26.94	0.5070	6.43
32.08	0.3580	4.28
37.20	0.2860	4.64
42.32	0.1580	5.53
47.43	0.1430	5.37
52.53	0.1150	5.63
57.62	0.0970	5.18
62.70	0.0646	5.97
67.76	0.0515	6.05
73.12	0.0409	10.28
78.16	0.0397	10.25
83.20	0.0408	8.50
88.21	0.0378	6.70
93.21	0.0309	5.84
98.20	0.0285	5.28

EP= 39.828 MEV

ANG(CM) (DEG)	Dσ/DΩ (MB/SR)	ERRθR (%)
12.35	0.6840	15.27
17.49	0.6220	9.77
22.63	0.5600	5.33
27.76	0.5350	3.40
32.60	0.3350	4.96
37.69	0.1660	5.68
42.81	0.1340	5.44
48.23	0.1260	7.48
53.32	0.1020	6.28
58.41	0.0947	5.89
63.17	0.0730	6.29
68.24	0.0502	5.79
73.60	0.0365	8.88
78.64	0.0317	7.62
83.66	0.0308	6.66
88.37	0.0306	7.02
93.37	0.0240	6.96
98.36	0.0180	6.33

CA40(P,P')CA40* EX= 7.921 MEV

EP= 24.926 MEV

ANG(CM) (DEG)	Dσ/DΩ (MB/SR)	ERRθR (%)
12.37	0.2510	48.90
17.53	0.3100	18.75
22.68	0.3340	10.00
27.82	0.3820	5.94
32.65	0.3840	5.92
37.78	0.3620	4.24
42.90	0.3530	4.84
48.34	0.3400	4.24
53.43	0.3180	3.99
58.53	0.2760	3.97
63.30	0.2220	3.81
68.37	0.1860	3.27
73.73	0.1500	3.84
78.78	0.1250	4.34
83.80	0.1080	4.57
88.51	0.0944	4.41
93.51	0.0831	4.50
98.50	0.0760	4.10

EP= 30.044 MEV

ANG(CM) (DEG)	Dσ/DΩ (MB/SR)	ERRθR (%)
12.36	0.2610	44.70
17.50	0.3030	12.50
22.65	0.3350	7.62
27.79	0.3820	3.94
32.61	0.3930	6.53
37.74	0.3880	3.34
42.85	0.3750	3.10
48.28	0.3340	3.57
53.29	0.2920	3.22
58.47	0.2320	3.69
63.23	0.1980	3.05
68.30	0.1620	3.09
73.66	0.1250	3.85
78.70	0.0944	4.25
83.73	0.0696	5.50
88.44	0.0610	4.40
93.44	0.0560	4.50
98.43	0.0518	4.51

EP= 34.775 MEV

ANG(CM) (DEG)	Dσ/DΩ (MB/SR)	ERRθR (%)
11.83	0.2820	55.00
16.97	0.3380	20.50
22.11	0.3910	11.33
26.94	0.4070	7.39
32.08	0.4240	4.51
37.20	0.4040	3.92
42.32	0.3640	3.36
47.43	0.3220	3.07
52.53	0.2530	3.06
57.62	0.2070	3.25
62.70	0.1670	3.43
67.76	0.1050	3.44
73.12	0.0723	6.82
78.16	0.0594	5.76
83.20	0.0485	5.85
88.21	0.0416	4.62
93.21	0.0367	4.93
98.20	0.0338	4.09

EP= 39.828 MEV

ANG(CM) (DEG)	Dσ/DΩ (MB/SR)	ERRθR (%)
12.35	0.2810	35.33
17.49	0.3380	16.67
22.63	0.4150	6.61
27.76	0.4430	3.76
32.60	0.4540	4.46
37.69	0.4470	3.30
42.81	0.3830	3.03
48.23	0.3290	3.73
53.32	0.2220	3.82
58.41	0.1540	4.16
63.17	0.1160	4.43
68.24	0.0805	4.51
73.60	0.0558	6.89
78.64	0.0456	5.41
83.66	0.0369	5.71
88.37	0.0285	6.03
93.37	0.0210	7.23
98.36	0.0185	6.06

CA40(P,P')CA40* EX= 8.097 MEV

EP= 24.926 MEV

ANG(CM) (DEG)	Dσ/DΩ (MB/SR)	ERRΘR (%)
12.37	0.5450	21.20
17.53	0.5740	15.00
22.68	0.5850	7.05
27.82	0.6300	4.66
32.65	0.5420	4.98
37.78	0.4820	3.44
42.90	0.4170	3.82
48.34	0.3180	4.74
53.43	0.2700	4.42
58.53	0.2240	4.90
63.30	0.1620	4.82
68.37	0.1280	4.00
73.73	0.1170	4.93
78.78	0.1120	4.85
83.80	0.1050	4.60
88.51	0.0923	4.29
93.51	0.0857	4.12
98.51	0.0756	4.24

EP= 30.044 MEV

ANG(CM) (DEG)	Dσ/DΩ (MB/SR)	ERRΘR (%)
12.36	0.4950	18.75
17.50	0.4850	22.00
22.65	0.4900	8.00
27.79	0.5060	3.76
32.61	0.4850	5.70
37.74	0.3720	3.68
42.85	0.2850	3.77
48.28	0.2180	4.80
53.29	0.1760	4.64
58.47	0.1420	5.33
63.23	0.1170	4.34
68.30	0.0930	4.10
73.66	0.0820	5.13
78.70	0.0756	5.26
83.73	0.0750	5.67
88.44	0.0732	4.20
92.44	0.0676	4.73
98.43	0.0610	4.20

EP= 34.775 MEV

ANG(CM) (DEG)	Dσ/DΩ (MB/SR)	ERRΘR (%)
11.83	0.3700	40.00
16.97	0.3670	22.20
22.11	0.3900	10.90
26.94	0.3840	6.91
32.08	0.3380	4.64
37.20	0.2800	4.56
42.32	0.2140	4.85
47.43	0.1460	5.02
52.53	0.1370	4.49
57.62	0.1200	4.65
62.70	0.1020	4.81
67.76	0.0867	4.34
73.12	0.0756	6.73
78.16	0.0735	7.17
83.20	0.0703	7.39
88.21	0.0641	3.71
93.21	0.0597	4.06
98.20	0.0534	3.82

EP= 39.828 MEV

ANG(CM) (DEG)	Dσ/DΩ (MB/SR)	ERRΘR (%)
12.35	0.4560	27.90
17.49	0.4500	16.42
22.63	0.4780	6.78
27.76	0.4480	3.68
33.60	0.3140	5.51
37.69	0.2460	4.84
42.81	0.1730	5.23
48.23	0.1380	6.53
53.32	0.1280	5.04
58.41	0.1130	5.15
63.17	0.0954	4.75
68.24	0.0783	4.78
73.60	0.0682	6.42
78.64	0.0645	4.96
83.66	0.0585	4.50
88.37	0.0488	5.59
93.38	0.0400	5.17
98.37	0.0304	4.83

CA40(P,P')CA40* EX= 8.361 MEV

EP= 24.926 MEV

ANG(CM) (DEG)	Dσ/DΩ (MB/SR)	ERRθR (%)
12.34	0.1820	61.80
17.52	0.2510	21.60
22.67	0.2940	10.60
27.81	0.3070	6.57
32.64	0.3120	7.14
37.77	0.3003	4.50
42.89	0.2930	4.96
48.32	0.2670	5.48
53.42	0.2560	4.75
58.52	0.2360	4.36
63.29	0.1970	5.20
68.36	0.1530	4.23
73.72	0.1370	4.40
78.74	0.1220	4.39
83.79	0.1090	4.45
88.40	0.1040	4.26
93.40	0.0960	4.26
98.40	0.0880	3.57

EP= 30.044 MEV

ANG(CM) (DEG)	Dσ/DΩ (MB/SR)	ERRθR (%)
12.36	0.2540	32.30
17.50	0.2880	15.70
22.66	0.3170	8.92
27.79	0.3470	4.02
32.61	0.3560	4.54
37.74	0.3360	3.92
42.85	0.3420	3.16
48.28	0.3030	3.64
53.38	0.2640	3.45
58.47	0.2150	3.85
63.23	0.1720	3.41
68.30	0.1550	3.13
73.66	0.1250	4.03
78.70	0.1050	3.90
83.73	0.1020	4.34
88.44	0.0936	3.70
93.45	0.0858	3.60
98.44	0.0774	3.58

EP= 34.775 MEV

ANG(CM) (DEG)	Dσ/DΩ (MB/SR)	ERRθR (%)
11.84	0.2910	61.75
16.98	0.3240	20.00
22.12	0.3650	13.06
26.95	0.3960	7.60
32.09	0.4150	3.94
37.21	0.3860	4.06
42.33	0.3760	3.03
47.44	0.3440	3.00
52.54	0.2900	2.97
57.63	0.2380	5.55
62.70	0.1830	3.51
67.77	0.1480	3.35
73.13	0.1160	5.27
78.17	0.0993	5.43
83.20	0.0934	5.05
88.22	0.0852	3.00
93.22	0.0785	3.25
98.21	0.0651	3.32

EP= 39.828 MEV

ANG(CM) (DEG)	Dσ/DΩ (MB/SR)	ERRθR (%)
12.35	0.3150	30.67
17.50	0.3670	16.53
22.63	0.4220	6.54
27.77	0.4350	3.00
32.58	0.4480	4.43
37.70	0.4350	3.30
42.82	0.4130	2.87
48.24	0.3820	3.93
53.33	0.3240	3.43
58.42	0.2260	3.39
63.12	0.1710	5.00
68.25	0.1260	4.06
73.61	0.1040	5.11
78.65	0.0855	4.64
83.68	0.0772	3.81
88.39	0.0723	4.39
93.39	0.0563	4.17
98.38	0.0357	4.32

CA40(P,P')CA40* EX= 8.412 MEV

EP= 24.926 MEV

ANG(CM) (DEG)	Dσ/DΩ (MB/SR)	ERRθR (%)
12.36	0.2500	29.16
17.52	0.2890	15.55
22.67	0.3210	8.09
27.81	0.3450	6.68
32.64	0.3340	6.53
37.77	0.3270	4.16
42.89	0.3050	5.06
48.32	0.2540	8.40
53.52	0.2200	8.60
58.52	0.2020	8.40
63.29	0.1870	7.80
68.36	0.1840	3.92
73.72	0.1620	8.10
78.76	0.1570	6.80
83.79	0.1350	3.92
88.40	0.1250	3.40
93.40	0.0970	6.40
98.40	0.0750	6.50

EP= 30.044 MEV

ANG(CM) (DEG)	Dσ/DΩ (MB/SR)	ERRθR (%)
12.36	0.2700	35.71
17.50	0.3150	17.85
22.66	0.3480	8.22
27.79	0.3520	4.43
32.61	0.3530	4.78
37.74	0.3460	3.80
42.85	0.3060	3.42
48.28	0.2450	8.00
53.38	0.1950	7.70
58.47	0.1540	8.00
63.23	0.1280	7.70
68.30	0.1240	6.20
73.66	0.1090	4.33
78.70	0.0960	3.78
83.73	0.0886	4.31
88.44	0.0680	6.80
93.45	0.0610	9.70
98.44	0.0480	9.50

EP= 34.775 MEV

ANG(CM) (DEG)	Dσ/DΩ (MB/SR)	ERRθR (%)
11.84	0.2940	55.50
16.98	0.3470	21.30
22.12	0.3660	12.70
26.95	0.3830	7.35
32.09	0.3740	4.21
37.21	0.3380	6.30
42.33	0.2800	6.50
47.44	0.2150	6.55
52.54	0.1550	7.60
57.63	0.1210	7.50
62.70	0.1050	7.80
67.77	0.1020	7.70
73.13	0.0875	6.15
78.17	0.0705	12.60
83.20	0.0620	12.90
88.22	0.0510	7.70
93.22	0.0420	8.50
98.21	0.0310	8.00

EP= 39.828 MEV

ANG(CM) (DEG)	Dσ/DΩ (MB/SR)	ERRθR (%)
12.35	0.3350	27.50
17.50	0.3620	14.00
22.63	0.4020	6.67
27.77	0.4170	3.12
32.58	0.3940	4.82
37.70	0.3430	6.90
42.82	0.2580	6.60
48.24	0.1830	10.00
53.33	0.1250	8.40
58.42	0.1030	8.60
63.12	0.0920	9.60
68.25	0.0770	4.70
73.61	0.0660	6.00
78.65	0.0520	5.55
83.68	0.0430	8.50
88.39	0.0358	8.40
93.39	0.0270	8.40
98.38	0.0180	8.40

CA40(P,P')CA40* EX= 8.557 MEV

EP= 24.926 MEV

ANG(CM) (DEG)	Dσ/DΩ (MB/SR)	ERRBR (%)
12.38	0.4980	26.20
17.54	0.4200	18.32
22.69	0.3780	9.45
27.83	0.3850	6.20
32.66	0.3500	6.55
37.79	0.3440	4.77
42.91	0.2840	5.17
48.34	0.2520	5.72
53.44	0.2320	5.13
58.54	0.2090	5.11
63.31	0.1720	5.34
68.38	0.1440	4.66
73.74	0.1280	4.77
78.79	0.1170	4.64
83.81	0.1170	4.67
88.52	0.1160	3.96
93.52	0.0990	3.91
98.52	0.0864	4.06

EP= 30.044 MEV

ANG(CM) (DEG)	Dσ/DΩ (MB/SR)	ERRBR (%)
12.37	0.5030	15.90
17.51	0.4020	13.40
22.66	0.3500	8.78
27.80	0.3420	4.31
32.62	0.3300	6.25
37.75	0.2560	4.61
42.86	0.2160	4.85
48.29	0.2020	4.96
53.39	0.1900	4.85
58.48	0.1850	4.07
63.24	0.1570	4.15
68.31	0.1270	3.81
73.67	0.0954	4.73
78.71	0.0752	5.26
83.74	0.0640	5.68
88.45	0.0530	5.65
93.46	0.0460	5.22
98.45	0.0410	4.96

EP= 34.775 MEV

ANG(CM) (DEG)	Dσ/DΩ (MB/SR)	ERRBR (%)
11.84	0.4530	36.00
16.98	0.3920	17.20
22.12	0.3540	12.33
26.95	0.3660	8.69
32.09	0.2910	5.22
37.21	0.2410	5.93
42.33	0.2090	4.96
47.44	0.1920	4.53
52.54	0.1850	4.10
57.63	0.1700	3.89
62.70	0.1450	3.95
67.77	0.1140	3.60
73.13	0.0891	7.05
78.17	0.0651	8.15
83.20	0.0505	8.47
87.92	0.0422	4.84
92.92	0.0350	5.50
97.91	0.0297	5.38

EP= 39.828 MEV

ANG(CM) (DEG)	Dσ/DΩ (MB/SR)	ERRBR (%)
12.35	0.4750	18.66
17.50	0.4206	14.67
22.63	0.3820	10.27
27.77	0.3306	4.89
32.58	0.2787	5.85
37.70	0.2161	5.47
42.82	0.1823	5.27
48.24	0.1860	5.77
53.33	0.1888	4.22
58.42	0.1565	4.37
63.18	0.1220	4.35
68.25	0.0954	4.26
73.61	0.0612	6.74
78.65	0.0460	7.25
83.68	0.0382	5.75
88.39	0.0295	7.44
93.39	0.0240	6.58
98.38	0.0180	5.98

CA40(P,P')CA40* EX= 3.743 MEV

EP= 24.996 MEV

ANG(CM) (DEG)	Dσ/DΩ (MB/SR)	ERRΘR (%)
17.52	0.2200	27.00
22.69	0.1300	15.00
27.84	0.1600	12.00
32.97	0.1330	12.00
42.92	0.0810	12.00
48.35	0.0770	16.00
53.45	0.0650	11.00
58.56	0.0550	14.00
63.32	0.0530	11.00
68.39	0.0570	9.00
73.75	0.0537	9.00
78.79	0.0452	10.00
83.92	0.0327	12.00
88.43	0.0248	12.00
93.43	0.0215	13.00
98.42	0.0180	12.00

EP= 30.044 MEV

ANG(CM) (DEG)	Dσ/DΩ (MB/SR)	ERRΘR (%)
17.51	0.2350	40.00
22.66	0.2160	15.00
27.81	0.1930	8.00
32.63	0.1220	13.00
37.76	0.0788	11.00
42.87	0.0692	11.00
48.30	0.0643	12.00
53.40	0.0640	11.00
58.49	0.0606	10.00
63.25	0.0448	9.00
68.32	0.0365	8.00
73.68	0.0292	11.00
78.72	0.0270	12.00
83.75	0.0280	10.00
88.46	0.0250	9.00
93.46	0.0170	11.00
98.45	0.0112	12.00

EP= 34.775 MEV

ANG(CM) (DEG)	Dσ/DΩ (MB/SR)	ERRΘR (%)
16.98	0.2400	16.00
22.12	0.2080	13.00
26.96	0.1360	14.00
32.10	0.1580	11.00
37.22	0.0913	12.00
42.34	0.0680	13.00
47.45	0.0485	14.00
52.55	0.0495	12.00
57.64	0.0502	9.00
62.71	0.0415	10.00
67.78	0.0320	9.00
73.14	0.0220	15.00
78.12	0.0200	16.00
83.21	0.0185	30.00
87.93	0.0138	11.00
92.93	0.0110	12.00
97.92	0.0090	12.00

EP= 39.828 MEV

ANG(CM) (DEG)	Dσ/DΩ (MB/SR)	ERRΘR (%)
17.50	0.2250	21.00
22.63	0.1950	15.00
27.78	0.1730	8.20
32.59	0.1290	11.00
37.71	0.0670	15.00
42.83	0.0456	14.00
48.25	0.0430	15.00
53.34	0.0460	12.00
58.42	0.0417	11.00
63.19	0.0320	12.00
68.26	0.0220	8.00
73.62	0.0146	15.00
78.66	0.0124	20.00
83.69	0.0125	11.00
88.40	0.0112	12.00
93.40	0.0088	11.00
98.39	0.0065	12.00

CA40(P,P')CA40* EX= 6.270 MEV

EP= 24.926 MEV

ANG(CM) (DEG)	Dσ/DΩ (MB/SR)	ERRθR (%)
27.82	0.2500	15.00
32.65	0.1580	12.00
37.78	0.1320	8.00
42.90	0.1050	10.00
48.34	0.0640	15.00
53.43	0.0420	20.00
58.53	0.0370	15.00
73.73	0.0350	12.00

EP= 30.044 MEV

ANG(CM) (DEG)	Dσ/DΩ (MB/SR)	ERRθR (%)
27.79	0.1830	11.00
37.74	0.0870	10.00
42.85	0.0720	9.00
48.28	0.0560	12.00
53.38	0.0410	13.00
63.23	0.0310	11.00
78.70	0.0207	12.00
83.70	0.0188	12.00
88.44	0.0126	11.00

EP= 34.770 MEV

ANG(CM) (DEG)	Dσ/DΩ (MB/SR)	ERRθR (%)
26.95	0.1300	13.00
32.09	0.0950	10.60
37.21	0.0560	16.00
42.33	0.0356	20.00
47.44	0.0297	16.40
52.54	0.0240	16.40
57.63	0.0226	16.50
73.13	0.0160	12.00
78.17	0.0144	20.00
83.20	0.0140	17.00
93.22	0.0094	12.00
98.21	0.0077	14.30

EP= 39.820 MEV

ANG(CM) (DEG)	Dσ/DΩ (MB/SR)	ERRθR (%)
27.77	0.1730	13.30
32.58	0.1080	10.60
37.77	0.0600	12.00
42.82	0.0360	18.50
48.24	0.0260	23.00
53.33	0.0192	20.50
58.42	0.0170	17.70
63.12	0.0160	17.00
68.25	0.0164	12.50
73.61	0.0125	22.00
78.65	0.0110	15.50
83.68	0.0094	13.70
88.39	0.0099	14.80
93.39	0.0102	11.20
98.38	0.0084	10.00

CA40(P,P')CA40* EX= 3.847 MEV

EP= 24.926 MEV

ANG(CM) (DEG)	Dσ/DΩ (MB/SR)	ERRθR (%)
27.53	0.0750	15.00
32.67	0.0830	16.00
42.93	0.0960	10.80
48.35	0.1160	10.23
53.46	0.1200	12.30
63.33	0.1220	12.40
68.40	0.1300	10.70
73.76	0.1300	9.80
78.80	0.1200	9.20
83.83	0.1130	9.60
88.54	0.1020	4.80
93.55	0.0980	4.44
98.53	0.0940	3.80

EP= 30.044 MEV

ANG(CM) (DEG)	Dσ/DΩ (MB/SR)	ERRθR (%)
27.50	0.0550	30.00
32.63	0.0700	15.50
37.76	0.0820	9.60
42.88	0.1000	8.10
48.30	0.1140	7.20
53.40	0.1200	9.80
58.49	0.1200	9.50
63.26	0.1190	8.70
68.33	0.1220	8.00
73.68	0.1250	8.00
78.73	0.1150	7.20
83.75	0.1090	4.00
88.47	0.0920	3.60
93.47	0.0850	4.00
98.46	0.0760	3.90

EP= 34.775 MEV

ANG(CM) (DEG)	Dσ/DΩ (MB/SR)	ERRθR (%)
26.96	0.0630	35.00
32.10	0.0720	15.00
37.22	0.1080	9.50
42.34	0.1200	9.60
47.45	0.1300	6.30
52.55	0.1200	10.70
57.64	0.1260	4.80
62.72	0.1220	4.30
67.79	0.1280	3.60
72.84	0.1200	3.00
78.18	0.1160	5.20
83.21	0.1000	5.30
87.93	0.0750	3.50
92.93	0.0570	3.70
97.92	0.0430	4.20

EP= 39.828 MEV

ANG(CM) (DEG)	Dσ/DΩ (MB/SR)	ERRθR (%)
27.46	0.0800	24.00
32.59	0.0860	15.00
37.72	0.0960	10.00
42.83	0.1050	9.20
48.24	0.1320	7.50
53.34	0.1400	5.20
58.43	0.1350	4.60
63.20	0.1400	4.60
68.26	0.1320	3.60
73.31	0.1220	3.50
78.66	0.1180	4.00
83.68	0.0980	6.40
88.40	0.0700	4.80
93.40	0.0480	4.00
98.39	0.0320	4.60

CA40(P,P')CA40* Ex= 8.188 MEV
EP=24.926 MEV

ANG(CM) (DEG)	Dσ/DΩ (MB/SR)	ERRθR (%)
27.82	0.0640	35.00
32.65	0.0660	25.00
48.34	0.0720	12.00
53.43	0.0750	12.00
58.53	0.0730	12.00
63.30	0.0720	10.00
68.37	0.0690	10.00
73.78	0.0600	9.00
83.81	0.0530	10.00
88.51	0.0500	9.00
93.51	0.0480	8.00
98.51	0.0460	8.00

CA40(P,P')CA40* Ex= 8.188 MEV
EP=34.775 MEV

ANG(CM) (DEG)	Dσ/DΩ (MB/SR)	ERRθR (%)
27.24	0.0310	17.00
32.08	0.0325	17.00
37.20	0.0350	17.00
42.32	0.0390	14.00
47.43	0.0440	11.00
52.53	0.0462	11.00
62.70	0.0386	11.00
73.12	0.0305	16.00
78.16	0.0264	17.00
83.20	0.0220	17.00
87.91	0.0196	11.00
92.91	0.0162	12.00
97.90	0.0120	11.00

CA40(P,P')CA40* EX= 8.974 MEV
EP=34.775 MEV

ANG(CM) (DEG)	Dσ/DΩ (MB/SR)	ERRθR (%)
26.89	0.0494	11.90
32.01	0.0537	16.80
37.12	0.0565	15.50
42.23	0.0580	12.90
47.33	0.0603	8.70
52.42	0.0622	9.40
57.50	0.0640	6.90
62.57	0.0563	6.50
67.63	0.0540	5.90
72.68	0.0448	5.30
78.02	0.0355	11.30
83.04	0.0287	11.50
87.76	0.0185	7.80
92.76	0.0147	9.40
97.75	0.0116	9.70

CA40(P,P')CA40* EX= 8.974 MEV
EP=39.828 MEV

ANG(CM) (DEG)	Dσ/DΩ (MB/SR)	ERRθR (%)
27.71	0.0451	14.90
32.52	0.0502	18.70
37.63	0.0510	22.20
42.74	0.0532	24.00
48.14	0.0585	13.70
53.23	0.0583	10.00
58.31	0.0566	7.70
63.07	0.0456	10.30
68.13	0.0409	7.10
73.48	0.0310	9.90
78.52	0.0225	7.80
83.54	0.0151	12.70
88.26	0.0129	14.00
93.26	0.0096	12.80
98.25	0.0090	9.80

CA40(P,P')CA40* EX= 9.025 MEV
EP=34.775 MEV

ANG(CM) (DEG)	Dσ/DΩ (MB/SR)	ERROR (%)
26.89	0.0518	10.80
32.01	0.0635	13.60
37.12	0.0656	13.20
42.23	0.0713	12.50
47.33	0.0670	12.60
52.42	0.0662	10.50
57.50	0.0616	9.00
62.57	0.0510	10.20
67.63	0.0456	9.20
72.68	0.0380	9.00
78.02	0.0320	14.40
83.05	0.0252	15.90
87.76	0.0200	10.70
92.76	0.0143	14.40
97.75	0.0118	14.50

CA40(P,P')CA40* EX= 9.025 MEV
EP=39.828 MEV

ANG(CM) (DEG)	Dσ/DΩ (MB/SR)	ERROR (%)
27.71	0.0622	17.20
32.52	0.0602	12.50
37.63	0.0614	15.70
42.74	0.0743	13.70
48.14	0.0765	11.60
53.23	0.0657	11.50
58.31	0.0574	9.00
63.08	0.0475	8.70
68.13	0.0417	8.30
73.18	0.0304	7.40
78.52	0.0220	10.10
83.55	0.0164	10.60
88.26	0.0120	14.00
93.26	0.0069	15.40

CA40(P,P')CA40* EX= 9.141 MEV
EP=34.775 MEV

ANG(CM) (DEG)	Dσ/DΩ (MB/SR)	ERROR (%)
22.12	0.2600	15.00
26.89	0.3173	8.60
32.01	0.3045	12.20
37.13	0.2774	5.16
42.23	0.2293	4.87
47.33	0.1880	4.58
52.42	0.1332	4.96
57.50	0.1063	5.27
62.57	0.0822	5.90
67.63	0.0782	5.00
72.68	0.0688	4.34
72.99	0.0720	7.12
78.02	0.0640	8.90
83.05	0.0550	7.77
87.76	0.0466	4.70
92.77	0.0300	6.30
97.76	0.0235	5.80

CA40(P,P')CA40* EX= 9.141 MEV
EP=39.828 MEV

ANG(CM) (DEG)	Dσ/DΩ (MB/SR)	ERROR (%)
48.14	0.1470	7.50
53.23	0.0805	7.20
58.31	0.0685	7.50
63.08	0.0606	8.00
68.14	0.0586	5.90
73.18	0.0485	6.10
78.52	0.0386	7.20
83.55	0.0290	7.60
88.26	0.0230	9.70
93.26	0.0146	10.40
98.25	0.0116	7.70

CA40(P,P')CA40* EX= 9.237 MEV
EP=34.775 MEV

ANG(CM) (DEG)	DσΩ/DΩ (MB/SR)	ERROR (%)
37.13	0.0476	14.70
42.23	0.0595	12.50
47.33	0.0610	8.90
52.42	0.0629	9.70
57.50	0.0633	7.00
62.57	0.0656	9.80
67.64	0.0622	8.20
72.99	0.0584	8.20
78.03	0.0535	8.60
83.05	0.0391	9.60
87.76	0.0370	7.60
92.77	0.0287	5.70
97.76	0.0206	8.90

CA40(P,P')CA40* EX= 9.237 MEV
EP=39.828 MEV

ANG(CM) (DEG)	DσΩ/DΩ (MB/SR)	ERROR (%)
58.31	0.0585	8.50
63.08	0.0575	8.30
68.14	0.0533	5.90
73.19	0.0507	5.80
78.53	0.0458	6.50
83.55	0.0418	6.10
88.26	0.0318	7.40
93.26	0.0262	6.80
98.25	0.0181	6.60

CA40(P,P')CA40* EX= 9.358 MEV
EP=34.775 MEV

ANG(CM) (DEG)	Dσ/DΩ (MB/SR)	ERRΘR (%)
22.12	0.1600	14.00
26.89	0.1840	10.70
32.01	0.1745	13.10
37.13	0.1610	6.70
42.24	0.1220	6.90
47.33	0.0984	6.60
52.42	0.0540	11.30
57.51	0.0390	9.80
62.58	0.0363	9.20
67.64	0.0336	7.80
72.99	0.0268	13.00
78.03	0.0245	15.40
83.05	0.0202	11.30
87.77	0.0165	8.60
92.77	0.0105	11.90
97.76	0.0097	11.00

CA40(P,P')CA40* EX= 9.411 MEV
EP=34.775 MEV

ANG(CM) (DEG)	Dσ/DΩ (MB/SR)	ERRΘR (%)
22.12	0.3600	13.00
26.89	0.3944	6.90
32.02	0.3640	7.70
37.13	0.3342	4.70
42.24	0.2492	4.20
47.34	0.2054	4.30
52.43	0.1683	3.80
57.51	0.1203	5.20
62.58	0.1170	5.20
67.64	0.1056	4.30
72.99	0.1013	6.00
78.03	0.0805	7.30
83.06	0.0677	7.00
87.77	0.0500	4.90
92.77	0.0390	4.80
97.76	0.0303	5.50

CA40(P,P')CA40* Ex= 9.540 MEV
EP=34.775 MEV

ANG(CM) (DEG)	Dσ/DΩ (MB/SR)	ERROR (%)
22.12	0.1080	13.00
27.20	0.1180	10.50
32.02	0.1230	12.00
37.13	0.1210	10.20
42.24	0.1130	8.00
47.34	0.0920	7.50
52.43	0.0650	8.00
57.51	0.0465	10.00
62.58	0.0330	10.50
67.64	0.0212	13.00
72.69	0.0197	11.00
78.03	0.0168	20.00
83.06	0.0140	20.00
87.77	0.0110	16.00
92.78	0.0080	15.00
97.77	0.0065	15.00

CA40(P,P')CA40* Ex= 9.590 MEV
EP=34.775 MEV

ANG(CM) (DEG)	Dσ/DΩ (MB/SR)	ERROR (%)
22.13	0.0850	20.00
26.90	0.0921	15.50
32.02	0.0900	13.10
37.13	0.0827	13.50
42.24	0.0657	10.50
47.34	0.0458	8.60
52.43	0.0333	13.00
57.51	0.0253	14.35
62.58	0.0250	10.25
67.64	0.0232	10.86
72.69	0.0179	10.40
72.99	0.0175	18.00
78.03	0.0153	21.00
83.06	0.0130	18.80
87.77	0.0087	14.60
92.78	0.0055	19.50
97.77	0.0048	14.40

CA40(P,P')CA40* EX= 9.637 MEV
EP=34.775 MEV

ANG(CM) (DEG)	Dσ/DΩ (MB/SR)	ERROR (%)
22.13	0.2100	15.00
26.90	0.1940	13.70
32.02	0.1365	8.40
37.13	0.1224	8.80
42.24	0.1080	7.20
47.34	0.0960	10.30
52.43	0.0893	6.50
57.51	0.0974	5.90
62.58	0.0948	12.80
67.64	0.0788	5.30
72.69	0.0504	5.50
78.03	0.0429	10.60
83.06	0.0254	14.00
87.77	0.0255	7.30
92.78	0.0206	7.90
97.77	0.0182	9.20

CA40(P,P')CA40* EX= 9.856 MEV
EP=34.775 MEV

ANG(CM) (DEG)	Dσ/DΩ (MB/SR)	ERROR (%)
26.90	0.0877	12.70
32.02	0.0954	10.50
37.13	0.1013	10.50
42.24	0.1063	8.10
47.34	0.1100	9.40
52.43	0.0987	6.30
57.51	0.0945	5.70
62.59	0.0783	6.10
67.65	0.0696	5.60
73.00	0.0434	10.20
78.04	0.0355	13.30
83.06	0.0266	13.70
87.78	0.0225	8.00
92.78	0.0152	10.40
97.77	0.0140	9.60

CA40(P,P')CA40* EX=10.045 MEV
EP=34.775 MEV

ANG(CM) (DEG)	Dσ/DΩ (MB/SR)	ERROR (%)
26.90	0.1080	19.40
32.02	0.1160	10.80
37.14	0.1185	9.70
42.24	0.1230	7.00
47.34	0.1140	10.60
52.43	0.1100	10.30
57.52	0.0985	5.90
62.59	0.0840	6.20
67.65	0.0624	6.00
72.70	0.0395	6.80
78.04	0.0345	12.60
83.07	0.0210	15.60
87.78	0.0195	8.50
92.78	0.0168	10.10
97.77	0.0128	8.20

CA40(P,P')CA40* EX=10.276 MEV
EP=34.775 MEV

ANG(CM) (DEG)	Dσ/DΩ (MB/SR)	ERROR (%)
22.13	0.1300	20.00
26.90	0.1497	19.00
32.02	0.1584	7.30
37.14	0.1590	8.80
42.25	0.1494	7.00
47.35	0.1274	7.90
52.44	0.0872	7.00
57.52	0.0662	7.90
62.59	0.0478	8.30
67.66	0.0410	8.00
72.71	0.0327	8.00
78.05	0.0327	14.10
83.07	0.0280	10.90
87.79	0.0250	7.30
92.79	0.0202	8.50
97.78	0.0175	8.30